REPORT DOCUMENTATION PAGE

AFRL-SR-AR-TR-05-

The public reporting burden for this collection of information is estimated to average 1 hour per response, including the tim gathering and maintaining the data needed, and completing and reviewing the collection of information. Send comments rega of information, including suggestions for reducing the burden, to Department of Defense, Washington Headquarters S (0704-0188), 1215 Jefferson Davis Highway, Suite 1204, Arlington, VA 22202-4302. Respondents should be aware that subject to any penalty for failing to comply with a collection of information if it does not display a currently valid OMB control PLEASE DO NOT RETURN YOUR FORM TO THE ABOVE ADDRESS.

6011

1. REPORT DATE *(DD-MM-YYYY)*	2. REPORT TYPE	3. DATES COVERED *(From - To)*
	Final Report	February 2000 - October 2004

4. TITLE AND SUBTITLE
Fundamental Issues Regarding the High Temperature Failure Properties of Graphite/Polyimide Fabric Composites

5a. CONTRACT NUMBER

5b. GRANT NUMBER
F49620-00-1-0159

5c. PROGRAM ELEMENT NUMBER

6. AUTHOR(S)
Professor M. S. Kumosa

5d. PROJECT NUMBER

5e. TASK NUMBER

5f. WORK UNIT NUMBER

7. PERFORMING ORGANIZATION NAME(S) AND ADDRESS(ES)
Center for Advanced Materials and Structures
Department of Engineering
University of Denver
2390 South York Street
Denver CO 80208

8. PERFORMING ORGANIZATION REPORT NUMBER

9. SPONSORING/MONITORING AGENCY NAME(S) AND ADDRESS(ES)
USAF/AFRL
AFOSR
801 N. Randolph Street
Arlington VA 22203

NA

10. SPONSOR/MONITOR'S ACRONYM(S)
AFOSR

11. SPONSOR/MONITOR'S REPORT NUMBER(S)

12. DISTRIBUTION/AVAILABILITY STATEMENT
Distribution Statement A. Approved for public release; distribution is unlimited.

13. SUPPLEMENTARY NOTES

14. ABSTRACT
In this work, a method based on X-ray diffraction (XRD) measurements of internal stresses in embedded metallic ellipsoidal inclusions is briefly described. The method has been recently developed for the determination of residual thermal stresses in high temperature graphite/polyimide composites. The effects of external bending loads and aging on the measurements of the internal stress in unidirectional and woven graphite fiber (T650-35)/polyimide (PMR-15) composites were examined in addition to several other factors which could influence the accuracy of the stress measurements. Such factors as the volume fraction of inclusions, their aspect ratios and the interaction between individual embedded inclusions were also evaluated in this study. It has been shown that despite its complexity the proposed method can be successfully applied to the evaluation of residual stresses in high temperature polymer matrix composites subjected to external loads and aging.

15. SUBJECT TERMS

16. SECURITY CLASSIFICATION OF:			17. LIMITATION OF ABSTRACT	18. NUMBER OF PAGES	19a. NAME OF RESPONSIBLE PERSON
a. REPORT	b. ABSTRACT	c. THIS PAGE			19b. TELEPHONE NUMBER *(Include area code)*
UU	UU	UU	UU	171	

JAN 10 2005

FUNDAMENTAL ISSUES REGARDING THE HIGH TEMPERATURE FAILURE PROPERTIES OF GRAPHITE/POLYIMIDE FABRIC COMPOSITES

FINAL REPORT

FEBRUARY 2000 – OCTOBER 2004

M. S. KUMOSA, PRINCIPAL INVESTIGATOR

CONTRIBUTORS:

P. K. PREDECKI, D. ARMENTROUT, B. BENEDIKT, M. GENTZ,
P. RUPNOWSKI, G. ODEGARD, K. SEARLES and L. KUMOSA

CENTER FOR ADVANCED MATERIALS AND STRUCTURES
DEPARTMENT OF ENGINEERING
UNIVERSITY OF DENVER
2390 SOUTH YORK STREET, DENVER, COLORADO 80208

SPONSORED BY:

AIR FORCE OFFICE OF SCIENTIFIC RESEARCH AND NASA GLENN
RESEARCH CENTER UNDER GRANT F49620-00-1-0159

20050125 143

TABLE OF CONTENTS

OBJECTIVES

Major research activities were undertaken between February 2000 and November 2004 in the Center for Advanced Materials and Structures at the University of Denver toward the development of experimental and computational methodologies to facilitate the analysis of failure mechanisms in graphite/PMR-15 composites subjected to biaxial shear dominated loads. The two primary goals of this research program were to (1) understand the mechanical behavior of unidirectional and woven graphite/polyimide composites based on medium (T-650) and high (M40J and M60J) modulus graphite fibers with PMR-15 and PMR-II-50 polyimide resins tested under biaxial, shear dominated stress conditions over a temperature range of 20°C to 316°C considering the effects of physical and chemical aging, and moisture, and (2) to develop a method for determining residual thermal stresses in the high temperature polymer matrix composites based on X-ray diffraction (XRD) measurements of strains in embedded metallic spherical inclusions.

EXECUTIVE SUMMARY

Graphite/polyimide composites are advanced materials that are widely used in aerospace applications at temperatures up to approximately 400°C [1-40]. A major limitation of woven fiber/polyimide systems is the inability of these materials to resist intralaminar and interlaminar damage initiation and propagation under shear-dominated biaxial loading conditions. Therefore, failure analyses of unidirectional and woven graphite/polyimide composites based on medium (T650-35) and high (M40J and M60J) modulus graphite fibers with PMR-15 and PMR-II-50 polyimide resins have been performed experimentally and numerically in this study [1-5,9-11,14-17,20-25, 27,28,30,31-35,37-40]. The composites were subjected to biaxial shear dominated stress conditions over a temperature range from 20°C to 316°C. Particular attention was given to the evaluation of damage development and its effect on the shear strengths of the woven composites using the Iosipescu shear and ±45° tensile tests. In support of the mechanical testing part of this research, the applications of the Iosipescu and ±45° tests for the room and high temperature failure analyses of woven graphite/polyimide

composites was numerically evaluated by performing non-linear finite element computations of these two tests. Then, visco-elastic and visco-elasto-plastic micro- and meso-stress distributions in the composites were conducted under several different biaxial shear dominated load cases considering the manufacturing cycles of the composites. The numerically predicted micro-stresses were subsequently used to explain the initiation of damage in the composites as a function of temperature, biaxial loads, strain rates and manufacturing conditions, among several other less critical factors. The effect of aging of the composites in air and in nitrogen on their mechanical response was also thoroughly evaluated. Since the transverse Young moduli and transverse coefficients of thermal expansion (CTE) of the T650-35, M40J and M60J fibers were either unknown (M40J and M60J) or inaccurate (T650-35), new numerical/experimental techniques were designed to evaluate these properties, as well as several other stiffness properties, from the macroscopic data for the unidirectional and woven composites based on the same fibers and used to determine the properties of the fibers.

Major advances were also made in this project in the development of an experimental/numerical technique for the determination of interlaminar residual stresses in unidirectional and woven graphite/polymer composites based on X-ray diffraction measurements of residual strains in embedded metallic inclusions [6-8,12,13,18,19,20,26,29,36]. The interlaminar residual stresses in the unidirectional and 8HS graphite/PMR-15 composites have been determined both experimentally and numerically as a function of the manufacturing process using the newly developed testing methodology. Then the method was used to evaluate the residual interlaminar stresses in the T650/PMR-15 composite as a function of bending deformations. In particular, the effect of large bending moments on the XRD measurements of the residual stresses in the particles was carefully examined and the limitations of the methodology were discussed. Subsequently, the method was used to evaluate the residual interlaminar stresses in the unidirectional and woven 8HS T650/PMR-15 composites subjected to aging either in air or nitrogen. To explain the effect of oxidation on the surface of the inclusions, a new analytical method for determination of thermal stress distributions around double inclusions embedded in an unbounded matrix due to a uniform temperature change has

been developed. Finally, such factors as the volume fraction of inclusions, their aspect ratios and the interaction between embedded inclusions were also evaluated in this study. It has been shown that despite its complexity, the proposed method can be successfully applied to the evaluation of residual stresses in high temperature polymer matrix composites subjected to external loads and aging.

Between February 2000 and December 2004 this research resulted in:

- Eighteen published papers in *Acta Materialia, Proceedings of the Royal Society, Composites Science and Technology, Composites Part A, Composites Technology & Research, Mechanics of Advanced Materials and Structures, and the Journal of Composite Materials.*
- Two journal papers submitted and two additional to be submitted in January 2005,
- Thirteen reviewed conference papers.
- Three completed and one to be completed (in Winter 2005) Ph.D. theses by Dr. G. Odegard, Dr. B. Benedikt, Dr. M. Gentz and Mr. P. Rupnowski.

As part of this program major technical interactions took place with Dr. J. K. Sutter and Dr. E. Shin from NASA Glenn Research Center. A significant portion of the funding for this work was provided by NASA in addition to supplying of numerous composite systems, conducting several quality control tests on the composites investigated in this project, and by openly sharing their extensive experience in the areas of composite manufacturing and testing. This project also provided important research support for NASA Glenn (see attached letter from Dr. J. K. Sutter) involved in a three year collaboration with Boeing to design, fabricate and test a lightweight high temperature polymer matrix composite (HTPMC) combustor support chamber for a rocket based combined cycle engine. The support structure was prepared from a high temperature composite material, based on M40J fiber and a PMR-II-50 polyimide resin. The chamber successfully survived hot-fire testing in March 2004.

Major Research Accomplishments

1. Introduction

Woven graphite/polyimide composites (Fig. 1) are advanced materials that are widely used in aerospace applications, which require high temperature capabilities up to approximately 400°C [1-40]. However, one of the limitations of such composites is their low strength under biaxial shear dominated loading conditions at room and elevated temperatures [2,3-5,9,11,14,16,17,20-24,28,30,34,38-40]. Under these loading conditions, intralaminar and interlaminar cracks develop in the composites at relatively low applied loads (Fig. 2). The shear strength of the composites is approximately ten times lower than their tensile strength and approximately five times lower than their compressive strength. In addition, the shear strength and shear stiffness of the composites are significantly reduced at elevated temperatures.

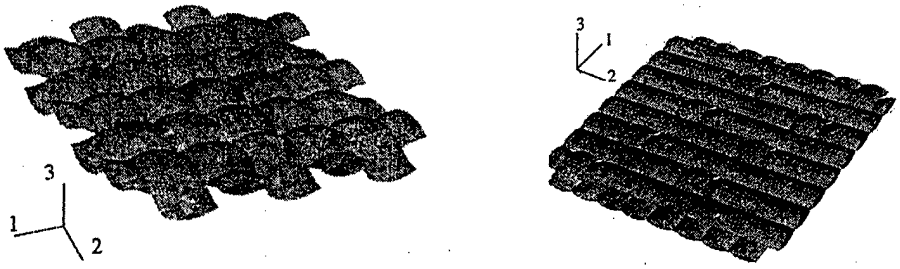

Figure 1. Woven fabric architectures; plain weave (left) and 8HS weave (right).

During manufacturing of graphite/polyimides, large residual thermal stresses are generated in the composites [6-8,11-20,22-24,26-29,34,38,40]. A greater discrepancy between the thermal expansion coefficients of the fibers and that of the resin, and a larger temperature difference between the manufacturing and in-service temperatures leads to the generation of higher residual thermal stresses. The non-zero state of stress at room temperature can significantly affect the shear strength of the composite materials, especially at low temperatures. In some graphite/polyimide woven systems the magnitudes of residual stresses from manufacturing can be so high that severe intralaminar tow micro-cracking can develop in the absence of external loads (Fig. 3) [20,

22,24]. The presence of such cracks could significantly affect the overall strength of the composites in service.

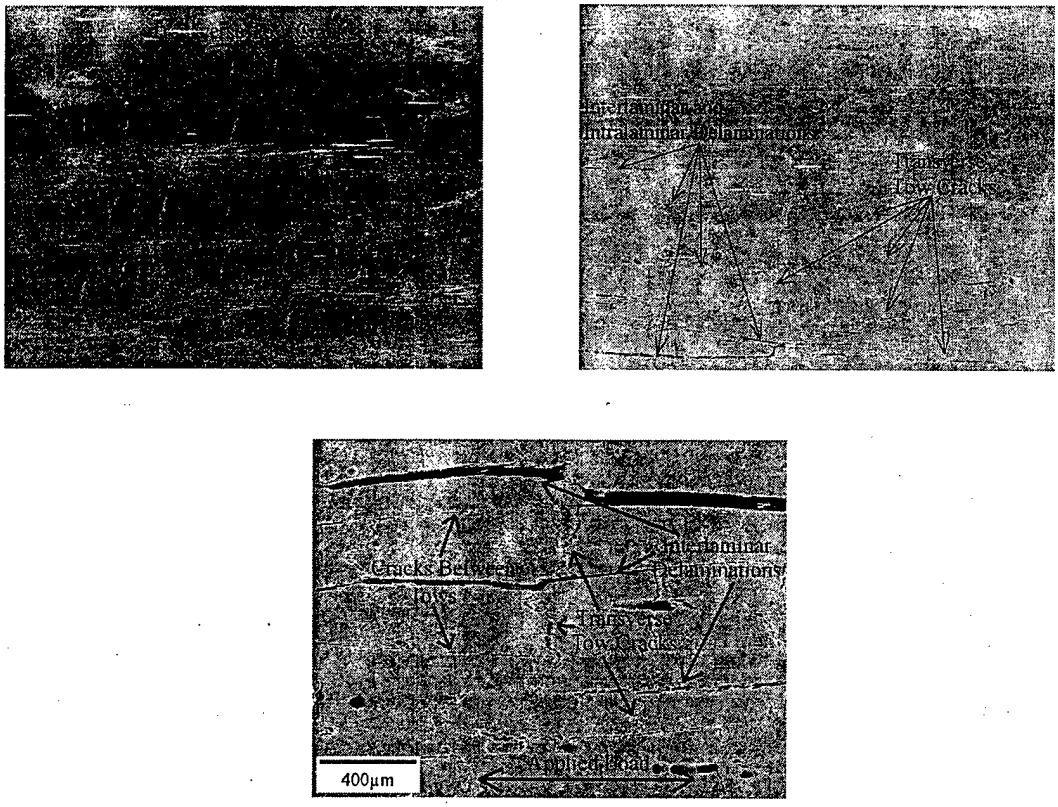

Figure 2. Stages of damage development in 8HS T650/PMR-15 subjected to biaxial shear dominated loads [3,9].

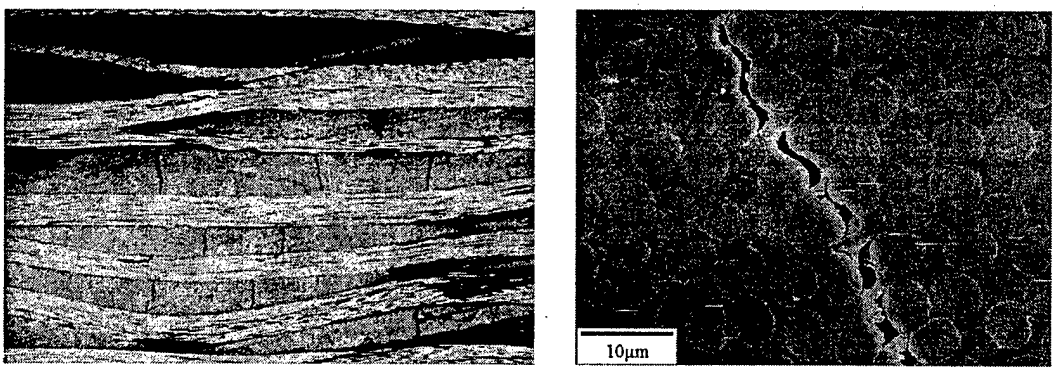

Figure 3. Micro-cracking after manufacturing in a graphite/polyimide composite [20,22,24].

2. Failure Analyses of T650-35/PMR-15, M40J/PMR-II-50 and M60/PMR-II-50 Composites

2.1. Non-linear macroscopic modeling of woven Iosipescu and ±45° specimens

The graphite fiber/polyimide woven composites were investigated in this research using mainly the Iosipescu shear and ±45° tensile tests. To understand the effects of specimen geometries, loading conditions, composite architectures, temperature, manufacturing, etc., both tests have been numerically evaluated using finite element techniques on the macro-, meso- and micro-levels under elastic, visco-elastic and visco elasto-plastic conditions [2,4,5,9-11,14-17,20,22-26-28,34,37,38,40].

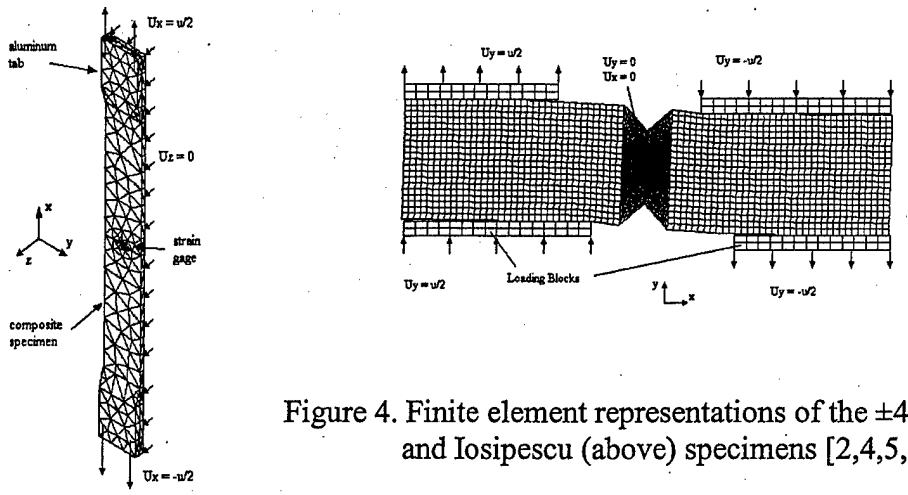

Figure 4. Finite element representations of the ±45° tensile (left) and Iosipescu (above) specimens [2,4,5,9,22].

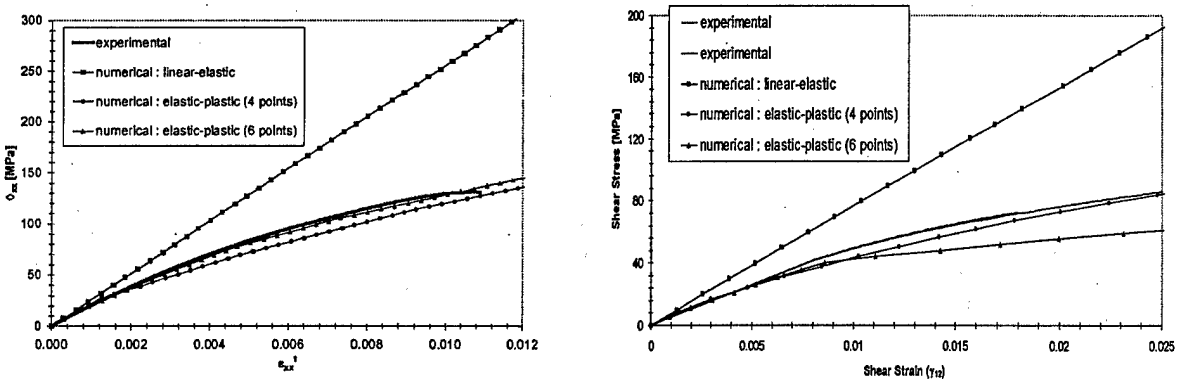

Figure 5. Room temperature shear stress/shear strain diagrams from the ±45° tensile (left) and Iosipescu shear (right) tests performed on the 8HS T650/PMR-15 composite [2,4,5,9,22].

An elastic-plastic, time-independent, macroscopic, homogenous model of an 8HS woven graphite/PMR-15 composite material has been developed by Odegard et al. [2] that predicts the non-linear response of the material subjected to shear-dominated biaxial loads. The model has been used to determine the response of the woven composite Iosipescu shear and ±45° tensile test specimens at room temperature in non-linear finite element analyses (Fig. 4) [2,4,5,9,22]. The finite element computations of the ±45° and Iosipescu tests were fully non-linear with the material, geometrical, and boundary contact non-linearities considered [2,4,5,9,22]. It has been shown that the numerically calculated stress-strain diagrams of the ±45° tensile specimens are very close to the experimentally obtained curves for small strains without inter- and intralaminar damage (Fig. 5).

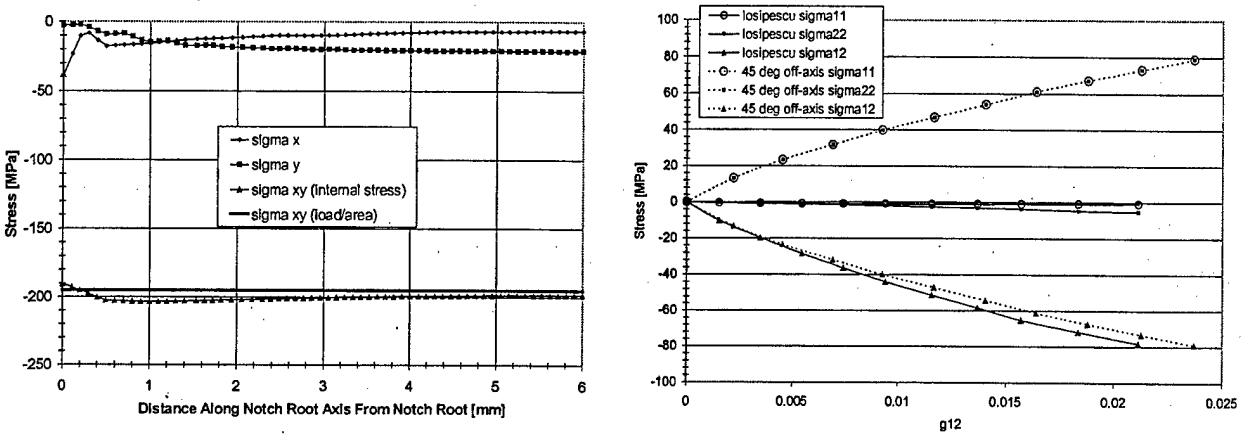

Figure 6. Stress distributions in the gage sections of the 8HS T650/PMR-15 Iosipescu shear (left) and ±45° tensile (right) specimens [2,4,5,9,22].

It was also indicated that the non-linear effects had to be considered in the modeling of the composite under in-plane shear dominated biaxial loads. Large differences were found in the mechanical response of the composite to shear when modeled under linear and non-linear conditions (Fig. 6). It was also shown [2,4,5,9,22] that the stress distributions in the Iosipescu and ±45° woven specimens were entirely different. In the gage sections of the woven Iosipescu specimens, the stress fields are essentially pure shear (Fig. 6, left) whereas the ±45° test generated biaxial tension/tension and shear stress fields (Fig. 6, right) [2,4,5,9,22].

2.2 Shear testing of 8HS T650-35/PMR-15, 4HS M40J/PMR-II-50 and 4HS M60J/PMR-II-50 composites

Failure analyses of woven graphite/polyimide composites based on T-650-35, M40J and M60J graphite fibers with either PMR-15 or PMR-II-50 polyimide resins have been performed [2-5,9,11,14,16,17,20-25,27,28,30,34,38-40]. The composites were tested at room and elevated temperatures using the Iosipescu shear and ±45° tensile tests. The T650/PMR-15 composite was tested as supplied, whereas the high stiffness composites based on either M40J or M60J graphite fibers with PMR-II-50 resin were tested as supplied and after thermal conditioning with and without moisture added. To explain the effect of temperature, residual thermal stresses and biaxial loads on the failure process of the composites, the visco-elastic computations of micro- and meso-stress distributions in the composites have been performed [13-20,22,23,25,27-29,31-35,38-40].

2.2.1 Woven 8HS T650-35/PMR-15 composite

It has been shown in this project that the mechanical behavior of the 8HS graphite/PMR-15 composite at room and elevated temperatures is very strongly dependent on the type of specimen used [2-4,9,11,14,16,17,20,22,28,34,40]. The ±45° test grossly underestimates the shear strength of the composite in comparison with the Iosipescu test at room and elevated temperatures (Fig. 7, Table 1). The critical shear stresses for the initiation of intralaminar damage determined from the ±45° tensile tests are also significantly lower than those determined from the Iosipescu tests (Table 1). It appears that the weakest failure mode for the 8HS woven composite tested at room and elevated temperatures is the combined in-plane shear and biaxial tension state of stress.

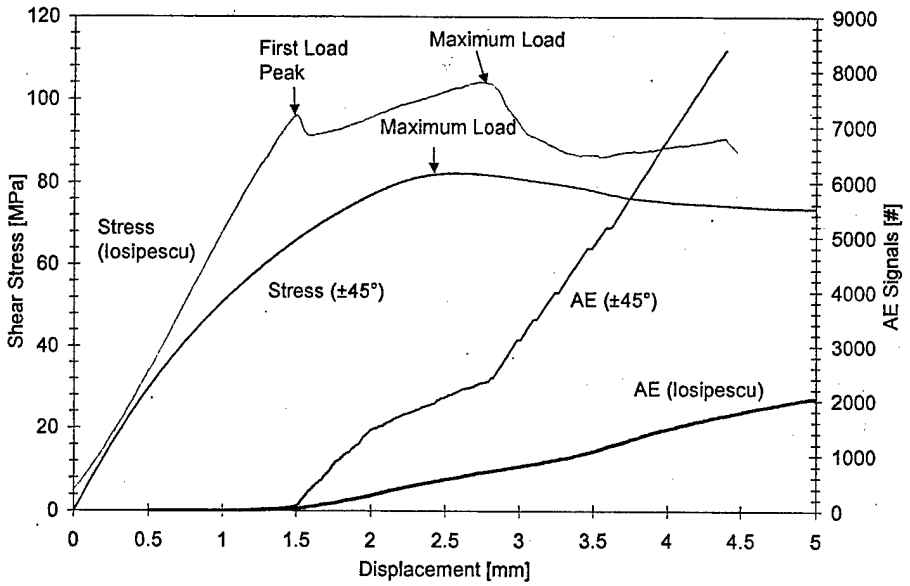

Figure 7. Shear stress vs. displacement and acoustic emission vs. displacement diagrams from the ±45° tensile and Iosipescu tests at room temperature [9].

It has also been clearly demonstrated in this project that the ±45° tensile tests are strongly affected by the specimen width [3-5,11,14,28]. This effect can be clearly seen in terms of the maximum loads (Fig. 8a) and the loads at the initiation of intralaminar damage (Fig. 8b) measured at room and elevated temperatures using advanced acoustic emission techniques.

Table 1. Shear stresses at the onset of intralaminar damage (determined by AE) and at the maximum loads from the ±45° tensile and Iosipescu tests at room and 315°C temperatures [3-5,9,11,14,28].

	Shear Stresses at the Onset of Intralaminar Damage [MPa]		Shear Stresses at Maximum Loads [MPa]	
Test	±45°	Iosipescu	±45°	Iosipescu
at RT	56.6 ± 2.0	94.8 ± 1.3	82.0 ± 0.15	105.8 ± 2.6
at 315°C	37.3 ± 5.2	59.9 ± 1.2	50.8 ± 6.0	71.8 ± 4.2

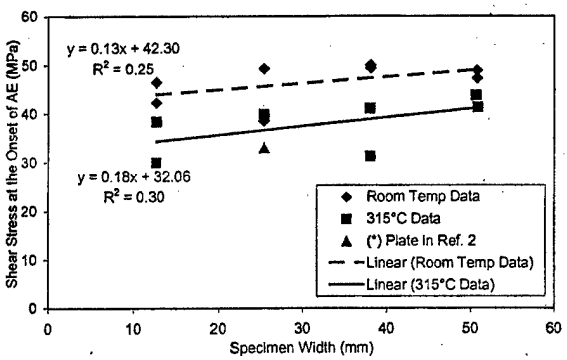

Fig. 8a Shear stresses at the maximum loads as a function of specimen width from the ±45° tensile tests performed at room and 315°C temperatures [3-5,11,14,28].

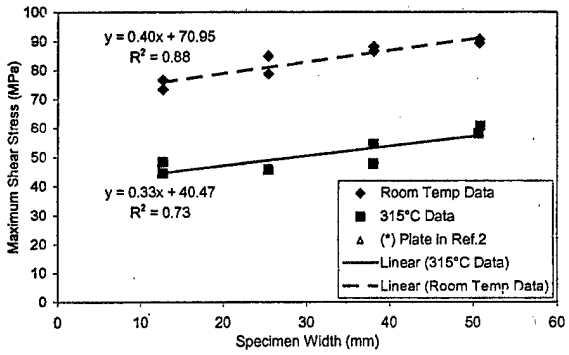

Fig. 8b Shear stresses at the onset of intralaminar damage as a function of specimen width from the ±45° tensile tests performed at room and 315°C temperatures [3-5,11,14,28].

2.2.2 4HS M40J/PMR-II-50 and M60J/PMR-II-50 composites

A very noticeable effect of residual thermal stresses was found on the initiation of intralaminar damage in the T650-35, M40J and M60J fiber composites, as determined by acoustic emission [16,17,20,22,24,28]. The large magnitudes of residual stresses in the M60J fiber composite resulted in the formation of the cracks under very low shear stresses at room temperature. At this temperature, the critical shear stresses for the initiation of tow cracking are much higher in the M40J/PMR-II-50 and the T-650/PMR-15 composites (see Table 2).

Table 2. Shear stresses at the onset of AE and at the maximum loads from the Iosipescu tests at room and 315°C temperatures performed on the as-supplied T-650/PMR-15, M40J/PMR-II-50 and M60J/PMR-II-50 composites (dry without thermal cycling) [24].

	At Room Temperature		At 315°C	
Composite System	Shear Stresses at the Significant Onset of AE [MPa]	Shear Stresses at Maximum Loads [MPa]	Shear Stresses at the Significant Onset of AE [MPa]	Shear Stresses at Maximum Loads [MPa]
T-650/PMR-15	94.8 ± 1.3	105.8 ± 2.6	59.9 ± 1.2	71.8 ± 4.2
M40J/PMR-II-50	30.3 ± 3.1	86.7 ± 2.7	56.5 (one test) (**54.9 ± 4.3)	61.2 ± 4.1
M60J/PMR-II-50	9.9 ± 2.5	63.8 ± 0.4	(*** 40.0 ± 5.8)	50.2 ± 0.8

Number of * are the number of tests with onset of AE after the maximum load.

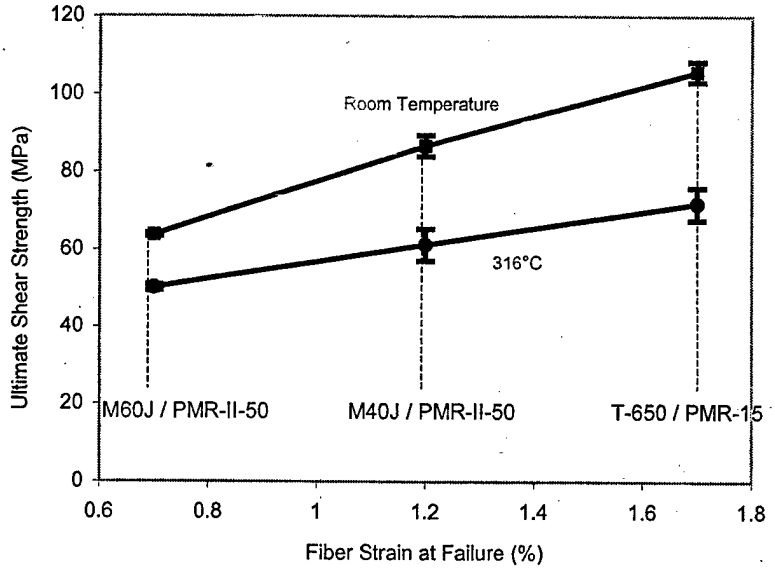

Figure 9. Shear strength of the as supplied T-650, M40J and M60J fiber composites at room temperature and 315°C as a function of the fiber strain at failure [16,17,20,22,24,28].

The room and high temperature (at 315°C) ultimate shear strengths of the as supplied T-650/PMR-15, M40J/PMR-II-50 and M60J/PMR-II-50 composite systems tested using the Iosipescu shear test increase linearly with the increased strain at failure of the T-650, M40J and M60J fibers (Fig. 9) [16,17,20,22,24,28]. No noticeable effect of the thermal conditioning and moisture on the shear strengths of the M40J and M60J fiber composites was observed.

The critical shear stresses for the initiation of new tow cracking in the M40J and M60J fiber Iosipescu specimens increased substantially after pre-conditioning [24,28]. This indicates that thermo-cycling (by the formation of additional tow cracks) and moisture can significantly relax the residual thermal stresses in the composites at room temperature. At 315°C the effect of the residual stresses on the initiation of damage in the as-supplied and pre-conditioned composites appears to be insignificant.

2.2.3 Effect of aging in nitrogen on the strength and stiffness of 8HS T650-35/PMR-15

In this part of the project the effect of aging in a nitrogen atmosphere at 315°C for times up to 1535 hours on the strength and stiffness of the 8HS T650/PMR-15 composite was studied [28]. Acoustic emission (AE) at the onset of damage was used as the criteria to determine if there are significant effects on the residual stress state of the composite as a function of aging time. The ±45° off axis tensile tests were performed at room temperature on the aged composite at a displacement rate of 1mm/min. until failure. The results of this experiment included mass loss, ultimate shear strength, stress at the initiation of damage as determined by AE, and the shear modulus, all as a function of aging time at 315°C in a nitrogen atmosphere. The shear modulus as a function of aging time is shown in Figure 10a whereas in Figure 10b the ultimate strength and the onset of AE from the ±45° tests are presented.

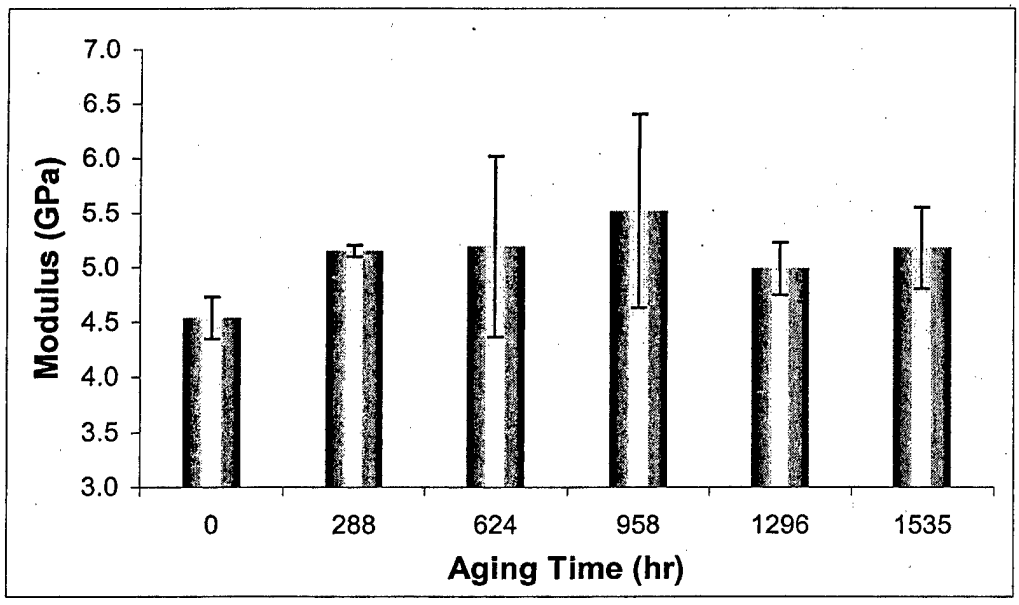

Figure 10a Shear modulus as a function of aging in nitrogen at 315°C [28].

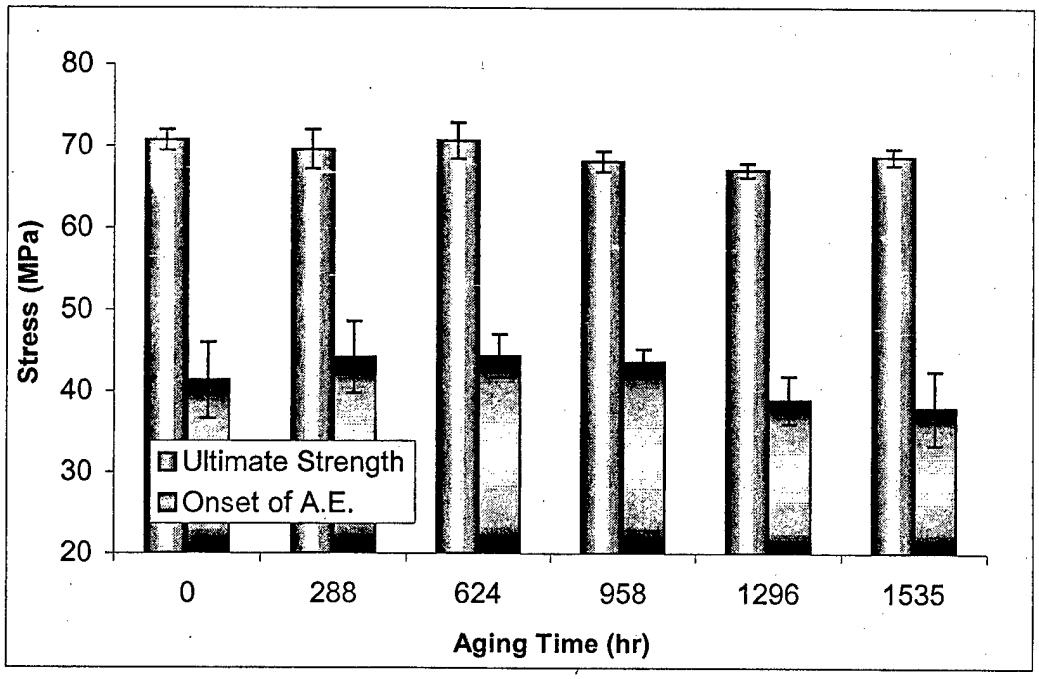

Figure 10b Ultimate strength and the onset of acoustic emission of the 8HS T650/PMR-15 composite following aging in nitrogen at 315°C [28].

It has been found that the only measurable effect of aging 8HS T650/PMR-15 in N_2 for up to 1535 hours at 315°C is a slight mass loss [28]. Because of the large variation in the measurement of the modulus (Fig. 10a) the only discernable difference in the modulus is between 0 and 288 hrs. of aging time with the modulus increasing approximately 12%. Comparing the modulus between 288 and 1535 hrs. the modulus is unchanged within the variability in the measurements. Aging the 8HS T650/PMR-15 composite in nitrogen at 316°C has very little effect on the ultimate shear strength (±45°), and the onset of intralaminar damage.

2.2.4 Other woven composite architectures investigated in this project

The support structure used by NASA is heated from the inside at a rate of approximately 95°C/sec. Therefore, absorbed ambient moisture absorbed in the 8HS M40/PMR-50 composite when vaporized during rapid heating may blister or delaminate the material.

To address this problem, five new M40J/PMR-II-50 composites were developed by NASA Glenn including two composites with out of plane stitching using fiberglass yarn [21,30]. The out of plane stitched material was developed specifically to address the rapid heating blistering performance of the composite even at the possible expense of decreasing the in-plane mechanical properties. The in-plane shear properties of the M40J/PMR-II-50 composites with various fiber geometries were evaluated [28] and compared with the baseline 4HS M40J/PMR-II-50 woven fabric composite tested previously, as well as with each other. These tests were performed at room temperature, at 315°C, and at 315°C after conditioning the specimens in a 50°C 80% R.H. environment for 916 hrs. Moisture absorption to saturation of the composites was also evaluated in the 50°C 80% R.H. environment.

The following composite architectures (Fig. 11) were used:

(I) 4HS Woven Fabric, Twelve ply 4HS fabric in a cross ply configuration, $[0_f, 90_f, 90_f, 0_f, 0_f, 90_f]_{1s}$, density 1.614 ± 0.011 g/cm^3, void content 1.1 ± 0.7%, T_g 383°C (G′ onset), FVF 58 ± 1%, average thickness 2.44mm,

(II) Uni-Tape Cross Ply, Twenty four ply unidirectional tape in a cross ply configuration, $[0, 90]_{6s}$, density 1.583 ± 0.014 g/cm^3, void content 3.0 ± 1.0%, T_g 370°C (G′ onset), FVF 56 ± 1%, average thickness 2.58mm,

(III) Uni-Woven Hybrid, Eight plys of 4HS fabric and eight plys of unidirectional tape, $[0_f, 90, 0, 90_f, 0_f, 0, 90, 90_f]_{1s}$, density 1.605 ± 0.007 g/cm^3, void content 1.7 ± 0.4%, T_g 380°C (G′ onset), FVF 58 ± 2%, average thickness 2.55mm,

(IV) Triaxial Braid, Equivalent to twelve ply fabric, density 1.562 ± 0.032 g/cm^3, void content 3.6 ± 1.5%, T_g 366°C (G′ onset), FVF 53 ± 4%, average thickness 2.62mm,

(V) Stitched Uni-Tape, Twenty four ply unidirectional tape in a cross ply configuration, $[0, 90]_{6s}$ Stitched with S2 glass (150 1/0), 4.23 mm spacing, density 1.570 ± 0.009 g/cm^3, void content 3.9 ± 0.6%, T_g 383°C (G′ onset), FVF 57 ± 2%, average thickness 2.78mm and

(VI) Stitched 4HS Woven Fabric, Twelve ply 4HS fabric in a cross ply configuration, $[0_f, 90_f, 90_f, 0_f, 0_f, 90_f]_{1s}$, Stitched with S2 glass (150 1/0), 4.23 mm spacing, density 1.515 ± 0.050 g/cm^3, void content 7.1 ± 2.2%, T_g 384°C (G′ onset), FVF 54 ± 4%, average thickness 2.72mm.

The matrix material used was PMR-II-50 for all the fiber architectures except for the stitched unidirectional tape. The stitched unidirectional tape used HFPE-II-52 with properties similar to PMR-II-50. The composites were tested using the Iosipescu test as supplied and preconditioned in a 50°C 80% R.H. environment for 916 hrs.

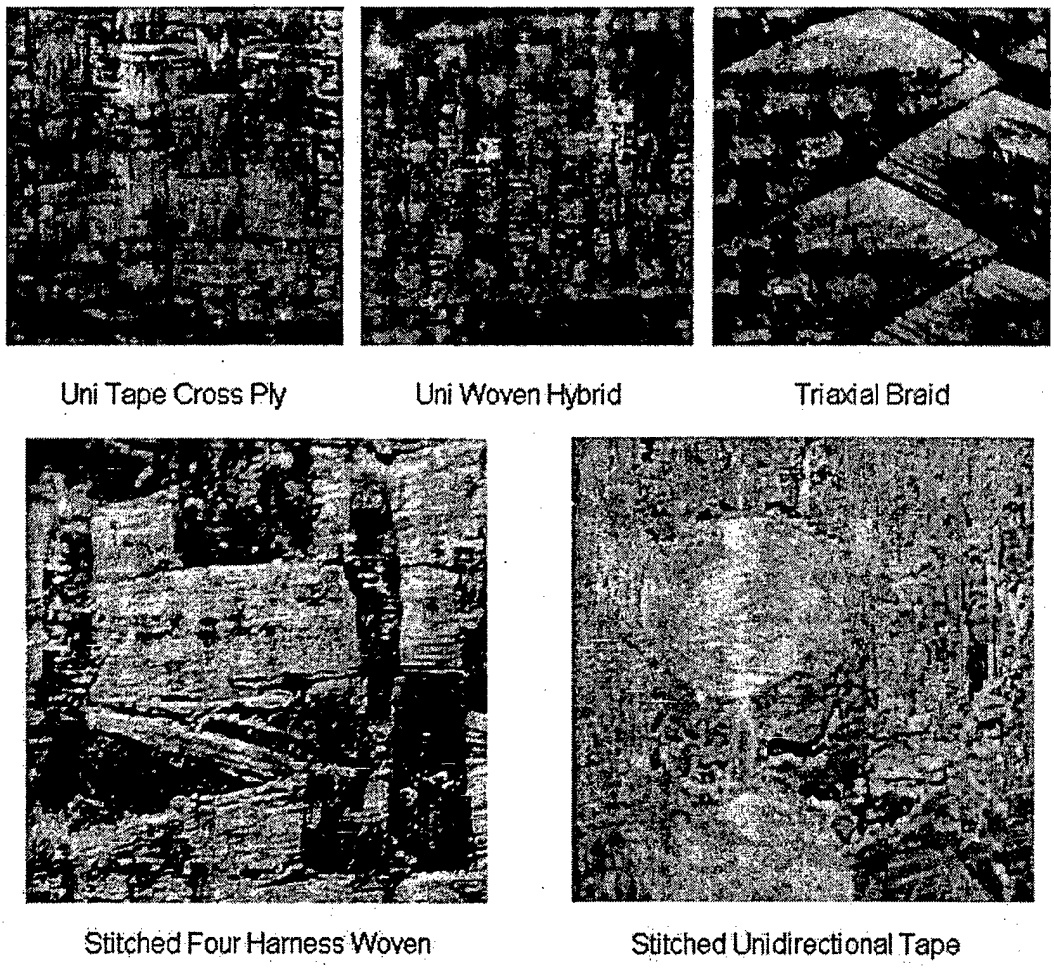

Figure 11. Surfaces of the composites [28].

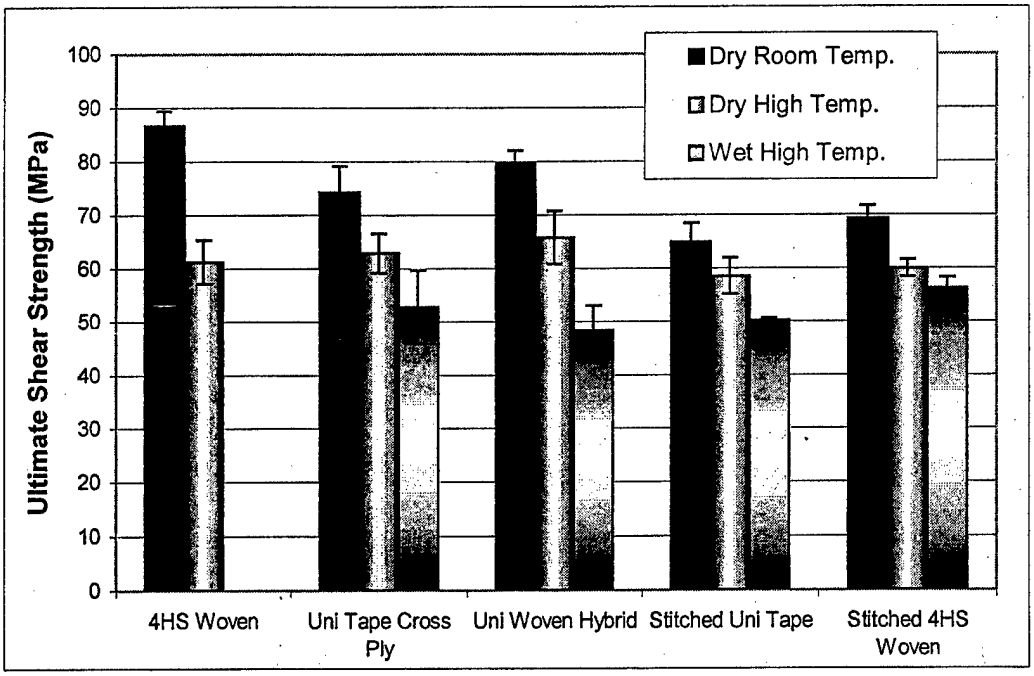

Figure 12. Comparison of the ultimate shear strength of the composites [28].

As an example, in Figure 12 the ultimate shear strength of the composites is compared to the onset of AE, dry at room temperature, dry at 315°C, and wet conditioned at 316°C, respectively. The complete description of the mechanical tests, SEM observations and the final results from this part of research can be found in [28].

3. Failure Predictions; Modeling of Micro- and Meso-Stresses

3.1 Micro- and meso stresses in unidirectional and 8HS T650-35/PMR-15 composites

In the macro-stress analysis of the Iosipescu shear and ±45° tensile specimens [2,9], the effect of composite manufacturing on the internal stress distributions was not considered. This was done however by performing the visco-elastic computations of both residual and applied stresses in the unidirectional and woven 8HS T650/PMR-15 composite on the meso- and micro-scales (Fig. 12) [13-20,22,23,25,27-29,31-35,38-40]. The composite manufacturing conditions, visco-elastic properties of the polyimide resin, orthotropic properties of the graphite fibers and composite architecture (weave type, fiber

distribution, etc.) were considered in the stress computations performed for a variety of in-plane biaxial loading conditions ranging from pure tension, biaxial tension along the warp and fill tows, biaxial tension and shear, and pure shear. The graphite fibers were assumed to be transversely isotropic with their longitudinal and transverse stiffness properties and coefficients of thermal expansions different. The polyimide matrix was modeled as a visco-elastic material with its stiffness properties changing with temperature and time (and with aging).

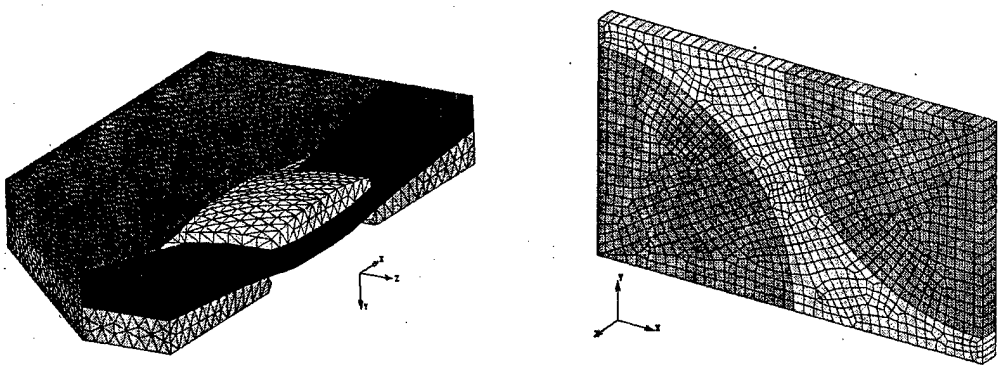

Figure 13. Finite element representations of the 8HS graphite/polyimide composite for the visco-elastic meso-stress (left) and micro-stress (right) analyses [13-20,22,23,25-29,31-35,38-40].

At first, the visco-elastic stress distributions and elastic properties in unidirectional graphite/polyimide composites as a function of the volume fraction of fibers have been determined [18,19]. The stress distributions were obtained by employing two different methods, namely the finite element method assuming either hexagonal or square fiber arrangements, and the Eshelby method modified by Mori and Tanaka to account for the presence of multiple fibers. It was shown that the Eshelby/Tanaka-Mori approach could be applied for the calculation of the stresses inside and outside the fibers provided the volume fraction of fibers does not substantially exceed either 35% (for the square fiber distributions) or 50% (for the hexagonal distribution) (Fig. 14a). The elastic constants of the unidirectional composite turned out to be less dependent on the orientation and the fibers' distribution. (Fig.14b). Therefore, the Eshelby/Mori – Tanaka approach was used to determine the stiffness properties of the densely packed tows in the graphite/polyimide composites [13-17,20,22,25-27-29,31-34,38-40].

The visco-elastic computations of the internal stresses on the meso- and micro-scales in the 8HS graphite (T650)/PMR-15 composite have shown that the local stress concentrations in the composite are very strongly dependent on the loading conditions (Table 3) [15,40]. Under biaxial loads consisting of biaxial tension applied in the direction of the warp and fill tows in addition to in-plane shear, there exist the largest principal stresses in the polyimide matrix at the fiber matrix interface. The meso-stress analysis has also shown that this type of biaxial loading creates the most favorable combination of meso- transverse and shear stresses for the initiation of transverse tow cracks in the composite. It has also been shown that for an accurate evaluation of stress distributions in the woven graphite/polyimide composites on both the meso- and micro-levels, the residual thermal stresses from composite manufacturing must be considered [14,15,40]. However, the proper simulation of internal stresses in the high temperature graphite polyimide composites subjected to any external loads in the presence of the residual stresses can only be accomplished if the visco-elastic properties of the polyimide resin are used.

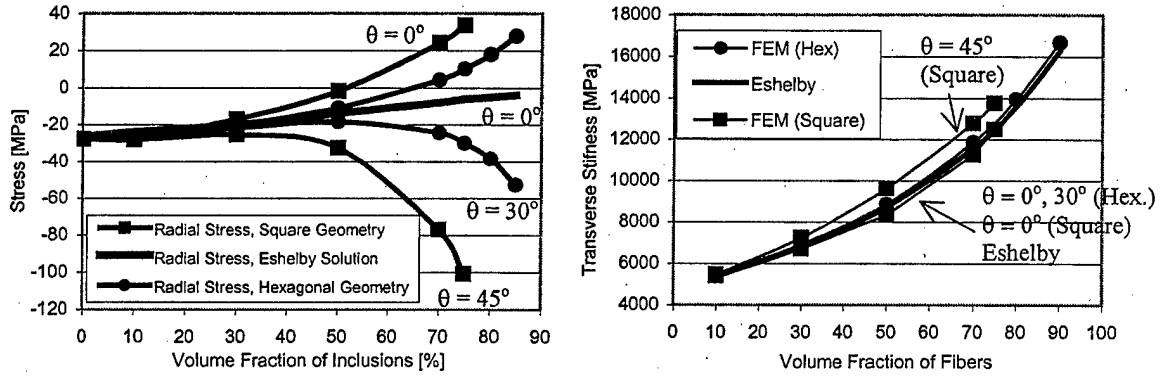

Figure 14. Finite element and analytical (visco-elastic Eshelby for multiple inclusions) results of the radial stresses in the matrix at the fiber/matrix interfaces (a, left), and the transverse stiffness (b, right) as a function of volume fractions in unidirectional T650/PMR-15 composites. The data in Figures 14a,b were determined for $\theta = 0°$ and $\theta = 45°$ (square fiber distribution) and $\theta = 0°$ and $\theta = °30°$ (hexagonal fiber distribution) [18,19].

Table 3. Meso- and micro-stresses in the center of the tow in the undulation region of 8HS T650/PMR-15 for various external in-plane loads at room temperature [15,40].

	Meso-stresses [MPa]				Micro-stresses [MPa]
Load case	σ_{XX} (transverse in-plane)	σ_{ZZ} (longitudinal in-plane)	σ_{YY} (transverse out of plane)	σ_{XZ} (in-plane shear)	Max. principal stresses in the matrix
Case 1 (ΔT only)	64	-119	18	-1	94
Case 2 (ΔT+TX)	79	-129	16	-1	107
Case 3 (ΔT+TZ)	68	145	20	-1	102
Case 4 (ΔT+S)	66	-98	19	108	208
Case 5 (ΔT+TX+TZ)	83	136	17	0	111
Case 6 (ΔT+TX+S)	81	-107	17	109	222
Case 7 (ΔT+TZ+S)	70	167	20	109	216
Case 8 (ΔT+TX+TZ+S)	85	158	18	110	230

(ΔT residual stresses only, TX(Y) applied in-plane tension along the tows, TZ transverse tension and S in-plane shear).

The stress data obtained from the micro- and meso-stress analyses agreed very well with the experimental strength results obtained by performing Iosipescu shear and ±45° tensile tests on the 8HS T650/PMR-15 composite at room and elevated temperatures [2-4,9,14]. Under almost pure in-plane shear (Iosipescu test), the shear stresses for the initiation of intralaminar damage and at the maximum loads were significantly higher than those from the case of biaxial tension and shear (±45° tensile test). This effect can be clearly seen in Table 1.

3.2 Failure prediction in 8HS T650-35/PMR-15 subjected to in-plane shear dominated loads at room and elevated temperatures,

Visco-elastic and elasto–plastic computations of micro- and meso-stresses in the 8HS T650-35 composite have been performed considering two external loading boundary conditions simulating either in-plane pure shear or in-plane biaxial tension in addition to shear [34,40]. An attempt was made to compare the critical loading conditions for the initiation of intralaminar damage in the composite subjected to the above two load cases at room temperature and at 315°C and to explain the damage initiation in the composite subjected to the Iosipescu and ±45° tensile tests.

Table 4. Maximum principal micro stresses at the initiation of damage in 8HS woven T650/PMR-15 composite [34,40].

	Micro Stress in the Resin [MPa]	
Test	±45°	Iosipescu
at RT	155 ± 9	200 ± 2
at 315°C	50 ±7	70 ±2

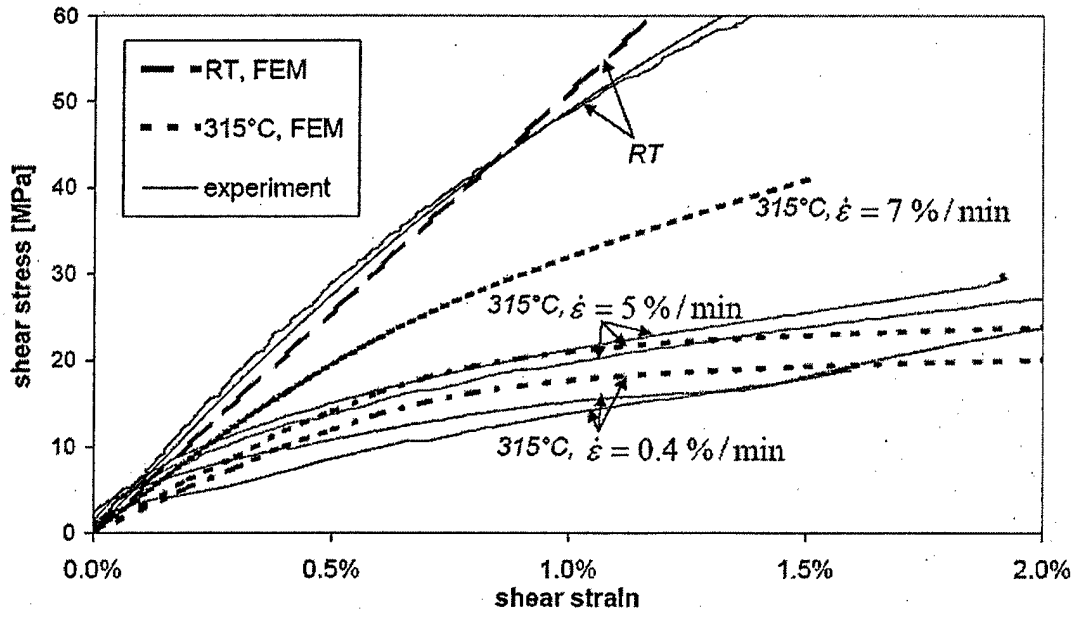

Figure 15. Macro response of unit-cell (predicted) and 8HS T650-35/PMR-15 composite (experimental) to biaxial load at room and elevated temperatures considering strain rate effect at 315°C [34,40].

The macro-response of the composite to the in-plane shear and biaxial loads (Fig. 15) was predicted at both temperatures and then validated by comparing it with the available experimental data [34,40]. The micro-stress calculations have shown (Table 4) that on the micro-scale, noticeably higher maximum principal stresses in the polyimide matrix in the vicinity of the graphite fibers were determined for the biaxial load case than in shear, both at room and high temperatures. It was shown that by using the numerical stress predictions, the experimentally observed differences can be explained in the initiation of tow micro-cracking in the woven composite subjected to the Iosipescu and ±45° tests at room and elevated temperatures.

3.3 Prediction of mechanical response of a unidirectional T650-35/PMR-15 composite as a function of temperature,

In this part if the project the mechanical response of a unidirectional T650-35/PMR-15 composite was analytically and numerically predicted as a function of temperature and subsequently compared [35,40] with the available experimental data from [1]. The Eshelby/Mori-Tanaka (E/M-T) method was used to predict the elastic properties of the composite whereas a finite element unit cell was employed to predict the stress vs. strain curves of the composite under elasto-plastic conditions. It was shown that for the temperature range from 25 to 315°C the predicted elastic properties of the composite agreed well with the experiment in the case of longitudinal and transverse (Fig. 16) Young's moduli. However, a significant discrepancy was noticed in the case of the longitudinal shear modulus. The comparisons for the transverse shear modulus and the longitudinal Poisson ratio were uncertain. The numerically predicted stress-strain curves of the composite agreed reasonably well with the experiment (Fig. 17) with the agreements between the model and the experiment depending on temperature and the type of loading [35,40].

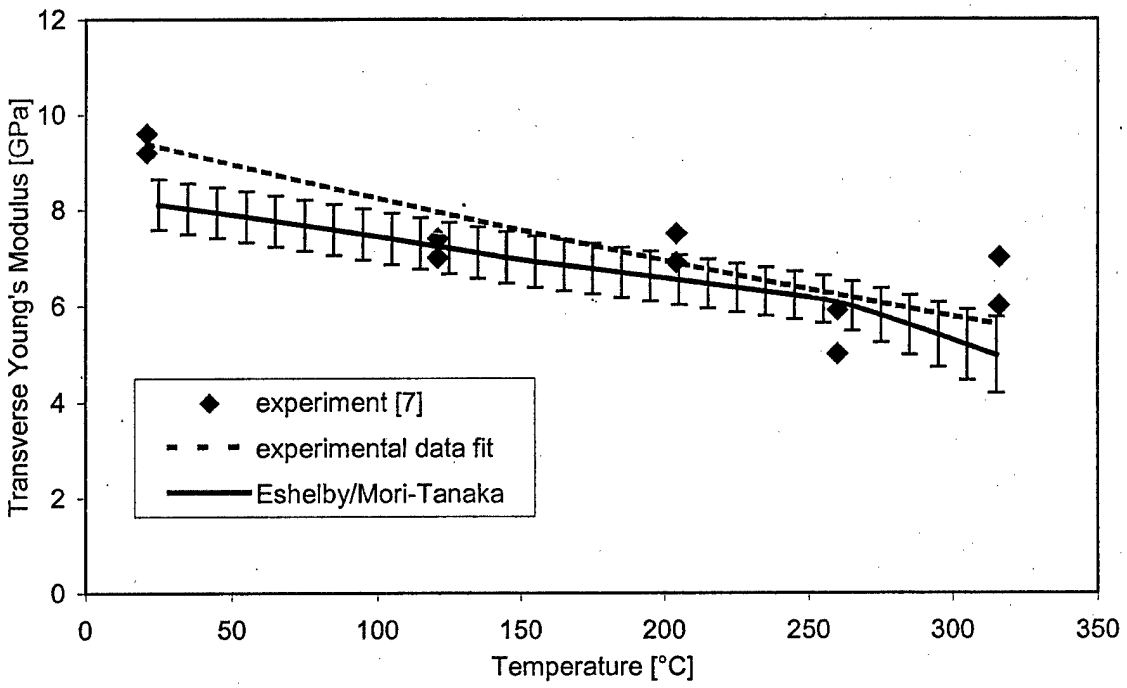

Figure16. Predicted and experimental transverse Young's modulus of unidirectional T650-35/PMR-15 as a function of temperature [35,40].

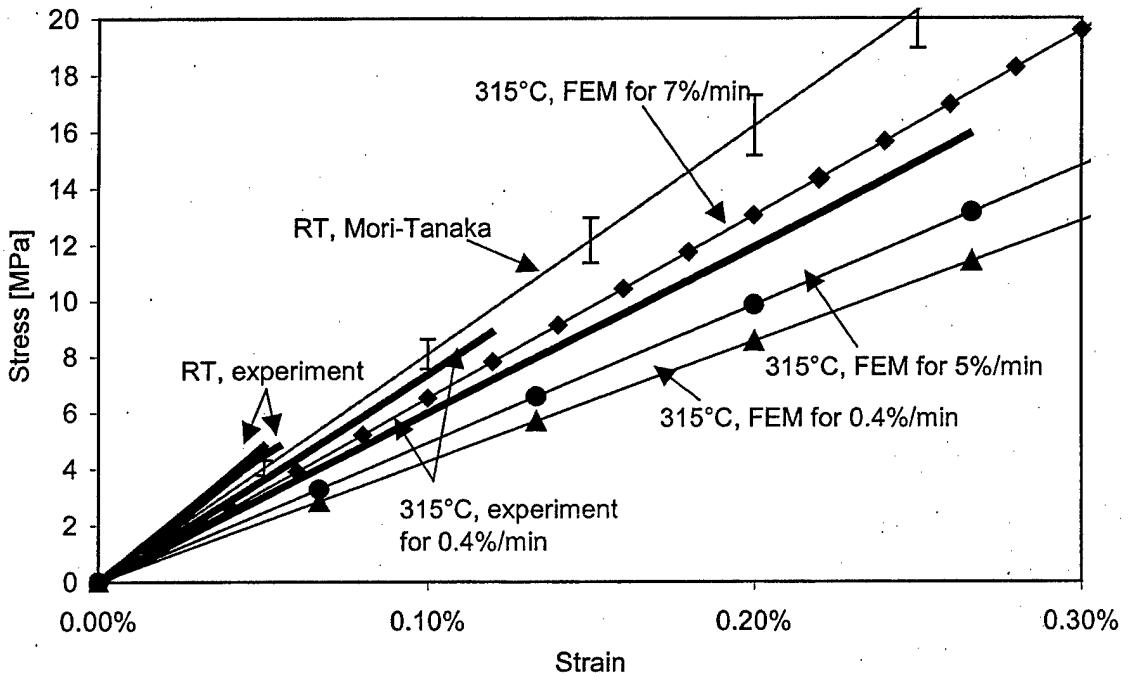

Figure 17. Predicted and experimental transverse stress vs. strain curves for unidirectional T650-35/PMR-15 at room temperature at 315°C for three different strain rates [35,40]. The data are shown for small transverse strains.

3.4 Predictions of residual stresses in unidirectional T650-35/PMR-15 as a function of aging in nitrogen.

The magnitude and distribution of residual aging stresses in a unidirectional T650-35/PMR-15 composite were also investigated [27,28]. First, a viscoelastic aging material model was developed by characterizing the isothermal aging strain and stress relaxation of neat PMR-15 polyimide. Then, the aging material model was applied to numerically evaluate the effect of matrix aging and cooling on the residual stress state of the unidirectional composite. It has been shown in this work that residual stresses in the composite are significantly affected by high temperature aging (Fig. 18). The magnitude of the residual stress in the composite caused by aging for one month at 315 °C was found to be comparable to the residual stress developed during cooling from 315°C to 25 °C.

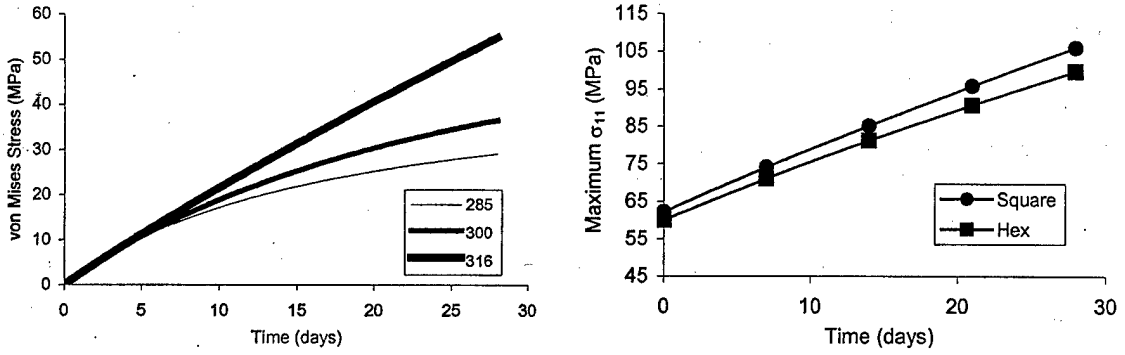

Figure 18. Comparisons of von Mises micro-stresses generated during aging at 285, 300 and 315°C (a, left) and of the first principle maximum stresses between the 70% V_f hexagonal and square models for aging at 315 °C with cooling (b, right) [27,28].

It was also shown in this work that reducing the isothermal aging temperature significantly affects aging strains and stresses [27,28]. Changing the isothermal aging temperature from 315 °C to 300 °C lowers the aging stress by as much as one third and from 315 °C to 288 °C by half. It was also found that aging maximum stresses between the square fiber array and the hexagonal fiber array were comparable. However, the stress distributions between architectures vary significantly. Although the maximum stresses are not significantly affected by fiber architecture, the volume fraction of fibers has a considerable effect on the aging and cooling stress.

3.5 Prediction of residual stresses and strength of 8HS T650-35/PMR-15 as a function of aging in nitrogen

The residual stresses in a woven 8HS T650-35/PMR-15 subjected to aging at 315°C in nitrogen have been determined using the finite element model of a woven unit-cell [38,40]. The aging stresses in the composite were predicted on a meso- scale for the aging times up to 1000 hours. In the simulations, the visco-elastic, age hardening and volumetric shrinkage effects were taken into account to describe the mechanical behavior of the polyimide resin at 315°C. The results from the stress calculations clearly showed that the internal stresses in the composite increased due to aging (Fig. 19). It was found, however, that the increase in the stresses was significantly reduced by stress relaxation. The model also showed that after 1000 hours the aging stresses in the composite were smaller than the thermal residual stresses caused just by cooling (Fig. 19). To verify the numerical model, the strength and stiffness of the composite was measured as a function of aging time [28]. It was observed that the numerical predictions agreed very well with the experimental results, which demonstrated no noticeable influence of aging on the strength and stiffness of the composite [38,40].

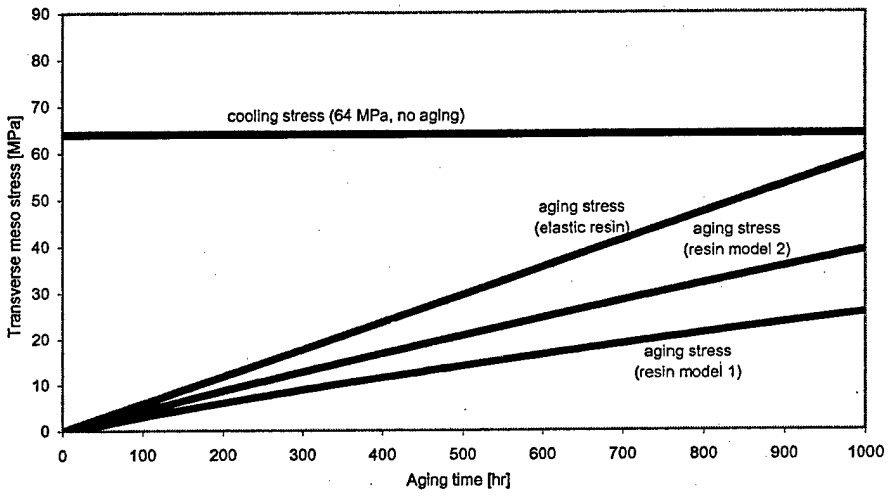

Figure 19. Transverse meso stresses in 8HS T650-35/PMR-15 as a function of aging in nitrogen at 315°C [38,40].

4. An Evaluation of Elastic Properties and Coefficients of Thermal Expansion of Graphite T650-35, M40J and M60J Fibers from Macroscopic Composite Input Data

A methodology has also been developed [25,31,32,33,40] for the evaluation of stiffness properties and temperature dependant coefficients of thermal expansion of continuous fibers from the macroscopic properties of either unidirectional or woven composites. It was used to measure the elastic properties and coefficients of thermal expansion of T650-35, M40J and M60J graphite fibers. The T650-35 fibers were embedded in a PMR-15 matrix, whereas the M40J and M60J fibers were embedded in a PMR-II-50 polyimide.

4.1 T650-35 fibers

At first, the new method was used to estimate the stiffness (Fig. 20) and thermal properties (Fig. 21) of T650-35 graphite fibers from the macroscopic input data of unidirectional and woven composites based on the same fibers embedded in a PMR-15 polyimide matrix [25,32,40]. The analysis was performed as a function of temperature and the fiber properties were determined from the composite properties in the temperature range from 20°C to 315°C. The macro-composite stiffness properties were measured by mechanical testing whereas the thermal properties of the composites were determined using a dilatometer. It was then followed by extraction of the fiber properties using the Eshelby/Mori-Tanaka model for unidirectional and finite element representative unit cells for woven systems under visco-elastic conditions.

It was shown that the temperature dependant coefficients of thermal expansion of the fibers could be estimated from the composite macro-data with significantly smaller errors than in the case of the elastic properties [25,32,40]. It was also shown that the errors in the evaluation of the elastic properties of the fibers from the macro unidirectional composite data could be significantly reduced if the fibers were placed in a stiff matrix material, much stiffer than the polyimide resin. The longitudinal and transverse coefficients of thermal expansions and the shear modulus of the T650-35 fibers determined from the unidirectional composite analysis were successfully verified in the

woven composite using the concept of a representative unit cell. This approach however could not be used to verify the transverse Young's modulus of the fibers.

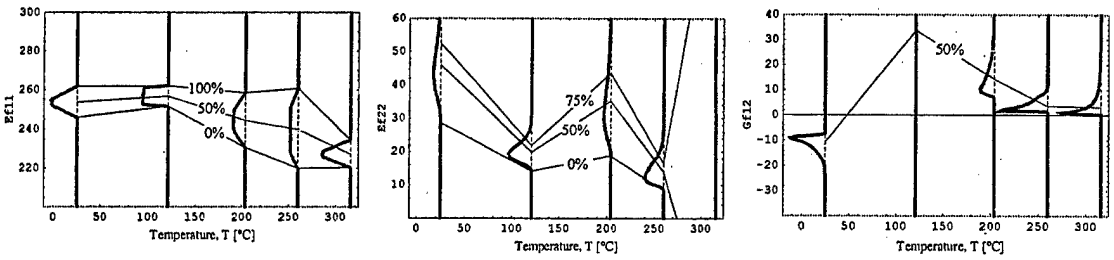

Figure 20. Probability distribution (thick lines) and cumulative distribution functions (thin lines) of calculated elastic properties of T650-35 fibers at five different temperatures; (a) longitudinal Young's modulus E_{f11} (left), transverse Young's modulus E_{f22} (middle), and longitudinal shear modulus G_{f12} (right) [25,32,40].

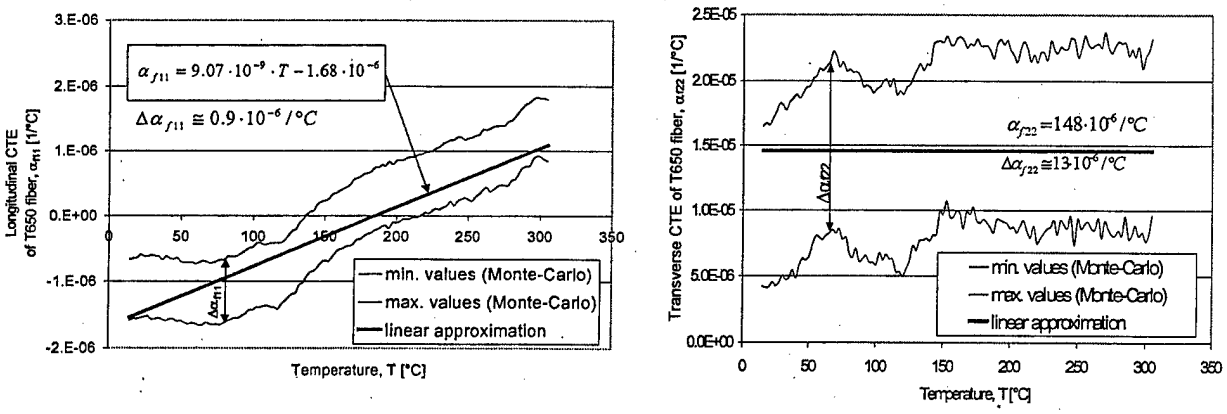

Figure 21. Longitudinal (a, left) and transverse (b, right) coefficients of thermal expansion of T650-35 graphite fibers from unidirectional composite macro-data [25,32,40].

4.2 T650-35, M40J and M60J fiber properties

In the second part of this research the three-component oscillator resonance method was employed to determine the room temperature elastic properties of the unidirectional and woven composites based on the T650-35, M40J and M60J fibers, and their neat resins [31,33,40]. Subsequently, the fiber properties were calculated (recalculated for the T650-35 fibers) from the unidirectional composite macro-data using the Eshelby/Mori-Tanaka

approach. For the woven composites, a finite element approach based on the concept of a representative volume element was employed to determine the elastic and thermal properties of the fibers.

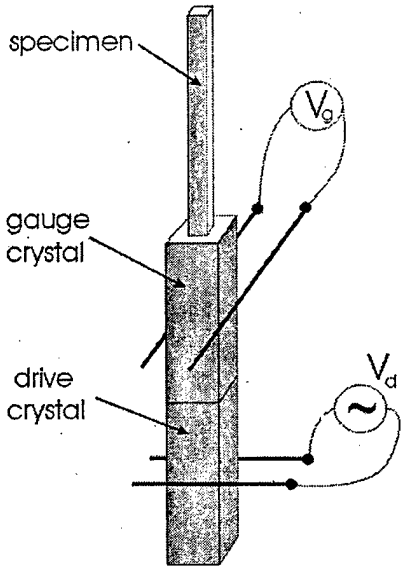

Figure 22. Schematic of three-component extensional oscillator [31,33,40].

Table 5. Elastic properties and thermal expansion coefficients of T650-35, M40J and M60J graphite fibers from different models [31,33,40].

Fiber	E_{fL} [GPa]	E_{fT} [GPa]	G_{fL} [GPa]	G_{fT} [GPa]	ν_{fL}	α_{fL} [10^{-6}/°C]	α_{fT} [10^{-6}/°C]	System	Models
T650-35	225 (±3)	15.4 (±0.7)	21.1 (±1.1)	5.8 (±0.4)	0.44 (±0.02)	-1.16 (±0.05)	13.5 (±1.1)	Uni.	Eshelby/ Mori-Tanaka
	224 (±3)	15.4 (±0.7)	-	-	-	-1.9 (±0.5)	12.9 (±1.5)	8HS	FE 8HS (slice)
	224 (±3)	15.4 (±0.7)	-	-	-	-1.9 (±0.7)	13.1 (±2.1)		FE 8HS (3D)
M40J	316 (±4)	13.4 (±3.7)	20.8 (±2)	3.9 (±0.1)	0.22 (±0.05)	-2.05 (±0.12)	6.9 (±6.3)	Uni.	Eshelby/ Mori-Tanaka
	344 (±2)	10.8 (±0.3)	-	-	-	-1.8 (±0.2)	8.8 (±1.7)	4HS	FE 4HS (slice)
M60J*)	500 (±2)	9.4 (±0.5)	-	-	-	-2.0 (±0.2)	18 (±4)	4HS	FE 4HS (slice)

*) It was assumed that for the M60J fiber G_{fL}= 20.8 ±10 GPa, G_{fT}=3.9 ±0.5 GPa and ν_{fL} =0.22 ±0.25.

In the case of the T650-35 fibers, both the longitudinal and transverse elastic and thermal properties of the fibers determined from the unidirectional and woven composites agreed very well with each other [31,33,40]. However, for the M40J fibers, noticeable differences were observed between the fiber properties determined from the unidirectional and woven system, which was attributed to the lack of transverse isotropy of the unidirectional system. Since the properties of the M60J fibers were evaluated only from the woven system, no direct comparison could be made between the properties obtained from the unidirectional and woven composite architectures. Overall, the methodology was shown to be highly applicable for the accurate determination of fiber properties from both unidirectional and woven systems [25,31,32,33,40].

5. Comparisons Between Unidirectional T650-35/PMR-15, M40J/PMR-II-50 and M60J/PMR-II-50 Aged in Nitrogen

The methodology developed in section 3.4, to predict the residual stress in the unidirectional T650/PMR-15 composite as a function of aging in nitrogen or aging with cooling [28], was subsequently used to predict the residual stress in the M40J/PMR-II-50 and M60J/PMR-II-50 composites as a function of aging with cooling. The material model for the PMR-II-50 matrix was also compared with the model used for the PMR-15 matrix [23,27,28,]. Shear relaxation mastercurves for PMR-II-50 at 371°C and for PMR-15 at 315°C are shown in Figure 23 for comparison.

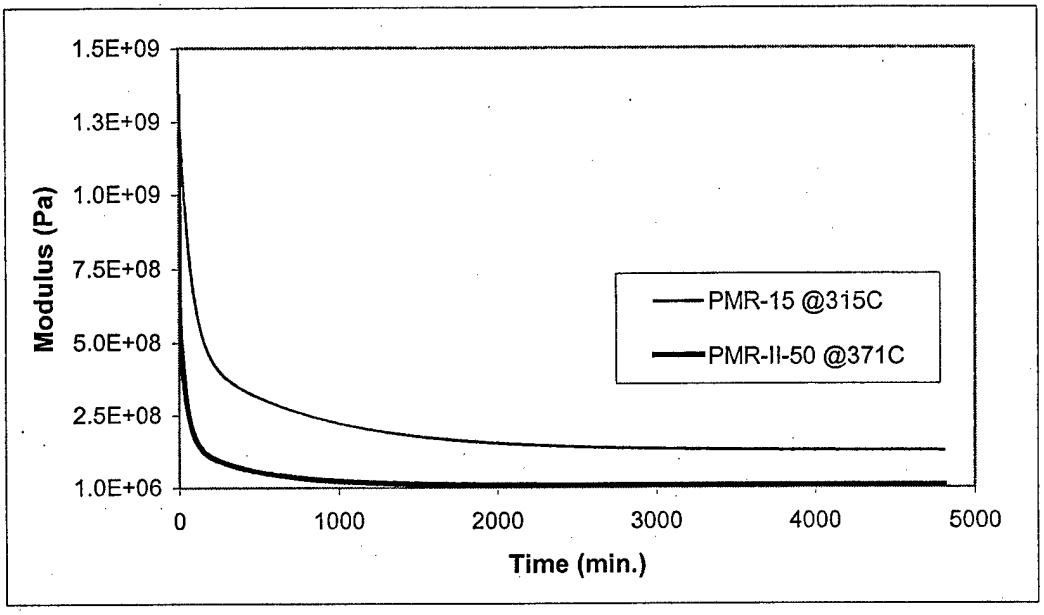

Figure 23. Comparison of shear relaxation mastercurves for the neat polymers PMR-II-50 at 371°C and PMR-15 at 315°C [28].

Figure 24 compares the predicted maximum first principle stresses in unidirectional M40J/PMR-II-50 and M60J/PMR-II-50 composites as a function of aging time at 315°C followed by cooling to 25°C. The analysis for the T650-35/PMR-15 composite aged at 316°C followed by cooling to 25°C is also included in Figure 24 [28].

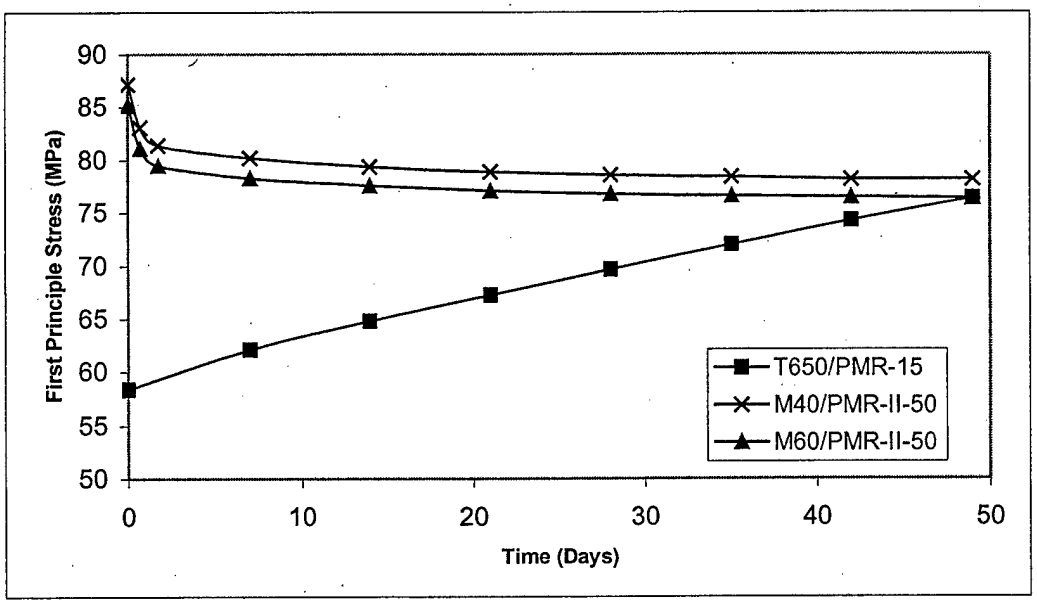

Figure 24. Comparison of the predicted maximum first principle stress as a function of aging time at 316°C for T650-35, M40J and M60J fiber woven composites [28].

Comparing the PMR-II-50 based composites to the PMR-15 based composite it can be seen from Figure 24 that the PMR-II-50 composites are unaffected by aging in N_2 at 316°C, in fact the stress from cooling from 371°C to 316°C is relaxed [28]. Contrary to the stress relaxing in the PMR-II-50 composites, the stress in the T650/PMR-15 composite increases with aging in nitrogen. Also the residual stresses formed during cooling from the postcuring temperatures for the PMR-II-50 composites and the PMR-15 composites is considerably different, approximately 28 MPa, this effect is from the 55°C difference in the processing temperatures between the PMR-II-50 and PMR-15 composites. In summary, the residual stress from cooling in the PMR-II-50 composites was approximately 30% higher than in the PMR-15 composite. Unexpectedly, the residual stress in the stiffer M60J fiber composite was slightly lower than that in the M40J lower modulus composite. It was also found that the PMR-II-50 is a better high temperature polymer, based on an activation energy/relaxation criteria [28].

6. Experimental Determination of Residual Stresses in Unidirectional and Woven Graphite Fiber/Polyimide Matrix Composite

A new methodology has been proposed [6-8,12,13,18,19,20,26,29,36] for the evaluation of interlaminar residual thermal stresses in unidirectional and woven polymer matrix composites based on XRD measurements of residual stresses in embedded crystalline inclusions in conjunction with the application of the visco-elastic Eshelby method for multiple inclusions. In the beginning of the project, two types of metallic inclusions were used, namely spherical aluminum (Al) and irregular silver (Ag) inclusions. The inclusions were distributed in the interlaminar regions of the composites between the first and second plies of the six ply unidirectional and four ply 8HS (Fig.25) composites. After the initial preliminary efforts, most of the XRD research in the subsequent years was conducted using the Al inclusions (Fig. 26).

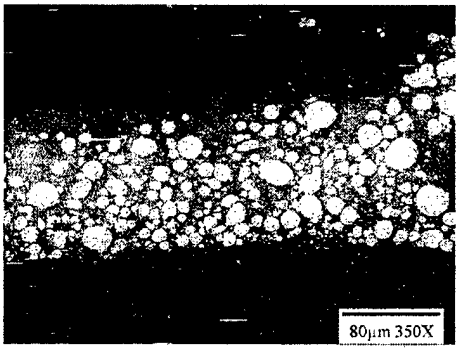

Fig. 25 Aluminum inclusions between 8HS plies in the graphite/PMR-15 composite [6,19].

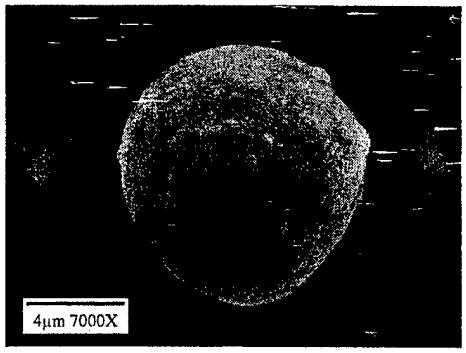

Fig. 26 Aluminum inclusion [6].

6.1 Residual interlaminar stresses as a function of bending

The method was used to determine residual interlaminar stresses in the unidirectional and 8HS T650-35/PMR-15 composites without and with externally applied bending loads (Fig. 27), and as a function of aging in nitrogen and in air.

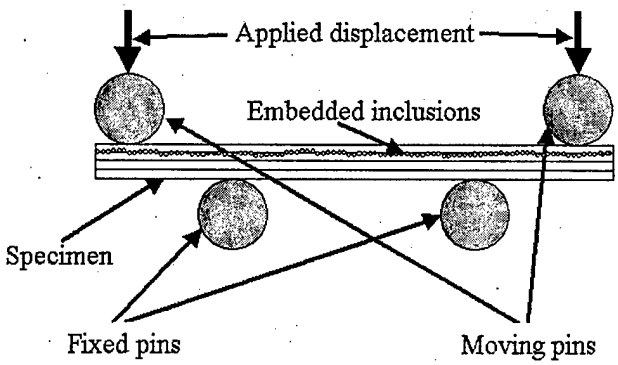

Fig. 27 X-ray four point bend tests; specimen configuration inside a four point bend fixture [7,19].

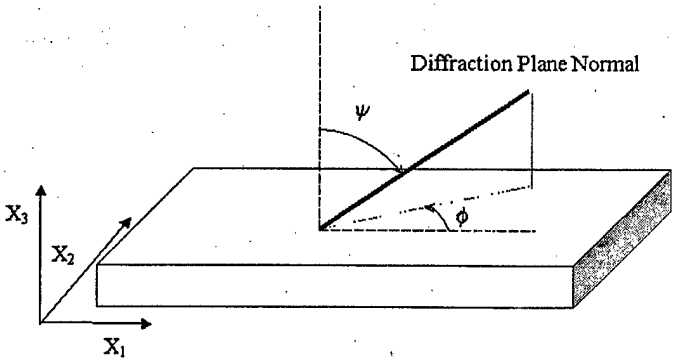

Fig. 28 The definition of angles ϕ and ψ with respect to the specimen coordinate system X_1, X_2 and X_3.

$$\varepsilon_{\phi=0,\psi} = \frac{d_{\phi=0,\psi} - d_0}{d_0} = (\varepsilon_{11} - \varepsilon_{33})\sin^2\psi + \varepsilon_{33} \qquad (1a)$$

$$\varepsilon_{\phi=90,\psi} = \frac{d_{\phi=90,\psi} - d_0}{d_0} = (\varepsilon_{22} - \varepsilon_{33})\sin^2\psi + \varepsilon_{33} \qquad (1b)$$

Using equations 1a and 1b the residual strains in the embedded particles can be determined. The definition of ϕ and ψ angles with respected to the specimen's coordinate system is shown in Figure 28. In equations 1a,b, d_o denotes the lattice spacing of either aluminum or silver for stress free inclusions and $d_{\phi,\psi}$ is the lattice spacing for the embedded inclusions. An example of the $\varepsilon_{\phi\psi}$ vs. $\sin^2\psi$ plot along with a straight least-squares line approximating the experiment is shown in Figure 29 whereas the residual stresses in the Al inclusions (experimental and numerical) as a function of bending are presented in Figure 30 [7,19].

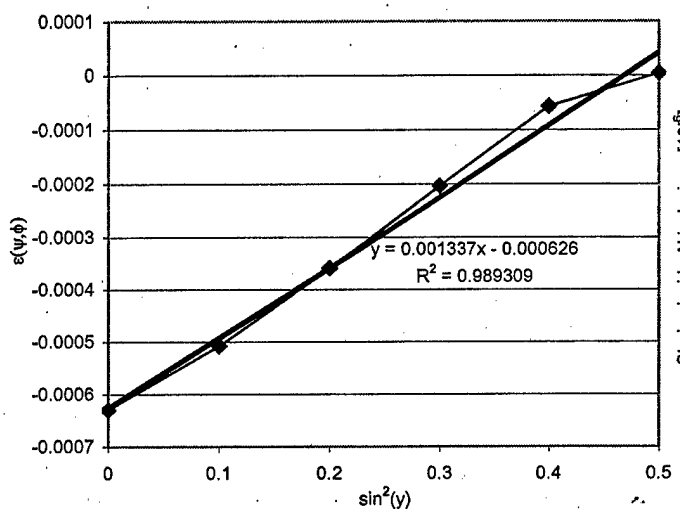

Fig. 29 An example of the $\sin^2\psi$ vs. $\varepsilon_{\phi\psi}$ plot [7,19].

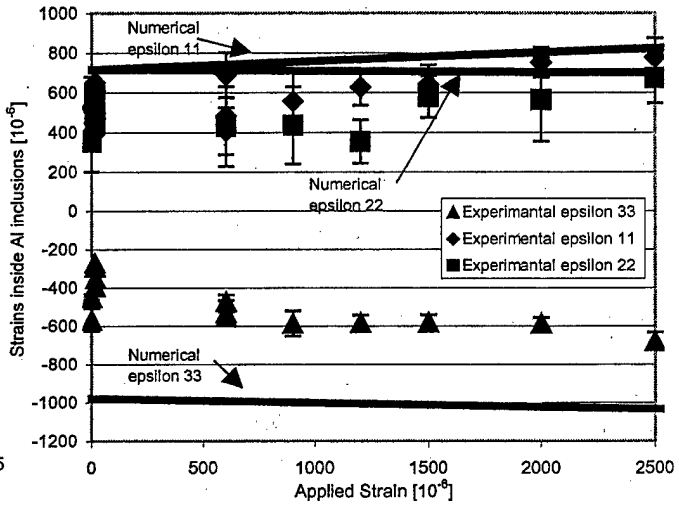

Fig. 30 X-ray and numerical strains inside Al inclusions as a function of applied strain [7,19].

The average interlaminar residual thermal stresses in the 8HS graphite/PMR-15 composite from the XRD measurements and the Eshelby model for multiple inclusions as well as from laminated plate theory with linear-elastic and visco-elastic assumptions are presented in Table 6 [13,19]. For comparison, the visco-elastic stresses in the unidirectional and woven graphite/PMR-15 systems are presented in Table 7 [13,10]. The data presented in Table 7 were obtained from the XRD tests performed with and without four-point bending.

Table 6. Interlaminar residual thermal stresses in the 8HS graphite/PMR-15 composite from XRD measurements and the Eshelby model for multiple inclusions as well as from laminated plate theory with linear-elastic and visco-elastic assumptions [13,19].

	X-Ray with Eshelby			Plate theory		
	σ_{11} [MPa]	σ_{22} [MPa]	σ_{33} [MPa]	σ_{11} [MPa]	σ_{22} [MPa]	σ_{33} [MPa]
Linear elastic	70.7± 17	71.1 ±17	36.7± 16	94	94	0
Visco-elastic	67.3 ±17	67.6 ±16	33 ±16	63.1	63.1	0

Table 7. Comparison between the interlaminar visco-elastic residual stresses in the unidirectional and woven (8HS) graphite/PMR-15 composites [13,19].

	Excluding bending			Including bending			
	σ_{11} [MPa]	σ_{22} [MPa]	σ_{33} [MPa]	σ_{11} [MPa]	σ_{22} [MPa]	σ_{33} [MPa]	Volume fraction of Al inclusions
Unidirectional	53.5± 9	39.6 ± 8	25 ± 5	55 ± 6	40.5 ± 5	26.6± 4	40 ±7%
8HS woven	67.3±17	67.6 ± 16	33 ± 16	62.3± 8	61.7 ± 8	27.6± 7	46 ±7.4%

It can be seen in Table 7 that the magnitudes of the interlaminar residual stresses along the fibers (σ_{11}, unidirectional) and along the tows ($\sigma_{11} = \sigma_{22}$, 8HS) in both the graphite/PMR-15 systems are high. The scatter in the XRD measurements is predominately caused by the non-uniform distribution of the particles and the non-uniform distribution of residual stresses in the composites. It should be strongly emphasized here that the accuracy of the entire analysis of the residual stresses is very strongly dependent on the physical properties of the investigated composite system. The temperature and time dependent physical properties of the composites and inclusions must be known for the accurate determination of the residual stresses either from laminate theory or from the XRD measurements of residual strains in the inclusions in conjunction with the Eshelby model. It has also been shown in this research there is a strong effect of inclusion type on the measured X-ray strains and stresses [6,19]. In

particular, the irregular silver inclusions significantly overestimated the residual stresses in the composites.

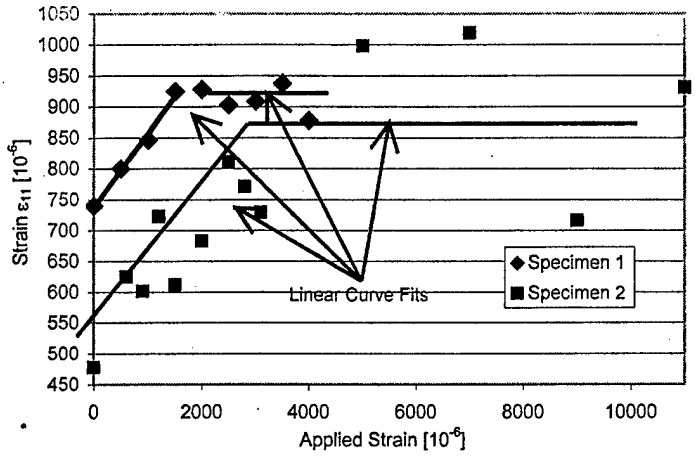

Figure 31. The ε_{11} strain components in Al particles as a function of bending strain in two unidirectional T650/PMR-15composite specimens [19,26].

The effect of large bending loads on strains and stresses inside aluminum particles embedded in the unidirectional and woven T650/PMR-15 composites has also been examined [19,26]. Under large four point bending loads, above certain critical loads, the normal stresses and strains in the Al particles no longer respond to an increase in the bending moments, reaching plateau values with increasing load (Fig. 31). This was attributed to the onset of plastic deformation of the inclusions. The plastic deformation of the Al particles in the case of the investigated graphite/PMR-15 composites was found to be beneficial [19,26]. It reduced the concentration of the normal stresses in the polymer matrix at the inclusion/matrix interface and thus reduced the possibility of interfacial fracture of the particles.

6.2 Effect of aging in air and in nitrogen

The unidirectional and woven graphite fiber T650-35)/PMR-15 composites with embedded aluminum inclusions were also investigated for their aging behavior either in nitrogen or air at 315°C for up to 1170 hours (Fig. 32) [19,29]. It was shown that the change of the thermal residual stresses in the composites subjected to aging could be

detected by measuring the state of stress in the embedded inclusions using XRD (Fig. 33).

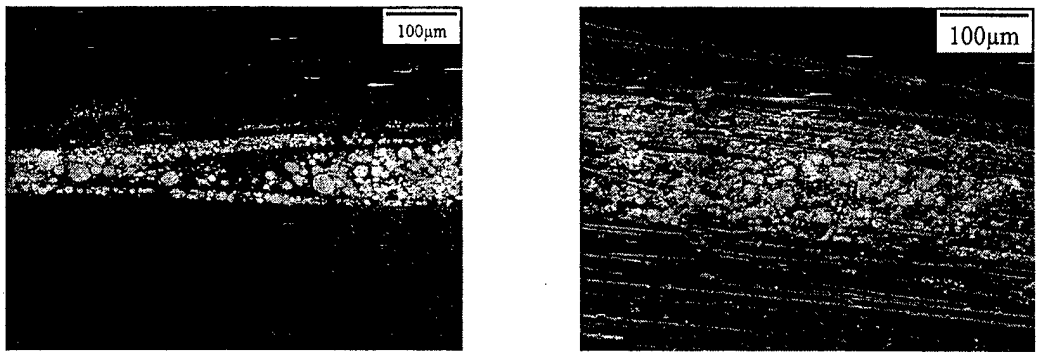

Figure 32. Unidirectional T650-35/PMR-15 system aged in nitrogen (a, left) and in air (b, right) for 1170 hours [19,29].

Subsequently, residual strains and stresses in the interlaminar regions of the composites were numerically estimated (Fig. 34) using the visco-elastic Eshelby/Mori-Tanaka method and classical lamination plate theory (CLPT).

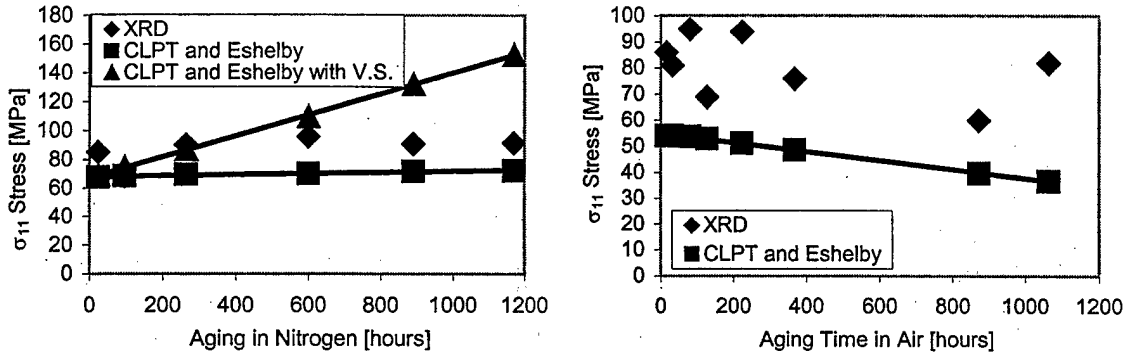

Figure 33. Residual σ_{11} stresses in Al inclusions embed in 8HS T650-35/PMR-15 aged in nitrogen (a, left) and in air (b, right) for 1170 hours [19,29].

It was shown in this project [19,29] that the residual strains and stresses in the inclusions as determined by XRD were noticeably affected by the aging conditions (Fig. 33). For the composite aged in nitrogen, good agreement was found between XRD and numerical

determinations of residual stresses in the inclusions and in the interlaminar matrix. However, for the composites aged in air, significant differences were observed between the experiment and the model. Large amounts of damage to the composites caused by oxidation and the volumetric shrinkage of the PMR-15 resin in air, which were not incorporated into the models, were responsible for the significant differences between the numerical predictions of the residual stresses and those determined from the XRD experiments.

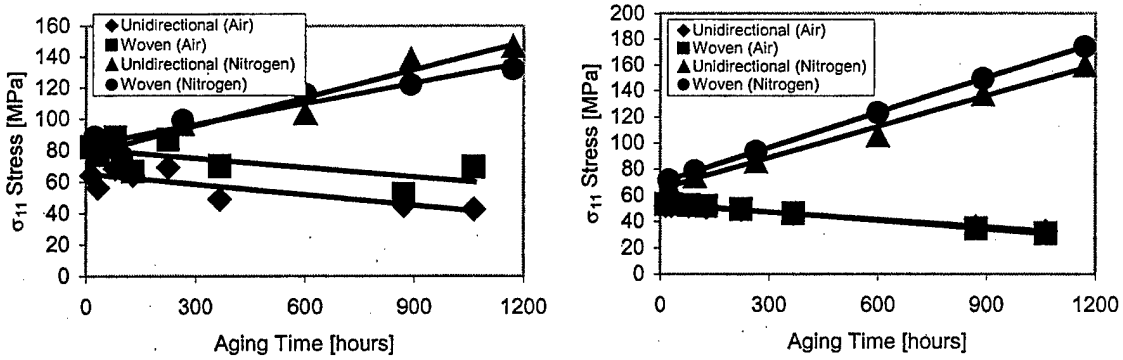

Figure 34. The σ_{11} interlaminar residual stresses in unidirectional and woven T650-35/PMR-15 composites aged in air and nitrogen calculated (a, left) from XRD using Eshelby/Mori-Tanaka method and (b, right) from CLPT [19,29].

6.3 Effects of inclusion volume fractions, their aspect ratios and their interactions on stress measurements

Finally, the effect of such factors as the volume fraction of inclusions (Fig. 35a), their aspect ratios (Fig. 35b) and the interaction between individual embedded inclusions (Table 8) on the accuracy of the XRD measurements were also evaluated in this study [19,36]. Despite several clearly identified disadvantages, the method can be recommended for the determination of residual stresses in polymer matrix composites with moderate to large residual stress concentrations, particularly with the use of higher intensity X-ray sources.

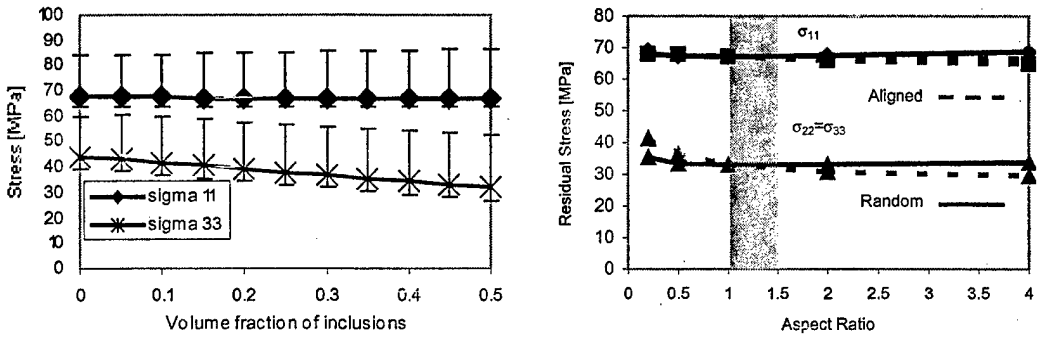

Figure 35. Residual stresses in 8HS T650-35/PMR-15 as a function of the volume fraction of embedded inclusions (a, left) and the aspect ratio of embedded Al inclusions (b, right) [19,36].

Table 8. Interlaminar stresses in 8HS T650-35/PMR-15 calculated as a function of the number of interacting inclusions and distribution patterns [36].

Number of inclusions	Random distribution			Simple cubic distribution			Eshelby/Mori-Tanaka		
	σ_{11} [MPa]	σ_{22} [MPa]	σ_{33} [MPa]	σ_{11} [MPa]	σ_{22} [MPa]	σ_{33} [MPa]	σ_{11} [MPa]	σ_{22} [MPa]	σ_{33} [MPa]
1	70.7	71.1	36.6	70.7	71.1	36.6	70.7	71.1	36.6
27	70.8	70.8	37.3	69.4	69.7	40.4			
125	70.6	70.9	38.1	69.2	69.3	41.1			

6.4 Thermal stress distributions in a composite reinforced with double spherical inclusions

A new method for the determination of thermal stress distributions around double inclusions embedded in an unbounded matrix due to a uniform temperature change was also developed [19] and used to explain the effect of surface oxidation of embedded Al inclusions on XRD stress measurements. As an example of the application of the

proposed model, thermal residual stresses in a composite reinforced with coated spherical inclusions were calculated in all three phases making up the composite. This was accomplished by combining the proposed analytical model with the Mori-Tanaka method to account for the presence of multiple inclusions. The effects of coating thickness and stiffness on the thermal residual stresses in the composite were evaluated. To validate the newly proposed analytical approach, the thermal residual stresses in the composite were also modeled by finite elements using the concept of a representative unit cell For a composite with 40% volume fraction of coated spherical inclusions, good agreements were found between the radial and tangential stresses calculated analytically and numerically (Fig. 36).

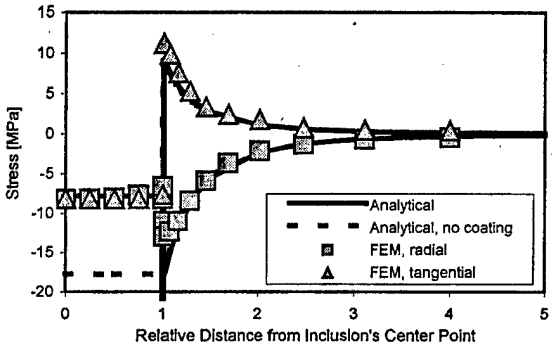

Figure 36a. Analytical and numerical thermal stress distributions around a single coated and a single uncoated spherical inclusion embedded in an unbounded matrix caused by $\Delta T = 100°C$ [19].

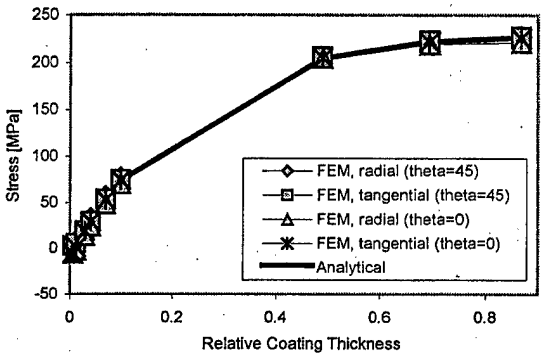

Figure 36b. Radial and tangential stress components inside a coated inclusion (at the interface) for 40% volume fraction of inclusions and a stiff coating [19].

Conclusions

In this project, a comprehensive combined numerical/experimental testing procedure has been developed for the determination of mechanical response of woven graphite/polyimide composites based on medium and high modulus graphite fibers subjected to either shear or biaxial shear dominated in-plane loads. The method was successfully used to determine the initiation of intralaminar damage and the shear strength of a woven 8HS T650/PMR-15 composite as a function of temperature and

aging. It was also used to investigate the mechanical response of M40J/PMR-II-50 with various fiber architectures and 4HS M60J/PMR-II-50 to shear at elevated temperatures. The experimental parts of this program were supported numerically by performing comprehensive macro-, meso- and micro-stress analyses of the composites under elasto-visco-plastic conditions. New techniques for measuring fiber properties from the macro-properties of their composites were also developed in this project and used to determine the properties of the fibers intended for the combustion chamber. It has been shown that the effect of residual thermal stresses on the prediction of intralaminar damage initiation in the high temperature polymer matrix composites must be considered. This effect can only be examined however, if the visco-elastic response of a polyimide matrix is considered in the meso- and micro-finite element computations. It has been shown that the initiation of intralaminar damage in the composites is very strongly dependent on the in-plane shear dominated loading conditions. It was also demonstrated in this research that the magnitudes and distributions of residual stresses in unidirectional and woven graphite fiber/polyimide composites aged in either nitrogen or air could be monitored experimentally by performing XRD measurements of residual strains in embedded metallic spherical inclusions. Most importantly, this research helped the NASA Glenn Research Center design, manufacture and successfully test the first polymer matrix composite based combustion chamber for the space shuttle applications.

References

(Complete List of Publications and Dissertations Based on F49620-00-1-0159)

1. Odegard, G. and Kumosa, M., Elastic-Plastic and Failure Properties of a Unidirectional Graphite/PMR-15 Composite at Room and Elevated Temperatures, Composites Science and Technology, Vol. 60, No. 16 (2000) pp. 2979-2988.

2. Odegard, G., Shear-Dominated Biaxial Failure Analysis of Polymer matrix Composites at Room and Elevated Temperatures, Ph.D. Thesis, Department of Engineering, University of Denver, Denver, Colorado, June 2000.

3. Odegard, G., Armentrout, D., Searles, K, Kumosa, L. and Kumosa, M., Failure Analysis of ±45° Off-Axis Woven Fabric Composite Specimens, Journal of Composites Technology & Research, Vol. 23, No. 3 (2001) pp. 205-224.

4. Kumosa, M., Predecki, P., Odegard, G., Searles, K., Benedikt, D., Armentrout, D., Kumosa, L., Gentz, M. and Sutter J.K., Analysis of Failure Mechanisms and Residual Stresses in Unidirectional and Woven Graphite/PMR-15 Composites Subjected to Shear Dominated Biaxial Loads, Proc. of High Temple Workshop XXI, Edit. DOD/NASA Laboratories and University of Dayton Research Institute, February 13- 15, 2001, Clearwater Beach, Florida, Z1- Z16.

5. Kumosa, M., Shear Dominated Failure Mechanisms in High Temperature Polymer Matrix Composites, Proc. of the 7th Summer School of Fracture Mechanics, Pokrzywna 18-22, June, 2001, Poland, Zeszyty Naukowe Politechniki Opolska, ISSN 1429-6055, pp. pp. 147-162.

6. Benedikt, B., Kumosa, M., Predecki, P.K., Kumosa, L. and Sutter, J.K., An Analysis of Residual Stresses in a Unidirectional Graphite/PMR-15 Composite Based on the X-Ray Diffraction Measurements, Composites Science and Technology, (2001), Vol. 61, No. 14 (2001) pp. 1977-1994.

7. Benedikt, B., Predecki, P., Kumosa, L., Armentrout, D., Sutter, J.K. and Kumosa, M., The use of X-ray Diffraction Measurements to Determine the Effect of Bending Loads on Internal Stresses in Aluminum Inclusions Embedded in a Unidirectional Carbon-Fiber/PMR-15 Composite, Composites Science and Technology, Vol. 61, No. 14 (2001) pp. 1995-2006.

8. Benedikt, B., Predecki, P.K., Kumosa, L. and Kumosa, M., Measurement of Residual Stresses in Polymer Matrix Fiber Reinforced Composites Based on X-Ray Diffraction, Advances in X-ray Analysis-Volume 45, Proceedings of the 50th Annual Conference on Applications of X-ray Analysis [Denver X-ray Conference], 30 July – 3 August 2001, Steamboat Springs, Colorado, USA ICDD 2002 ISSN 1097-002, pp. 218-224.

9. Kumosa, M., Odegard, G., Armentrout, D., Kumosa, L., Searles, K. and Sutter J.K., Comparison of the ±45° Off-Axis and Iosipescu Shear Tests for Woven Fabric Composite Materials, Journal of Composites Technology & Research, Vol. 24, (2002) pp. 3-16.

10. Searles, K., Odegard, G. and Kumosa, M., The Effect of Eccentric Loads on the Macroscopic Strain and Stress Distributions in Woven Fabric Iosipescu Specimens, J. Composite Materials, Vol. 36, No. 5 (2002) pp. 571-588.

11. Kumosa, M. P.K. Predecki, Armentrout, D., Benedikt, B., Rupnowski, P., Gentz, M., Kumosa, L., and Sutter, J.K., Fundamental Issues Regarding the High Temperature Failure Properties of Graphite/Polyimide Fabric Composites Subjected to Biaxial Shear Dominated Loads, in the Proceedings of the 22nd High Temple Workshop, Edit. DOD/NASA Laboratories and University of Dayton Research Institute, January 2002, Santa FR, New Mexico, pp. L.1-L.15.

12. Benedikt, B., Gentz, M., Kumosa, L., Predecki, P.K., Armentrout, D., KUMOSA, M. and Sutter, J.K., The Use of X-ray Diffraction Measurements to Determine the Effect of Aging on Residual Stresses in Unidirectional and Woven Graphite/Polyimide Composites, the 51st Annual Denver X-Ray Conference, Colorado Springs, August 2002, International Center for Diffraction Data, Advances in X-ray Analysis, Volume 46, pp. 112-118.

13. Benedikt, B., Rupnowski, P., Kumosa, L., Sutter J.K., Predecki, P.K. and Kumosa, M., Determination of Interlaminar Residual Thermal Stresses in a Woven 8HS Graphite/PMR-15 Composite using X-Ray Diffraction Measurements, Mechanics of Advanced Materials and Structures, Vol. 9 (2002) pp. 375-394.

14. Gentz, M. Armentrout, D., Rupnowski, P., Kumosa, L., Sutter, J.K., and Kumosa, M., Mechanical Behavior of a Woven Graphite/PMR-15 Composite at Room and Elevated Temperatures Determined from the ±45° Tensile and Iosipescu Shear Tests, Journal of Composites Technology & Research, Vol. 25, Issue 1 (2003) pp. 22-34.

15. Rupnowski, P. and Kumosa, M., Meso- and Micro-Stress Analyses in an 8HS Graphite/Polyimide Woven Composite Subjected to Biaxial In-Plane Loads at Room Temperature, Composites Science and Technology, Vol. 63, No. 6 (2003) pp. 785-799.

16. Kumosa, M. Gentz, M., Armentrout, D., Rupnowski, P., Kumosa, L., Shin, E. and Sutter, J.K., Analysis of Failure Mechanisms in Woven Graphite/Polyimide Composites with Medium and High Modulus Graphite Fibers Subjected to In-Plane Shear, Proceedings of the High Temple Workshop XXIII, Edit. DOD/NASA Laboratories and University of Dayton Research Institute, 10-13 February 2003, Jacksonville, Florida, pp. E1-E13.

17. Kumosa, M., Gentz, M., Rupnowski, P. Armentrout, D., Kumosa, L., Shin, E., and Sutter, J.K., Mechanical Behavior of Woven Graphite/Polyimide Composites with Medium and High Modulus Graphite Fibers Subjected to Biaxial Shear Dominated Loads, Proceedings of the 14th International Conference on Composite Materials (ICCM-14,) July 14-18, 2003, San Diego, California, 2003, paper #1493.

18. Benedikt, B., Rupnowski, P. and Kumosa, M., Visco-Elastic Stress Distributions and Elastic Properties in Unidirectional Composites with Large Volume Fractions of Fibers, Acta Materialia, Vol. 51, No. 12 (2003) pp. 3483-3493.

19. Benedikt, B., Analysis of Residual stresses in Graphite fiber/PMR-15 Composites, Ph.D. Thesis, Department of Engineering, University of Denver, Denver, Colorado, June 2003.

20. Kumosa, M., An Investigation of Damage Initiation in Woven Graphite Fiber/Polyimide Composites Subjected to Shear, 3rd International Conference on Fracture and Damage, 2-4 September 2003, Paderborn, Germany.

21. Eugene, E., Thesken J. C., Sutter, J. K., Chuang, K., Kumosa, M., et. al, Effects of Fiber Reinforcement Architecture on the Hydrothermal-Mechanical Performance of Polyimide Matrix Composites for Aeropropulsion Applications Proc. 14th International Conference on Composite Materials (ICCM-14.) July 14-18, 2003, San Diego, California, 2003, paper #1429.

22. Kumosa, M., An Investigation of Damage Initiation in Woven Graphite Fiber/Polyimide Composites Subjected to Shear, Key Engineering Materials, Vols. 251-252 (2003) pp. 447-456.

23. Gentz, M., Benedikt, B., Kumosa, M. and J. Sutter, Residual Stresses in Unidirectional Carbon Fiber/Polyimide Composites as a Function of Aging, Proc. 8th Japan International SAMPE Symposium, Nov. 18-21, 2003, pp. 565-568.

24. Gentz, M., Armentrout, D., Rupnowski, P., Kumosa, L. Shin, E., Sutter, J.K., and Kumosa, M., In-Plane Shear Testing of Woven Graphite/Polyimide Composites with Medium and High Modulus Graphite Fibers at Room and 316°C Temperatures, Composites Science and Technology, Vol. 64, No. 2 (2004) pp. 203-220.

25. Kumosa, M., Rupnowski, P., Gentz, M. and Sutter, J. K., An Evaluation of Elastic Properties and Coefficients of Thermal Expansion of Medium and High Modulus Graphite Fibers, High Temple Workshop XXIV, Sacramento, California, 2-5 February, 2004, pp. CC1-CC11.

26. Benedikt, B., Kumosa, M., Armentrout, D., Kumosa, L., Sutter, J.K., and Predecki, P.K., Analysis of Stresses in Aluminum Particles Embedded Inside Unidirectional and Woven Graphite/Polyimide Composites Subjected to Large Bending Loads, Mechanics of Advanced Materials and Structures, Vol. 11, Issue 1, (2004) pp. 31-49.

27. Gentz, M., Benedikt, B., J. K. Sutter, and Kumosa, M., Residual Stresses in Unidirectional Graphite Fiber/Polyimide Composites as a Function of Aging, Composites Science and Technology, Vol. 64 (2004) pp. 1671-1677.

28. Gentz, M., Mechanical Response of Graphite/Polyimide Composites at Elevated Temperatures, Ph.D. Thesis, Department of Engineering, University of Denver, Denver, Colorado, August 2004.

29. Benedikt, B., Gentz, M., Kumosa, L., Rupnowski, P., Sutter, J. K., Kumosa, M., X-ray Diffraction Experiments on Aged Graphite Fiber/Polyimide Composites

with Embedded Aluminum Inclusions, Composite Part A, Vol. 35 (2004) pp. 667-681.

30. Shin, E. E., Sutter, J., Bubnick, J., Thesken, J., and Kumosa, M., Property-Performance Assessment of Polymer Matrix Composites for Rapid Heat-up Aeropropulsion Applications, High Temple Workshop XXIV, Sacramento, California, 2-5 February, 2004, pp. M1- M18.

31. Rupnowski, P. and Kumosa, M., Determination of the Elastic and Thermal Properties of Graphite Fibers from the Unidirectional and Woven Composite Data, in the Proceedings of the Eleventh International Conference on Composites or Nano Engineering, August 8-14, 2004, Hilton-Head Island, South Carolina, USA.

32. Rupnowski, P., Gentz, M., Sutter, J. K. and Kumosa, M., An Evaluation of Elastic Properties and Coefficients of Thermal Expansion of Graphite Fibers from Macroscopic Composite Input Data, Proceedings of the Royal Society: Mathematical, Physical and Engineering Sciences, 10.1098/rspa.2004.1358.

33. Rupnowski, P., Gentz, M., Sutter, J. K. and Kumosa, M., An Evaluation of the Elastic Properties and Coefficients of Thermal Expansion of Medium and High Modulus Graphite Fibers, Composites Part A, Vol. 36 (2004) pp. 327-338.

34. Rupnowski, P., Gentz, M., Sutter, J. K., and Kumosa, M., Mechanical Response of a Woven Graphite/Polyimide Composites to in-Plane Shear Dominated Loads at Room and Elevated Temperatures, Acta Materialia, Vol. 52, No. 19 (2004) pp. 5603-5613.

35. Rupnowski, P., Gentz, M. and Kumosa, M., Mechanical Response of o Unidirectional Graphite Fiber/polyimide Composite as a function of Temperature, Composites Science and Technology, submitted in November 2004.

36. Benedikt, B., Kumosa, M. and Predecki, P. K., An Evaluation of Residual Stresses in Graphite/PMR-15 Composites by X-ray Diffraction, Acta Materialia, submitted in December 2004.

37. Kumosa, M. and Odegard, G. Unidirectional and Woven Composite Iosipescu Specimens Subjected to Biaxial Loads, Composites Part B, to be submitted in January 2005.

38. Rupnowski, P., Gentz, M, Benedikt, B, Sutter, J. K. and Kumosa, M., The Response of a Woven Graphite/Polyimide Composite to Aging in Nitrogen, Acta Materialia, to be submitted in January 2005.

39. Gentz, M., Rupnowski, P., Kumosa, M. and J. K. Sutter, Residual Stress in Unidirectional Graphite Fiber/PMR-II-50 Polyimide Composites Aged in Air and Nitrogen, High Temple 2005, Point Clear, Alabama, February 2005, submitted.

40. Rupnowski, P., Multi-Scale Damage Initiation Analysis in Woven Graphite Fiber/Polyimide Composites, Department of Engineering, University of Denver, Denver, Colorado, expected completion, Winter 2005.

Abstracts of Ph.D. Dissertations Completed in this Project

I. Shear-Dominated Biaxial Failure Analysis of Polymer Matrix Composites at Room and Elevated Temperatures" by Gregory Morris Odegard, Ph.D. Dissertation, Department of Engineering, University of Denver, Denver, completed June 2000.

This dissertation addresses the influence of shear-dominated biaxial stresses on the behavior of unidirectional and woven fabric polymer-matrix composites at room and elevated temperatures. The experimentally determined elastic-plastic properties of the various composite materials have been examined and applied to finite element analyses of shear-dominated biaxial tests: the standard Wyoming Iosipescu, biaxial Iosipescu, and off-axis tensile tests. The numerically determined internal stresses and strains have been used to study the failure behavior of the shear test specimens and the composite materials. It has been determined that while the Iosipescu test may be used to determine the shear modulus of unidirectional and woven-fabric composite and the interlaminar shear strength of woven-fabric composites, it is inadequate for the determination of intralaminar shear strength of unidirectional composites. Also, a series of off-axis tensile tests have been conducted on the unidirectional graphite/PMR-15 composite at room and various elevated temperatures. The elastic-plastic and failure properties have been determined for each temperature, and relations have been generated that describe the properties as a function of temperature.

II. "Analysis of Residual Stresses in Graphite Fiber/PMR-15 Composites" by Bartlomiej J. Benedikt, Ph.D. Dissertation, Department of Engineering, University of Denver, Denver, completed in June 2003.

This dissertation addresses the problem of determining the thermal residual stresses in unidirectional and woven graphite/PMR-15 composites from the aluminum inclusions embedded between the first and second plies of 6-ply unidirectional and 4-ply woven laminates. The stresses in the inclusions have been measured using X-ray Diffraction (XRD) from 422 aluminum reflections. The experimentally obtained values of the stress field in the embedded inclusions have been subsequently used to calculate the average thermal residual stresses in the composites. The visco-elastic Eshelby method has been used to obtain the residual stresses in the polymer matrix from the stresses in the embedded inclusions. The magnitudes of the thermal residual stresses calculated from the XRD experiments and the Eshelby method have been compared with the results given by the visco-elastic CLPT (inter-laminar model) and the Eshelby method (intra-laminar model). In order to further verify the obtained results, the composite specimens have been subjected to 4-point bending conditions. The total stresses and strains in the Al particles caused by the residual thermal stresses in the composite and the applied stresses generated by a four point bending fixture have been measured by XRD for different bending moments. It has been shown that for small bending displacements the stresses in the embedded inclusions were increasing linearly with the applied bending moment, however for large bending displacements the stresses in the embedded inclusions stabilized, which suggested that the embedded inclusions were deforming plastically. The proposed methodology was also used to investigate the effect of the matrix degradation on the thermal residual stresses. The unidirectional and woven composite specimens have been aged in air and nitrogen for 1064 hours and 1170 hours at 315°C, respectively. The residual thermal stresses in the embedded aluminum particles have been monitored during this experiment. In the last part of this dissertation, the effects of inclusions shape, distribution, and formation of an aluminum oxide film on a surface of the inclusions, on the calculated thermal residual stresses in the composites was investigated.

III. "Mechanical Response of Graphite/Polyimide Composites at Elevated Temperatures" by Mark Gentz, Department of Engineering, University of Denver, Denver, Colorado, August 2004.

In this research the in-plane Iosipescu shear test and the ± 45° biaxial shear test have been used to characterize the shear properties of woven T650-35/PMR-15, M60JB/PMR-II-50, and M40JB/PMR-II-50 composites at room temperature and 316°C. Along with the characterization of the woven composites, the shear properties of five other fiber architectures, including out of plane stitching, using the M40JB fiber and PMR-II-50 matrix have been investigated and compared with the baseline four harness woven M40JB/PMR-II-50 composite at room temperature and at 316°C. For each of these composites an indication of their residual stress state has been determined using an acoustic emission criterion as the onset of the initiation of damage. The ± 45° biaxial shear test along with acoustic emission has also been used to determine if the residual stress state of a T650-35/PMR-15 composite changes as a function of isothermal aging time in a 316°C nitrogen environment. Time and temperature models of the combined dilatational and deviatoric response of the neat resin matrix materials have been developed. These material models have been used numerically with the idealized geometry of two dimensional unidirectional composites. It was determined experimentally that the ultimate shear strength of the eight harness T650-35/PMR-15 is greater at room and high temperature, as determined by the Iosipescu shear test versus the ± 45° test. However, the moduli determined by both tests compare well. The ultimate shear strength determined by the ± 45° test is also noticeably dependant on the specimen width. From experiment it was determined that the ultimate shear strength for the M60JB/PMR-II-50, M40JB/PMR-II-50, and T650-35/PMR-15 composites is a function of the strain to failure of the fibers. It has been found from experimental analysis that the residual stress level in the woven M60JB/PMR-II-50 and M40JB/PMR-II-50 is greater than in the T650-35/PMR-15 composite which agreed with the observations made by modeling the unidirectional composites. Also, it was numerically determined that the unidirectional M60JB/PMR-II-50 and M40JB/PMR-II-50 composites were unaffected by

aging in N_2 at 316°C and slightly affected the T650-35/PMR-15 aged under the same conditions.

IV. **"Multiscale Stress and Damage Initiation Analyses in Graphite/Polyimide Composites" by Przemyslaw Rupnowski, Ph.D. Dissertation, Department of Engineering, University of Denver, in preparation, expected completion March 2005.**

PERSONNEL SUPPORTED

Four graduate Ph.D. students were involved in this project between February 2000 and November 2004, namely Dr. G. Odegard, Dr. B. Benedikt, Dr. M. Gentz and Mr. P. Rupnowski. These four students of the Materials Science graduate program in the Department of Engineering at the University of Denver were supervised by Dr. M. Kumosa.

Dr. G. Odegard graduated in June 2000 with a Ph.D. in Materials Science at DU and was hired by the NASA Langley Research Center where he worked in the subsequent four years with Dr. T. Gates in his composite group. Dr. B. Benedikt graduated in June 2003 also with a Ph.D. in Materials Science from DU. He was immediately hired by the Las Alamos National Laboratory where he is presently employed by their Weapon response Group (ESA-WR) as a Postdoctoral Research Associate. Dr. M. Gentz graduated in August 2004 with a Ph.D. and is presently employed by DU as a Research Assistant Professor. Mr. P. Rupnowski is presently finishing his Ph.D. research. He should be able to defend his doctoral thesis in the Winter/Spring of 2005.

In addition, Dr. P. K. Predecki, Professor Emeritus, Dr. D. Armentrout, Research Assistant Professor, and Mr. Lucas Kumosa, Research Scientist, were also involved in this project. Their primary responsibilities were: mechanical testing of composites and measurement of acoustic emission (D. Armentrout) and SEM analysis and strain gage

application (L. Kumosa) whereas Professor Predecki was helping Dr. Kumosa supervising the graduate students.

INTERACTIONS/TRANSITIONS

This study was performed in very close collaboration with the NASA Glenn Research Center. A major portion of the entire funding came from NASA to support research activities in this program. The composite materials investigated in the project were manufactured and supplied by NASA. The NASA Glenn Research Center also performed several quality control tests on the materials investigated in this study. We are especially grateful to Dr. J. Sutter and Dr. E. Shin of NASA Glenn for their very strong support of this study. In addition we have interacted with several companies involved in the combustion chamber project run by NASA Glenn. The statement below was issued by NASA Glenn in March 2004.

"A lightweight high temperature polymer matrix composite (HTPMC) combustor support chamber for a Rocket Based Combined Cycle engine successfully survived hot-fire testing at ATK-GASL. This testing concludes a three year collaboration between NASA Glenn and Boeing to design, fabricate and test the support structure and fulfills a GPRA (Government Performance Reform Act) milestone for the UEET (Ultra-efficient Engine Program). The support structure was prepared from a high temperature composite material, PMR-II-50. In addition to satisfying an important technical milestone, this activity is noteworthy because it constitutes a number of 'firsts.' This is the first application for Rocketdyne of a high temperature polymer matrix composite in a space propulsion component. Successful completion of this test will enable Rocketdyne to explore other applications for HT PMCs in their engines. It is also the first time that a full-scale PMC structure has been tested at GASL. Experience gained from this testing will enable GASL to more easily test similar structures. In addition to Rocketdyne, this effort involved the participation of twenty-four companies (component designers, fabricators, resin/materials suppliers, etc.), universities (U of Dayton Research Institute, **U of Denver**), and the Air Force Materials Lab. This effort utilized GRC expertise and facilities in the Life Prediction (5920), Structural Mechanics and Dynamics (5930) Branches, and Engineering and Technical Services Directorate. This project was supported by the former HOTPC program and is currently funded by UEET-Highly Loaded Light Weight Compressors and Turbines." [NASA Glenn]"

According to Dr. Sutter of NASA Glenn, the chamber (below) survived 5 days of testing wherein multiple tests "conditioned" this structure with 4000 deg F air and repeated

internal pressuring that simulated the RBCC component.

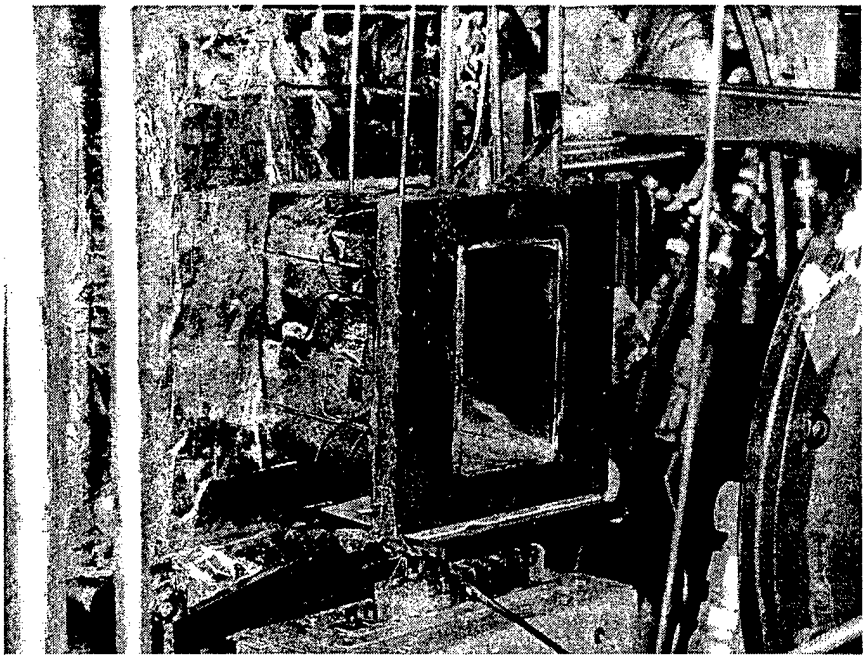

Letter From Dr. J. K. Sutter to Dr. M. Kumosa

December 13, 2004

RPM/5150

Dr. Maciej Kumosa
University of Denver
Department of Engineering
Denver, Colorado 80210

Dear Maciek,

I wanted to let you know how much I appreciated all your help over the past five years. You and your group have demonstrated an exceptional ability to adapt your research on our high temperature polymer composite systems. But it is not just your ability to change focus, your relentless desire to precisely know how these materials behave has led to several poignant discoveries on these polymer systems that are inordinately difficult to characterize and subsequently understand. As I reflect on your groups' contributions, here are a few of the highlights that I take away from your research:

- Diligently examining and refining tests led to a better understand biaxial stress states in high temperature composites. Despite many years of research you performed earlier in your career on Iosipescu shear tests, you were willing to re-examine that research by performing a thorough comparison of this test with other methods (± 45 degree off-

axis). Your critical evaluation of these two test methods led you to reconsider conclusions derived from your earlier work. That level of integrity in your research convinced me that collaborating with you on future projects would be an honest affair. Ultimately, this research provided a clear understanding of the residual stresses that high temperature polymer composites retain after processing. This knowledge will go a long way in developing reliable light-weight components for both space and military applications.

- Collaborative efforts with co-workers such as Dr. Predecki (University of Denver) were invaluable in our research geared towards embedding particulates with a composite structure. The lifetime differences you discovered in aging HT polymer composites in air versus nitrogen are now, for the first time, accounted for in models that no longer contain conflicts when predicting residual stresses. That contribution is multi-faceted. This work significantly contributes to our current applications for carbon fiber PMR-15 composites but also to future high temperature applications—perhaps even those that require coatings for thermo-oxidative and erosion protection.
- Development of an understanding of the transverse coefficient of thermal expansion for Toray's M carbon fibers led to our selection of the best combination of fiber and resin for the successful hot-fire testing of a hypersonic engine containing a lightweight polymer matrix composite component at ATK-General Applied Science Laboratory (GASL). In addition to satisfying an important technical milestone, this activity is noteworthy because it constitutes a number of "firsts." This is the first application for Boeing Rocketdyne of a HTPMC in a space propulsion component. It is also the first time that a full-scale Polymer Matrix Composite (PMC) structure has been tested at GASL. Your contribution to this project enabled our team towards a robust component design which demanded that the composite structure remain dimensionally stable despite an incredible rapid increase in temperature during the hot-fire rocket engine testing. In addition to Boeing, this effort involved the participation of twenty four companies (component designers, fabricators, resin/materials suppliers), as well as the Air Force Materials Lab (AFML). Therefore, you and the University of Denver received extensive exposure to many of the leaders in our aerospace industry—certainly those intimate with its composites industry.

Finally and on a personal note, I'd like to congratulate you on your ability to successfully motivate your undergraduate and graduate students. On several occasions, I've spoken with many of your students. They have gained your relentless trait to fully understand a complex problem. That will serve them well in their future efforts regardless if in science, engineering or their personal lives. Again thank you and I look forward to working with you in the future.

James K. Sutter, Ph.D.
Project Manager for High Temperature Polymer Matrix Composites
Materials Division

P.S. NASA code of ethics prohibits us from using NASA letterhead for letter of this nature.

Attachments

(selected journal publications published or submitted for publication in the last six months of the project)

Available online at www.sciencedirect.com
SCIENCE DIRECT®
Composites Science and Technology 64 (2004) 1671–1677
COMPOSITES SCIENCE AND TECHNOLOGY
www.elsevier.com/locate/compscitech

Residual stresses in unidirectional graphite fiber/polyimide composites as a function of aging

M. Gentz, B. Benedikt, J.K. Sutter [1], M. Kumosa *

Center for Advanced Materials and Structures, Department of Engineering, University of Denver, 2390 South York Street, Denver, CO 80208-3807, USA

Received 21 August 2003; accepted 2 December 2003
Available online 10 February 2004

Abstract

In this research, the magnitude and distribution of residual aging stresses in unidirectional graphite fiber/polyimide composites were investigated. First, a viscoelastic aging material model was developed by characterizing the isothermal aging strain and stress relaxation of neat PMR-15 polyimide. Then, the aging material model was applied to numerically evaluate the effect of matrix aging and cooling on the residual stress state of a unidirectional graphite fiber (T-650)/polyimide (PMR-15) composite. It has been shown in this work that residual stresses in the composite are significantly affected by high temperature aging. Most importantly, the magnitude of the residual stress caused by aging in N_2 at 316 °C for one month was found to be comparable to the cooling stress in the composite.
© 2004 Elsevier Ltd. All rights reserved.

Keywords: Unidirectional composites; C. Residual stresses

1. Introduction and background

Residual stresses in high temperature polymer matrix composites occur not only from the differences in the thermal expansions of the fiber and matrix materials [1], but also from the reduction in volume of the matrix material at high temperatures. For PMR-15 polyimide/carbon fiber composites the structural changes at high temperatures are due to physical and chemical aging as well as thermal degradation of the glass forming matrix material [2–4]. Aging and cooling residual stresses in woven polyimide matrix carbon fiber composites may be high enough to create transverse tow micro-cracks [5]. Examples of such micro-cracks are shown in Figs. 1(a) and (b). To determine the residual stress state in a composite structure manufactured with high temperature polyimides the physical properties of the polyimide as functions of time, temperature, physical aging, chemical aging, and thermal degradation are required. The analysis may be simplified, however, by measurement of the polyimide properties in an inert atmosphere. This is done to restrict the changes in the polyimide to physical aging and cross-linking. Contrary to polyimide resins, which will undergo significant changes in their physical properties with time and temperature, the properties of the carbon fibers are stable at elevated temperatures relative to the polyimide [2–4].

The isothermal stress relaxation response for a continuously aging material may be modeled by the Kohlrausch function [6]

$$\frac{G(t)}{G(0)} = e^{(-t/\tau_s)^{\beta_s}}, \tag{1}$$

where $G(0)$ is the shear modulus at $t = 0$, τ_s is a shear stress relaxation time constant, and β_s is a shear stress relaxation fractional exponent between 0 and 1. Similarly, isothermal length relaxation for a continuously aging material may be modeled by

* Corresponding author. Tel.: +1-303-871-3807; fax: +1-303-871-4450.
E-mail address: mkumosa@du.edu (M. Kumosa).
[1] Present address: NASA Glenn Research Center at Lewis Field, 21000 Brookpark Road, Cleveland, OH 44135, USA.

0266-3538/$ - see front matter © 2004 Elsevier Ltd. All rights reserved.
doi:10.1016/j.compscitech.2003.12.006

$$\frac{L(t)}{L(0)} = e^{(-t/\tau_l)^{\beta_l}}, \quad (2)$$

with the initial length $L(0)$, τ_l the length relaxation time constant, and β_l a length relaxation fractional exponent between 0 and 1. Then, if β_s and β_l are constant for the isothermal relaxations at different temperatures, the activation energy for each process, shear and length relaxation, may be determined. Linearizing the Arrhenius equation with ΔH the activation energy and R the gas constant and plotting $\ln \tau$ determined from Eqs. (1) and (2) vs. $1/T$ for each isothermal process yields the activation energy for shear and length relaxation in a neat polymer

$$\ln \tau = -\frac{\Delta H}{RT} + \ln \tau_0. \quad (3)$$

If the activation energy for each process is the same it may be used as a common shift function, A, with T_r the reference temperature

$$A = \frac{\Delta H}{RT}\left(\frac{1}{T_r} - \frac{1}{T(t)}\right). \quad (4)$$

The reduced time (ξ) is defined as [7]

$$\xi = \int_0^t e^A \, dt'. \quad (5)$$

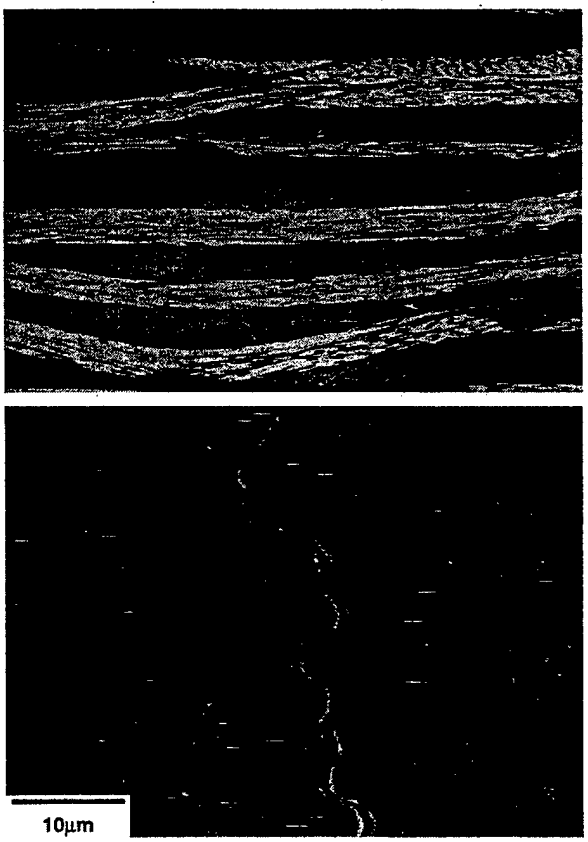

Fig. 1. Transverse tow micro-cracks in a woven graphite fiber polyimide composite [5]. Individual tow micro-crack from (a) [5].

In this manner, a reference mastercurve for each process may be used at all temperatures. The use of a thermorheological simple model for the shear relaxation response of a constant aging material and a thermostructural simple model for constant aging length relaxation enables the reduction of the effect of temperature with constant aging on shear and length relaxation into the time domain. Then, a material model may be combined with the structure's geometry in a finite element model to determine the state of stress as a function of time and temperature during constant aging using Eq. (6) [8]

$$\sigma(\xi) = \int_0^\xi G(\xi - \xi')\frac{d\tau}{d\xi'} d\xi' + \int_0^\xi K(\xi - \xi')\frac{d\Delta}{d\xi'} d\xi'. \quad (6)$$

In Eq. (6), G is the shear modulus, K is the bulk modulus, τ is the shear strain and is the volumetric strain.

2. Experimental procedures and results

A Netzsch 402C dilatometer was used to determine the isothermal aging strain of neat PMR-15 polyimide. Postcured neat PMR-15 polyimide supplied by NASA Glenn was cut into specimens approximately 10×5×4 mm. Prior to dilatometry, the specimens were dried in a vacuum desiccator at 110 °C for 24 h. The specimens were loaded into the dilatometer, the dilatometer was evacuated and backfilled with N_2. The temperature of the specimen was ramped from 25 to 365 °C at 5 °C/min held at 365 °C for 15 min and then cooled at 10 °C/min to the test temperature. The specimen was then held at the isothermal test temperature for up to four weeks. Data was collected at a rate of five samples per minute for the first hour followed by one sample per minute for the remainder of the test.

The length relaxation data was fitted using the normalized Kohlrausch function, Eq. (2), with a constant β_l of 0.50. Using the same approach, the shear relaxation data of Roberts et al. [9] was fitted using the normalized Kohlrausch function, Eq. (1), with β_s a constant 0.35. The τ_ls for the length relaxation and τ_ss for the shear relaxation were used in Eq. (3) to determine the activation energy for thermostructural and thermorheological simplicity of neat PMR-15.

Fig. 2 shows the energy rate determined from the length relaxation as well as from the shear stress relaxation. The activation energies for the length and shear relaxations were determined to be within two percent of each other. The average activation energy divided by the gas constant for the two processes, $\Delta H/R = 34016$, was used in Eq. (4) for a common shift function. An illustration of the fitted and normalized non-equilibrium aging curves from isothermal length dilatometery on PMR-15 is shown in Fig. 3. In Fig. 4 the curves from Fig. 3 are mastercurved to 316 °C using Eq. (5).

Since no long-term continuous aging shear relaxation data for neat PMR-15 is presently available, the shear

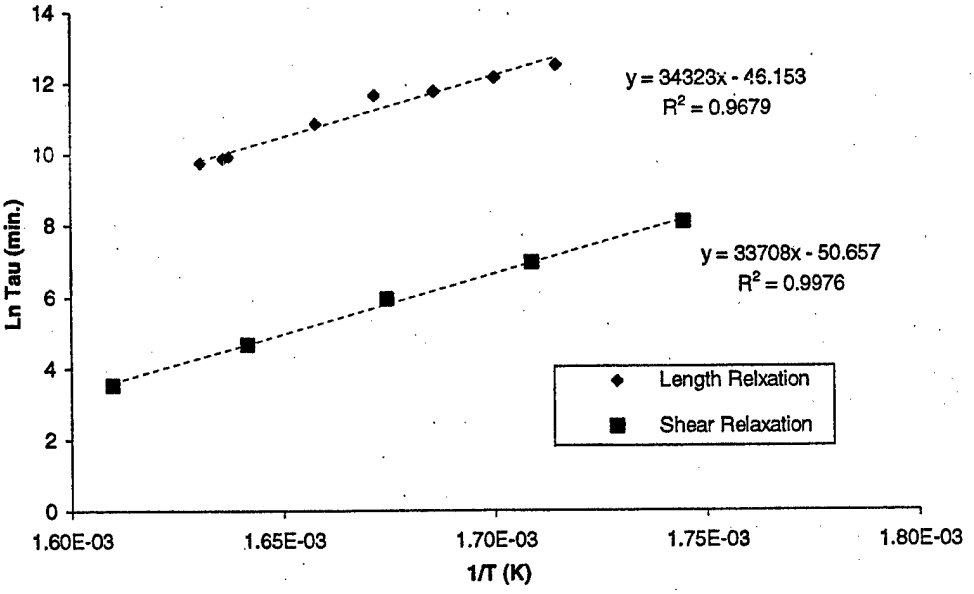

Fig. 2. Comparison of shear and length relaxation energies for neat PMR-15.

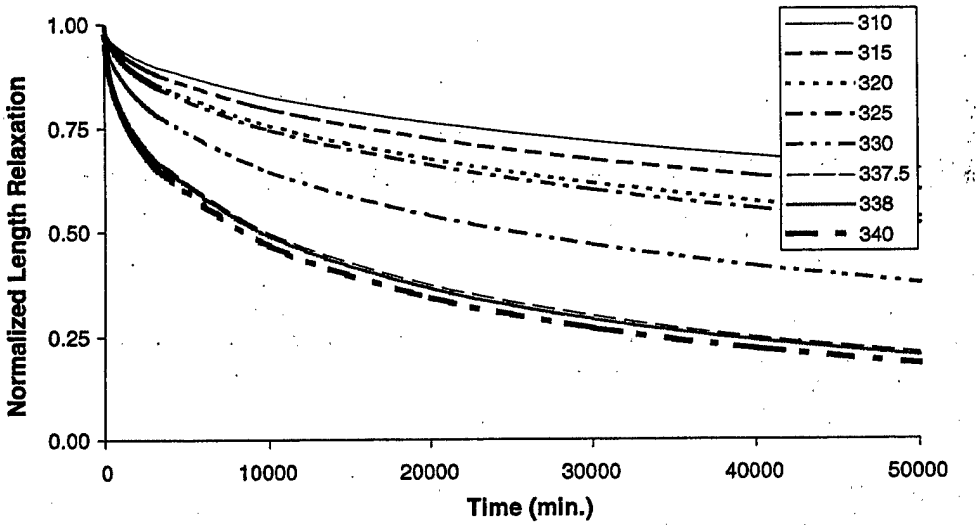

Fig. 3. Normalized length relaxation of PMR-15 neat polymer.

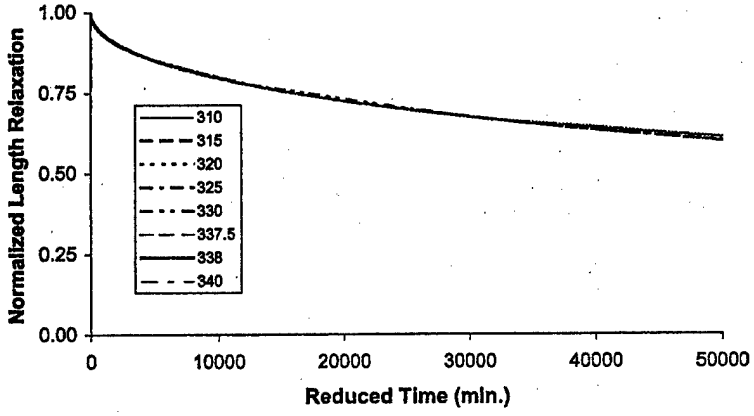

Fig. 4. Mastercurve of isothermal length relaxation for PMR-15 at 316 °C.

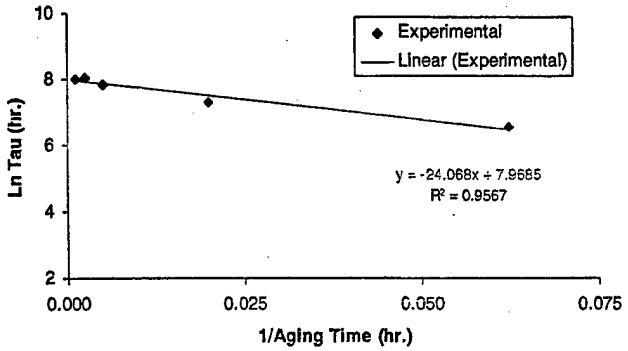

Fig. 5. τ as a function of aging time.

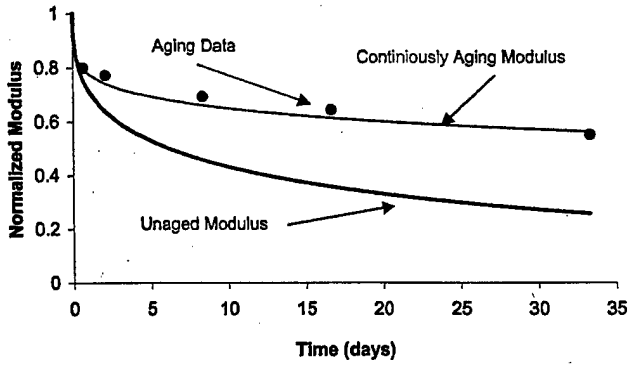

Fig. 6. Continuously aging shear modulus mastercurve for PMR-15.

stress relaxation modulus for continuously aging neat PMR-15 in nitrogen at 316 °C was derived using Kamvouris' [4] short-time test data (about 30 min), for neat PMR-15 that was aged for times up to 800 h. in N_2 at 316 °C. Structural aging simplicity was assumed (constant β), and a rate of change of τ for aged neat PMR-15 was determined from

$$\tau = \tau_0 e^{(-C/t_a)}, \tag{7}$$

where C is a material constant with units of time and t_a is the aging time. From Eq. (8), τ at aging times up to 800 h. in N_2 at 316 °C may be determined. The curve of

$$\ln \tau = -C\left(\frac{1}{t_a}\right) + \ln \tau_0, \tag{8}$$

is shown in Fig. 5. The normalized shear modulus of neat PMR-15 aged in N_2 as a function of time for continuous aging derived from Eq. (8) is shown in Fig. 6. For comparison, an extrapolation of the short-term modulus data from Roberts et al. [9] is also included in Fig. 6.

3. Numerical analysis

The continuously aging length and shear relaxation mastercurves for PMR-15 as well as an activation energy based shift function have been derived in the previous section. In this section, numerical predictions of the residual stress state in an idealized unidirectional carbon fiber/PMR-15 composite will be determined using finite elements following Eq. (6).

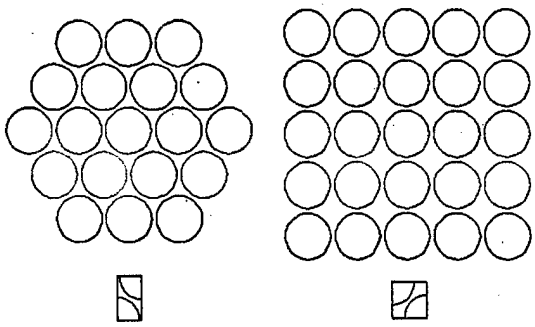

Fig. 7. Hexagonal (left) and square (right) fiber arrays along with their unit cell representations (bottom).

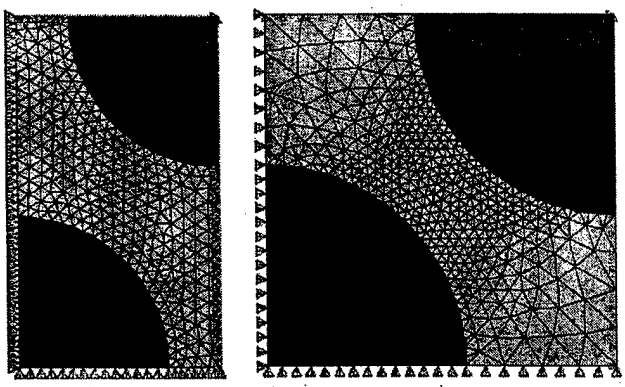

Fig. 8. Finite element representations of the hexagonal (left) and square (right) unidirectional composite models.

The effects of aging and cooling strains on the residual stresses in a unidirectional graphite fiber/PMR-15 composite were examined using two simple unidirectional composite models, specifically the hexagonal and square unit cells (Fig. 7). These models are representations of the center of an infinite hexagonal or square array of fibers [10]. The finite element representations of the two models are shown in Fig. 8. For each unit cell shown in Fig. 8, the left edge nodal displacements were constrained in the horizontal direction, whereas the lower edge nodal displacements were constrained in the vertical direction. The right edge nodal displacements were consistent in the horizontal direction and the top edge displacements were consistent in the vertical direction.

The PMR-15 polyimide matrix was modeled using six-node two-dimensional plane strain elements with the isotropic properties of the neat polymer developed and described above. The T-650 graphite fibers were modeled with two-dimensional six-node plane strain aniso-

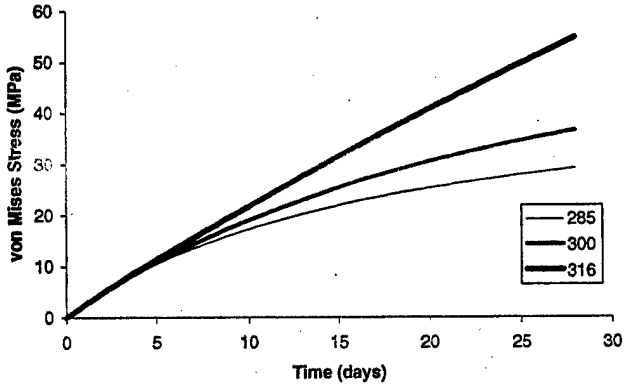

Fig. 9. Comparison of von Mises stress generated during aging at 285, 300, and 316 °C.

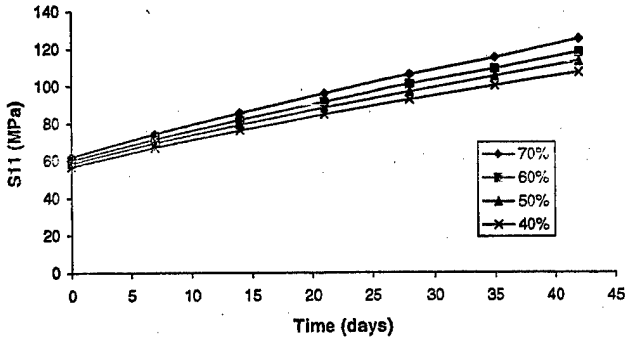

Fig. 10. Comparison of the first principle stress generated during aging with cooling at 316 °C for the 40–70% square unit cell models.

tropic linear elastic elements using the mechanical properties from Peebles [11]. The simulations directly follow postcuring at 316 °C and assume a stress free initial state. The simulations consisted of: (1) cooling from 316 to 25 °C in 15 min with no isothermal aging and (2) isothermal aging at 316 °C for up to six weeks followed by cooling to 25 °C in 15 min. Isothermal aging was also simulated at 316, 300, and 285 °C without cooling (3). The simulations for isothermal aging at 300 and 285 °C commenced after cooling from 316 °C to the aging temperature in 1 min.

Representative results from the numerical analysis are presented in Figs. 9–12 to briefly indicate the effects of aging temperature and cooling, fiber volume fraction and fiber architecture on the residual stresses in the composite. For example, a comparison of the maximum von Mises stresses generated during aging without cooling at 285, 300, and 316 °C for the square unit cell with 50% V_f is shown in Fig. 9. In Fig. 10, a comparison of the maximum first principle stresses for the 40%, 50%, 60%, and 70% V_f square unit cell for aging with cooling

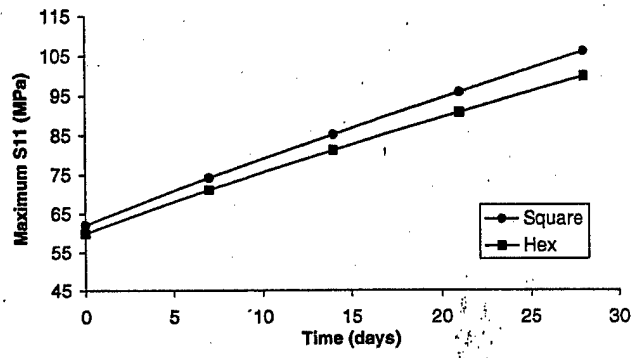

Fig. 11. Comparison of the first principle maximum stresses between the 70% V_f hexagonal and square models for aging at 316 °C with cooling.

at 316 °C is also presented. In addition to Fig. 11, the first principle maximum stresses between the 70% V_f hexagonal and square models for aging at 316 °C with cooling to room temperature are shown. To better illustrate the effect of the two different geometries on the residual stress distribution, the von Mises stress

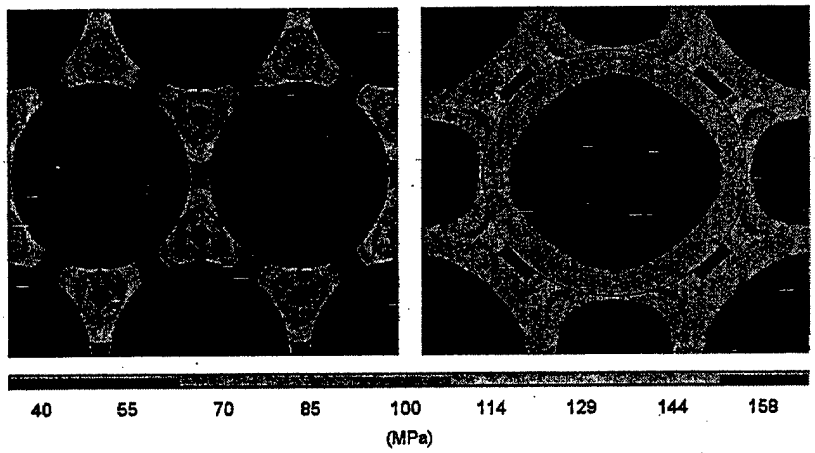

Fig. 12. Comparison of von Mises stress fields between the 70% V_f hexagonal (left), and square (right) unit cell models for aging at 316 °C with cooling.

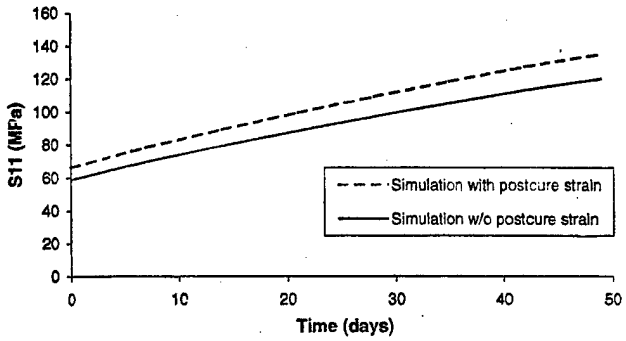

Fig. 13. Comparison of maximum first principle stresses for the FEA 50% V_f square unit cell model with and without the addition of postcure strain for aging at 316 °C with cooling.

contours for the case of aging at 316 °C and cooling to room temperature are shown in Fig. 12.

The results presented in Figs. 9–12 were obtained without considering the effect of postcuring strains. However, it was found that during postcuring at 316 °C for 16 h the aging strain of neat PMR-15 was approximately 0.2%. The effect of the additional strain that occurs during postcure is shown in Fig. 13. In this figure, the maximum first principle stress from the 50% V_f square unit cell model after aging in nitrogen at 316 °C for up to six weeks with cooling, with and without the addition of the postcure strain, are compared. No data is available for the change in the shear relaxation modulus of PMR-15 during postcure therefore this simulation assumed that the shear relaxation function is unaffected by the postcuring.

4. Discussion

The data presented in Figs. 9–13 clearly show that the residual stresses in the composite are strongly affected by the aging and cooling conditions as well as the composite architecture. For example, after six weeks of aging with cooling the difference between the first principle maximum stresses for the 70% and 40% V_f square unit cell models was 17% and the difference between the 50% and 40% V_f square unit cell models was 6% (Fig. 10). From Fig. 11, after four weeks of aging with cooling the difference between the maximum first principle stress from the 70% V_f hexagonal and square unit cell models was 6%. Accordingly, the difference in the maximum first principle stresses between geometries is approximately the same as a change of 10% volume fraction of fibers.

Although the maximum stresses are comparable between geometries, square vs. hexagonal, the stress fields are not, as shown in Fig. 12. In Fig. 12, the square unit cell (right), center fiber is outlined and shows a von Mises stress gradient through the fiber. Conversely for the hexagonal unit cell (left), there is no stress gradient through the fiber.

Referring to the fiber distribution shown in Fig. 1(b), it is easy to imagine a unidirectional composite made up of random distributions of hexagonal and square arrays of fibers. Therefore, when the unidirectional composite is cooled or aged it may have stress distributions representing combinations of the two stress fields shown in Fig. 12. Importantly, during aging large residual stresses in graphite fiber/polyimide composites are generated which should not be ignored in any stress analysis involving high temperature aged polymers.

The effect of aging on residual stresses in the composites can also be observed from the data obtained by Benedikt et al. [12]. Benedikt determined the interlaminar stress in a 50–53% V_f T650/PMR-15 unidirectional composite by measuring the change in lattice spacing of embedded aluminum particles, as illustrated in Fig. 14. The residual stresses in the composite were determined from the residual strains in the particles using the Eshelby [13]/Mori–Tanaka method [14] after aging in nitrogen at 316 °C for up to six weeks then cooling to room temperature and measuring using X-ray diffraction (XRD). The calculations of the residual stresses in the composite were performed with and without the addition of aging strains [12]. However, the effect of aging strains, from both postcuring and aging, was

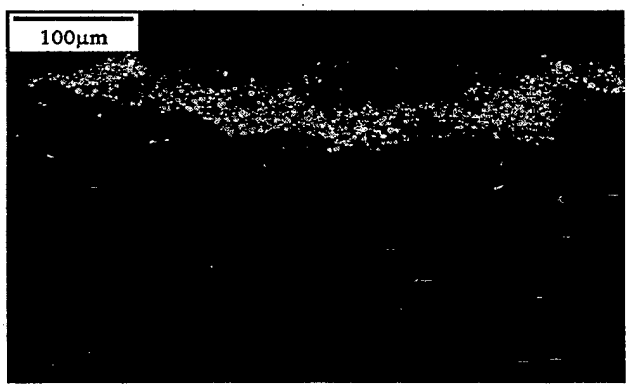

Fig. 14. Cross-section of unidirectional T-650/PMR-15 with embedded aluminum particles.

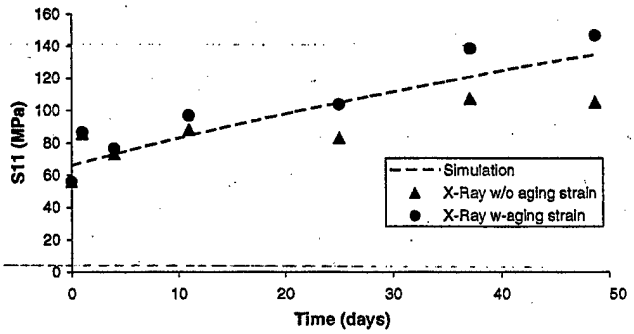

Fig. 15. Comparison of X-Ray residual stress and FEA simulation for aging at 316 °C with cooling.

present in the XRD residual strain data for the inclusions [12].

Fig. 15 compares the first principle interlaminar residual stress calculated using the Eshelby/Mori–Tanaka method from the residual X-ray stresses in the inclusions with and without the effect of aging strain [12], with the maximum first principle stresses determined in this study using the 50% V_f square unit cell model including postcuring strains. It can be seen that the residual stresses in the composite during postcuring determined from XRD [12] and numerically in this study are in very good agreement. This implies that the two independent approaches yielded the same residual stress data with aging. It also shows that for the proper interpretation of the XRD data the effect of the aging strains must be included.

5. Conclusions

1. It has been shown in this research that the stress developed during high temperature aging of a unidirectional T-650/PMR-15 composite is significant. The magnitude of the residual stress in the composite caused by aging for one month at 316 °C was found to be comparable to the residual stress developed during cooling from 316 to 25 °C.
2. Reducing the isothermal aging temperature significantly affects aging strains and stresses. Changing the isothermal aging temperature from 316 to 300 °C lowers the aging stress by as much as one third and from 316 to 288 °C by half.
3. Aging maximum stresses between the square fiber array and the hexagonal fiber array are comparable. However, the stress distributions between architectures vary significantly. Although the maximum stresses are not significantly affected by fiber architecture, the volume fraction of fibers has a considerable affect on the aging and cooling stress.

Acknowledgements

The Air Force Office of Scientific Research and NASA Glenn Research Center supported this research under joint Grant F49620-00-1-0159. Additional funds were provided by the National Science Foundation and the University of Denver from a Major Research Instrumentation Program; Instrument Development and Acquisition Grant No. CMS-99777-35.

References

[1] Benedikt B, Kumosa M, Predicki PK, Kumosa L, Castelli MG, Sutter JK. An analysis of residual thermal stresses in a unidirectional graphite/PMR-15 composite based on the X-ray diffraction measurements. Compos Sci Technol 2001;61(14):1977–94.
[2] Bowles KJ, Jayne D, Leonhardt TA. Isothermal aging effects on PMR-15 resin. SAMPE Quarter 1993:2–9.
[3] Tsuji LC, McManus HL, Bowles KJ. Mechanical properties of degraded PMR-15 resin. ASTM STP 2000;1357:3–17.
[4] Kamvouris JE, Roberts GD, Pereira JM, Rabzak C. Physical and chemical aging effects in PMR-15 neat resin. ASTM STP 1997;1302:243–58.
[5] Gentz M, Armentrout D, Rupnowski P, Kumosa L, Shin E, Sutter J, et al. In-plane shear testing of medium and high modulus woven graphite fiber reinforced/polyimide composites. Compos Sci Technol 2004;(64):203–20.
[6] Kohlrausch R. Ueber das dellmann'sche elektrometer. Ann Phys 1847;72:353–405.
[7] Muki R, Sternberg E. On transient thermal stresses in viscoelastic materials with temperature dependent properties. J Appl Mech 1961;28:193–207.
[8] ANSYS Theory Manual, Ver. 6.1; 2003. p. 1 [chapter 4.6].
[9] Roberts GD, Malarik DC, Robaidek JO. Viscoelastic properties of addition-cured polyimides used in high temperature polymer matrix composites. NASA Technical Memorandum 1991;1.15: 103768.
[10] Adams D. Inelastic analysis of a unidirectional composite subjected to transverse normal loading. J Compos Mater 1970; (4):310–28.
[11] Peebles LH. Carbon fibers: formation structure, and properties. Boca Raton, FL: CRC Press; 1994. p. 75.
[12] Benedikt B, Gentz M, Kumosa L, Predicki P, Armentrout D, Kumosa M et al. The use of X-ray diffraction measurements to determine the effect of aging on residual stresses in unidirectional and woven graphite/polyimide composites. Compos A 2004, in press.
[13] Eshelby JD. The determination of the elastic field of an ellipsoidal inclusion, and related problems. Proc Roy Soc 1957;(A241):376–96.
[14] Mori T, Tanaka K. Average stress in matrix and average elastic energy of materials with misfitting inclusions. Acta Metall 1973;(21):571–4.

Available online at www.sciencedirect.com
SCIENCE DIRECT®
Acta Materialia 52 (2004) 5603–5613
Acta MATERIALIA
www.actamat-journals.com

Mechanical response of a woven graphite/polyimide composite to in-plane shear dominated loads at room and elevated temperatures

P. Rupnowski [a], M. Gentz [a], J.K. Sutter [b], M. Kumosa [a,*]

[a] *Department of Engineering, Center for Advanced Materials and Structures, University of Denver, 2390 S. York St. Denver, CO 80208, USA*
[b] *NASA Glenn Research Center at Lewis Field, 21000 Brookpark Rd., Cleveland, OH 44135, USA*

Received 3 June 2004; received in revised form 16 August 2004; accepted 18 August 2004
Available online 25 September 2004

Abstract

In this work, the effect of two types of in-plane shear dominated loads on the initiation of intralaminar damage has been evaluated in an 8-harness satin (8HS) T650-35/PMR-15 (graphite/polyimide) composite tested at room and elevated temperatures. The composite was subjected to either pure in-plane shear or combined biaxial tension and shear, which represented the stress conditions in the gage sections of the Iosipescu shear and ±45° tensile tests, respectively. The stress distributions in the composite were determined as a function of load and temperature by performing non-linear stress computations on the micro-, meso- and macro-levels. Both the concept of representative micro- and meso-unit-cells and the viscoelastic Eshelby/Mori–Tanaka approach were used in the analyses. The macro-response of the composite to the in-plane shear and biaxial loads was predicted at both temperatures and then validated by comparing it with the available experimental data. The micro-stress calculations have shown that on the micro-scale noticeably higher maximum principal stresses in the polyimide matrix in the vicinity of the graphite fibers were determined for the biaxial load case than in pure shear, both at room and high temperatures. It was shown that by using the numerical stress predictions, the experimentally observed differences can be explained in the initiation of tow micro-cracking in the woven composite subjected to the Iosipescu and ±45° tests at room and elevated temperatures.
© 2004 Acta Materialia Inc. Published by Elsevier Ltd. All rights reserved.

Keywords: Woven graphite/polyimide composites; Shear response; Modeling; Finite element method; Failure prediction; Elevated temperature

1. Introduction

Graphite fiber/polyimides are advanced composite systems suitable for aerospace applications that require high specific strength and stiffness at elevated temperatures [1–24]. Especially, woven systems are quite popular in aerospace applications. However, one of the limitations of such composites is their low shear strength under shear and biaxial shear dominated loads both at room and elevated temperatures [4,6,10,11,14,19], which can lead to premature failures of aerospace components. Since the composites are manufactured at relatively high temperatures, due to the mismatch in the coefficients of thermal expansion of the fibers and the polyimide resins, large residual thermal stresses exist in these materials [8,9,13,15,16,19–21]. These stresses can significantly influence the strength properties of the composites and, in particular, their resistance to damage initiation under shear and shear dominated biaxial loads [19].

To evaluate the response of woven composites to shear, the Iosipescu shear and ±45° tensile tests can be employed (see Fig. 1(a) and (b)) [25,26]. The application of these two tests in the shear testing of the composites has been particularly successful in the failure analysis of the 8HS T650-35/PMR-15 system both at room and elevated temperatures [4,6,10,11,14,19]. The shear strength

* Corresponding author. Tel.: +1 303 871 3807; fax: +1 303 871 4450.
E-mail address: mkumosa@du.edu (M. Kumosa).

1359-6454/$30.00 © 2004 Acta Materialia Inc. Published by Elsevier Ltd. All rights reserved.
doi:10.1016/j.actamat.2004.08.019

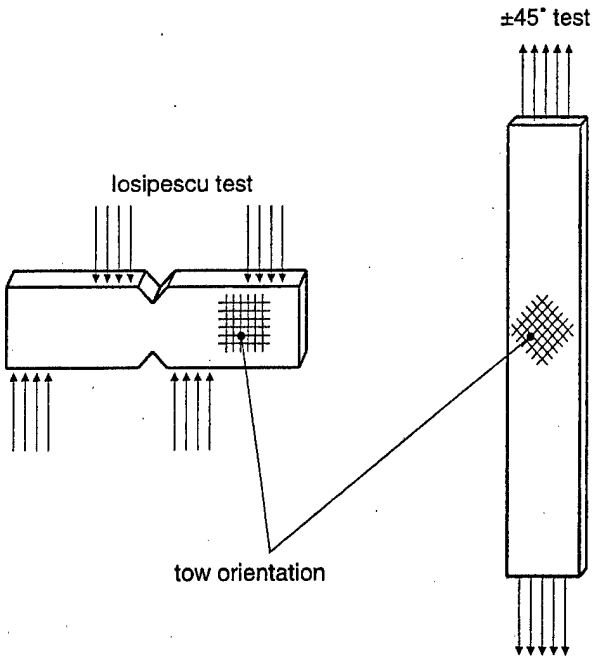

Fig. 1. Schematics of Iosipescu shear and ±45° tension tests as applied to woven composites.

of the composite was determined from these tests and the critical shear stresses for the initiation of intralaminar damage in the composite were estimated by monitoring acoustic emission (AE) [10,11,14]. The shear strength results from the room and high temperature testing of the composite are shown in Table 1.

The data presented in Table 1 were obtained by testing the woven Iosipescu and ±45° specimens on a MTS 809 system at a displacement rate of 1 mm/min. The Iosipescu specimens were tested in an environmental chamber whereas infrared lamps were used to heat the ±45° specimens. AE was monitored during testing using wide band sensors at room temperature and resonant sensors at high temperature. Detailed descriptions of the testing conditions, specimen preparation and the limitations encountered in the testing procedures can be found in [10,11,14].

The data in Table 1 clearly show that the shear stress at the initiation of the intralaminar tow micro-cracking in the 8HS T650-35/PMR-15 composite (see Fig. 2) is lower in the case of the ±45° tensile test than for the Iosipescu test both at room temperature and at 315 °C. It was suggested that this effect could have resulted from the fact that in the ±45° test the composite was subjected to biaxial tension along the warp and fill tows and in-plane shear loads whereas in the gage section of the woven Iosipescu specimens the stress field was predominately pure in-plane shear [6,11]. To further examine this effect Rupnowski and Kumosa [15] performed meso- and micro-viscoelastic finite element computations of stresses in the composite subjected to various in-plane uniaxial, shear and biaxial loads at room temperature. It was shown that the combined effect of residual stresses and external applied loads had a greater influence on the micro-stresses if the composite was subjected to the loading conditions produced by the ±45° test (combined biaxial tension and shear) than if the load case simulated the Iosipescu shear test (predominately in-plane shear). Even more importantly, the combined effect of biaxial tension and in-plane shear was

Table 1
Shear stresses at the onset of intralaminar damage and shear strength of 8HS T650-35/PMR-15 tested at room temperature and at 315 °C [10,11,14]

Test	Shear stresses at the onset of intralaminar damage [MPa]		Shear strength [MPa]	
	±45°	Iosipescu	±45°	Iosipescu
at RT	52.6 ± 6.1	94.8 ± 1.3	82.0 ± 0.15	105.8 ± 2.6
at 315 °C	37.3 ± 5.2	59.9 ± 1.2	50.8 ± 6.0	71.8 ± 4.2

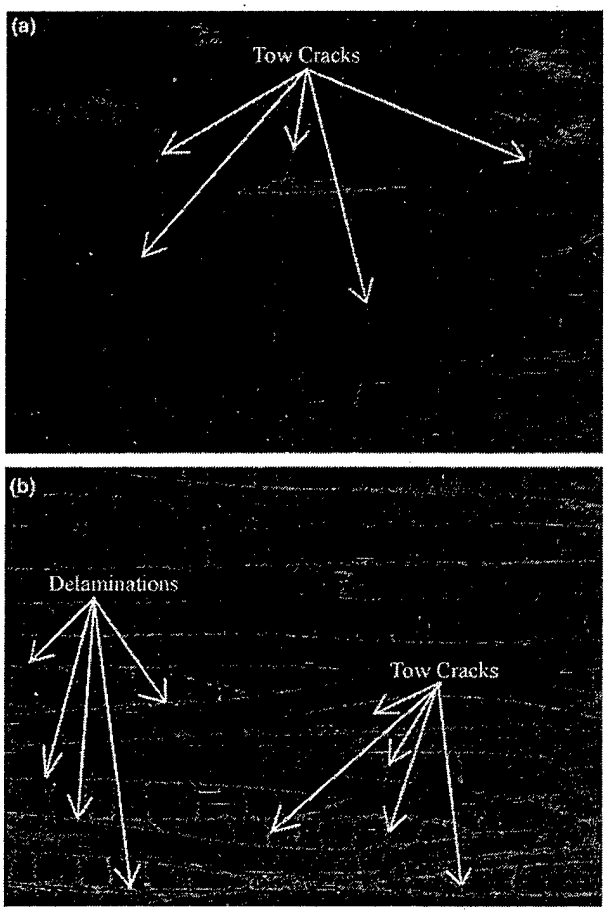

Fig. 2. Damage initiation and progression in 8HS T650-35/PMR-15 subjected to shear dominated loads at room temperature; (a) tow micro-cracking and (b) damage at maximum load [10,11].

determined to generate the highest micro-stresses in the matrix inside the tows, among all in-plane simple and biaxial load cases [15].

In our previous work [15], the micro- and meso-visco-elastic stress analyses of the 8HS T650-35/PMR-15 system were performed only at room temperature. In this research, the previous stress investigation is extended to higher temperatures, up to 315 °C. An attempt is made here to compare the failure process of the composite subjected to Iosipescu and ±45° tests not only at room temperature but also at the elevated temperature, which could be expected in-service (315 °C).

2. Material characterization

2.1. Composite

A detailed description of the investigated composite, its architecture, quality control, manufacturing, stiffness and thermal properties, etc. was already presented in [10,11,14]. In this work, only the most important information about the composite is listed. The composite consisted of sixteen 8HS plies and was manufactured and postcured (for 16 h in air) at 315 °C. The cooling rate was 1.3 °C/min. The composite had an average volume fraction of fibers of 61.1% and its glass transition temperature was 342 °C. The volume fraction of voids, as determined from acid digestion tests was less than 1.5%.

2.2. Fibers

The elastic and thermal parameters of the T650-35 fibers were measured by Rupnowski et al. [22,24] and are shown in Table 2. The fiber stiffness properties (E_{fL} – longitudinal Young's modulus, E_{fT} – transverse Young's modulus, G_{fL} – longitudinal shear modulus, G_{fT} – transverse shear modulus, ν_{fL} – longitudinal Poison's ratio) were determined in [22,24] by measuring the stiffness constants of a unidirectional composite based on the same fibers and resin by the three-component oscillator resonance method [24] and then extracting the fiber properties from the composite macro-data using the inverse Eshelby/Mori–Tanaka approach [22,27,28]. The same numerical technique was used to determine the coefficients of thermal expansion of the fibers (α_{fL} – longitudinal and α_{fT} – transverse) from the composite macro-data obtained using a dilatometer.

2.3. Polyimide resin

The mechanical behavior of PMR-15 is significantly influenced by elevated temperatures and strain rates, leading to the reduction of its stiffness and strength properties (see Fig. 3). As examples of these effects, the data in Fig. 3 are shown at room and 315 °C temperatures. The response of the PMR-15 was measured by mechanical testing using 90 mm long dog bone-shape specimens with 15 mm gauge sections and the axial strain was measured using a high temperature extensometer (Epsilon 3555 Un-Cooled). The high temperature tests were performed in a temperature controlled environmental chamber. The strain rate effect is illustrated in the high temperature data only by showing three sets of most representative stress/strain curves (two at each strain rate) for three different strain rates (0.4, 5 and 7%/min). A strain rate effect was not observed at room temperature therefore it was not shown in Fig. 3. Also, the stress/strain curve at room temperature is an average curve representing six independent tests. The Young's modulus at room temperature was 3.7 ± 0.4 GPa. The modulus at high temperature was lower and strain rate dependent. At 0.4, 5 and 7%/min, the Young's' moduli were 1.6, 1.9 and 2.8 GPa, respectively (average of two tests for each condition). The dashed line shown in Fig. 3 as a linear extension of the high temperature data at 7%/min was used in the numerical prediction, which will be explained later on in this work.

In the calculations of micro- and meso-stresses caused by manufacturing and mechanically applied loads at room temperature, a temperature dependent visco-elastic model of PMR-15 [8,29,30] was employed.

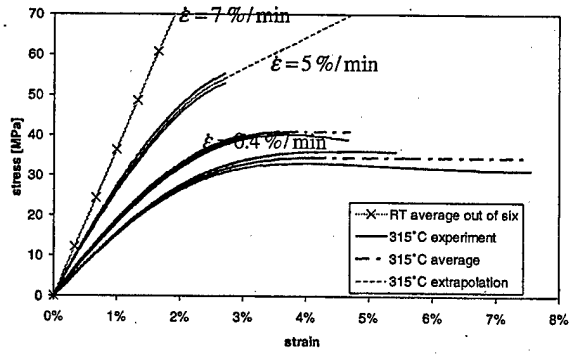

Fig. 3. Stress vs. strain curves for PMR-15 at room temperature and at 315 °C tested at three different strain rates.

Table 2
Elastic properties and coefficients of thermal expansion of T650-35 fibers [22,24]

	E_{fL} [GPa]	E_{fT} [GPa]	G_{fL} [GPa]	G_{fT} [GPa]	ν_{fL}	α_{fL} [10^{-6}/°C]	ν_{fT} [10^{-6}/°C]
Fiber T650-35	224 ± 3	15.4 ± 0.5	21.1 ± 1.1	5.8 ± 0.4	0.44 ± 0.02	−1.2 ± 0.05	13.5 ± 0.8

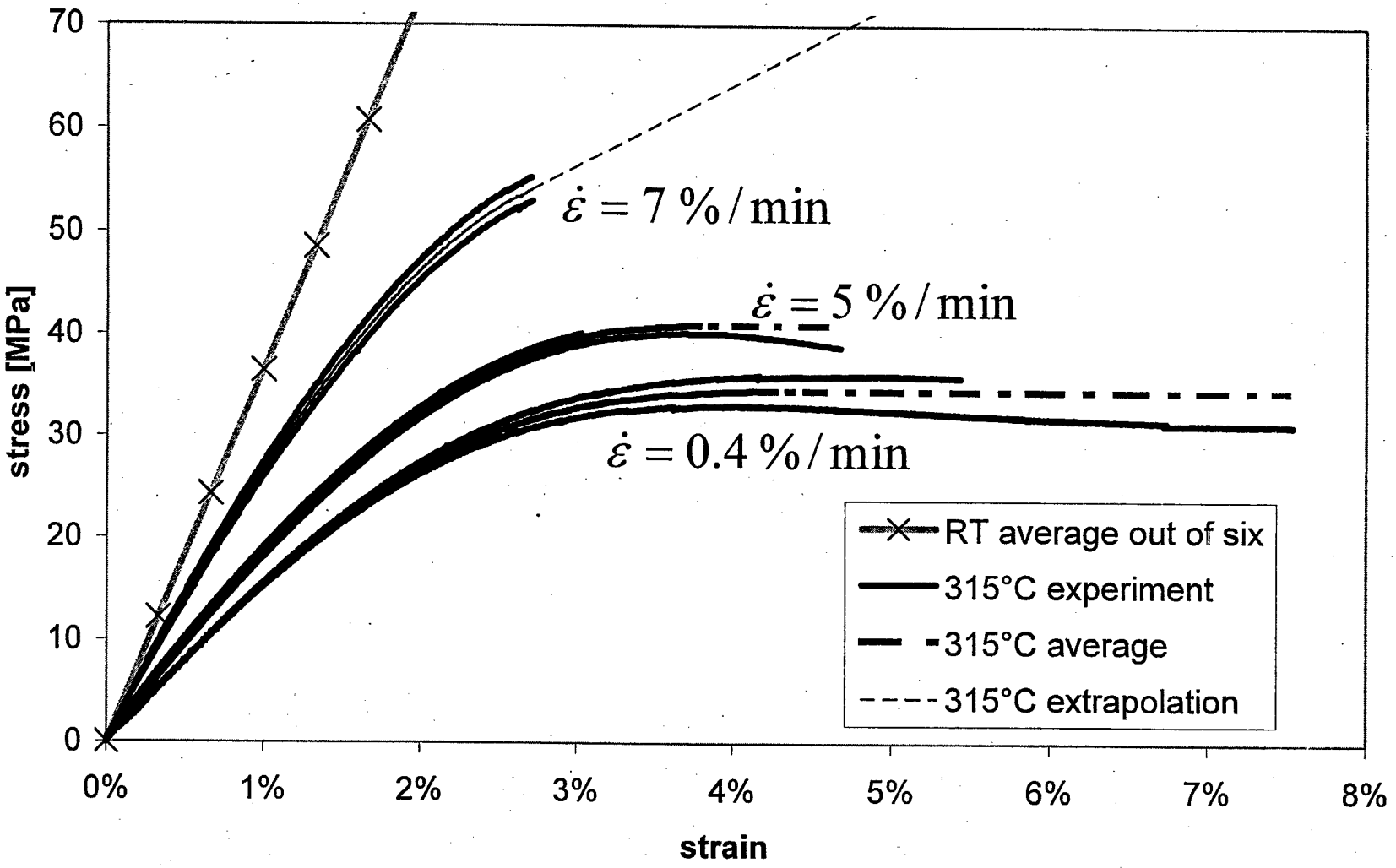
70
60
50
40
30
20
10
0
stress [MPa]
0%
1%
2%
3%
4%
5%
6%
7%
8%
strain
$\dot{\varepsilon} = 7\,\%/\min$
$\dot{\varepsilon} = 5\,\%/\min$
$\dot{\varepsilon} = 0.4\,\%/\min$
RT average out of six
315°C experiment
315°C average
315°C extrapolation

Figure 3.

To describe the behavior of the composite at 315 °C an elasto-plastic model of PMR-15 was used.

2.3.1. Visco-elastic model of PMR-15

Following [8,29,30], a visco-elastic formula for the shear modulus $G_m(t,T)$ of PMR-15 as a function of time and temperature for temperatures ranging from room temperature to 348 °C was used according to Eqs. (1)–(4).

$$G_m(t,T) = G_m(\xi, T_{\text{ref}}), \tag{1}$$

$$G_m(t,T_{\text{ref}}) = 603.9 + 519.2\exp(-t/11.13) + 100.9\exp(-t/325.5) + 116.5\exp(-t/3977), \tag{2}$$

where

$$\xi(t) = \int_0^t \frac{\mathrm{d}t'}{a_h[T(t')]}, \tag{3}$$

$$a_h(T) = 10^{\text{Exp}(0.41(-T+348)^{0.28}-4.3)}, \tag{4}$$

with $T_{\text{ref}} = 288$ °C.

In the above equations time t is expressed in seconds, temperature T in °C and G_m in MPa. Using Eqs. (1)–(4) and assuming that the Poisson's ratio v_m of PMR-15 is constant (0.36), the range of the effective Young's and shear moduli E_m and G_m could be derived for a given temperature and time.

The temperature dependant coefficient of thermal expansion, α_m, of neat PMR-15 was measured between 25 and 315 °C and is given by the following expression [22]:

$$\alpha_m = a^2(T + 273.15\ ^\circ\text{C})[1 - 0.809aT - 258(aT)^3 + 21828(aT)^5], \tag{5}$$

where $a = 3.64 \times 10^{-4}/^\circ$C. The relationship described by Eq. (5) is based on the experimental data obtained using length dilatometry.

2.3.2. Elasto-plastic model of PMR-15

To evaluate the response of the woven composite at 315° an elasto-plastic model of the resin was assumed. The effect of strain rate was also considered following the data shown in Fig. 3. For a strain rate of 7%/min the elastic limit was estimated to be approximately 20 MPa with the total and plastic strains at failure equal to 2.7% and 0.75%, respectively. The elastic limits for the other two strain rates, 0.4%/min and 5%/min, were 12 and 15 MPa, respectively with noticeably larger total and plastic strains at failure. In the calculation of micro-stresses in the woven composite only the data for a strain rate of 7%/min, shown in Fig. 3, were considered. Since the micro-stress analysis required large stress data, the average high temperature results at 7%/min in Fig. 3, were linearly extended for the purpose of the numerical simulations.

3. Micro- and meso-stress calculations

The numerical analyses of the micro- and meso-stresses are comprised of the following three steps. First, either the Eshelby/Mori–Tanaka approach [27,28] or a micro-unit-cell model was employed to obtain the properties of the tows. Then, the properties of the tows were introduced into a meso-unit-cell representing the 8HS woven composite. Subsequently, the meso-unit-cell was subjected to mechanical loads simulating either pure in-plane shear (Iosipescu) or combined shear and biaxial tension (±45°) stress fields and, consequently, the meso-stresses and strains in the composite were calculated. Finally, the meso-strains obtained in several locations of the 8HS unit-cell were transferred back into the micro-unit-cell and the micro-stresses inside the tows in those locations were numerically determined at room temperatures and at 315 °C as a function of load for the two load cases.

3.1. Micro-stress modeling

The micro-scale three-dimensional hexagonal FE representation of a unidirectional tow with a volume fraction of fibers, f, of 72% is shown in Fig. 4. The assumed volume fraction of fibers agreed with experimental observations [31]. Since the stresses in the hexagonal unit-cell do not depend on the x_3 coordinate, the thickness of the model d can be arbitrarily chosen. In or-

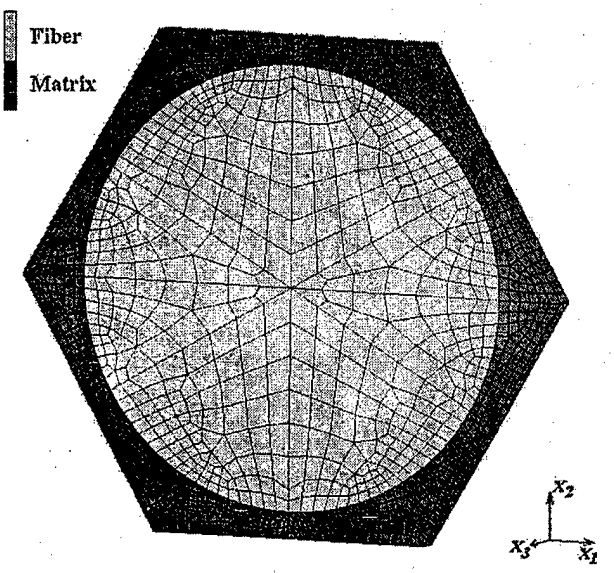

Fig. 4. Finite element representation of unidirectional tow with 72% volume fraction of fibers.

der to reduce the computation time, the most suitable approach is to construct the mesh that consists of only one element layer, as shown in Fig. 4. Twenty-node isoparametric distorted three-dimensional brick elements were employed to build the micro-unit-cell.

The following periodic boundary conditions were applied [32]:

$$U_i(0,0,d/2) = 0 \tag{6}$$

for the faces perpendicular to the fiber axis

$$U_i(x_1,x_2,d/2) = U_i(x_1,x_2,-d/2) + \langle\varepsilon_{i3}\rangle d \tag{7}$$

for $x_1 \in [-a/3,a/3]$, $x_3 \in [-d/2, d/2]$

$$U_i(x_1,b,x_3) = U_i(x_1,-b,x_3) + \langle\varepsilon_{i2}\rangle 2b \tag{8}$$

for $x_1 \in [-2a/3,-a/3]$, $x_3 \in [-d/2, d/2]$

$$U_i(x_1 + a, -\sqrt{3}\cdot x_1 - b, x_3) = U_i(x_1, -\sqrt{3}\cdot x_1 - 2b, x_3) + \langle\varepsilon_{i1}\rangle a + \langle\varepsilon_{i2}\rangle b, \tag{9}$$

$$U_i(x_1 + a, \sqrt{3}\cdot x_1 + b, x_3) = U_i(x_1, \sqrt{3}\cdot x_1 + 2b, x_3) + \langle\varepsilon_{i1}\rangle a + \langle\varepsilon_{i2}\rangle(-b). \tag{10}$$

In the above equations $a = \sqrt{\pi\sqrt{3}/(2f)}$, $b = a\cdot\sqrt{3}/3$, and $\langle\varepsilon_{ij}\rangle$ denotes the volume averaged strain in the unit-cell and U_i is the displacement vector. $\langle\varepsilon_{ij}\rangle$ equals $\langle\varepsilon_{ji}\rangle$ and the radius of the graphite fibers was taken to be 1.

3.2. Homogenization of tows

The temperature-dependent viscoelastic behavior of the tows was assumed for the residual and mechanical stress determination at room temperature. For the elevated temperature calculations an elasto-plastic model of the tows was used. In this work the approach used to obtain the viscoelastic properties of the tows at room temperature was the same as the one presented in [15], based on the Eshelby/Mori–Tanaka model. It should be also noted that, according to [16], the Eshelby/Mori–Tanaka model agrees closely with the response of a finite element representation of the hexagonal micro-unit-cell.

The elasto-plastic behavior of the tows at 315 °C was obtained by introducing the elasto-plastic properties of PMR-15 from Fig. 3, for strain rates of 0.4, 5 and 7%/min, to the micro-unit-cell shown in Fig. 4. The effective response of the micro-unit-cell was numerically determined for six simple load cases where only one diagonal component of the stress tensor was assumed to be non-zero. The corresponding six strain–stress curves for σ_{11}, σ_{22}, σ_{33}, σ_{12}, σ_{13} and σ_{23} for a strain rate of 7%/min are shown in Fig. 5. The response of the unit-cell to the other two strain rates was analogous. The obtained data clearly show that the mechanical behavior of the unit-cell strongly depend on the loading conditions. It can also be seen that the stress–strain curves are non-linear even at small strains except for the longitudinal tension case. A small non-linear effect in the longitudinal data was also found for σ_{33} greater than 1000 MPa. The Young's and shear moduli and the elastic limits determined for the micro-unit-cell are listed in Table 3.

In Fig. 5 the two transverse tension curves (σ_{11} and σ_{22}) and the two longitudinal shear curves (σ_{23} and σ_{13}) are almost identical. This means the elasto-plastic hexagonal unit-cell exhibits almost perfect isotropic symmetry in the x_1–x_2 plane. This result agrees with the observations in [16] regarding the behavior of a linear elastic hexagonal unit-cell.

For the meso finite element modeling it was necessary to select an elasto-plastic material model of the unidirectional tows that would be able to reproduce the behavior of the hexagonal micro-unit-cell shown in Fig. 5. In this research, the anisotropic elasto plastic model of Hill [33] was employed to numerically model the tows. In order to verify the applicability of the model the transverse tension σ_{22} vs. ε_{22} curve of the hexagonal unit-cell was taken as the master-curve in Hill's model [33]. Then, using the data in Table 3, the Hill's model response was obtained for the other load cases and compared

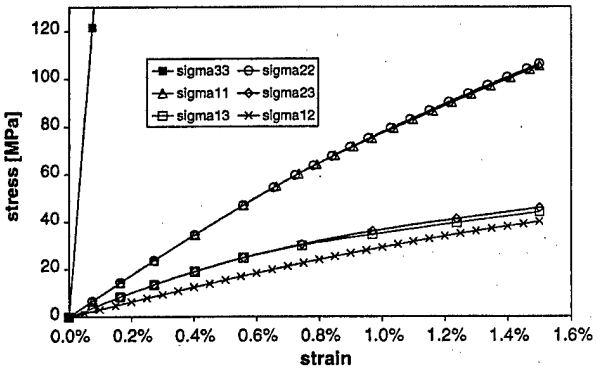

Fig. 5. Effective stress–strain curves for hexagonal unit-cell with elasto-plastic matrix subjected to a strain rate of 7%/min at 315 °C.

Table 3
Properties of elasto-plastic hexagonal micro-unit-cells at three strain rates

Strain rate [%/min]	Longitudinal tension			Transverse tension			Longitudinal shear			Transverse shear		
	7	5	0.4	7	5	0.4	7	5	0.4	7	5	0.4
Young's or shear modulus [GPa]	162	162	162	8.7	7.0	6.3	5.0	3.7	3.1	3.1	2.5	2.2
Elastic limit [MPa]	1000	950	900	20	17	15	9	7.5	6.6	10	8.5	7.5

with the corresponding curves determined from the micro-unit-cell (Fig. 6). It can be seen in Fig. 6 that the predictions from the unit-cell and the Hill model are almost identical.

3.3. Meso modeling

Fig. 7 illustrates a finite element representation of one-half of a meso 8HS unit-cell. For clarity, the configuration of the fill and weft yarns (tows) is shown in this figure without the resin rich regions. The model was prepared based on SEM images of the 8HS T650-35/PMR-15 composite [15]. The mesh consists of 26220 isoparametric 4 node tetragonal elements. Symmetric stacking of woven layers was assumed and the periodic boundary conditions taken from [32] were applied. The total and tow volume fractions of fibers and the size of the meso-unit-cell were adjusted to match the values obtained using the acid digestion test [11,14] and SEM observations [31].

The evaluation of the meso-stresses at room temperature consisted of the following two steps. In the first step, the residual stresses in the meso-unit-cell were determined by simulating the last stage of the manufacturing process during which the composite was cooled down from the postcuring temperature at 315 °C to room temperature. The temperature dependent viscoelastic properties of the resin and the tows were used during this stage. It was also assumed that there were no residual thermal stresses in the composite at the beginning of the cooling cycle. In the second step, either pure shear or biaxial loads were applied to the meso-unit-cell. For the calculations at 315 °C, no residual stress determination was necessary and the mechanical loads could be directly applied simulating either pure shear or biaxial tension.

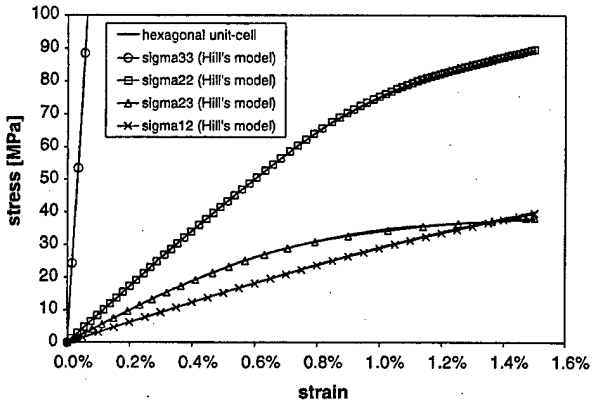

Fig. 6. Response of hexagonal unit-cell vs. Hill's model for a strain rate of 7%/min.

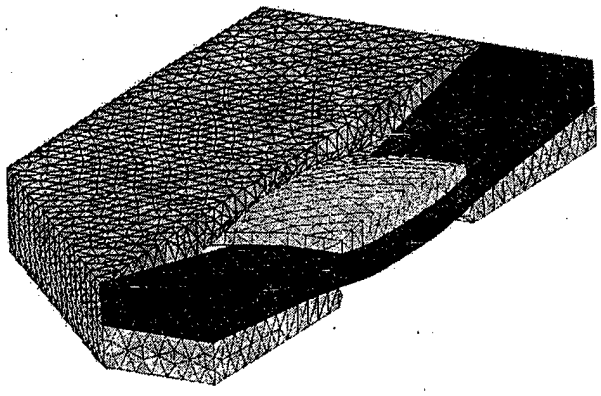

Fig. 7. Three-dimensional finite element representation of one-half of 8HS unit-cell. Resin pockets are not shown for simplicity.

For both room and elevated temperature computations the macro loads $\sigma_{ij}^{\text{macro}}$ (either pure shear or combined shear with biaxial tension) were at first applied to the meso-unit-cell. This can be written as:

$$\langle \sigma_{ij}^{\text{meso}} \rangle = \sigma_{ij}^{\text{macro}}, \tag{11}$$

where $\langle \sigma_{ij}^{\text{meso}} \rangle$ denotes the volume averaged stresses in the meso 8HS unit-cell. Consequently, the meso-stress distributions in the homogenous tows and the resin rich pockets were obtained. Then, for several selected locations inside the tows, the calculated local meso-stresses $\sigma_{ij}^{\text{meso}}$ were used as the boundary conditions in the micro hexagonal unit-cell according to the following expression:

$$\langle \sigma_{ij}^{\text{micro}} \rangle = \sigma_{ij}^{\text{meso}}. \tag{12}$$

As a result of the micro-scale computations, the micro-stresses $\sigma_{ij}^{\text{micro}}$ in the individual fibers, in the surrounding matrix and at the fiber/resin interface were determined. Eqs. (11) and (12) are expressed here in terms of stresses. However, the equivalent form for the strain tensors is also valid since the homogenous Hill model accurately describes the mechanical behavior of the hexagonal micro-unit-cell.

4. Failure prediction in 8HS T650-35/PMR-15 composite

4.1. Macro-response of meso-unit-cell to biaxial load

The numerically predicted macro shear stress vs. shear strain curves for the 8HS meso-unit-cell calculated at RT and at 315 °C for the biaxial/shear loading are shown in Fig. 8. For comparison, the experimentally determined shear stress vs. shear strain curves (two representative curves for each case) for the composite tested at room temperature and at 315 °C using the ±45° test are also presented in Fig. 8. An attempt was made to obtain the composite data at the three strains rates following the rates in the resin testing (0.4, 5 and 7%/min). However, it was found that at 7%/min the shear stress/shear strain curves for the composite exhibited far too

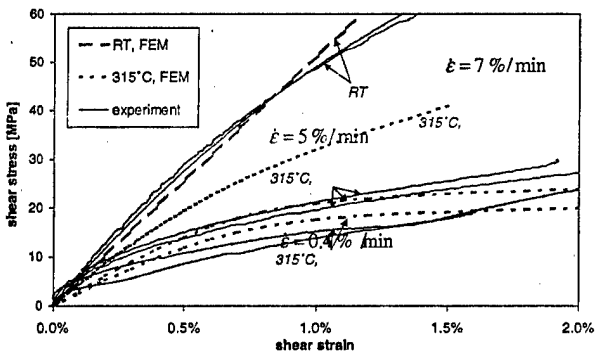

Fig. 8. Macro response of unit-cell (predicted) and 8HS T650-35/PMR-15 composite (experimental) to biaxial/shear load at room and elevated temperatures considering strain rate effect at 315 °C.

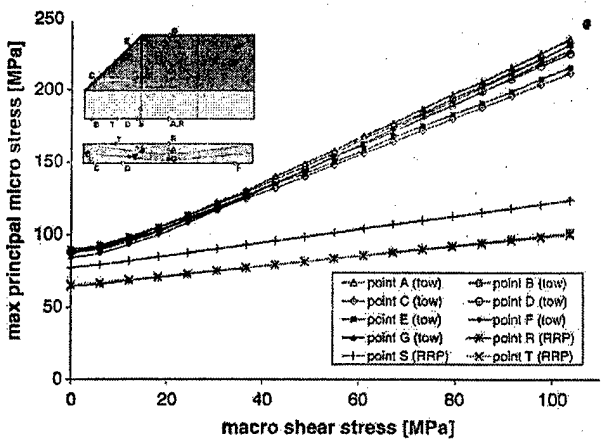

Fig. 9. Room temperature micro-stresses in the matrix at several locations of the meso-unit-cell subjected to combined biaxial tension and shear load.

much scatter. Therefore, these data are not shown in Fig. 8 for comparison with the numerical results.

It can be seen in Fig. 8 that overall the numerical predictions at room temperature agree well with the experiment for the ±45° test up to approximately 1.2% strain, despite the fact that the experimental curves appear to be slightly non-linear even for small loads. Above this strain, the experimental curves are highly non-linear due to damage initiation and progression [6]. Also, the experimental data at 315 °C followed reasonably well the predicted response at 0.4 and 5%/min considering the amount of scatter always present in the experimental results. Most importantly, the strain rate effect can be clearly seen both in the experiment and the model.

From the numerical data in Fig. 8, the shear moduli of the composite were also predicted at both temperatures. At room temperature, the predicted shear modulus of the composite was found to be 5.11 GPa which compared quite well with the experimental data from [11,14] ranging from 5.0 to 6.0 GPa. The numerically predicted modulus was found to be exactly the same for the shear and biaxial/shear load cases. It was shown experimentally that the values of the shear modules of the composite determined from the Iosipescu and ±45° tests were also quite similar [11]. At 315 °C, the modulus was predicted to be 4.27 GPa at 7%/min for shear strains smaller than 0.1% and was the same for both loading conditions. The predicted moduli at 0.4 and 5%/min were 3.1 and 2.7 GPa which could not be compared with the experiment due to the significant amount of scatter in the curves shown in Fig. 8 for small strains.

4.2. Micro-stress distributions as a function of load and temperature

To be able to predict the initiation of intralaminar damage in the 8HS woven T650-35/PMR-15 composite, the distributions of micro-stresses as a function of temperature and external loads must be determined. Fig. 9 illustrates the maximum principal stress in the resin in several locations of the composite subjected to biaxial/shear loads (±45° test) at room temperature. Seven locations (points A–G) were selected inside the tows and the micro-stresses at these points were determined using the micro-unit-cell. The remaining three points (R, S and T) were located in the resin-rich pockets of the meso-unit-cell. The results show that the stresses in the resin inside the tows were in a relatively small range from 212 to 236 MPa for an external macro-shear stress of 100 MPa. Also, the stresses in the resin pockets were quite uniform ranging from 100 to 123 MPa for the same external load. The stress distributions under pure in-plane shear were very similar to the biaxial/shear case. At high temperature the trends in the shear stress distributions were also similar with the stresses in the tows, approximately two times higher than in the resin pockets, however, the magnitudes of the stresses at 315 °C were significantly lower.

4.3. Failure initiation in Iosipescu and ±45° tests

The values of the maximum principal micro-stresses in the matrix between the fibers at point A (see Fig. 9) of the meso-unit-cell at room temperature and at 315 °C are shown in Figs. 10 and 11, respectively. The maximum principal micro-stresses were calculated as a function of external macro-shear loads for the cases of in-plane pure shear (Iosipescu) and biaxial/shear (±45°) loads. It can be seen in Fig. 10 that when no external loads are applied at room temperature, the micro-stress is equal to the residual principal micro-stress in the matrix. When external shear macro-loads are applied, the micro-stresses in the matrix increase at room and elevated temperatures for both the Iosipescu and ±45° off-axis load cases. It can be observed however that micro-stresses increase more rapidly in the ±45° case than in the case of the Iosipescu test both at room (see Fig. 10) and elevated (see Fig. 11) temperatures.

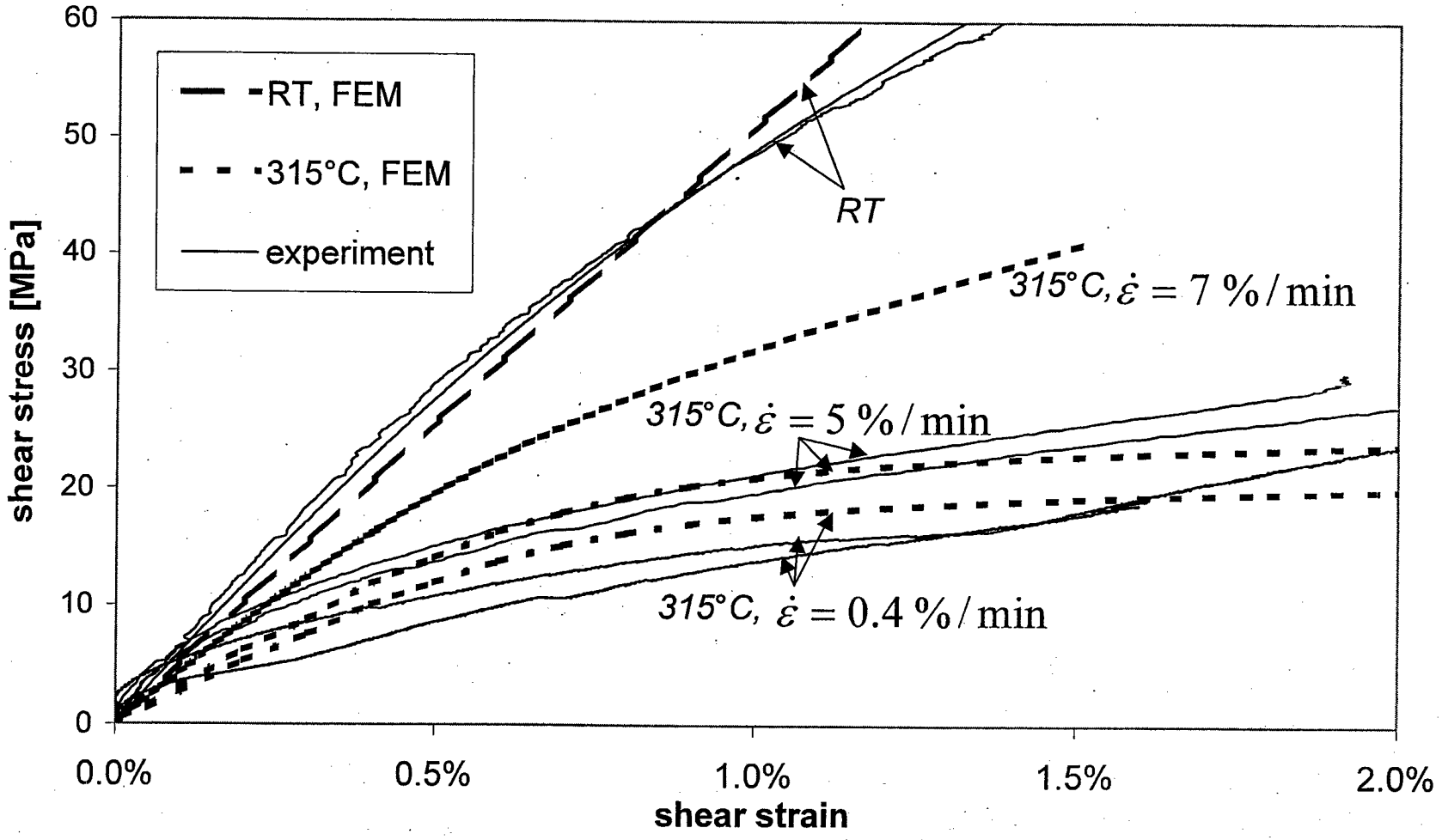
60
50
40
30
20
10
0
shear stress [MPa]
RT, FEM
315°C, FEM
experiment
RT
315°C, $\dot{\varepsilon} = 7\ \%/\min$
315°C, $\dot{\varepsilon} = 5\ \%/\min$
315°C, $\dot{\varepsilon} = 0.4\ \%/\min$
0.0%
0.5%
1.0%
1.5%
2.0%
shear strain

Figure 8.

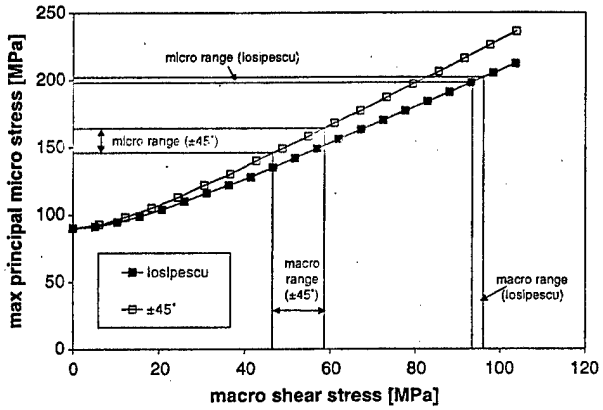

Fig. 10. Micro maximum principal stress in the matrix at room temperature for point A.

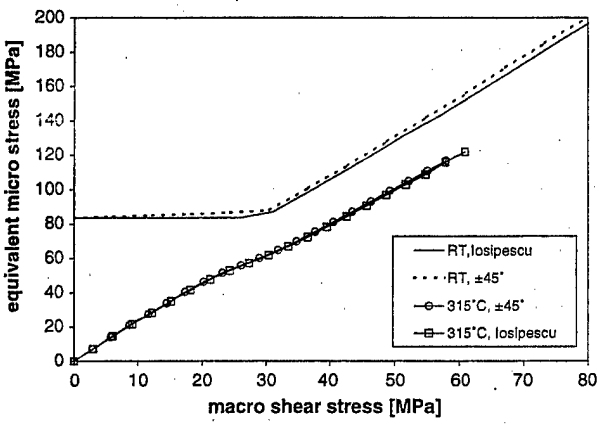

Fig. 12. Micro equivalent stresses in the matrix at point A at room and elevated temperatures.

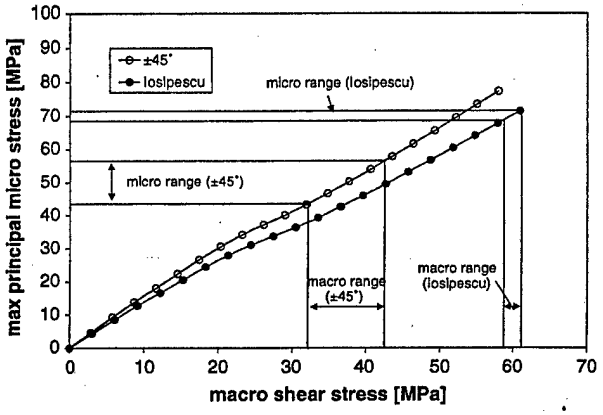

Fig. 11. Micro maximum principal stress in the matrix at 315 °C for point A.

In Figs. 10 and 11, in addition to the calculated maximum principal micro-stresses in the matrix, the possible ranges of micro-stresses at failure are also indicated for the two test conditions. The stresses were determined from the critical macro-shear stresses for the significant onset of AE [10,11,14], which were assumed to be the critical loads for the initiation of tow micro-cracking in the composite. The principal micro-stresses in the matrix for the initiation of tow micro-cracking for the Iosipescu and ±45° tests at room temperature and at 315 °C were also determined and are shown in Table 4.

Table 4
Maximum principal micro-stresses at the initiation of damage at point A in 8HS woven T650/PMR-15 composite

Test	Micro-stress in the resin [MPa]	
	±45°	Iosipescu
at RT	155 ± 9	200 ± 2
at 315 °C	50 ± 7	70 ± 2

The effect of loading conditions (in-plane pure shear vs. combined biaxial and shear) on the initiation stresses can be seen if the principal micro-stresses in the matrix are compared for the two load cases. However, if the maximum equivalent (von Mises) micro-stresses in the matrix are obtained (Fig. 12) no difference in the stresses can be seen between the Iosipescu shear and ±45° test. Therefore, the differences in the two tests regarding the initation stresses can only be observed if the maximum principal stress criterion is applied.

5. Discussion

The micro- and meso-stress analyses in the woven T650-35/PMR-15 composite were performed to predict the initiation of intralaminar failure of the composite both at room temperature and at 315 °C under in-plane shear and biaxial/shear loads. It is important to be able to either measure or predict the initiation of damage in the composite since the strength of the composite under in-plane shear is less than 10% of its ultimate tensile strength [10,11,14]. The strength is even lower if the composite is subjected to biaxial tension along the warp and fill tows in addition to shear. Under these two loading conditions woven composites exhibit the lowest resistance to damage initiation, which can be especially low at elevated temperatures [14]. This already low resistance to damage could be further reduced by chemical and physical aging due to the increase in residual stresses with aging and chemical degradation [21,23]. Moreover, the effects of manufacturing on the resistance to damage initiation in the composites can be significant [19].

The room temperature visco-elastic approach used in this research has also been previously applied in the residual stress analysis of unidirectional and woven

T650-35/PMR-15 systems [13]. Since the numerical predictions of the residual stresses could be experimentally verified, high confidence was gained regarding the accuracy of the visco-elastic data. Moreover, the good agreement between the shear stress vs. shear strain diagrams up to 1.2% strain at room temperature illustrated in Fig. 8 further supports the argument that the physical properties of the matrix and the elastic properties of the fibers were correctly assumed.

The high temperature analysis required an approach which would also consider the plastic and strain rate effects. It was shown that based on the non-linear response of the neat polyimide resin, the elasto-plastic properties of the tows and the woven system could be predicted at 315 °C by employing the meso- and micro-unit-cell models. Also, the strain rate effect was correctly accounted for due to the good agreement between the experimental and numerical data shown in Fig. 8. It was also observed that the elasto-plastic behavior of the tows could be very accurately described by Hill's model for anisotropic materials. Therefore, Hill's model could be used as a link that allows for the load transfer between the micro- and the meso-scale computations.

Certainly, shear testing of woven composites is not a straightforward process. There are several highly undesirable effects, which can affect the shear strength data. Some of the effects were quite apparent in the failure analysis of the 8HS T650-35/PMR-15 system. Despite the fact that the Iosipescu shear and ±45° tensile tests are popular in the shear testing of woven composites, none of them is without significant problems. Let us evaluate both tests to be able to comprehend the complexity of the problem.

First of all, the stress field in the gage section of the ±45° specimens is biaxial with tensile normal stresses along the fill and warp tows and shear stresses being of the same magnitude [6,11]. This obviously affects the micro-stresses [15] and the initiation of intralaminar failure [10,11,14]. In addition, the edge effect in the ±45° specimens is substantial both at room [10] and elevated [14] temperatures significantly affecting the initiation of damage and the ultimate composite strength. For example, at room temperature the shear strength of the 12.5 mm wide ±45° 8HS T650-35/PMR-15 specimens was found to be as low 75 MPa and as high as 92 MPa for the 50 mm wide specimens [10]. At 315 °C the edge effect was observed to be almost as strong [14]. This means that any damage initiated in the gage section of the ±45° specimens is affected by the edge effect. This also means that the edge effect needs to be incorporated into the micro- and meso-finite element models, which cannot be done at present.

In the Iosipescu specimens, the edge effect must also be present. Since no detailed analysis of the edge effect in the woven graphite/polyimide Iosipescu specimens has ever been conducted, it is impossible to evaluate the influence of the edge effect on the strength data in Table 1. However, there is another highly undesirable effect which makes the monitoring of damage initiation in the woven Iosipescu specimens very difficult both at room and elevated temperatures. On loading, the initiation of damage does not usually occur in the 8HS T650-35/PMR-15 composite in the specimen gage sections [11]. Instead, interlaminar cracks were observed to occur on the notch faces of the specimens due to out of plane shear and tension stresses present in these areas (see Fig. 13(a)). Very similar effects have been observed to occur in the shear testing of unidirectional composites using the Iosipescu test [34]. Instead of intralaminar failures due to shear developing in the specimen gage sections, tensile cracks have been observed to initiate along the notches (see Fig. 13(b)) at stresses far below those required to initiate pure shear failure. Obviously, if AE is used to monitor the failure process in woven Iosipescu specimens the initiation of damage outside the specimen gage section will not be distinguished from the failure in the gage section. Therefore, the stress data for initiation of intralaminar damage in the woven Iosipescu specimens are affected by the damage occurring outside the gage section.

It has also been shown in this research that the strain rate effect at high temperature is strong both in the case of the neat resin (Fig. 3) and its woven composite (Fig. 8). In order to compare the two tests (Iosipescu vs. ±45°) and predict micro-failure of the composite irrespective of the specimen geometry, the strain rate effects in the ±45° and Iosipescu tests must be considered. This however, could not be accomplished without making some questionable assumptions affecting significantly the numerical comparison of the two tests at high temperature. The numerical predictions of the micro-stresses in the composite for the shear and biaxial/shear loads at high temperature were obtained for a strain rate of 7%/min. However, even in this case the data had to be linearly extended following the dashed line shown in Fig. 3, otherwise the predicted average meso-stresses would be too low to be comparable with the macro-stresses at failure in Table 2. It can be immediately

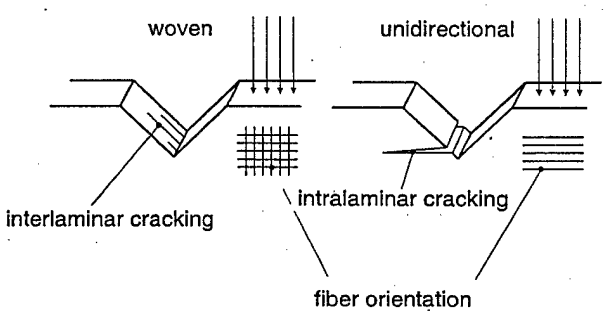

Fig. 13. Locations of damage initiation in unidirectional and woven Iosipescu specimens.

observed that the same approach could not be used for the other two strain rates since the extension of the other curves would be horizontal.

According to Table 1 and Fig. 11, the range of macro-stresses for the initiation of tow micro-cracking for the Iosipescu (shear) test is 94.8 ± 1.3 MPa, whereas the range for the ±45° test was 59.9 ± 1.2 MPa. Using the data in Fig. 3 for 0.4 and 5%/min strain rates, the predicted macro-stresses in the composite would always be significantly below the experimentally observed ranges. Only the extension of the data for a strain rate of 7%/min allowed these ranges to be approached and exceeded. However, the assumed strain rate of 7%/min differed from the strain rates of the Iosipescu and ±45° tests at 315 °C which were approximately 5%/min and 0.3%/min, respectively for an axial displacement rate of 1 mm/min. This means that the high temperature modeling of the ±45° test did not represent the actual testing conditions, grossly overestimating the actual micro-stresses.

Considering all of the above complexities and inaccuracies in the shear testing of woven graphite/polyimide composites, the only approach is to compare the experimental data with high quality numerical predictions. Again, there are also serious problems on the modeling side of the approach, as stated above, which can lead to significant errors in the failure predictions. Therefore, instead of comparing the actual magnitudes of micro-stresses in both specimens, trends in stress distributions should be examined as a function of temperature and loading conditions. Certainly, the micro-stress data presented in Figs. 10 and 11 and in Table 4 agree very well with the experimental results in Table 1. Since the principal micro-stresses in the matrix at room temperature and at 315 °C are higher for the biaxial/shear load case (±45°) than under in plane shear (Iosipescu), this clearly explains why the initiation of intralaminar damage in the Iosipescu specimens was always observed to occur at significantly higher shear stresses than in the case of the ±45° test (see Table 1).

The accuracy of the micro-failure predictions can easily be observed in the data presented in Table 4. Since the criterion for failure of tow micro-cracking should be the same in both specimen geometries for a given temperature and strain rate, the maximum principal micro-stresses for the initiation of micro-failure in the matrix between the fibers shown in this table should also be the same, irrespective of the assumed boundary conditions. This is however, not the case both at room temperature and at 315 °C. At room temperature and at 315 °C the ratios of the micro-stresses in the matrix (maximum principal) between the Iosipescu and ±45° test are 1.29 and 1.4, respectively. In a perfectly accurate analysis the ratios should be one. The fact that the ratios are above one clearly shows the error in the entire combined numerical/experimental failure prediction approach presented in this work. It seems that at room temperature the dominant factor affecting the accuracy of the prediction is the edge effect which was not considered in the model. The uncertainty of the experimental macro-stresses at failure in the Iosipescu test, as discussed above, also contributed to the observed difference in the numerically predicted micro-strengths in Table 4. At high temperature, in addition to the above two effects, the differences in the experimental strain rates of the Iosipescu and ±45° test, and the assumed strain rate in the modeling further contributed to the overall errors in the failure predictions.

Another issue in the failure predictions is the location of failure. If the data presented in Fig. 9 are analyzed, it can be noticed that under external loads the maximum principal micro-stresses in the matrix inside the tows increase much more rapidly that the stresses in the resin rich pockets. Therefore, the tows are the regions where the intralaminar tow micro-cracks should be observed at first. Also, since the maximum micro-stresses were found to be very similar in different locations inside the tows, it can be concluded that the distribution of tow micro-cracking in the composite should be uniform at the initiation of damage. These predictions agree very well with the SEM observations described in [10,11,14,19].

6. Conclusions

Visco-elastic and elasto-plastic computations of micro- and meso-stresses in an 8HS T650-35 composite have been performed considering two external loading boundary conditions simulating either in-plane pure shear or in-plane biaxial tension in addition to shear. An attempt was made to compare the critical loading conditions for the initiation of intralaminar damage in the composite subjected to the above two load cases at room temperature and at 315 °C and to explain the damage initiation in the composite subjected to the Iosipescu and ±45° tensile tests. When comparing the mechanical behavior of the composite subjected to the two tests, significant experimental and numerical problems were encountered. This made the exact comparison of the two tests less accurate with regard to damage initiation. However, the experimentally observed trends in the micro-stresses at failure agreed well with the numerical simulations both at room temperature and at 315 °C. It was also shown that the macro-response of the composite to shear could be accurately predicted as a function of temperature and in-plane shear dominated loads if the actual composite architecture as well as the fiber and matrix properties are considered in the numerical analysis.

Acknowledgements

This research was supported by the Air Force Office of Scientific Research and NASA Glenn Research Center under joint grant F49620-00-1-0159. Additional funds were also provided by the National Science Foundation and the University of Denver from a Major Research Instrumentation Program; Instrument Development and Acquisition grant# CMS-9977735.

References

[1] Wilson D. High Perf Polym 1993;5:77.
[2] Searles K, McCarthy J, Kumosa M. Comp Sci Technol 1998;58:1607.
[3] Gao F, Boniface L, Ogin SL, Smith PA, Greaves RP. Comp Sci Technol 1999;59:123.
[4] Searles K, Odegard G, Castelli M, Kumosa M. J Comp Mater 1999;33:2038.
[5] Seferis JC, Chung K, Buehler FU, Takatoya T. Polymer Degrad Stab 2000;68:43.
[6] Odegard G, Searles K, Kumosa M. J Mech Comp Mater Struct 2000;7:129.
[7] Odegard G, Kumosa M. Comp Sci Technol 2000;60:2979.
[8] Benedikt B, Kumosa M, Predecki PK, Kumosa L, Castelli MG, Sutter JK. Comp Sci Technol 2001;61:1977.
[9] Benedikt B, Predecki P, Kumosa L, Armentrout D, Sutter JK, Kumosa M. Comp Sci Technol 2001;61:1995.
[10] Odegard G, Armentrout D, Searles K, Kumosa L, Sutter JK, Kumosa M. Comp Tech Res 2001;23:204.
[11] Kumosa M, Odegard G, Armentrout D, Kumosa L, Sutter JK. Comp Tech Res 2002;24:3.
[12] Sutter K. Proceedings of the High Temple Workshop XXII 2002. p. 21.
[13] Benedikt B, Rupnowski P, Kumosa L, Sutter JK, Predecki PK, Kumosa M. Mech Adv Mater Struct 2002;9:375.
[14] Gentz M, Armentrout D, Rupnowski P, Kumosa L, Sutter JK, Kumosa M. J Comp Tech Res 2003;25:22.
[15] Rupnowski P, Kumosa M. Comp Sci Technol 2003;63:785.
[16] Benedikt B, Rupnowski P, Kumosa M. Acta Mater 2003;51:3483.
[17] Han MH, Nairn JA. Comp Part A 2003;34:978.
[18] Allerd RE, Wesson SP, Shin EE, Inghram L, McCorkle L, Papadopoulos D, et al. High Perf Polym 2003;15:395.
[19] Gentz M, Armentrout D, Rupnowski P, Kumosa L, Shin E, Sutter JK, et al. Comp Sci Technol 2004;64:203–20.
[20] Benedikt B, Kumosa M, Armentrout D, Kumosa L, Sutter JK, Predecki PK. Mech Adv Mater Struct 2004;11:31.
[21] Benedikt B, Gentz M, Kumosa L, Rupnowski P, Sutter JK, Kumosa M. Comp Part A 2004;35:667.
[22] Rupnowski P, Gentz M, Sutter JK, Kumosa M. Proc R Soc: Math, Phys Eng Sci, in press.
[23] Gentz M, Benedikt B, Kumosa M, Sutter JK. Comp Sci Technol 2004;64:1671.
[24] Rupnowski P, Gentz M, Sutter JK, Kumosa M. Comp Part A, in press.
[25] ASTM. D5379/D5379M-98.
[26] ASTM. D3518/D3518M-94 (2001).
[27] Eshelby JD. Proc R Soc London 1957;A241:376.
[28] Mori T, Tanaka K. Acta Metall 1973;21:571.
[29] Roberts GD, Malarik DC, Robaidek JO. NASA Tech Memorandum 1991;103768:10.
[30] Swan SA. Aging effects on fracture properties of polyimide neat resin. MSc Thesis: University of Houston; 1997.
[31] Searles K, Odegard G, Kumosa M. Comp Part A 2001;31:1627.
[32] Whitcomb JD, Chapman CD, Tang X. J Comp Mater 2000;34:724.
[33] Hill R, editor. The mathematical theory of plasticity. Oxford: Clarendon Press; 1983.
[34] Odegard G, Kumosa M. Comp Sci Technol 2000;60:2917.

10.1098/rspa.2004.1358

FirstCite e-publishing

THE ROYAL SOCIETY

An evaluation of elastic properties and coefficients of thermal expansion of graphite fibres from macroscopic composite input data

BY P. RUPNOWSKI[1], M. GENTZ[1], J. K. SUTTER[2] AND M. KUMOSA[1]

[1] *Center for Advanced Materials and Structures, Department of Engineering, University of Denver, 2390 S. York Street, Denver, CO 80208, USA* (mkumosa@du.edu)

[2] *NASA Glenn Research Center at Lewis Field, 21000 Brookpark Road, Cleveland, OH 44135, USA*

Received 4 August 2003; accepted 12 May 2004

In this work, a methodology has been presented for the evaluation of stiffness properties and temperature-dependent coefficients of thermal expansion of continuous fibres from the macroscopic properties of either unidirectional or woven composites. The methodology was used to determine the stiffness and thermal properties of T650-35 graphite fibres from the macroscopic input data of unidirectional and woven composites based on the same fibres embedded in a PMR-15 polyimide matrix. In the first part of the analysis, the fibre properties were determined directly from the unidirectional composite macro data using the inversed Eshelby–Mori–Tanaka approach. Subsequently, certain fibre properties were additionally evaluated indirectly from the woven composite, using the finite-element method and the concept of a representative unit cell.

It has been shown that the temperature-dependent coefficients of thermal expansion of the fibres can be estimated from the unidirectional composite macro data with significantly smaller errors than in the case of the elastic properties. It has also been shown that the errors in the evaluation of the elastic properties of the fibres from the macro unidirectional composite data could be significantly reduced if the fibres were placed in a stiff matrix material: much stiffer than the polyimide resin. The longitudinal and transverse coefficients of thermal expansions and the shear modulus of the T650-35 fibres determined from the unidirectional composite analysis were successfully verified by investigating the woven composite.

Keywords: graphite fibres; properties; indirect methods; elastic constants; coefficients of thermal expansion; Eshelby–Mori–Tanaka

1. Introduction

For the accurate determination of micro- and meso-stress distributions in composite materials, the physical properties of their constituents must be known *a priori*. The difficulties associated with the proper characterization of fibre and matrix properties in the numerical simulations of internal micro-stresses have recently been encountered

© 2004 The Royal Society

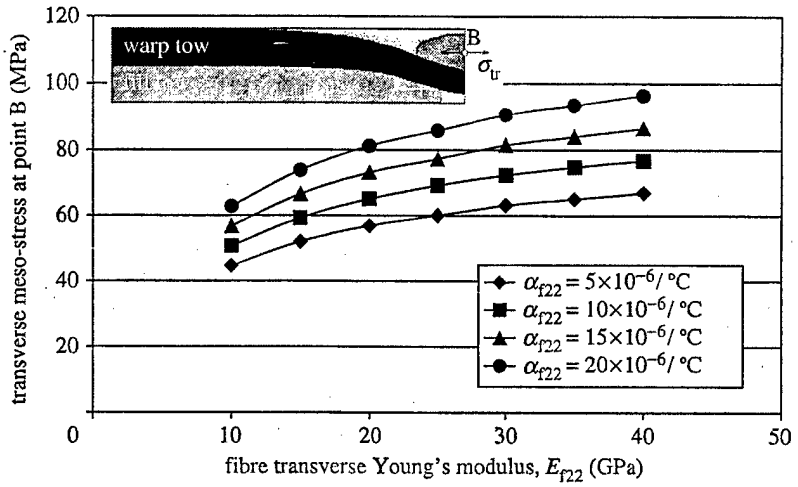

Figure 1. Effects of E_{f22} and α_{f22} on transverse meso-stress in a woven 8HS composite.

in the failure analysis of advanced unidirectional and woven graphite fibre/polyimide matrix composite systems for aerospace applications (Rupnowski & Kumosa 2003; Gentz *et al.* 2003, 2004). Since these composite systems always exhibit large residual thermal stresses, an accurate determination of the internal stress distributions in the composites on the micro-level is critical for the prediction of their failure properties. Obviously, the final results of any numerical simulations of micro-stress distribution in a composite material will be very strongly dependent on its architecture, manufacturing and loading conditions, and on the physical properties of its constituents.

Usually, the longitudinal properties of graphite fibres are readily available from fibre manufacturers. However, their transverse properties such as the transverse stiffness and coefficient of thermal expansion are frequently not accessible. Good examples of this are M40J and M60J high-stiffness graphite fibres (Gentz *et al.* 2004). These fibres are currently being used as the reinforcing material in high-temperature polyimide matrix composites for certain aerospace applications (Sutter 2002). Since these composites develop large residual stresses during manufacturing resulting, in some cases, in tow micro-cracking (Gentz *et al.* 2004), the accurate determination of their mechanical strength is critical for their successful application. This cannot be accomplished, however, if the magnitudes and distributions of residual stresses in the composites at different stages of manufacturing and in-service are not correctly established.

It can be easily shown, using the methods developed and presented by Rupnowski & Kumosa (2003), that the residual stresses in woven T650-35/PMR-15 graphite/polyimide composites on both the micro- and meso-scale clearly depend on the elastic and thermal properties of the graphite fibres. The transverse stiffness of the fibres E_{f22} and the transverse coefficient of thermal expansion α_{f22} are especially important in the residual stress analysis of these composites. However, the published values of E_{f22} and α_{f22} of T650-35 graphite fibres vary significantly. The transverse stiffness of T650-35 fibres was reported to be in a range from 13.8 GPa to 40 GPa (Wagoner & Bacon 1989; Peebles 1995; Donnet *et al.* 1998; Searles *et al.* 2001; Russell 1989; Benedikt *et al.* 2001*a*, 2002). The value of the transverse coeffi-

cient of thermal expansion (CTE) was found to be $7.8 \times 10^{-6}\ ^{\circ}\mathrm{C}^{-1}$ by Wagoner & Bacon (1989) and $10.0 \times 10^{-6}\ ^{\circ}\mathrm{C}^{-1}$ by Benedikt *et al.* (2001*a*, 2002). Such a large discrepancy and uncertainty in the elastic constants of graphite fibres result in significant problems when performing micro- or meso-stress simulations. The transverse residual stresses in the tows of an eight-harness-satin (8HS) woven T650-35/PMR-15 composite could change by up to 30% (figure 1) when the transverse properties of graphite fibres are varied in the range given above.

Similar difficulties have arisen in the modelling of micro- and meso-stresses in woven composites based on the T650-35, M40J and M60J fibres subjected to in-plane shear-dominated loads (Gentz *et al.* 2004). When modelling micro-stresses due to shear, the value of a fibre's shear modulus G_{f12} should also be known with high accuracy. For T650-35 fibres, the values of G_{f12} have been reported, ranging from 23.1 to 27 GPa (Wagoner & Bacon 1989; Peebles 1995; Donnet *et al.* 1998; Benedikt *et al.* 2001*a*, 2002). For other fibres, such as M40J and M60J, these properties are unknown.

Generally, one can consider direct (ASTM 1989, 2004) and indirect (e.g. Wagoner & Bacon 1989; Kowalski 1986) methods for the evaluation of fibre's thermal and elastic properties. The direct methods can be successfully employed to determine the E_{f11} and α_{f11} of graphite fibres. However, direct measurements of the transverse or shear properties of graphite fibres can be difficult to perform due to the small diameter of the fibres (*ca.* 6.8 μm for T650-35 fibres). Therefore, indirect measurements could be more feasible (Wagoner & Bacon 1989; Kowalski 1986). The indirect evaluation of fibre properties consists firstly of obtaining the macroscopic data of the composite and the pure matrix. Then, based on micro- and meso-mechanical models, one can extract the stiffness and CTEs of fibres. This method not only seems plausible, but also, in contrast to the direct measurements of individual filaments, it gives fibre properties that are averaged over the entire specimen.

There are errors associated with all experimental measurements. Therefore, when the macroscopic properties of a composite, obtained, for example, by mechanical testing, are used, it is important to verify what the magnitudes of the experimental errors are and how they influence the final results of the indirect method. However, no one has attempted to perform a multi-parameter analysis of errors associated with the determination of fibre properties from the composite macroscopic data. The basic work in the field of determining fibre properties was done by Wagoner & Bacon (1989). Their data were subsequently cited in many publications (for example, Peebles 1995; Donnet *et al.* 1998) and the same accuracy was always used. For example, all values of the shear moduli are given with an accuracy of 0.1 GPa, which corresponds to 0.4% error in the case of the T650-35 fibre. However, as will be shown further in this paper, just because of the presence of voids in the composite (1% volume fraction), the error in the indirect evaluation of G_{f12} is at least 11% in the case of T650-35/PMR-15 composite. Thus, even a small error in the input data will yield a large discrepancy in the output results.

Taking into consideration the substantial error sensitivity, it seems obvious that, besides the application of an indirect technique, a detailed accuracy analysis must be performed. In this paper, a classical error analysis based on the differentials (Taylor 1982) and Monte Carlo (Landau & Binder 2000) methods applied to the inversed Eshelby–Mori–Tanaka model (Eshelby 1957; Mori & Tanaka 1973) will be employed to compute the errors in the indirect evaluation of graphite fibre properties. This

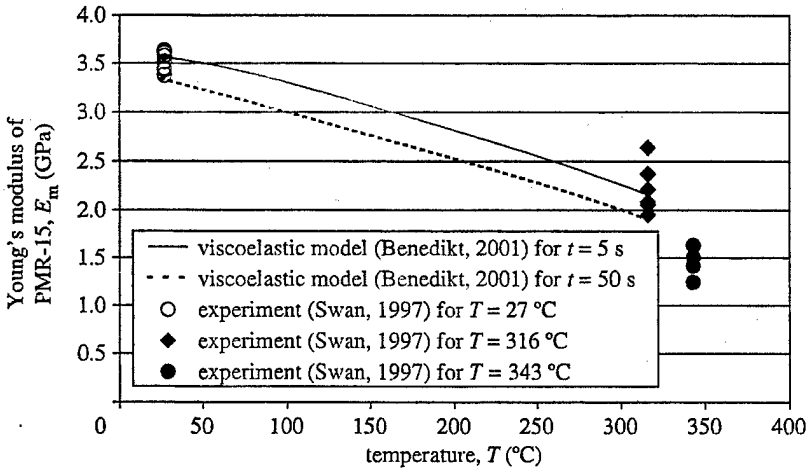

Figure 2. Young's modulus of PMR-15 as a function of temperature. Results taken from Benedikt *et al.* (2001*a*, 2002), based on those of Roberts *et al.* (1991) and Swan (1997).

approach will not only result in the error estimation, but will also indicate which input parameters need to be measured, and how accurately, in order to obtain reliable information about the graphite fibres. Additionally, composites with different matrices will be examined in order to design a composite system that is the least sensitive to the input parameters' errors.

2. Macroscopic input properties

Unidirectional and woven 8HS T650-35/PMR-15 composites were considered in this analysis. The available macroscopic input data for the micro-analysis, namely the elastic properties and CTEs of the composites and their PMR-15 polyimide resin were taken from Odegard & Kumosa (2000*a*, *b*), Searles *et al.* (2001) and Benedikt *et al.* (2001*a*, 2002). In addition, several other properties, not available in the open literature, were measured in this study.

(*a*) *PMR-15 polyimide resin*

PMR-15 is a thermoset polyimide resin for high-temperature applications with a glass transition temperature of *ca.* 345 °C. Swan (1997) determined the stress–strain response of PMR-15 for three temperatures (27, 315 and 343 °C) at a constant strain rate of 4.5% min^{-1}. Roberts *et al.* (1991) performed more detailed studies of the viscoelastic properties of the resin in the temperature range from 288 to 343 °C. Based on the data presented by Roberts *et al.* (1991) and Swan (1997), Benedikt *et al.* (2001*a*, 2002, 2004) proposed a viscoelastic formula for the shear modulus of PMR-15 as a function of time and temperature $G_{\mathrm{m}}(t, T)$ of PMR-15 for temperatures ranging from room temperature to 348 °C, according to equations (2.1).

$$G_{\mathrm{m}}(t, T) = G_{\mathrm{m}}(\xi, T_{\mathrm{ref}}), \tag{2.1\,a}$$

$$G_{\mathrm{m}}(t, T_{\mathrm{ref}}) = 10^{(\exp(0.16(-\log(t+0.001)+6.5)^{0.5})+7.5)}, \tag{2.1\,b}$$

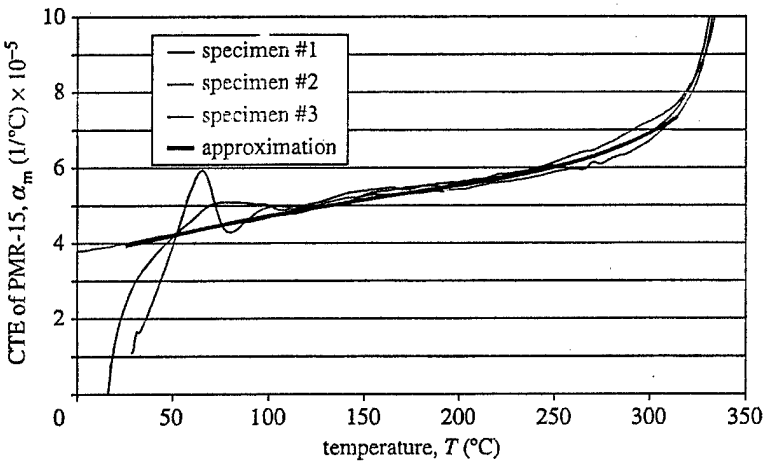

Figure 3. Thermal expansion coefficient of PMR-15 as a function of temperature from three specimens.

where

$$\xi(t) = \int_0^t \frac{\mathrm{d}t'}{a_h[T(t')]}, \tag{2.1 c}$$

$$a_h(T) = 10^{\exp(0.41(-T+348)^{0.28}-4.3)}, \tag{2.1 d}$$

with $T_{\mathrm{ref}} = 288\ ^\circ\mathrm{C}$. Using the above equation and assuming that the Poisson ratio for PMR-15 is constant (0.36), the range of the effective Young modulus E_{m} could be derived for any given temperature and time (figure 2 and table 1). The range of values of E_{m} obtained by changing time t from 5 to 50 s was considered in the error analysis as an uncertainty of the Young modulus. It should be stated that equation (2.1 *b*) is only valid for t ranging from 0 to $10^{6.5}$ s.

The temperature-dependent CTEs of neat PMR-15 at different temperatures were measured in this study using a Netzsch DIL 402C dilatometer. The same technique was used later on to determine the temperature-dependent CTEs of the unidirectional and woven composites both in and out of plane. All samples were dried before testing in vacuum at 110 °C for 24 h.

Three tests were performed on three different neat resin specimens. All three curves $\alpha_{\mathrm{m}}(T)$ were very similar (see figure 3) and could be described by

$$\alpha_{\mathrm{m}} = a^2(T + 273.15\ ^\circ\mathrm{C})[1 - 0.809aT - 258(aT)^3 + 21828(aT)^5], \tag{2.2}$$

where $a = 3.64 \times 10^{-4}\ ^\circ\mathrm{C}^{-1}$.

It is important to emphasize that the above approximation is accurate only from 25 to 315 °C and that in this range the discrepancy between different specimens is *ca.* $\Delta\alpha_{\mathrm{m}} = 6 \times 10^{-6}\ ^\circ\mathrm{C}^{-1}$.

(*b*) *Unidirectional T650-35/PMR-15 composite*

The elastic properties of a unidirectional T650-35/PMR-15 composite at room temperature and elevated temperatures were measured by Odegard & Kumosa

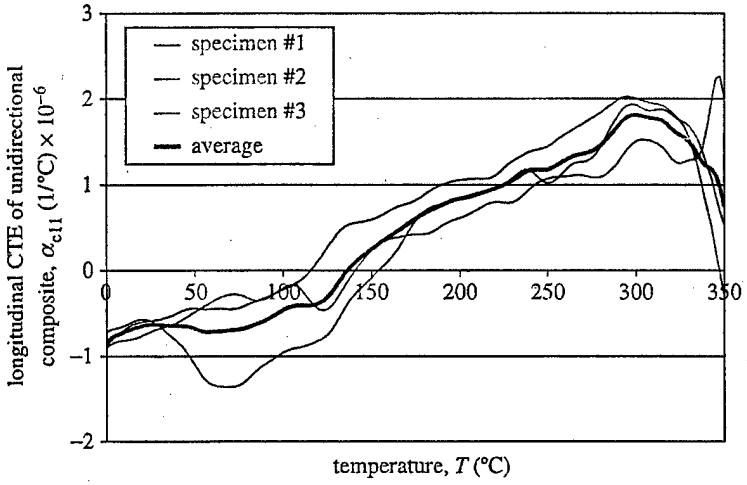

Figure 4. Longitudinal thermal expansion coefficient of unidirectional T650-35/PMR-15 composite as a function of temperature from three specimens.

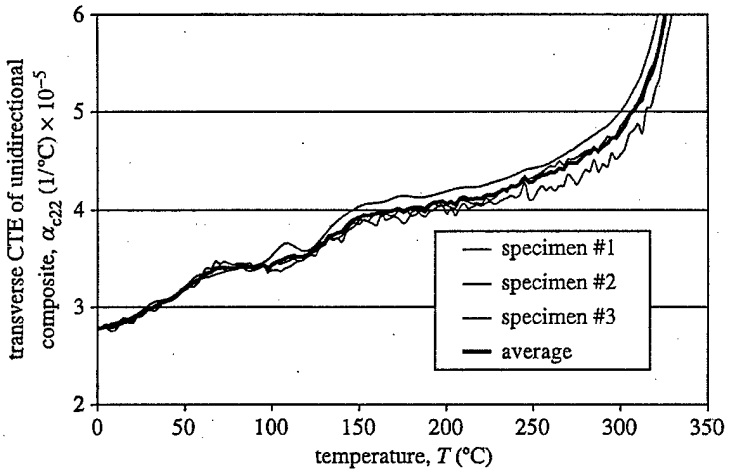

Figure 5. Transverse thermal expansion coefficient of unidirectional T650-35/PMR-15 composite as a function of temperature from three specimens.

(2000*a*). The tensile modulus along the fibres, E_{c11}, transverse modulus, E_{c22}, Poisson ratio along the fibres, ν_{c12}, transverse Poisson ratio, ν_{c23}, and the shear modulus, G_{c12}, were obtained at four different temperatures. For each temperature, either two or three specimens were tested with a displacement rate of 0.5 mm min^{-1}. In some cases, significant scatter in the elastic constants was observed. Due to the small number of tests, a proper evaluation of the scatter could not be performed. The elastic properties are presented in table 2, where Δ is the difference between the largest and smallest values of the properties at each temperature.

The longitudinal and transverse CTEs of the unidirectional composite were measured at temperatures ranging from −50 °C to 350 °C using three specimens for each fibre orientation (see figures 4 and 5). The largest differences between the measure-

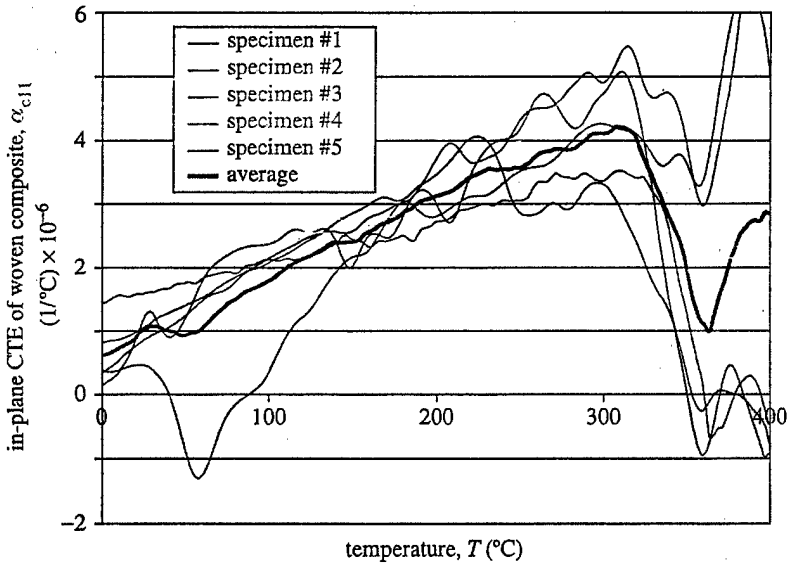

Figure 6. In-plane coefficient of thermal expansion of 8HS T650-35/PMR-15 composite as a function of temperature from five specimens.

ments were *ca.* $0.75 \times 10^{-6}\,^{\circ}\mathrm{C}^{-1}$ for α_{c11} and $3.5 \times 10^{-6}\,^{\circ}\mathrm{C}^{-1}$ for α_{c22}, respectively. The average values of the coefficients were used in subsequent calculations.

(*c*) *8HS T650-35/PMR-15 woven composite*

For the woven 8HS T650-35/PMR-15 system the shear modulus G_{c12} at room temperature was taken to be 5.5 ± 0.5 GPa (Kumosa *et al.* 2002), whereas the values of $E_{c11} = E_{c22}$ and v_{c12} were taken to be 76.9 ± 6.2 GPa and 0.08 ± 0.03, respectively, following Searles *et al.* (2001).

The in-plane (figure 6) and out-of-plane (figure 7) coefficients of thermal expansion of the woven composite as a function of temperature were measured in this study. The data shown in figure 6 were obtained from five specimens, whereas in the case of the out-of-plane CTE (figure 7) only three specimens were tested. It was found that the thermal expansion of the woven system in the out-of-plane direction was very similar to the behaviour of the neat PMR-15 resin and to the transverse response of the unidirectional composite. However, the in-plane CTE of the woven composite was dominated by the stiff fibres and therefore was much smaller than the out-of-plane CTE. The in-plane thermal expansion of the woven system was significantly larger than the expansion of the unidirectional composite along the fibres. It was also noted that both woven and unidirectional composite CTEs along the fibres exhibited temperature dependence.

3. Numerical procedures

Graphite fibres are anisotropic materials which can be described by five independent elastic constants, namely E_{f11}, E_{f22}, v_{f12}, v_{f23} and G_{f12} and two CTEs (α_{f11} and α_{f22}). There are a few significant differences between the analysis of unidirectional

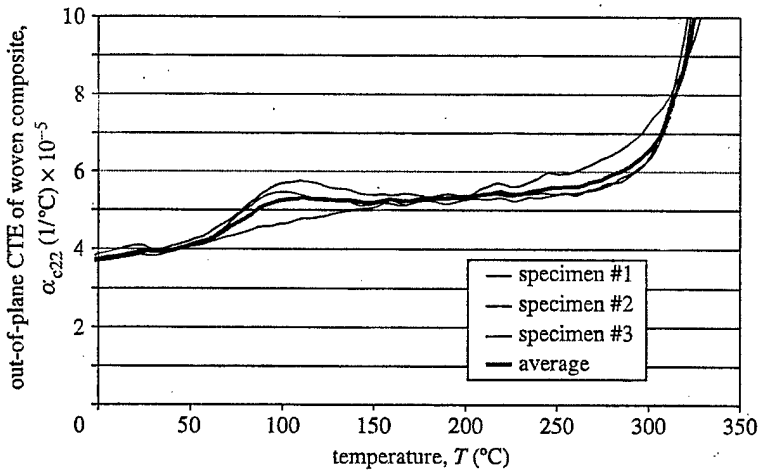

Figure 7. Out-of-plane coefficient of thermal expansion of 8HS T650-35/PMR-15 composite as a function of temperature from three specimens.

and woven systems. In the first case, a few analytical micro-mechanical models are available (e.g. Chamis 1984; Hashin 1979; Eshelby 1957; Mori & Tanaka 1973), which allow the expression of the macroscopic data of a unidirectional composite in terms of the properties of its constituents. Therefore, it is relatively easy to invert these equations and express the fibres' properties in terms of the macroscopic data of the composite and its neat resin. Another advantage of the exact, analytical micro-models of unidirectional composites is that a multi-parameter error analysis can be carried out using well-known differential (Taylor 1982) or Monte Carlo (Landau & Binder 2000) methods.

Contrary to the models for unidirectional composites, there are no available accurate, analytical models for woven composites. Therefore, numerical approximation must be used in order to derive the properties of a woven composite from the properties of its components, using, for example, finite-element (FE) techniques. The main disadvantages of the numerical micro/meso models for woven composites are that they cannot be inverted (from macro to micro) and the preparation of FE representations of woven composites is usually very time consuming. Due to these limitations, in this work the analyses of the woven system were used for one-parameter estimation only and for verification of the results that were obtained from the unidirectional system.

(*a*) *Evaluation of fibre elastic properties from unidirectional composite*

In this work, the approach taken by Eshelby (1957) and Mori & Tanaka (1973) was chosen to evaluate the fibre stiffness properties from the elastic properties of the unidirectional composite. It has been shown recently by Benedikt *et al.* (2003) that, in spite of the fact that the Eshelby–Mori–Tanaka model assumes uniform stress inside ellipsoidal inclusions, it agrees with the FE approach. In particular, it was found that the stiffness of an FE hexagonal unit cell was almost the same as the prediction from the Eshelby model with the Mori–Tanaka extension even when the volume fraction of fibres was very high (e.g. 70%). Secondly, contrary to FE or

Table 1. *Young's modulus of PMR-15 as a function of temperature*
(After Benedikt *et al.* (2001*a*, 2002) based on Roberts *et al.* (1991) and Swan (1997).)

temperature (°C)	resin properties	
	E_m (GPa)	ΔE_m (GPa (%))
21	3.36–3.57	0.21 (6)
121	2.90–3.20	0.3 (10)
204	2.51–2.79	0.28 (11)
260	2.23–2.50	0.27 (11)
315	1.90–2.15	0.25 (12)

iterative methods, the Eshelby approach is an entirely analytical model and therefore can be inverted, and the error analysis can be easily performed.

The Eshelby–Mori–Tanaka equation that expresses the stiffness matrix of a composite C_c in terms of the stiffness matrices of fibres C_f and matrix C_m can be found, for example, in Hull & Clyne (1996). The inversion of this expression, so that the stiffness matrix of fibres C_f can be evaluated, results in the formula

$$C_f = \left[\left(\frac{1}{f_v}-1\right)C_m(I-S)(C_m^{-1}-C_c^{-1})+I\right]\left[C_m^{-1}-(S-f_v(S-I))(C_m^{-1}-C_c^{-1})\frac{1}{f_v}\right]^{-1}, \tag{3.1}$$

where S is the Eshelby tensor in the matrix form, I denotes a 6×6 unity matrix and f_v stands for the volume fraction of fibres. Assuming that the composite and fibres are transversely isotropic, then their stiffness matrices that appear in formula (3.1) are related to the five independent engineering elastic constants by

$$C = \begin{bmatrix} E_{11}^{-1} & -v_{12}/E_{11} & -v_{12}/E_{11} & 0 & 0 & 0 \\ & E_{22}^{-1} & -v_{23}/E_{22} & 0 & 0 & 0 \\ & & E_{22}^{-1} & 0 & 0 & 0 \\ & & & \dfrac{2(1+v_{23})}{E_{22}} & 0 & 0 \\ & \text{sym.} & & & G_{12}^{-1} & 0 \\ & & & & & G_{12}^{-1} \end{bmatrix}^{-1} \tag{3.2}$$

The other important parameter that appears in equation (3.1) is the volume fraction of fibres f_v. In the unidirectional graphite/PMR-15 composite this parameter was measured by the acid digestion test (Benedikt *et al.* 2001*b*), and the average value of 53% was obtained. The void content was found to be less than 2% (Benedikt *et al.* 2001*b*). In the analysis presented in this paper, the effect of voids will be taken into account by varying the volume fraction of fibres in the range 52–54%.

Monte Carlo simulations, based on the inverse Eshelby–Mori–Tanaka model (equation (3.1)), were performed to obtain the elastic properties of T650-35 fibres for five specific temperatures (21, 121, 204, 260 and 315 °C). Each simulation consisted of 10^5 calculation steps. During each step, the input data (i.e. the elastic constants of the unidirectional composite and neat resin, and the volume fraction of fibres) were randomly chosen from the range defined by the assumed error ranges. The specific

Table 2. *Elastic properties of unidirectional T650-35/PMR-15 composite from Odegard & Kumosa (2000a)*

temperature (°C)	composite properties			
	E_{c11} (GPa)	E_{c22} (GPa)	v_{c12}	G_{c12} (GPa)
21	134.4–137.8 $\Delta = 3.4$ (3%)	9.2–9.6 $\Delta = 0.4$ (4%)	0.40–0.42 $\Delta = 0.02$ (5%)	5.3–7.8 $\Delta = 2.5$ (38%)
121	137.4–137.7 $\Delta = 0.3$ (0.2%)	7.0–7.4 $\Delta = 0.4$ (7%)	0.42–0.51 $\Delta = 0.09$ (20%)	3.5–3.8 $\Delta = 0.3$ (8%)
204	125.8–135.8 $\Delta = 10$ (8%)	6.9–7.5 $\Delta = 0.6$ (8%)	0.38–0.43 $\Delta = 0.05$ (12%)	2.4–2.9 $\Delta = 0.5$ (18%)
260	119.9–136.7 $\Delta = 17$ (14%)	5.0–5.9 $\Delta = 0.9$ (17%)	0.42–0.54 $\Delta = 0.12$ (25%)	1.2–2.2 $\Delta = 1.0$ (58%)
315	120.0–123.0 $\Delta = 3.0$ (3%)	6.0–7.0 $\Delta = 1.0$ (15%)	0.43– 0.58 $\Delta = 0.15$ (30%)	0.6–2.4 $\Delta = 1.8$ (120%)

values of error for each property were discussed above and are shown in tables 1 and 2. When the random process was executed, it was assumed that the probability is uniform in the given range. For example, according to table 2, the transverse Young's modulus E_{c22} of the unidirectional composite at 21 °C was randomly drawn from the range 9.2–9.6 GPa, and the probability of drawing any number in this range was the same. Next, for the drawn set of input data, the inverse Eshelby–Mori–Tanaka equation (3.1) was applied. Finally, the obtained results of the calculations led to the probability density function and cumulative probability density for all five unknown elastic constants of the T650-35 fibres.

(*b*) *Evaluation of fibre CTE from unidirectional composite*

For the calculations of micro- or meso-residual stresses in unidirectional and woven composites, it is important to know the CTEs of the fibres. In the case of graphite fibres the longitudinal and transverse CTEs (α_{f11} and α_{f22}) can potentially be a function of temperature. In this section, a methodology for extracting α_{f11} and α_{f22} from the macroscopic properties of a unidirectional graphite composite is presented.

Using the Eshelby–Mori–Tanaka model, the CTEs of the fibres were determined employing the following formula:

$$\alpha_f(T) = \frac{1}{f_v} C_f^{-1}[(C_m(T) - C_f)(S - f_v(S - I)) - C_m(T)](\alpha_m(T) - \alpha_c(T)) + \alpha_m(T), \quad (3.3)$$

where α_f, α_m and α_c denote the column vectors of the CTEs for the fibres, matrix and composite, respectively. The above equation was obtained by the inversion of the well-known formula published, for example, in Hull & Clyne (1996). According to equation (3.3), in order to find the thermal expansion coefficients of a fibre α_f, the stiffness matrices of that fibre and the neat resin must be known.

Thus, it can be seen that there are many input parameters involved in equation (3.3), and each of them is not exactly known. The uncertainties of the input data may consequently result in substantial errors in the output value of α_f. In

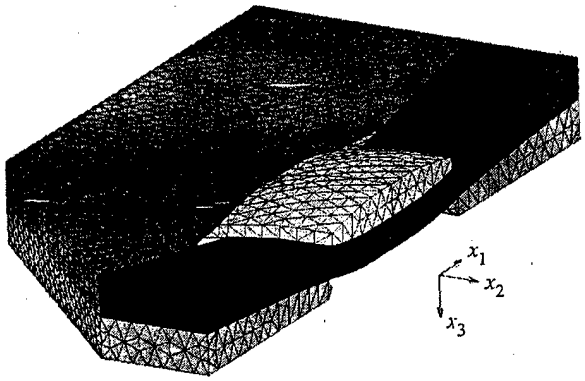

Figure 8. Three-dimensional FE representation of 8HS unit cell. Resin pockets are not shown in this figure.

this work, the average values of the fibre's CTEs and their errors were obtained by employing equation (3.3) and the Monte Carlo simulations. The analyses of α_f were performed for temperatures ranging from room temperature to *ca.* 315 °C in 2 °C increments. For each temperature increment, the maximum and minimum values of the fibres' CTEs were determined.

(*c*) *Evaluation of fibre elastic properties from woven composite*

The properties of graphite fibres can also be hypothetically obtained from macro-properties of woven composites. In order to do this, micro- and meso-scale models are required that relate the properties of the fibres to the macro-properties of the composites. There are many semi-analytical models available in the literature (e.g. Ishikawa & Chou 1983; Walsh & Ochoa 1996; Naik & Ganesh 1996; Naik 1995) that can be used to predict the stiffness of woven composite systems. All of them are based on the concept of a unit cell in which the stress and/or strain distribution are assumed in advance (usually it is constant stress or strain). It seems that the most accurate results can be obtained from the FE model of a unit cell representing a woven composite, since in such a model it is not necessary to assume in advance any strain and stress distributions.

A three-dimensional FE representation of an 8-harness satin (8HS) unit cell was prepared (figure 8) to investigate the effect of fibre properties on the elastic response of the woven composite (Rupnowski & Kumosa 2003). For any given set of fibre elastic properties, the FE representation allowed for the calculations of the following independent elastic constants of the woven composite: E_{c11}, E_{c33}, G_{c12}, ν_{c12} and ν_{c31} (where '3' denotes the out-of-plane direction). The results obtained could be subsequently compared with the experimental results for the 8HS T650-35/PMR-15 composite. Due to the limited available experimental data, the prediction of fibre properties could be based only on the in-plane properties of the composite.

As already stated, a FE model is not as comfortable to work with as an analytical one. In particular, it works only in one direction: it allows us to find the properties of the woven composite from the properties of its constituents (fibres and resin), i.e.

$$C_{8HS} = f(C_f, C_m, f_v, a), \tag{3.4}$$

where C_{8HS} is the stiffness of the 8HS woven composite, f_v is the volume fraction of fibres inside the tows, a stands for all necessary geometric parameters, and C_f represents five unknown elastic constants of the fibres. The opposite approach is not possible because the FE method is not able to provide the properties of the fibres (or tows) when the information about the matrix and woven composite is given. In other words, the FE model cannot be inverted, since it does not provide f^{-1} in the relation

$$C_f = f^{-1}(C_{8HS}, C_m, f_v, a). \tag{3.5}$$

Therefore, in order to obtain f^{-1} other techniques, such as, for example, optimization or Monte Carlo, need to be employed. Noting that it was necessary to deal with a five-dimensional space (five parameters are unknown) and assuming that optimization will require 10 simulations per one unknown parameter it can be shown that this gives 10^5 combinations. Thus, a full multi-dimensional FE analysis would take an unrealistic amount of time.

After taking into consideration the fact that not all elastic constants of the 8HS graphite/PMR-15 woven system are known, and that the multi-parameter FE simulations are very time consuming, the following simplified approach was used in this work. It is reasonable to assume that the in-plane Young modulus of a woven composite E_{c11} depends mainly on the unknown longitudinal and transverse Young moduli of the fibres (E_{f11} and E_{f22}), whereas the effect of the other elastic constants of the fibres can be neglected, i.e.

$$E_{c11} = f(C_f, C_m, f_v, a) \approx g(E_{f11}, E_{f22}, C_m, f_v, a). \tag{3.6}$$

For the T650-35 fibres, the value of E_{f11} is well known as it can be easily measured. Therefore, we can reduce our problem to a one-dimensional analysis with the relation $E_{c11} = h(E_{f22})$, which can be simply inverted in order to obtain E_{f22}.

Likewise, we can assume that G_{c12} is mainly a function of G_{f12}, C_m, f_v and a, whereas the contribution of the other fibre elastic constants, namely E_{f11}, E_{f22}, v_{f12} and v_{f23}, is very small. Thus, again we need to deal with only one parameter relation, which after inversion can potentially provide a good approximation of the shear modulus of the fibres, assuming that the shear modulus of the woven composite is given.

(*d*) *Evaluation of CTEs of 8HS T650-35/PMR-15 woven composite*

The FE model shown in figure 8 can also be used to predict the thermal response of the 8HS T650-35/PMR-15 composite and in particular its CTEs. By changing temperature, the model can predict the thermal strains and, consequently, by differentiating with respect to temperature, the thermal expansion coefficients can be calculated. In other words it can be said that the FE model of the 8HS system provides a numerical relation in the form of

$$\alpha_C(T) = f(C_m(T), C_f, \alpha_f(T), \alpha_m(T), a). \tag{3.7}$$

Ideally, this relation should be inverted to obtain α_f as a function of temperature T. However, it should be remembered that full multi-parameter FE method/Monte Carlo simulations are feasible but very time consuming. Therefore, after taking into consideration the time limitation, the FE thermal model was used in this work to

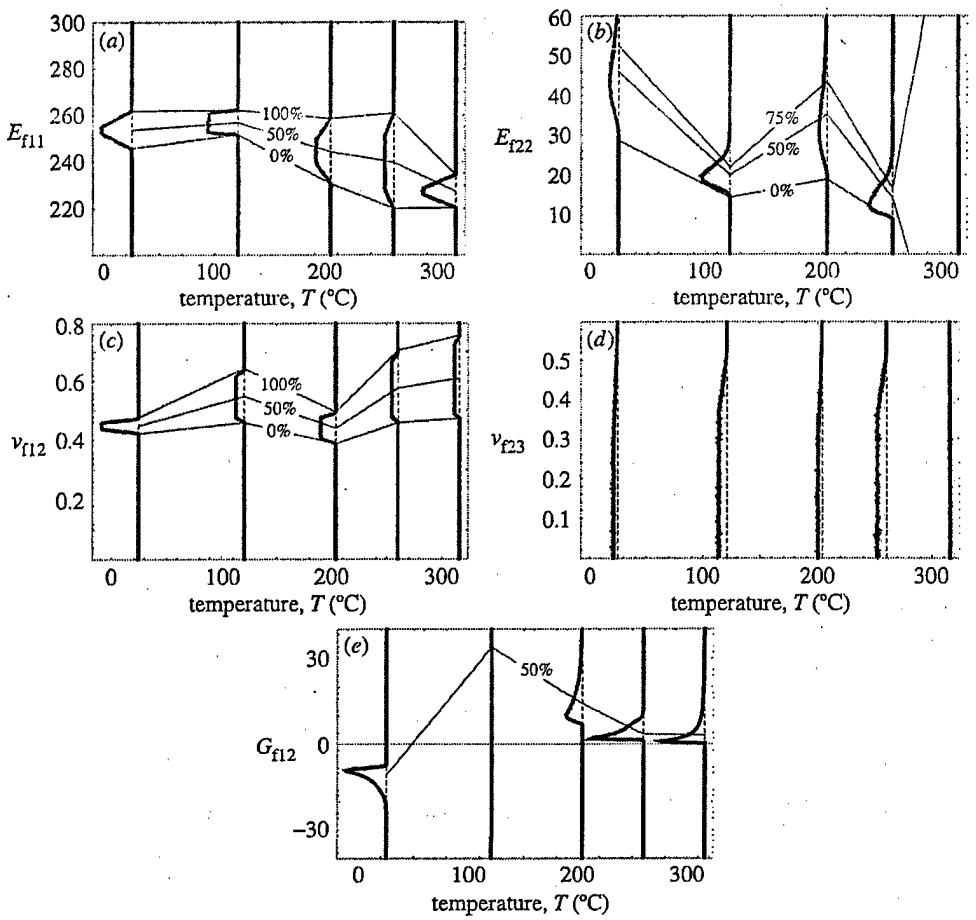

Figure 9. Probability distribution (thick lines) and cumulative distribution functions (thin lines) of calculated elastic properties of T650-35 fibres at five different temperatures: (*a*) longitudinal Young's modulus E_{f11}; (*b*) transverse Young's modulus E_{f22}; (*c*) longitudinal Poisson's ratio ν_{f12}; (*d*) transverse Poisson's ratio ν_{f23}; (*e*) longitudinal shear modulus G_{f12}.

verify whether the fibre thermal properties estimated from the unidirectional composite were accurate. The verification consisted of comparing the experimental data with the numerically predicted response of the woven system.

4. Results and discussion

(*a*) *Fibre properties determined from unidirectional composite*

The probability distribution and cumulative distribution functions of the calculated elastic properties for the T650-35 fibres at five different temperatures are shown in figure 9. In this figure, the vertical thick lines represent the probability distribution functions (PDFs) of the resultant elastic properties of the fibres. In each case, the probability is zero for very small and very large values of a given fibre property. The peaks in the middle of the PDF line correspond to the range where the actual value

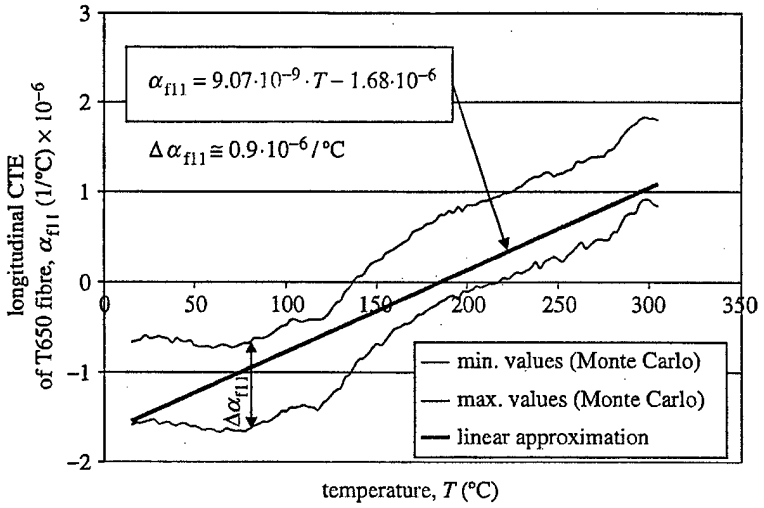

Figure 10. Determination of α_{f11} from thermal properties of T650-35/PMR-15 unidirectional composite.

of a specific property is expected. In figure 9 the cumulative distribution functions (CDFs) are also presented. For example, in figure 9*a*, the thin CDF lines denoted as 0% and 100% form a region containing all calculated values of E_{f11}.

The data presented in figure 9*a* clearly shows that the longitudinal Young modulus of fibres, E_{f11}, is somewhere between 230 and 260 GPa. According to figure 9*b*, E_{f22} could be greater than 12 GPa if the results for 315 °C are excluded. The upper limit of E_{f22} is not well defined in figure 9*b*, since values even larger than 60 GPa could be found. It should be noted that the data for E_{f22} are much more difficult to interpret than the E_{f11} case. The PDF peaks representing the distribution of E_{f22} are very wide at temperatures 21, 204 and 315 °C. The other problem is that the positions of the PDF peaks in figure 9*b* are not temperature independent. Therefore, in this case the most probable value of E_{f22} could not be accurately determined. This could be caused by systematic and/or random experimental errors in the input data, especially at high temperatures.

As illustrated in figure 9*c* the longitudinal Poisson ratio, ν_{f12}, was found to be between 0.4 and 0.8. However, if only the more credible, low temperature (21–204 °C) data are taken into account, then the possible region of ν_{f12} becomes 0.4–0.6. Figure 9*d* clearly shows that the transverse Poisson ratio ν_{f23} could not be determined. This was expected, since no value of the corresponding transverse Poisson ratio of the composite ν_{c23} could be found in the literature and used as the input data.

The predicted values of the longitudinal shear modulus G_{f12} of the fibres are depicted in figure 9*e*. According to the PDF line at 21 °C, only negative values of G_{f12} were obtained from the Monte Carlo simulation. This questionable result suggests that there must be a substantial, systematic error in the input data. Most probably the shear modulus used for the unidirectional composite, G_{c12}, as measured by Odegard & Kumosa (2000*a*) was significantly overestimated. For the same reasons, the calculations of G_{f12} at 121 °C and for higher temperatures could not give any reliable estimates.

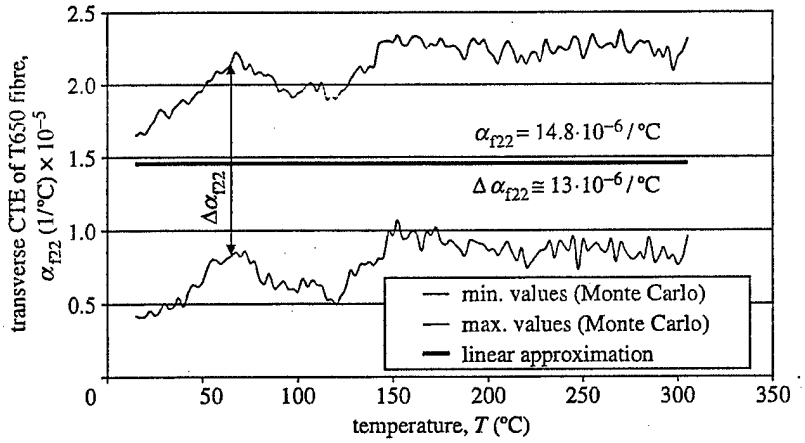

Figure 11. Determination of α_{f22} from thermal properties of T650-35/PMR-15 unidirectional composite.

The estimated thermal expansion coefficients of the fibres are shown in figures 10 and 11 as a function of temperature. The range between the curves in figures 10 and 11 corresponding to the minimal and maximal values is the location where the most probable values are expected. Using a regression technique, the best fit was estimated for the calculated data. In the case of α_{f22}, a constant, temperature-independent value equal to $14.8\times10^{-6}\ ^{\circ}\mathrm{C}^{-1}$ was found (figure 11). In the case of α_{f11}, it was not possible to find a constant value that would stay between the maximum and minimum curves for all considered temperatures. Thus, contrary to the previous case, a linear dependence had to be assumed and the best-fit approximation resulted in the empirical relation

$$\alpha_{f11} = 9.07 \times 10^{-9}T - 1.68 \times 10^{-6}, \tag{4.1}$$

which is valid from room temperature to 315 °C. In this formula the units of T and α_{f11} are °C and $^{\circ}\mathrm{C}^{-1}$, respectively.

The distance between the maximum and minimum values in figures 10 and 11 constitutes the uncertainty of the calculated CTEs of the T650-35 fibre. It can be seen that the errors of the calculated CTEs that stem from the uncertainties in the input parameters are approximately equal to 0.9×10^{-6} and $13\times10^{-6}\ ^{\circ}\mathrm{C}^{-1}$ for α_{f11} and α_{f22}, respectively. It is also interesting to note that these error values were found to be practically temperature independent.

The transverse coefficient of thermal expansion, α_{f22}, of the T650-35 graphite fibres was found to be essentially independent of temperature, if the data presented in figure 11 are examined. However, the longitudinal coefficient, α_{f11}, seems to be quite strongly dependent on temperature. It can be seen in figure 10 that the predicted vales of α_{f11} range from $-1.5\times10^{-6}\ ^{\circ}\mathrm{C}^{-1}$ to almost $2.0\times10^{-6}\ ^{\circ}\mathrm{C}^{-1}$. The fact that the predicted values of α_{f11} were found to significantly change with temperature cannot be blamed on the accuracy of the analysis performed. Therefore, the effect observed in figure 10 is mostly likely physically possible. This would also agree with the observations made by Wolff (1987) regarding the change in axial thermal strains of T50 fibres, indicating that α_{f11} for graphite fibres could be strongly temperature dependent.

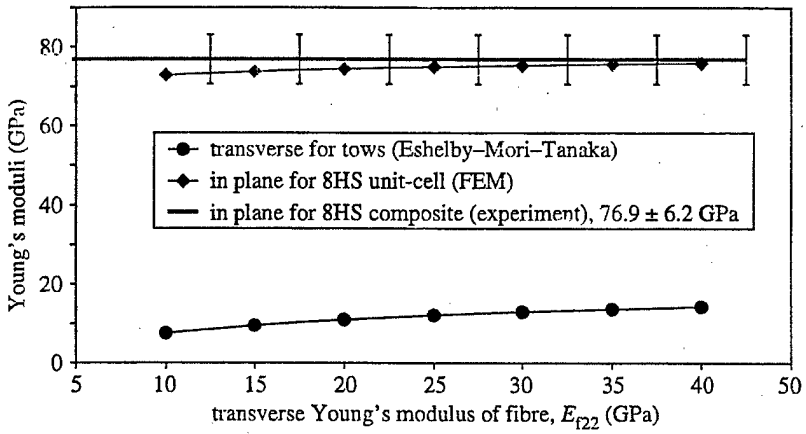

Figure 12. In-plane Young's modulus of 8HS unit cell and the transverse Young modulus of tows as a function of E_{f22}.

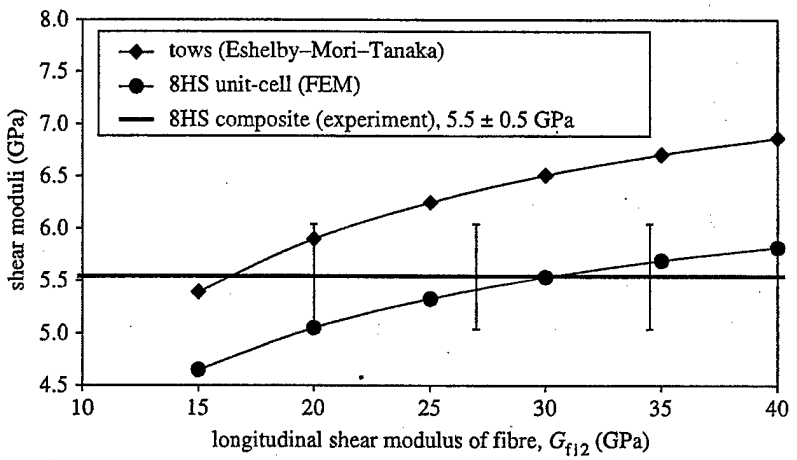

Figure 13. In-plane shear modulus of 8HS unit cell and tows as a function of G_{f12}.

(*b*) *Fibre properties from woven composite*

The stiffness of the woven composite was also numerically simulated at room temperature as a function of the elastic properties of the fibres. Subsequently, the predicted stiffness of the composite was compared with the experimental results to independently verify the stiffness of the T650-35 fibres determined from the unidirectional composite analysis. The obtained results are shown in figures 12 and 13. Due to the limitations discussed in § 3 *c*, *d*, only one-parameter analyses were performed for the in-plane Young modulus $E_{c11} = E_{c22}$ (figure 12) and for the in plane shear modulus G_{c12} (figure 13) of the woven composite. These properties were numerically predicted as a function of E_{f22} and G_{f12} of the fibres. In addition, the predicted transverse stiffness and the longitudinal shear modulus of the unidirectional T650-35/PMR-15 tows calculated from equation (3.1), and the experimental data (Searles

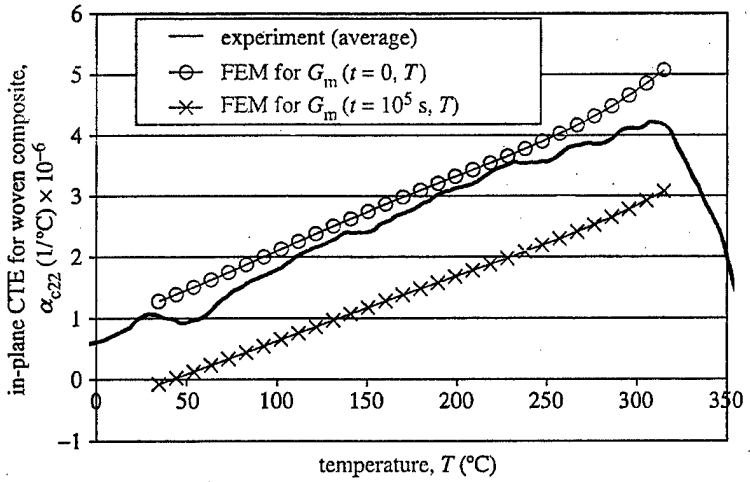

Figure 14. Numerical and experimental in-plane CTEs for 8HS T650-35/PMR-15 composite as a function of temperature.

et al. 2001; Kumosa *et al.* 2002) with error bars for the woven composite are shown in figures 12 and 13.

It can be seen in figure 12 that the transverse tensile modulus of graphite fibres cannot be accurately predicted from the analysis of the in-plane stiffness properties of woven systems. For a wide range of E_{f22} values, the calculated in-plane Young modulus of an 8HS composite based on PMR-15 was only weakly dependent on the fibre property (figure 12). This of course also applies to the T650-35 fibres investigated in this study. However, the longitudinal shear modulus of the fibres can be quite accurately predicted if the experimental errors in the macroscopic shear modulus measurements are sufficiently small, significantly smaller than for the data shown in figure 13. Nevertheless, even for the large scatter in the experimental macro-data shown in figure 13, the predicted longitudinal modulus of the T650-35 fibres cannot be smaller than 20 GPa, which agrees very well with Wagoner & Bacon (1989).

The study performed on the unidirectional composite allowed for the evaluation of the thermal expansion coefficients for the T650-35 graphite fibres (α_{f11} and α_{f22}). For the purpose of an additional verification, these values were subsequently employed in the FE model of the 8HS unit cell to find out if the prediction of the model matches the measured thermal behaviour of the T650-35/PMR15 woven composite. Both the measured and numerically predicted CTEs of the woven system are depicted in figures 14 and 15.

The results shown in figures 14 and 15 for the woven composites were obtained from the unit cell with the PMR-15 matrix behaving according to equations (2.1 *a*)–(2.1 *d*). This was done to evaluate the effect of matrix viscoelasticity on the calculations performed for time t values of either 0 or 10^5 s. No effect of matrix viscoelasticity can be seen in figure 15 for the out-of-plane thermal expansion of the composites. However, this effect is visible in the data presented in figure 14 for the in-plane expansion. Most importantly, the experimental data are either between the numerical data calculated for $t = 0$ s and $t = 10^5$ s (see figure 14) or very close to both of them (figure 15). The data presented in figure 14 and 15 clearly show that the

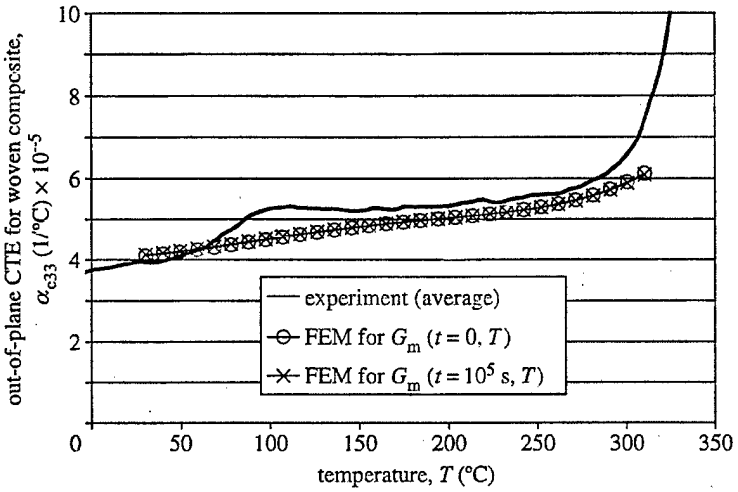

Figure 15. Numerical and experimental out-of-plane CTEs for 8HS T650-35/PMR-15 composite as a function of temperature.

thermal expansion coefficients of the T650-35 fibres were correctly determined in the unidirectional composite analysis.

(*c*) *Error analysis and optimization of the indirect technique for a unidirectional composite system*

It has been shown above that the errors related to the indirect calculations of the fibre elastic properties can be very large in some cases. Therefore, it is important to ascertain the correlation between the errors of the input and output parameters for a unidirectional composite system. It is also important to determine which input data influence the accuracy of the obtained micro-results the most. To answer these questions, a one-parameter study, based on equation (3.1), was performed. At first, the average values of all input parameters were assumed (see the first column in table 3) for the elastic properties of matrix (E_m, υ_m) and unidirectional composite ($E_{c11}, E_{c22}, \upsilon_{c12}, \upsilon_{c23}, G_{c12}$) and for the volume fraction of fibres f_v. The input parameters were assumed to be of the unidirectional T650-35 fibre composite and its PMR-15 resin. Subsequently, using the inverse Eshelby–Mori–Tanaka model (equation (3.1)), the variations in the fibres' properties (outputs) were investigated when only one of the input parameters was changed by ±2.5, ±5 and ±10% around the average value. The other input parameters were kept constant at the same time. The resulting correlation matrix is presented in table 3.

The obtained data clearly show that the errors of the calculated elastic constants of fibres are very high in some cases. For example, only a ±2.5% variation of f_v (volume fraction of fibres) results in a ±27% uncertainty of the G_{f12} estimates. This means that the relative error, in this case, is increased more than ten times. In addition to f_v, the calculated value of G_{f12} is also strongly related to the matrix properties (E_m and υ_m) and to the longitudinal shear modulus of the composite. For all these parameters the output error is much higher than the error in the input data. From table 3 one can also observe that in order to predict the transverse Young modulus

Table 3. *Error correlations in the computation of elastic properties of T650-35 graphite fibres*

input parameter	change (±) in input parameter (%)	changes (±) in output parameters (%)					
		E_{f11} 241 GPa	E_{f22} 20 GPa	υ_{f12} 0.2	υ_{f23} 0.4	G_{f12} 27 GPa	G_{f23} 7.1 GPa
E_m	2.5	—	7.5	0	0.5	18	6.5
3.64 GPa	5	—	13	0.5	1.5	42	13
	10	—	28	1	3	190	29
ν_m	2.5	—	3	4	14	4.5	1
0.36	5	—	6.5	8	28	9	1.5
	10	—	12	17	55	19	3
E_{c11}	2.5	2.5	—	—	0	—	—
129 GPa	5	5	—	—	0.5	—	—
	10	10	—	—	0.5	—	—
E_{c22}	2.5	—	9	0	0.5	—	9
8.1 GPa	5	—	18	0.5	1	—	18
	10	—	37	1	2.5	—	37
υ_{c12}	2.5	—	—	6	0	—	—
0.27	5	—	—	11	0.5	—	—
	10	—	—	23	0.5	—	—
υ_{c23}	2.5	—	0.5	0	11	—	3
0.49	5	—	1	0.5	23	—	6
	10	—	1.5	1	47	—	12
G_{c12}	2.5	—	—	—	—	21	—
3.81 GPa	5	—	—	—	—	46	—
	10	—	—	—	—	155	—
f_v	2.5	2.5	7	1.5	2	27	7.5
0.52	5	5	14	3.5	4.5	69	15
	10	10	30	7	9.5	1140	34

of fibres, E_{f22}, the values of E_{c22}, E_m, υ_m and f_v must be measured accurately, since when these input constants vary by ±2.5% then the uncertainty of the output value, E_{f22}, becomes ±9, ±7.5, ±3 and ±7%, respectively. This observation becomes even more important if we realize that the total output error will be ±14% (Taylor 1982) when the discrepancies of all individual input data are taken into account simultaneously.

It should also be emphasized that the components of the correlation matrix (table 3) depend on the assumed average elastic properties of the composite and its matrix, and on the volume fraction of fibres. Naturally, it is possible that a composite system with different initial macro-data could be less sensitive to the errors of the input parameters. It can be observed in table 3 that, due to the high error sensitivity, in order to obtain the stiffness properties of the T650-35 graphite fibres from the unidirectional graphite/PMR-15 system, the initial macro-data need to be measured very accurately. Therefore, it might be interesting to reverse the problem

and determine whether it is possible to design a composite system that will be significantly less sensitive to the measurement errors, and that will allow a more accurate prediction of the graphite fibre properties. The only feasible method to design a more suitable system is to change either the matrix or the volume fraction of fibres, or both of them. The effect of the volume fraction of fibres on the determination of fibre properties is easy to deduce. It is believed that the larger the number of fibres in a composite, the easier it is to measure the fibre properties. Therefore, only high-quality (low-void-content) composite systems with the highest possible volume fractions of fibres should be used to perform indirect calculations of fibre elastic and thermal properties from the macro-data. In this work, an effort was made to verify whether the calculated errors could be minimized by increasing the matrix Young's modulus E_{m}.

From equations (3.1) and (3.2), it can be inferred that $F = F(E_{\mathrm{m}}, v_{\mathrm{m}}, C, f_{\mathrm{v}})$ where F and C denote five independent elastic constants of fibres and a unidirectional composite, respectively. Then, assuming input errors are small and independent, the relative error of the output parameter can be calculated using (Taylor 1982):

$$\begin{aligned}\delta F_i &= \frac{100\%}{F_i}\Delta F_i \\ &= \frac{100\%}{F_i}\left\{\left(\frac{\partial F_i}{\partial E_{\mathrm{m}}}\Delta E_{\mathrm{m}}\right)^2 + \left(\frac{\partial F_i}{\partial v_{\mathrm{m}}}\Delta v_{\mathrm{m}}\right)^2 + \sum_{k=1}^{5}\left(\frac{\partial F_i}{\partial C_k}\Delta C_k\right)^2 + \left(\frac{\partial F_i}{\partial f}\Delta f\right)^2\right\}^{1/2}.\end{aligned} \tag{4.2}$$

The above equation expresses the uncertainty of the fibre elastic constant δF_i in terms of E_{m}, v_{m}, C and f_{v}, provided that all measurement errors $(\Delta E_{\mathrm{m}}, \Delta v_{\mathrm{m}}, \Delta C_k, \Delta f)$ are known. However, C can be evaluated as a function of F, E_{m}, v_{m} and f_{v}. Consequently, the errors of the fibre elastic constants δF_i become dependent only on the matrix stiffness E_{m} if we assume that v_{m}, F and f_{v} are known. This process can be summarized by the following expression:

$$\begin{aligned}\delta F_i &= \delta F_i(E_{\mathrm{m}}, v_{\mathrm{m}}, C, f_{\mathrm{v}}) = \delta F_i(E_{\mathrm{m}}, v_{\mathrm{m}}, C(F, E_{\mathrm{m}}, v_{\mathrm{m}}), f_{\mathrm{v}}) \\ &= \delta F_i(E_{\mathrm{m}}, v_{\mathrm{m}}, F, f_{\mathrm{v}}) = \delta F_i(E_{\mathrm{m}}).\end{aligned} \tag{4.3}$$

Figure 16 shows the results of the calculations based on equation (4.3) for $\Delta E_{\mathrm{c}11} = \Delta E_{\mathrm{c}22} = \Delta G_{\mathrm{c}12} = \Delta G_{\mathrm{c}23} = \Delta E_{\mathrm{m}} = \Delta G_{\mathrm{m}} = 0.1$ GPa, $\Delta v_{\mathrm{c}12} = \Delta v_{\mathrm{c}23} = \Delta v_{\mathrm{m}} = 0.01$, $\Delta f_{\mathrm{v}} = 0.01$ and for the elastic constants of the fibres taken from the first row of table 3. Based on the results depicted in figure 16, it can be concluded that, for low stiffness matrices, such as PMR-15, the errors of the evaluated fibre properties, $E_{\mathrm{f}22}$, $G_{\mathrm{f}12}$ and $G_{\mathrm{f}23}$ are very high. They can be substantially reduced, however, if a stiff matrix is used to fabricate a unidirectional graphite fibre composite. The resultant errors would be much smaller if a matrix with a Young modulus of at least 18 GPa is used. According to figure 16, the optimal condition for the measurement of $E_{\mathrm{f}22}$ and $G_{\mathrm{f}12}$ of the T650-35 fibres would be a unidirectional T650-35 fibre composite with the matrix stiffness of 22 GPa for the tensile modulus and 66 GPa for the shear modulus.

The methodology presented in this work can be used not only to estimate certain physical properties of long fibres from the macro-properties of unidirectional or woven composites. It can also be used to evaluate errors and their significance in

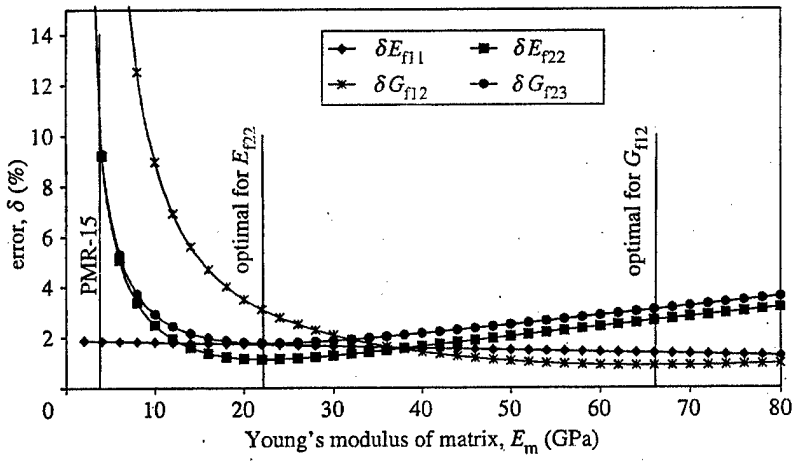

Figure 16. Errors of the indirect measurements of fibre properties as a function of the matrix Young modulus.

the experimentally determined macroscopic properties of the composites. Such errors always exist, especially in high-temperature research on graphite/polyimide composite materials (Odegard & Kumosa 2000*a*; Gentz *et al.* 2003). A good example of these errors is to be found in the high-temperature data of the unidirectional T650-35/PMR-15 composite (Odegard & Kumosa 2000*a*). The importance of the errors in the design process might not be significant. However, when the data are used to extract the micro-fibre properties the errors in the macro-data of the composites suddenly become very significant.

5. Conclusions

A combined experimental/analytical methodology, based on the Eshelby–Mori–Tanaka model, was used to determine the elastic properties of T650-35 fibres from the macroscopic elastic properties of a unidirectional T650-35/PMR-15 composite for temperatures ranging from 25 to 315 °C. It was shown, by employing the Monte Carlo simulation, that this method is very sensitive to the experimental errors in the macroscopic input data. The temperature-dependent CTEs of the T650-35 graphite fibres were also evaluated from the macro-data for the unidirectional composite as a function of temperature. Contrary to the elastic constants, much smaller errors were determined in the case of the thermal properties of the T650-35 fibres.

It has been shown, based on the FE modelling of an 8HS woven composite and the in-plane experimental data of this system, that it is impossible to predict the transverse stiffness of the T650-35 fibres. In contrast, the longitudinal shear modulus of the fibres can be evaluated from the woven composite, provided that the in-plane shear modulus of the composite is measured with high accuracy. The FE modelling of the woven composite was found to be very useful in verifying the results obtained from the analysis of the unidirectional system.

The errors of indirect determination of the transverse and shear moduli of graphite fibres from the properties of a unidirectional composite are very high when the composite is based on a low modulus polymer resin such as PMR-15. In order to minimize

these errors, the macro-properties of the composite must be measured with greater accuracy or the matrix must be replaced with a much stiffer material.

This research was supported by the Air Force Office of Scientific Research and NASA Glenn Research Center under joint grant F49620-00-1-0159. Additional funds were also provided by the National Science Foundation and the University of Denver, CO, USA, from a Major Research Instrumentation Program, Instrument Development and Acquisition grant no. CMS-9977735. The authors thank Professor P. K. Predecki for his comments on this paper.

References

ASTM 1989 Standard test method for tensile strength and young's modulus for high modulus single-filament materials. American National Standards Institute, Standard no. D3379-75.

ASTM 2004 Standard test methods for properties of continuous filament carbon and graphite fiber tows. American National Standards Institute, Standard no. D4018-99.

Benedikt, B., Predecki, P. K., Kumosa, L., Armentrout, D., Sutter, J. K. & Kumosa, M. 2001*a* The use of X-ray diffraction measurements to determine the effect of bending loads on internal stresses in aluminum inclusions embedded in a unidirectional graphite fiber/PMR-15 composite. *Compos. Sci. Tech.* **61**, 1995–2006.

Benedikt, B., Kumosa, M., Predecki, P. K., Kumosa, L., Castelli, M. G. & Sutter, J. K. 2001*b* An analysis of residual thermal stresses in a unidirectional graphite/PMR-15 composite based on the X-ray diffraction measurements. *Compos. Sci. Tech.* **61**, 1977–1994.

Benedikt, B., Rupnowski, P., Kumosa, L., Sutter, J. K., Predecki, P. K. & Kumosa, M. 2002 Determination of interlaminar residual thermal stresses in a woven 8HS graphite/PMR-15 composite using X-ray diffraction measurements. *Mech. Adv. Mater. Struct.* **9**, 375–394.

Benedikt, B., Rupnowski, P. & Kumosa, M. 2003 Viscoelastic stress distributions and elastic properties in unidirectional composites with large volume fractions of fibers. *Acta Mater.* **51**, 3483–3493.

Benedikt, B., Kumosa, M., Armentrout, D., Kumosa, L., Sutter, J. K. & Predecki, P. K. 2004 Analysis of stresses in aluminum particles embedded inside unidirectional and woven graphite/polyimide composites subjected to large bending loads. *Mech. Adv. Mater. Struct.* **9**(1), 31–49.

Chamis, C. C. 1984 Simplified composite micromechanics equations for hydral, thermal and mechanical properties. *SAMPE Q.* **15**, 14–23.

Donnet, J. B., Wamg, T. K., Peng, J. & Rebouillat, S. 1998 *Carbon fibers*, 3rd edn, p. 336. New York: Marcel Dekker.

Eshelby, J. D. 1957 The determination of the elastic field of an ellipsoidal inclusion, and related problems. *Proc. R. Soc. Lond.* A **241**, 376–396.

Gentz, M., Armentrout, D., Rupnowski, P., Kumosa, L., Sutter, J. K. & Kumosa, M. 2003 Mechanical behavior of a woven graphite/PMR-15 composite at room and elevated temperatures determined from the $\pm 45^\circ$ tensile and Iosipescu shear tests. *J. Comp. Tech. Res.* **25**, 22–34.

Gentz, M., Armentrout, D., Rupnowski, P., Kumosa, L., Shin, E., Sutter, J. K. & Kumosa, M. 2004 In plane shear testing of medium and high modulus woven graphite fiber reinforced/polyimide composites. *Compos. Sci. Tech.* **64**, 203–220.

Hashin, Z. 1979 Analysis of properties of fiber composites with anisotropic constituents. *J. Appl. Mech.* **46**, 543–550.

Hull, D. & Clyne, T. W. 1996 *An introduction to composite materials*, 2nd edn. Cambridge University Press.

Ishikawa, T. & Chou, T. W. 1983 Nonlinear behavior of woven fabric composites. *J. Compos. Mater.* **17**, 399–413.

Kowalski, I. M. 1986 Determining the transverse modulus of carbon fibers. *SAMPE J.* **22**, 38–42.

Kumosa, M., Odegard, G., Armentrout, D., Kumosa, L., Searles, K. & Sutter, J. K. 2002 Comparison of the ±45° off-axis and Iosipescu shear tests for woven fabric composite materials. *J. Compos. Tech. Res.* **24**, 3–16.

Landau, D. P. & Binder, K. 2000 *A guide to Monte Carlo simulations in statistical physics.* Cambridge University Press.

Mori, T. & Tanaka, K. 1973 Average stress in matrix and average elastic energy of materials with misfitting inclusions. *Acta Metall.* **21**, 571–574.

Naik, R. A. 1995 Failure analysis of woven and braided fabric reinforced composites. *J. Compos. Mater.* **29**, 2334–2363.

Naik, N. K. & Ganesh, V. K. 1996 Failure behavior of plain weave fabric laminates under on-axis uniaxial tensile loading. II. Analytical predictions. *J. Compos. Mater.* **30**, 1779–1822.

Odegard, G. & Kumosa, M. 2000*a* Elastic-plastic and failure properties of a unidirectional carbon/PMR-15 composite at room and elevated temperatures. *Compos. Sci. Tech.* **60**, 2979–2988.

Odegard, G. & Kumosa, M. 2000*b* Non-linear analysis of woven fabric-reinforced graphite/PMR-15 composites under shear-dominated biaxial loads. *Mech. Compos. Mater. Struct.* **7**, 129–152.

Peebles, L. H. 1995 *Carbon fibers*, p. 75. Boca Raton, FL: Chemical Rubber Company.

Roberts, G. D., Malarik, D. C. & Robaidek, J. O. 1991 Viscoelastic properties of addition-cured polyimides used in high temperature polymer matrix composites, composites design, manufacturing, and applications. In *Proc. 8th Int. Conf. Composite Materials* (ed. S. W. Tsai & G. S. Springer), pp. 12-H-1–12-H-10. Society for Advanced Materials and Process Engineering, Covina, CA.

Rupnowski, P. & Kumosa, M. 2003 Meso- and micro-stress analyses in an 8HS graphite/polyimide woven composite subjected to biaxial in plane loads at room temperature. *Compos. Sci. Tech.* **63**, 785–799.

Russell, J. D. 1989 Carbon/graphite fibers. In *Engineered materials handbook, vol. 1: composites*, 3rd edn, § 2, p. 49. ASM International.

Searles, K., Odegard, G. & Kumosa, M. 2001 Micro- and mesomechanics of 8-harness satin woven fabric composites. I. Evaluation of elastic behavior. *Composites* A **31**, 1627–1655.

Sutter, K. 2002 Higher operating temperature propulsion components. *Proc. High Temple Workshop XXII, DOD/NASA Laboratories and University of Dayton Research Institute, 21–24 January 2002, Santa Fe, NM.* DOD/NASA Laboratories and University of Dayton Research Institute.

Swan, S. A. 1997 Aging effects on fracture properties of polyimide neat resin. MSc thesis, University of Houston, TX, USA.

Taylor, J. R. 1982 *An introduction to error analysis*, p. 174. Oxford University Press.

Wagoner, G. & Bacon, R. 1989 Elastic constants and thermal expansion coefficients of various carbon fibers. In *Proc. 19th Biennial Conf. on Carbon, State College, PA* (extended abstract), pp. 296–297.

Walsh, T. J. & Ochoa, O. O. 1996 Analytical and experimental mechanics of woven fabric composites. *Mech. Compos. Mater. Struct.* **3**, 133–152.

Wolff, E. G. 1987 Stiffness–thermal expansion relationships in high modulus carbon fibers. *J. Compos. Mater.* **21**, 81–97.

Composites Part A, Vol. 36 (2004) pp. 327-338

An Evaluation of the Elastic Properties and Thermal Expansion Coefficients of Medium and High Modulus Graphite Fibers

P. Rupnowski, M. Gentz, J. K. Sutter*
and M. Kumosa

Center for Advanced Materials and Structures
Department of Engineering, University of Denver
2390 S. York St. Denver, CO 80208

***NASA Glenn Research Center at Lewis Field**
21000 Brookpark Rd.
Cleveland, OH 44135

Abstract

In this work, the elastic properties and coefficients of thermal expansion of T650-35, M40J and M60J graphite fibers were determined from the macroscopic properties of either unidirectional and/or woven composites of these fibers embedded in polyimide resins. The T650-35 fibers were embedded in a PMR-15 matrix, whereas the M40J and M60J fibers were embedded in a PMR-II-50 polyimide. The three-component oscillator resonance method was employed to determine the elastic properties of the unidirectional and woven composites and their neat resins. The macroscopic coefficients of thermal expansion of the composites and the neat resins were measured by length dilatometry. Subsequently, the fiber properties were calculated from the unidirectional composite macro-data using the Eshelby/Mori-Tanaka approach. For the woven composites, a finite element approach based on the concept of a representative volume element was employed to determine the elastic and thermal properties of the fibers. In the case of the T650-35 fibers, both the longitudinal and transverse elastic and thermal properties of the fibers determined from the unidirectional and woven composites agreed very well with each

other. However, for the M40J fibers, noticeable differences were observed between the fiber properties determined from the unidirectional and woven system, which was attributed to the lack of transverse isotropy of the unidirectional system. Since the properties of the M60J fibers were evaluated only from the woven system no direct comparison could be made between the properties obtained from the unidirectional and woven composite architectures. Overall, the methodology was shown to be highly applicable for the accurate determination of fiber properties from both unidirectional and woven systems.

1. Introduction

For the accurate determination of internal stress distributions in advanced composite systems, the elastic and thermal properties of their constituents must be known. This is especially true in the case of high temperature graphite/polyimide composites [1-22]. Since these composites are manufactured at relatively high temperatures, large residual stresses can exist in the composites after manufacturing due to the mismatch in the thermal expansion coefficients and the elastic properties of the graphite fibers and polyimide resins [8,9,12,14,15,18,19,20,22]. In some cases, multiple transverse micro cracking in the tows of woven graphite/polyimide composites can occur as a result of the high residual thermal stresses (Figure 1) [18]. In order to predict the critical stress conditions of tow micro cracking in the composites one needs to know the elastic and thermal properties of the fibers as well as those of neat polyimide resins.

To describe the mechanical and thermal behavior of graphite fibers, five elastic and two thermal constants must be measured. The longitudinal Young's modulus and longitudinal coefficient of thermal expansion can be directly determined by performing standard tests on a single filament or strand. The other fiber properties, such as the transverse Young's and longitudinal shear moduli, can be obtained by indirect methods [23-26].

In recent work, the elastic properties of T650-35 fibers were evaluated indirectly from the macroscopic elastic properties of a unidirectional T650-35/PMR-15 composite for temperatures ranging from 25°C to 315°C and then numerically and experimentally verified in a woven system based on the same fibers and polyimide resin [21]. It was shown however that when the fiber mechanical properties were determined from the composite properties obtained by conventional mechanical tests, the final results were strongly dependent on the experimental errors in the macroscopic input data. However, the estimates of the thermal fiber properties were found to be significantly less dependent on the accuracy of the macro-data of the composite.

In this work, an improved version of the combined analytical and numerical procedure that had been developed and presented in Ref. 21 was used to evaluate the elastic and thermal properties of M40J and M60J fibers at room temperature from their composite macro-data. These high modulus graphite fibers are used in certain aerospace applications, which require significantly higher stiffness at the expense of slightly reduced strength. Since the stiffness macro-data of the composites were obtained in this research by the three-component oscillator resonance method, instead of conventional mechanical testing (see [21]), the T650-35/PMR-15 composites were re-tested and the properties of the T650-35 fibers were determined and then compared with the data presented in Ref. 21 and with the properties of the M40J and M60J fibers.

2. Investigated Composite Systems

To determine the properties of the T650-35, M40J and M60J fibers the following graphite fiber/polyimide composites were examined in this study: unidirectional T650-35/PMR-15, eight harness satin (8HS) woven T650-35/PMR-15, unidirectional M40J/PMR-II-50, four harness satin (4HS) woven M40J/PMR-II-50 and a woven 4HS M60J/PMR-II-50 composite. For comparison, the mechanical properties and the longitudinal and transverse coefficients of thermal expansion (CTE_L and CTE_T) of the T650-35, M40J and M60J graphite fibers taken from the available literature, are shown in Table 1. It can be seen in

Table 1 that several properties of the M40J and M60J fibers were not available at the start of this project.

The available data of the average fiber, resin and void contents as well as the glass transition temperatures T_g of the five composite systems examined are presented in Table 2 for comparison. The composites were manufactured at the NASA Glenn Research Center (GRC). The T650-35 fiber composites were manufactured and post-cured at 316°C, whereas the M40J and M60J fiber composites were manufactured and post-cured at 371°C. Detailed descriptions of their manufacturing procedures, composite architectures and selected properties can be found in Ref. 18.

3. Experimental Methods

3.1. Oscillator resonance measurements

The three-component oscillator resonance method [27-30] was employed to determine the elastic properties of the unidirectional and woven graphite/polyimide composites and their neat PMR-15 and PMR-II-50 polyimide resins. The testing setup consisted of two piezoelectric oscillators (see Figure 2). The first oscillator vibrated in the extensional mode enabling the determination of Young's modulus, whereas the second oscillator operated in the torsional mode so that the torsional modulus of the specimen could be measured.

Each oscillator consisted of two piezoelectric quartz crystals cemented together. The first crystal rod, called the drive crystal was responsible for generating either an extensional or torsional standing wave. The second crystal, called the gauge crystal was responsible for monitoring the vibrations. A neat resin or composite specimen was attached to the top of the gauge crystal. The vibrations of the whole system were generated by applying a sinusoidal voltage with an amplitude, U_d, of approximately 1 volt to the metal coatings of the drive crystal. Simultaneously, the voltage amplitude, U_g, across the metal coatings of the gauge crystal was monitored. For a fixed U_d, the value of U_g was a function of the

frequency of the applied voltage. To measure the stiffness of a specimen, one had to find the specific value of frequency that corresponds to the maximum U_g. This characteristic value of frequency was the resonance frequency, f_{res}, of the entire vibrating oscillator.

The resonance frequency of the oscillator without an attached specimen, f_q, was 49.877 and 49.817 kHz for the extensional and torsional setup, respectively. With an attached specimen, f_{res} increased or decreased depending on the natural frequency of the specimen, f_{spec}. After measuring f_{res}, the natural frequency of the specimen, f_{spec}, could be calculated from equation (1) [27]:

$$f_{spec} = \sqrt{\frac{m_Q}{m_S}(f_{res}^2 - f_q^2) + f_{res}^2} \tag{1}$$

where m_Q and m_S denote, respectively, the mass of the piezoelectric crystals and of the specimen. In the torsional setup case, equation (1) is valid provided that the diameters of the specimen and the crystal are the same. Once f_{spec} is known, the Young's, E, or torsional, G, modulus of a specimen can be found from expression (2):

$$E \text{ or } G = \rho\left(\frac{f_{spec}L}{n}\right)^2 \tag{2}$$

In the above formula, L and ρ represent the length and density of the specimen, and n denotes a constant number equal to a multiple of 0.5. It should be also noted that equation (1) is valid only when f_{spec} is close to f_{res}. Therefore, only specimens of specific L/n ratios could be measured using the three-component oscillator resonance method.

Using the oscillator resonance technique, the elastic properties (E_m, G_m) of neat PMR-15 and PMR-II-50 polyimides as well as the in plane and out of plane Young's moduli of the woven composites were measured directly. For the unidirectional composites, the resonance technique allowed for the determination of the three Young's and two torsional

moduli (E_L, in-plane E_T, out of plane E_T, $G_\perp$ and $G_\parallel$). Then, based on the torsional moduli ($G_\perp$, $G_\parallel$) and assuming that the material is transversely isotropic, the values of the longitudinal and transverse moduli (G_L and G_T) were obtained following the method described in detail in reference [30].

All specimens used in this work were fabricated either from neat resin or composite plates of approximately 5 mm thickness. For thicker specimens, several plates were stacked together and glued using an epoxy-based cement. The specimens for the torsional tests and for measuring the out of plane Young's moduli of the woven composites were all prepared this way. To examine the effect of the glue on the measurements, four cemented specimens of the neat PMR-15 resin were prepared. The Young's moduli of the cemented and homogenous specimens of PMR-15 were tested and subsequently compared.

3.2. Mechanical testing

The longitudinal Poisson's ratios (v_L) of the unidirectional composites could not be measured using the resonance method. Therefore, for the unidirectional T650-35/PMR-15 composite the ratio was taken from Ref. 7 and for the unidirectional M40J/PMR-II-50 system it was measured by performing conventional mechanical uniaxial tests. For this purpose two 0° specimens 215 mm long and 22 mm wide with two rosette strain gages attached to both sides of each specimen were tested at a strain rate of 1mm/min.

3.3. Measuring coefficients of thermal expansion (CTEs) and volume fraction of fibers

Length dilatometry using a Netzsch DIL 402C dilatometer was employed to determine the coefficients of thermal expansion of the neat PMR-15 and PMR-II-50 resins and of the unidirectional and woven composites. Only the CTEs at 20°C were needed for this work. For the unidirectional systems, the measurements were performed in the direction parallel and perpendicular to the fibers. For the woven composites, the tests were performed in and out-of-plane.

4. Properties of Polyimide Resins and Composites

The properties of the neat PMR-15 and PMR-II-50 resins, unidirectional and woven composites are shown in Table 3, 4 and 5, respectively. The average values of the properties (AVG) with the standard deviation of the mean (SDOM) [31] are included with the data for each tested specimen. Additionally, the volume fractions of fibers are shown for all the investigated composites. The number of specimens in each test varied from three to eleven. In some cases tests were repeated on the same specimen. For such tests both results are shown in one cell of the tables.

The data presented in Tables 3-5 clearly show that the natural frequency method used to determine the elastic parameters of the neat resins and the composites appears to be very precise. When the tests were repeated more than once on the same specimen, the difference was less than 0.8%. The coefficients of variance (COV) in the elastic property measurements, not reported in Tables 3-5, were usually lower than 2%. Only the tests for the out of plane Young's moduli of the woven composites yielded higher discrepancies as the maximum value of the COV reached 4.5% in the case of the M40J/PMR-II-50 woven system. It can also be seen in the data presented in Table 3 that the results obtained from the homogeneous and the cemented specimens of PMR-15 were very similar. This implies that the three thin layers of glue in the cemented specimens introduced no effect on the Young's modulus measurements. Consequently, it was assumed that the out-of - plane and torsional properties of the composites measured on the cemented specimens were also not affected by the glue.

The thermal behavior of the composites was found to be highly anisotropic since the values of CTE in the direction of the fibers were very small compared to other directions. It was also observed that for the neat resins, the transverse direction of the unidirectional composites and the out of plane direction of the woven systems, the COV was less than 10%, whereas the longitudinal CTEs of the unidirectional composites and the in-plane

CTEs of the woven systems exhibited much higher discrepancy with the COV above 10%.

5. Fiber Property Evaluations

5.1. Macro-input data

For the fiber property calculations the average values of the data shown in Table 3-6 were used. However, it has been shown in Ref. 21 that errors in input data can substantially influence the uncertainty of the output fiber properties. Therefore, an error analysis was also carried out in this study. According to Ref. 31, the best estimation of random measurement errors is the standard deviation of the mean, also included in Tables 3, 4 and 5. By considering the SDOM values as uncertainties of the input data, the associated errors of the fiber properties could be also determined. In Table 6, the transverse Young's moduli and transverse CTEs of the unidirectional systems with their assumed errors are shown. These were used in the calculations of the fiber properties. The average values were obtained by averaging the properties measured in and out-of-plane. The assumed errors were actually the coefficients of variance of all the data from the in and out of plane measurements.

5.2. Fiber properties from unidirectional composites

To determine the properties of the fibers (E_{fL}, E_{fT}, v_{fL}, G_{fT}, G_{fL}, α_{fL} and α_{fT}) from the unidirectional composites and to model the tows in the woven systems the Eshelby/Mori-Tanaka model [32-34] was used. The application of this model for describing mechanical behavior of unidirectional composites with a volume fraction of fibers (f_v) higher than 50% has been not been widely accepted. This problem has been recently investigated in Ref. 15 by comparing the Eshelby/Mori-Tanaka and FEM approaches. It was found that the Eshelby/Mori-Tanaka model could provide only approximate stresses and strains distribution when f_v exceeded 50%. However, the Eshelby/Mori-Tanaka approach was

found to be accurate for the elastic property evaluations of unidirectional composites even with very high values of f_v [15].

Elastic properties

The Eshelby/Mori-Tanaka approach provides the following equation that expresses the stiffness matrix of the fibers, C_f, in terms of the stiffness matrix of the composite, C_c, and of the resin, C_m [21, 32-34]:

$$C_f = [(\frac{1}{f_v} - 1) C_m (I - S)(C_m^{-1} - C_c^{-1}) + I][C_m^{-1} - (S - f_v(S - I))(C_m^{-1} - C_c^{-1})\frac{1}{f_v}]^{-1} \qquad (3)$$

In the above equation S stands for the Eshelby tensor in matrix form, I denotes a 6 by 6 unit matrix and f_v is the volume fraction of fibers. Assuming transversely isotropic symmetry for the fibers and composite, the stiffness matrices C_c and C_f in equation (3) can be related to the five independent engineering elastic constants by:

$$C = \begin{bmatrix} E_L^{-1} & -\nu_L / E_L & -\nu_L / E_L & 0 & 0 & 0 \\ & E_T^{-1} & E_T^{-1} - \frac{1}{2} G_T^{-1} & 0 & 0 & 0 \\ & & E_T^{-1} & 0 & 0 & 0 \\ & & & G_T^{-1} & 0 & 0 \\ & sym. & & & G_L^{-1} & 0 \\ & & & & & G_L^{-1} \end{bmatrix}^{-1} \qquad (4)$$

Equation (4) can also be used to describe the matrix C_m provided that $E_L = E_T = E_m$, $G_L = G_T = G_m$ and $\nu_L = E_m/2/G_m - 1$, where E_m and G_m denote respectively the Young's and shear moduli of the resin.

Coefficients of thermal expansion

Again, using the Eshelby/Mori-Tanaka method, the coefficients of thermal expansion of the fibers can be determined from [18, 32-34]:

$$\alpha_f = \frac{1}{f_v} C_f^{-1}[(C_m - C_f)(S - f_v(S - I)) - C_m](\alpha_m - \alpha_c) + \alpha_m \qquad (5)$$

where α_f, α_m, and α_c are the column vectors of the CTEs for the fibers, matrix and composite, respectively. According to equation (5), in order to find the thermal expansion coefficients of a fiber, α_f, the stiffness matrix of that fiber, C_f, must be known, or calculated using equation (3).

5.3. Fiber properties from woven composites

To determine the elastic (E_{fL}, E_{fT}) and thermal (α_{fL}, α_{fT}) properties of the fibers from the woven composites, finite element method (FEM) and an optimization technique were employed. Using finite element representations of woven systems the macro mechanical properties of the composites can be obtained when the properties of the constituents (matrix and fibers) are known. To reverse this relation and obtain the fiber properties from the macro data of the composites, the optimization technique was used.

The finite element representations of the woven composites were based on the concept of a meso- unit-cell. In the modeling of the 8HS T650-35/PMR-15 composite both fully 3D and single-slice models [14] were used. The modeling of the 4HS systems with the M40J and M60J fibers was based only on the single-slice models (see Figure 4). Each model consisted of the warp and fill tows and small pockets of neat resin. The geometry and size of the tows were taken from the SEM images of the woven composites. By assuming that each tow is a unidirectional composite, mechanical properties of the tows could be determined using the Eshelby/Mori-Tanaka approach. The volume fraction of fibers

inside the tows was adjusted so that the global volume fraction of fibers in the whole unit-cell matched the value obtained from the acid digestion test shown in Table 2.

The mesh shown in Figure 3 was built using thetrahedral isoparametric elements. Periodic boundary conditions were applied to the faces of the unit cell following Ref. 35. A more detailed description of the model can be found in Ref. 14. The geometrically simplified, so-called single-slice FE models of 4HS and 8HS woven composites are depicted in Figure 4. The single-slice models are also 3D, however, in their design only the weave undulations in the warp direction were taken into account, whereas the undulations in the fill direction were neglected (see Figure 5). This simplification makes the stresses and strains along the z-coordinate constant. The thickness of the single-slice meshes equaled the size of one finite element. Periodic boundary conditions applied to the single-slice model took the following form:

$$\begin{aligned} u_X(0,y,z) &= 0 \quad u_X(-l,y,z) = -<\varepsilon_X>\cdot l \\ u_Y(x,0,z) &= 0 \quad u_Y(x,h,z) = <\varepsilon_Y>\cdot h \\ u_Z(x,y,0) &= 0 \quad u_Z(x,y,-t) = -<\varepsilon_Z>\cdot t \end{aligned} \tag{6}$$

where l, h and t represent the dimensions of the mesh and $<\varepsilon_i>$ stands for the average strain in the i-th direction.

Elastic properties

Using the finite element models in Figures 3 and 4 the stiffness properties of a woven composite can be calculated assuming that the matrix and fiber properties and the volume fraction of fibers in the composite are known. However, in this study the problem had to be reversed, since the properties of the composites were known and the objective was to determine the fiber properties. To simplify the problem it was assumed that only the Young's moduli of a fiber (E_{fL} and E_{fT}) are to be determined whereas the values of ν_{fL}, G_{fT}, G_{fL} are already known. In the case of the M40J and T650-35 fiber composites, these values were taken from the analysis of the unidirectional systems. For the M60J fiber

composite these values were assumed to be the same as for the M40J fiber. Consequently, the analyses became not five- but only two-dimensional with the goal of determining numerically the values of E_{fL} and E_{fT} according to the following function:

$$E_{fL}, E_{fT} = f(E_{cIP}, E_{cOP}, \nu_{fL}, G_{fT}, G_{fL}, E_m, G_m, f_v, a_i), \quad (7)$$

To obtain the unknown values of E_{fL} and E_{fT}, a two-parameter iterative optimization (Figure 6) was performed for each woven system. At first, the initial values of E_{fL} and E_{fT} were arbitrarily selected. Next, a finite element simulation was run to obtain the composite properties. Then, by comparing the calculated and measured values of the in and out of plane Young's moduli of the composite (E_{cIP} and E_{cOP}), the initially assumed values of E_{fL} and E_{fT} were modified. This procedure was repeated until the measured (see Table 5) and calculated stiffness properties of the composite converged. Usually, after five to six steps the proper values of E_{fL} and E_{fT} could be determined using a 0.1% convergence criterion.

Coefficients of thermal expansion

The algorithm employed to determine the CTEs of the fibers, α_{fL} and α_{fT}, was similar to the algorithm used in the determination of the elastic properties. The goal was to solve the following problem:

$$\alpha_{fL}, \alpha_{fT} = g(\alpha_{cIP}, \alpha_{cOP}, E_{fL}, E_{fT}, \nu_{fL}, G_{fT}, G_{fL}, \alpha_m, E_m, G_m, f_v, a_i), \quad (8)$$

where α_{cIP}, α_{cOP} denote the in and out of plane CTEs of a woven composite.

Iterative optimization was used and the values of α_{fL} and α_{fT} were calculated assuming 0.1% convergence.

5.4. Error analysis

A differential-based approach was used to estimate the errors of the determined fiber properties. Generally, a function that describes a fiber property can be designated by $y = y(x_1, x_2, x_3, ..., x_n)$ where x_i is a set of n input parameters. In this case y represents either an inversed Eshelby/Mori-Tanaka or an inverse finite element based model. The input parameters x_i were measured experimentally; therefore, they are known only with some finite accuracies. According to Ref. 31, if Δx_i is a small random error in x_i, then the uncertainty of the output Δy (fiber property) can be calculated using expression (9):

$$\Delta y(x_1, x_2, ..., x_n, \Delta x_1, \Delta x_2, ..., \Delta x_n) = \sqrt{\sum_{i=1}^{n} \left(\frac{\partial y}{\partial x_i} \Delta x_i \right)^2} \tag{9}$$

In the analysis of the unidirectional composites the analytical Eshelby/Mori-Tanaka formulas 3-5 were employed to describe the function y. Therefore, the partial derivatives $\partial y / \partial x_i$ in equation (9) could be evaluated analytically. However, in the case of the woven systems, closed form expressions for the fiber properties are not available. Therefore, the partial derivatives had to be estimated numerically using the following expression:

$$\frac{\partial y(x_1, x_2, ..., x_i, ...x_n)}{\partial x_i} \cong \frac{y(x_1, x_2, ..., x_i + h, ...x_n) - y(x_1, x_2, ..., x_i, ...x_n)}{h}, \tag{10}$$

where h is much smaller than x_i.

In the error analysis, the input parameter error Δx_i equaled the SDOM which are given in Tables 3-6. This means that there is a 78% probability that the actual fiber property is in the range $y \pm \Delta y$.

According to equation (9), in order to estimate the total error of the fiber property, Δy, one must know all input parameter errors Δx_i. In the case of the finite element analysis of the 8HS woven composite, all the input parameters errors were determined in this study except for the error of the geometrical parameters Δa_i. The effect of Δa_i on the output errors of the fiber properties ($\Delta E_{fL}, \Delta E_{fT}, \Delta \alpha_{fL}, \Delta \alpha_{fT}$) is believed to be small and was therefore neglected in this study. After this simplification, according to equations (7) and (9) the error ΔE_{f11} can be described by the following formula:

$$\Delta E_{fL}^2 \cong \left(\frac{\partial E_{fL}}{\partial E_{cIP}}\Delta E_{cIP}\right)^2 + \left(\frac{\partial E_{fL}}{\partial E_{cOP}}\Delta E_{cOP}\right)^2 + \left(\frac{\partial E_{fL}}{\partial \nu_{fL}}\Delta \nu_{fL}\right)^2 + \left(\frac{\partial E_{fL}}{\partial G_{fL}}\Delta G_{fL}\right)^2 + \left(\frac{\partial E_{fL}}{\partial G_{fT}}\Delta G_{fT}\right)^2 + \left(\frac{\partial E_{fL}}{\partial E_m}\Delta E_m\right)^2 + \left(\frac{\partial E_{fL}}{\partial G_m}\Delta G_m\right)^2 + \left(\frac{\partial E_{fL}}{\partial f_v}\Delta f_v\right)^2 \quad (11)$$

A similar method was also employed to determine $\Delta E_{fT}, \Delta \alpha_{fL}\ \Delta \alpha_{fT}$.

6. Properties of T650-35, M40J and M60J fibers

6.1. Individual fiber properties

The elastic properties and CTEs of the T650-35, M40J and M60J graphite fibers obtained in this study from the unidirectional and woven composite macro-data are shown in Table 7. The longitudinal E_{fL} and transverse E_{fT} Young's moduli of the T650-35 fibers were determined using the Eshelby/Mori-Tanaka, single-slice and fully 3D finite element models. The three approaches yielded almost identical values for the longitudinal and transverse stiffness properties, equal to 224 GPa and 15.4 GPa, respectively, very similar to the properties listed in Table 1. Also, the other stiffness properties such as G_{fT}, G_{fL}, ν_{fL} were very close to the properties listed in Table 1.

The longitudinal and transverse coefficients of thermal expansion of the T650-35 fibers from the three approaches were found to be similar, especially in the case of the

transverse coefficient ranging from 12.9 to 13.5 $\times 10^{-6}$/°C. The longitudinal coefficient were found ranging from –1.16 to –1.9 $\times 10^{-6}$/°C, depending on the method used. If compared to the data from other sources presented in Table 1 the transverse coefficients determined in this study were two times higher than the coefficient listed in Table 1. The absolute value of the longitudinal coefficient determined here was also almost two times larger than in Table 1.

Not all properties of the T650-35 fibers evaluated in this study agreed well with the properties of the fibers presented in Ref. 21. The numerical techniques used here and in Ref. 21 were similar. The only significant difference was related to the determination of the macro-composite properties, which in Ref. 21, were obtained purely by conventional mechanical testing. If we consider only the room temperature data, the fiber properties from Ref. 21 are as follows: E_{fL} ranging from 246 to 262GPa, E_{fT} from 29 to 114 GPa, G_{fL} from 20GPa to unspecified upper limit, and v_{fL} ranging from 0.42 to 0.48. Clearly, large discrepancies exist in the results of the transverse and shear moduli of the fibers obtained in this project compared with those in Ref. 21. These discrepancies could be even larger if the elevated temperature results from Ref. 21 were considered in this comparison.

It has been shown in Ref. 21 that the accuracy of the input macro-data for a composite is critical for the accurate evaluation of the properties of its fibers. In this study, two independent approaches based on unidirectional and woven analyses with two different composite systems independently tested and independently analyzed numerically using two different schemes for their fiber properties yielded almost identical results for the E_{fL} and E_{fT} values of the T650-35 fibers. This clearly indicates that the precision of the three-component oscillator resonance method which was used in this study to determine the macro- stiffness properties of the composites is very high.

The coefficients of thermal expansion of the T650-35 fibers presented in Ref. 21 range from –1.6 to –0.7$\times 10^{-6}$/°C for α_{fL} and from 5 to 17$\times 10^{-6}$/°C for α_{fT} as obtained from the unidirectional composite. This agrees well with the data in this research for the

unidirectional composite with α_{fL} equal to -1.16×10^{-6} /°C and α_{fT} equal to 13.5×10^{-6}/°C. Since the coefficients from the woven analyses were not obtained in Ref. 21 they could not be compared with the data from this study. More importantly, the average values of the coefficients are very similar, however, the range of scatter is much smaller in the data shown in Table 7. This should be attributed to much better estimates of the fiber elastic properties obtained here than in Ref. 21 which, of course, according to equation (5) affected the calculations of the thermal properties of the fibers.

For the M40J fiber, significant differences were found between the values of E_{fL} and E_{fT} obtained from the analysis of the unidirectional and woven composites. The difference was 7% for E_{fL} and 21% for E_{fT}. These discrepancies are most likely caused by the fact that the unidirectional M40J/PMR-II-50 system does not exhibit transverse isotropy. The lack of transverse isotropy in the unidirectional system based on the M40J fibers can be easily observed in Table 4 if the in and out of plane transverse stiffness values are compared. The difference between these two values is approximately 20%. Since the difference in the in and out of plane transverse stiffness properties of the unidirectional M40J/PMR-II-50 was not incorporated into the Eshelby/Mori-Tanaka model (only the average value was used) this must have been responsible for the significant difference in the estimated stiffness properties of the M40J fiber. It should also be noticed in Table 7 that the longitudinal modulus from the woven system analysis (344 GPa) is quite close to the value provided by Toray (377 GPa) [36].

The lack of transverse isotropy is also evident in the results of the transverse coefficients of thermal expansion of the unidirectional composite shown in Table 4. In this case the difference between the in and out of plane values was found to be almost 29%. Consequently, the estimated transverse CTEs of the M40J fiber from the unidirectional composite (6.9×10^{-6}/°C) were noticeably different than the property determined from the woven composite analysis (8.8×10^{-6}/°C).

Since only the woven system was used for the analysis of the M60J fibers, direct comparisons between the results from the unidirectional and woven composite analyses

could not be made. However, the properties obtained in this study can be compared with the data provided by Toray in Table 1. The longitudinal modulus obtained here was 500 GPa versus the modulus from Toray of 588GPa which is quite acceptable considering all the possible factors which could be responsible for this difference. However, α_{fL} equal to -2.0×10^{-6}/°C from this study does not compare well with the value from Toray of -1.1×10^{-6}/°C.

6.2 Comparison between T650-35, M40J and M60J fiber properties

A meaningful comparison of the elastic properties and CTEs of the three fibers, T650-35, M40J and M60J, obtained in this study is rather difficult due to the problems already discussed. For instance, the lack of transverse isotropy observed in one system (unidirectional M40J/PMR-II-50) and not observed in another (unidirectional T650-35/PMR-15) could add a significant effect to the final estimates of the fiber properties. Another factor which could noticeably affect the measurements of the composite mechanical properties and the extractions of the mechanical fiber properties is intralaminar tow micro-cracking from manufacturing, especially for the woven 4HS M60J/PMR-II-50 system [18]. The 4HS M40J/PMR-II-50 composites also showed evidence of tow micro-cracking after manufacturing. Cleary, significant tow micro-cracking must affect the composite stiffness measurements and the final estimates of the fiber stiffness and coefficients of thermal expansion. Since no tow micro-cracking has been observed, in the absence of external loads, in the two T650-35/PMR-15 systems the T650-35 properties determined here are not affected by this effect. In addition, the unidirectional T650-35 based system was transversely isotropic.

Despite all of the above problems the final estimates of the longitudinal fiber properties agree well with the data from other sources presented in Table 1. As expected the longitudinal stiffness values of the T650-35 fiber were lower than for the M40J fiber and even lower that that of the M60J fibers following the initial trend shown in Table 1. It seems that the trend in the transverse stiffness properties is just opposite with the transverse Young's moduli decreasing from the T650-35 to M40J and M60J fibers. No

obvious trend could be noticed in the values of the coefficients of thermal expansion of the three fibers.

7. Conclusions

1. A combined experimental and numerical methodology for the evaluation of fiber properties from the composite macro-data has been presented in this research. The methodology is based on the measurements of the elastic and thermal macro-properties of unidirectional and woven composites by the three-component oscillator resonance method and dilatometry. It is then followed by extraction of the fiber properties using the Eshelby/Mori-Tanaka model for unidirectional and finite element representative unit cells for woven systems.

2. High quality estimates of the elastic properties and coefficients of thermal expansion of the T650-35 graphite fibers were obtained in this research. Almost the same values of the properties were obtained from the unidirectional and woven analyses which were carried out almost independently of each other using two different composite architectures based on the same graphite fibers embedded in a PMR-15 polyimide resin.

3. Despite the fact that exactly the same approaches were used to determine the properties of the M40J fibers the final results were less accurate than in the case of the T650-35 fibers, especially for the transverse fiber properties. It was suggested however that the lack of transverse isotropy of the unidirectional M40J/PMR-II-50 system could be predominately responsible for the noticeably difference in the fiber properties obtained from the unidirectional and woven analyses. The properties of the M60J fibers could not be independently verified since only one composite architecture was investigated.

REFERENCES

1. Wilson D. Recent Advances in Polyimide Composites, High Performance Polymers, 1993, 5(2), p. 77-95.

2. Searles K., McCarthy J. and Kumosa M. An Image Analysis Technique for Evaluating Internal Damage in Graphite/Polyimide Fabric Composites, Composites Science and Technology, 1998, 58, p. 1607-1619.

3. Gao F., Boniface L., Ogin S. L., Smith P.A. and Greaves R.P., Damage Accumulation in Woven-Fabric CFRP Laminates under Tensile Loading: Part 1. Observation of Damage Accumulation, Composites Science and Technology, 1999, 59(1), p. 123-136.

4. Searles K., Odegard G., Castelli M. and Kumosa M., Failure Investigation of Graphite-Polyimide Fabric Composites at Room and Elevated Temperatures using the Biaxial Iosipescu Test, Journal of Composite Materials, 1999, 33(22), p. 2038-2080.

5. Seferis J.C., Chung K., Buehler F.U and Takatoya T., Heat and Water Mass Transfer Modeling in Polyimide Based Advanced Composites, Polymer Degradation and Stability, 2000, 68(1), p. 43-51.

6. Odegard G., Searles K. and Kumosa M., Non-Linear Analysis of Woven Fabric-Reinforced Graphite/PMR-15 Composites Under Shear-Dominated Biaxial Loads, J. Mechanics of Composite Materials and Structures 2000, 7(2), p. 129-152.

7. Odegard G. and Kumosa M., Elastic-Plastic and Failure Properties of a Unidirectional Graphite/PMR-15 Composite at Room and Elevated Temperatures, Composites Science and Technology 2000, 60, p. 2979-2988.

8. Benedikt B., Kumosa M., Predecki P.K., Kumosa L., Castelli M.G. and Sutter J.K., An Analysis of Residual Thermal Stresses in a Unidirectional Graphite/PMR-15 Composite Based on the X-ray Diffraction Measurements, Composites Science and Technology, 2001, 61(14), p. 1977-1994.

9. Benedikt B., Predecki P., Kumosa L., Armentrout D., Sutter J. K. and Kumosa M., The Use of X-Ray Diffraction Measurements to Determine the Effect of Bending Loads on Internal Stresses in Aluminum Inclusions Embedded in a Unidirectional Carbon-Fiber/PMR-15 Composite, Composites Science and Technology, 2001, 61(14), p. 1995-2006.

10. Kumosa M., Odegard G., Armentrout D., Kumosa L. and Sutter J. K., Comparison of the ±45° Off Axis and Iosipescu Shear Tests for Woven Fabric Composite Materials, Composites Technology & Research, 2002, 24, p. 3-16.

11. Sutter K. Higher Operating Temperature Propulsion Components, Proc. of the High Temple Workshop XXII, Edit. DOD/NASA Laboratories and University of Dayton Research Institute, Santa Fe, New Mexico, January 2002, p. 21-24.

12. Benedikt B., Rupnowski P., Kumosa L., Sutter J. K., Predecki P. K. and Kumosa M., Determination of Interlaminar Residual Thermal Stresses in a Woven 8HS Graphite/PMR-15 Composite Using X-ray Diffraction Measurements. Mechanics of Advanced Materials and Structures, 2002, 9, p. 375-394.

13. Gentz M., Armentrout D., Rupnowski P., Kumosa L., Sutter J.K. and Kumosa M., Mechanical Behavior of a Woven Graphite/PMR-15 Composite at Room and Elevated Temperatures Determined from the ±45° Tensile and Iosipescu Shear Tests, Journal of Composites Technology & Research, 2003, 25, p. 22-34.

14. Rupnowski P. and Kumosa M., Meso- and Micro-Stress Analyses in an 8HS Graphite/Polyimide Woven Composite Subjected to Biaxial In-Plane Loads at Room Temperature, Composites Science and Technology 2003, 63(6), p. 785-799.

15. Benedikt B., Rupnowski P. and Kumosa M., Visco-Elastic Stress Distributions and Elastic Properties in Unidirectional Composites with Large Volume Fractions of Fibers, Acta Materialia, 2003, 51(12), p. 3483-3493.

16. Han M. –H. and Nairn J. A., Hygrothermal Aging of Polyimide Matrix Composite Laminates, Composites Part A, 2003, 34(10), p. 978-986.

17. Allerd R. E., Wesson S. P., Shin E. E., Inghram L., McCorkle L., Papadopoulos D., Wheeler D. and Sutter J. K., The Influence of Sizing on the Durability of High-Temperature Polymer Composites, High Performance Polymers, 2003, 15(4), p. 395-419.

18. Gentz M., Armentrout D., Rupnowski P., Kumosa L., Shin E., Sutter J. K. and Kumosa M., In-Plane Shear Testing of Woven Graphite/Polyimide Composites with Medium and High Modulus Graphite Fibers at Room and 316°C Temperatures, Composites Science and Technology, 2004, 64, p. 203-220.

19. Benedikt B., Kumosa M., Armentrout D., Kumosa L., Sutter J. K. and Predecki P. K., Analysis of Stresses in Aluminum Particles Embedded Inside Unidirectional and Woven Graphite/Polyimide Composites Subjected to Large Bending Loads, Mechanics of Advanced Materials and Structures, 2004, 11(1), p. 31-49.

20. Benedikt B., Gentz M., Kumosa L., Rupnowski P., Sutter J. K., Predecki P. K. and Kumosa M., X-Ray Diffraction Experiments on Aged Graphite Fiber/Polyimide Composites with Embedded Aluminum Inclusions, Composites Part A, 2004, 35, p. 667-681.

21. Rupnowski P., Gentz M., Sutter J. K. and Kumosa M., An Evaluation of Elastic Properties and Coefficients of Thermal Expansion of Graphite Fibers from Macroscopic Composite Input Data, Proceedings of the Royal Society: Mathematical, Physical and Engineering Sciences, in press, 2004.

22. Gentz M., Benedikt B., Kumosa M., and Sutter J. K., Residual Stresses in Unidirectional Carbon Fiber/Polyimide Composites as a Function of Aging, Composites Science and Technology, 2004, 64, p. 1671-1677.

23. Kowalski I. M. Determining the Transverse Modulus of Carbon Fibers. SAMPE Journal, 1986, 22, p. 38-42.

24. Wagoner G. and Bacon R. Elastic constants and thermal expansion coefficients of various carbon fibers. Extended Abstr., 19th Biennial Conf. on Carbon, State Collage, Pennsylvania, 1989, p. 296-297.

25. Peebles L. H., Carbon Fibers, CRC Press,1995, p. 75.

26. Donnet J.B., Wamg T. K., Peng J. & Rebouillat S. Carbon Fibers, 3rd ed, Marcel Dekker Inc., 1998, p. 336.

27. Armstrong J. H., A Study of Hydrogen Induced Cracking in Iron, Phd. Dissertation, University of Denver, June 1958.

28. Robinson W.H., Carpenter S.H. and Tallon J.L., Piezoelectric Method of Determining Torsional Mechanical Damping Between 40 and 120 kHz, Journal of Applied Physics, 1974, 45(5), p. 1975-1981.

29. Devine S.D. and Robinson W.H., Piezoelectric Method of Determining Mechanical Properties of a small sandwich specimen at 30 to 200 kHz, Journal of Applied Physics 1977, 48(4), p. 1437-1441.

30. Read D.T. and Ledbetter H.M., Elastic Properties of Boron-aluminum Composite at Low Temperatures, Journal of Applied Physics, 1977, 48(7), p. 2827-2831.

31. Taylor J. R., An Introduction to Error Analysis, Oxford University Press, 1982.

32. Eshelby J.D., The Determination of the Elastic Field of an Ellipsoidal inclusion, and Related Problems, Proc. R. Soc. London, 1957, A241, p. 376-396.

33. Mori T. and Tanaka K., Average Stress in Matrix and Average Elastic Energy of Materials with Misfitting Inclusions, Acta Metall., 1973, 21, p. 571-574.

34. Hull D. and Clyne T.W., An Introduction to Composite Materials. Cambridge University Press, 2nd ed., 1996.

35. Whitcomb J. D., Chapman C.D. and Tang X., Derivation of Boundary Conditions for Micromechanics Analyses of Plain and Satin Weave Composites, Journal of Composite Materials, 2000, 34(9), p. 724-47.

36. M40J and M60J Data Sheet, Toray Carbon Fibers America, Inc.

Acknowledgments

This research was supported by the Air Force Office of Scientific Research and NASA Glenn Research Center under joint grant F49620-00-1-0159. Additional funds were also provided by the National Science Foundation and the University of Denver from a Major Research Instrumentation Program; Instrument Development and Acquisition grant# CMS-9977735.

Figure Captions

Figure 1. Cross-sections of woven 8HS T650-35/PMR-15 (a), 4HS M40J/PMR-II-50 (b) and 4HS M60J/PMR-II-50 (c) composites after manufacturing and post curing [18].

Figure 2. Schematic of three-component extensional oscillator.

Figure 3. Fully three dimensional finite element representation of an 8HS woven composite.

Figure 4. Single-slice finite element representations of 4HS and 8HS woven composites.

Figure 5. Transformation steps from a fully three dimensional to single-slice model.

Figure 6. Numerical procedures for determining longitudinal and transverse Young's moduli of graphite fibers

Table 1. Selected mechanical properties and CTEs of the T650-35, M40J and M60J graphite fibers.

Properties / Fibers	E_L [GPa]	E_T [GPa]	ν_L	G_L [GPa]	G_T [GPa]	Strength [GPa]	Strain at Failure [%]	CTE_L [10^{-6}/°C]	CTE_T [10^{-6}/°C]
T650-35*	243	13.8	0.29	23.1	5.0	4.55	1.7	-0.84	7.8
M40J**	377	N/A	N/A	N/A	N/A	4.41	1.2	-0.83	N/A
M60J**	588	N/A	N/A	N/A	N/A	3.92	0.7	-1.1	N/A

*) stiffness and thermal properties from [26] and strength from [36]

**) from [36]

Table 2. Average fiber, resin, void contents and T_g for the five composite systems [8,18].

Properties / Composites	Fiber by volume [%]	Matrix by weight [%]	Void fraction [%]	T_g [°C]
UNI. T650-35/PMR-15	55.6	36.4	1.5	~342
8HS T650-35/PMR-15	61.1	31.6	1.2	342
UNI. M40J/PMR-II-50	56.8	38.0	0.5	~389
4HS M40J/PMR-II-50	58.8	35.2	1.9	389
4HS M60J/PMR-II-50*	63.8	33.9	1.3	376

*) unidirectional M60J/PMR-II-50 composite was not available for this study.

Table 3. Properties of PMR-15 and PMR-II-50 resins

Property	Specimen								AVG
	#1	#2	#3	#4	#5	#6	#7	#8	±SDOM
PMR-15									
E [GPa]	4.02	4.02	4.05	3.97	3.97	3.93	3.95		4.00 ±0.3%
	3.98*	4.01*	4.04*	4.02*					
G [GPa]	1.48*	1.45*	1.46*	1.43*	1.45*				1.46 ±0.6%
α [10^{-6}/°C]	39.9	40.3	38.9	38.5	39.6	40.2			39.6 ±0.7%
PMR-II-50									
E [GPa]	4.40	4.36	4.33	4.32	4.29	4.31	4.31	4.30	4.33 ±0.3%
G [GPa]	1.63*	1.65*	1.67*	1.65*					1.64 ±0.5%
α [10^{-6}/°C]	38.9	38.5	38.2	38.3	39.2	37.6			38.4 ±0.6%

*) glued specimens

Table 4. Mechanical properties of unidirectional composites

Property	Specimen						AVG ±SDOM
	#1	#2	#3	#4	#5	#6	
T650-35/PMR-15							
E_L [GPa]	125	130	128	128	123	126	126.7 ±0.8%
in plane E_T [GPa]	8.32	8.36	8.41	8.23	8.16		8.30 ±0.5%
out of plane E_T [GPa]	8.16*	8.15*	8.31*	8.27*	8.16*	8.18*	8.21 ±0.3%
G_L [GPa]	4.19*	4.19*	4.22*	4.22*	4.20*		4.20 ±0.2%
G_T [GPa]	2.70*	2.88*	2.84*				2.81 ±1.9%
ν_L	0.40**	0.41**	0.42**				0.41 ±1.4%
α_L [10^{-6}/°C]	-0.71	-0.58	-0.59				-0.62 ±6.7%
in plane α_T [10^{-6}/°C]	29.0	29.4	29.5				29.3 ±0.5%
out of plane α_T [10^{-6}/°C]	27.7	33.4	31.0	31.2			30.8 ±3.8%
fiber content [vol. %]	56.3	55.3	55.2				55.6 ±0.6%
M40J/PMR-II-50							
E_L [GPa]	188	180	183	178	180	181	181.7 ±0.8%
in plane E_T [GPa]	9.00 8.97	8.82 8.84	8.91	8.97	8.72	8.94	8.90 ±0.4%
out of plane E_T [GPa]	7.19*	7.25*	7.34*	7.14*	6.95*	7.16*	7.17 ±0.7%
G_L [GPa]	4.77*	4.75*	4.81*	4.61*			4.73 ±0.9%
G_T [GPa]	2.55*	2.63*	2.57*	2.55*	2.61*		2.58 ±0.6%
ν_L	0.31	0.27	0.21				0.26 ±11%
α_L [10^{-6}/°C]	-1.39	-1.79	-1.80	-1.42			-1.6 ±7%
in plane α_T [10^{-6}/°C]	20.9	21.0	17.8				20.1 ±5.3%
out of plane α_T [10^{-6}/°C]	26.4	27.2	26.4				26.7 ±1.0%
fiber content [vol. %]	57.3	57.0	56.1				56.8 ±0.6%

*) glued specimens, **) data taken from Ref.. 7.

Table 5. Mechanical properties of woven composites

Property	Specimen								AVG ±SDOM
	#1	#2	#3	#4	#5	#6	#7	#8	
8HS T650-35/PMR15									
in plane E [GPa]	70.7	70.3	69.4	69.2	69.9				69.9 ±0.4%
out of plane E [GPa]	10.9*	10.4*	10.8*	10.3*	10.4*	10.3*	10.4*		10.5 ±0.8%
in plane α [10^{-6}/°C]	1.58	1.16	1.04	0.46	0.85	1.02			1.02 ±14.7%
out of plane α [10^{-6}/°C]	38.7	40.9	38.5	39.4					39.4 ±1.4%
fiber content [vol. %]	59.7	62.1	61.4						61 ±1.2%
4HS M40J/PMRII50									
in plane E [GPa]	98.8	98.9	99.5	98.1	99.6	97.5	98.3		98.7 ±0.3%
out of plane E [GPa]	9.11*	8.63*	8.71*	9.29*	9.41*	8.17*	8.97*	8.74*	8.88 ±1.6%
in plane α [10^{-6}/°C]	-0.25	-0.46	0.18	-0.08	-0.67				-0.25 ±58%
out of plane α [10^{-6}/°C]	30.5	35.0	36.0	37.7	37.1				35.3 ±3.6%
fiber content [vol. %]	59.4	58.6	58.5						58.8 ±0.5%
4HS M60J/PMRII50									
in plane E [GPa]	152	153	153	152	152				152.2 ±0.2%
out of plane E [GPa]	8.20*	8.09*	7.92*	8.02*	8.11*	7.87*	8.10*		8.04 ±0.5%
in plane α [10^{-6}/°C]	-0.89	-0.47	-0.90	-1.4					-0.91 ±21%
out of plane α [10^{-6}/°C]	35.8	36.7	40.4	40.6	40.9				38.9 ±2.8%
fiber content [vol. %]	63.7	63.7	63.9						63.8 ±0.1%

*) glued specimens

Table 6. Transverse properties (average between in plane and out of plane direction) of unidirectional composites used for the fiber property calculations.

	average values and assumed errors
T650-35/PMR15	
E_T [GPa]	8.25 ±1.1%
α_T [10^{-6}/°C]	30.4 ±5.1%
M40J/PMRII50	
E_T [GPa]	8.03 ±11.2%
α_T [10^{-6}/°C]	23.4 ±16%

Table 7. Elastic properties and thermal expansion coefficients of T650-35, M40J and M60J graphite fibers from different models.

Fiber	E_{fL} [GPa]	E_{fT} [GPa]	G_{fL} [GPa]	G_{fT} [GPa]	ν_{fL}	α_{fL} [10^{-6}/°C]	α_{fT} [10^{-6}/°C]	System	Models
T650-35	225 (±3)	15.4 (±0.7)	21.1 (±1.1)	5.8 (±0.4)	0.44 (±0.02)	-1.16 (±0.05)	13.5 (±1.1)	Uni.	Eshelby/ Mori-Tanaka
	224 (±3)	15.4 (±0.7)	-	-	-	-1.9 (±0.5)	12.9 (±1.5)	8HS	FE 8HS (slice)
	224 (±3)	15.4 (±0.7)	-	-	-	-1.9 (±0.7)	13.1 (±2.1)		FE 8HS (3D)
M40J	316 (±4)	13.4 (±3.7)	20.8 (±2)	3.9 (±0.1)	0.22 (±0.05)	-2.05 (±0.12)	6.9 (±6.3)	Uni.	Eshelby/ Mori-Tanaka
	344 (±2)	10.8 (±0.3)	-	-	-	-1.8 (±0.2)	8.8 (±1.7)	4HS	FE 4HS (slice)
M60J*)	500 (±2)	9.4 (±0.5)	-	-	-	-2.0 (±0.2)	18 (±4)	4HS	FE 4HS (slice)

*) It was assumed that for the M60J fiber G_{fL}= 20.8 ±10 GPa, G_{fT}=3.9 ±0.5 GPa and ν_{fL} =0.22 ±0.25

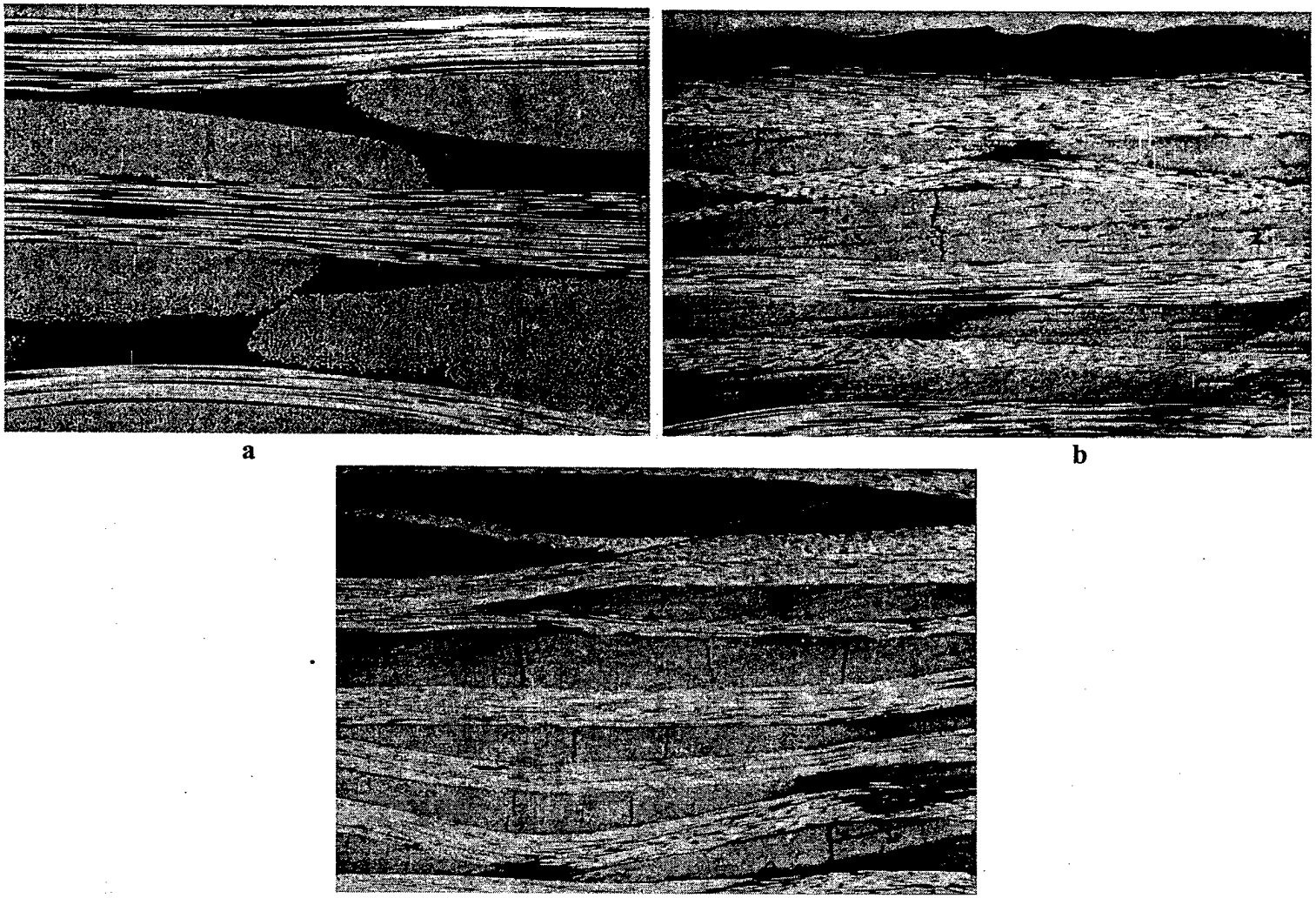

Figure 1). Cross-sections of woven 8HS T650-35/PMR-15 (a), 4HS M40J/PMR-II-50 (b) and 4HS M60J/PMR-II-50 (c) composites after manufacturing and post curing [18].

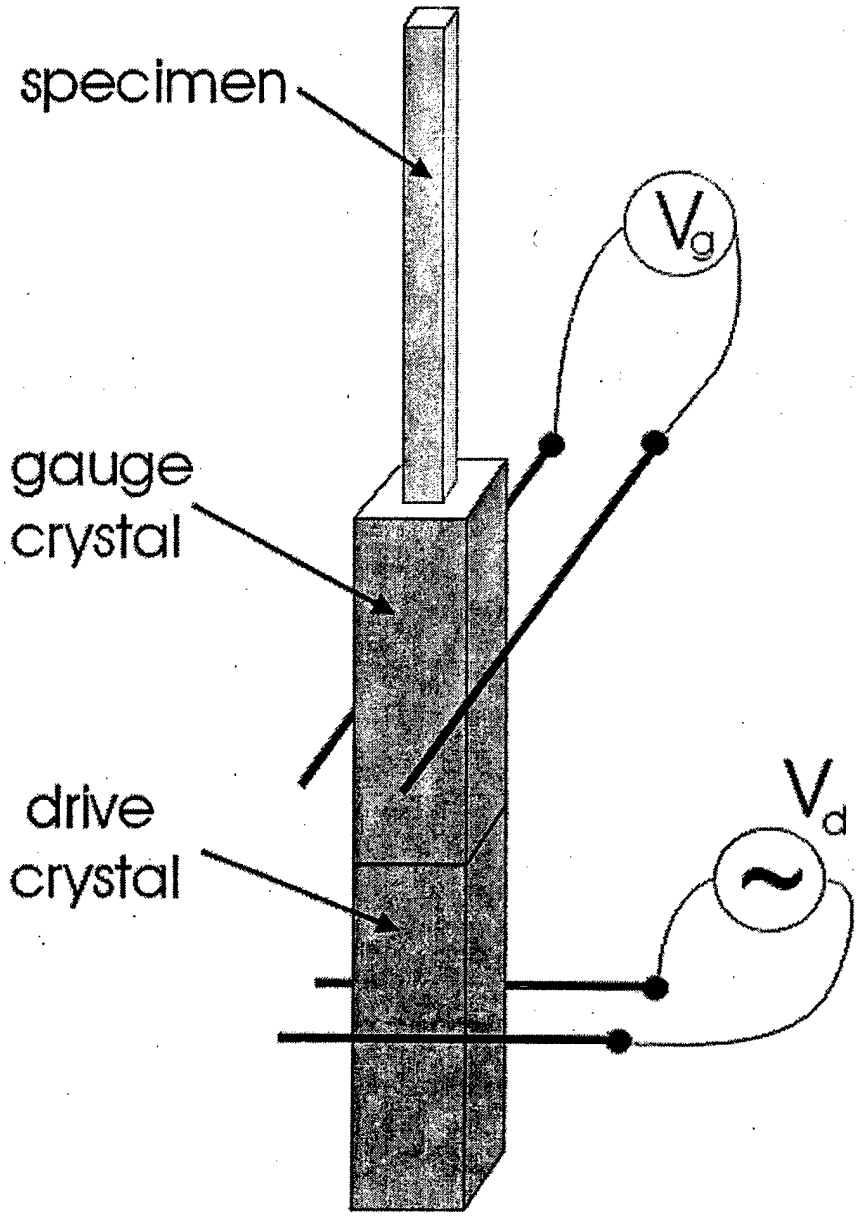

Figure 2). Schematic of three-component extensional oscillator.

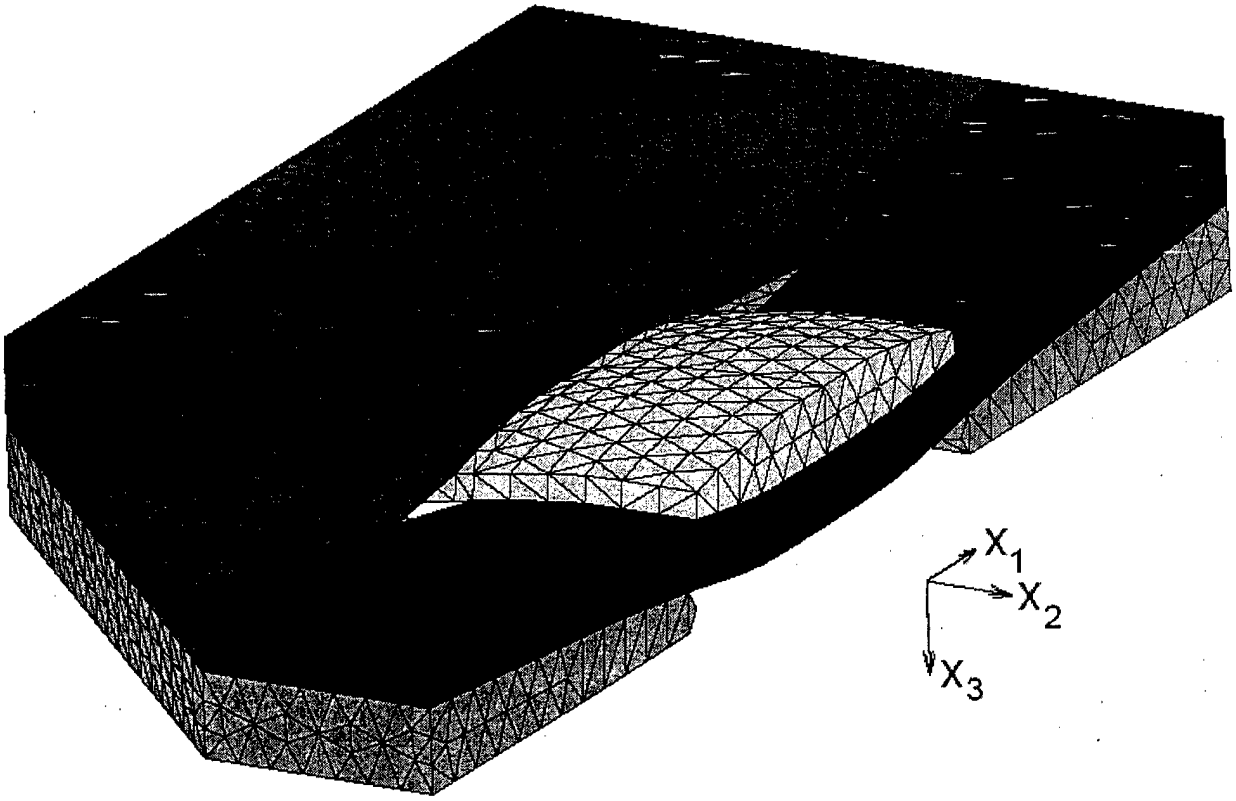

Figure 3). Fully three dimensional finite element representation of an 8HS woven composite.

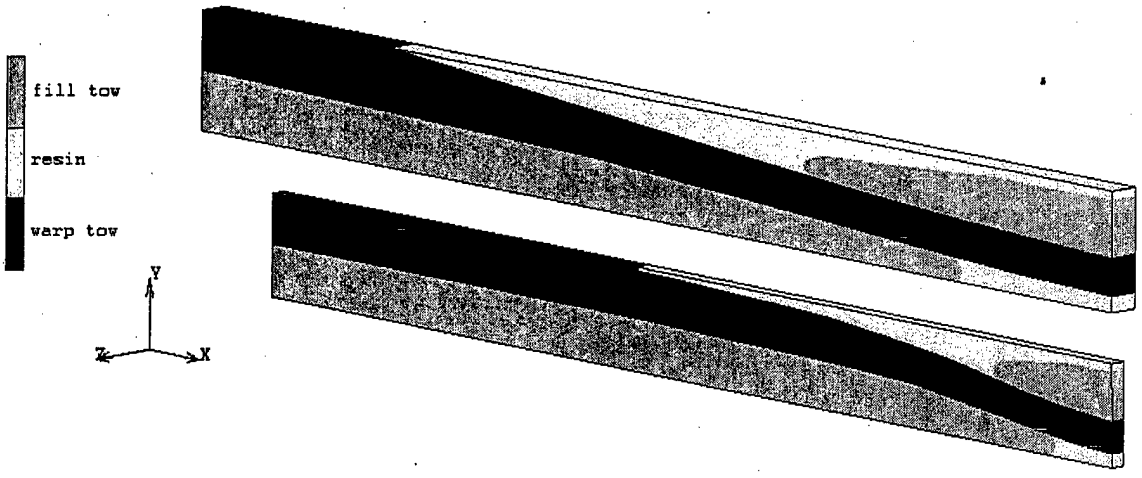

Figure 4). Single-slice finite element representations of 4HS and 8HS woven composites.

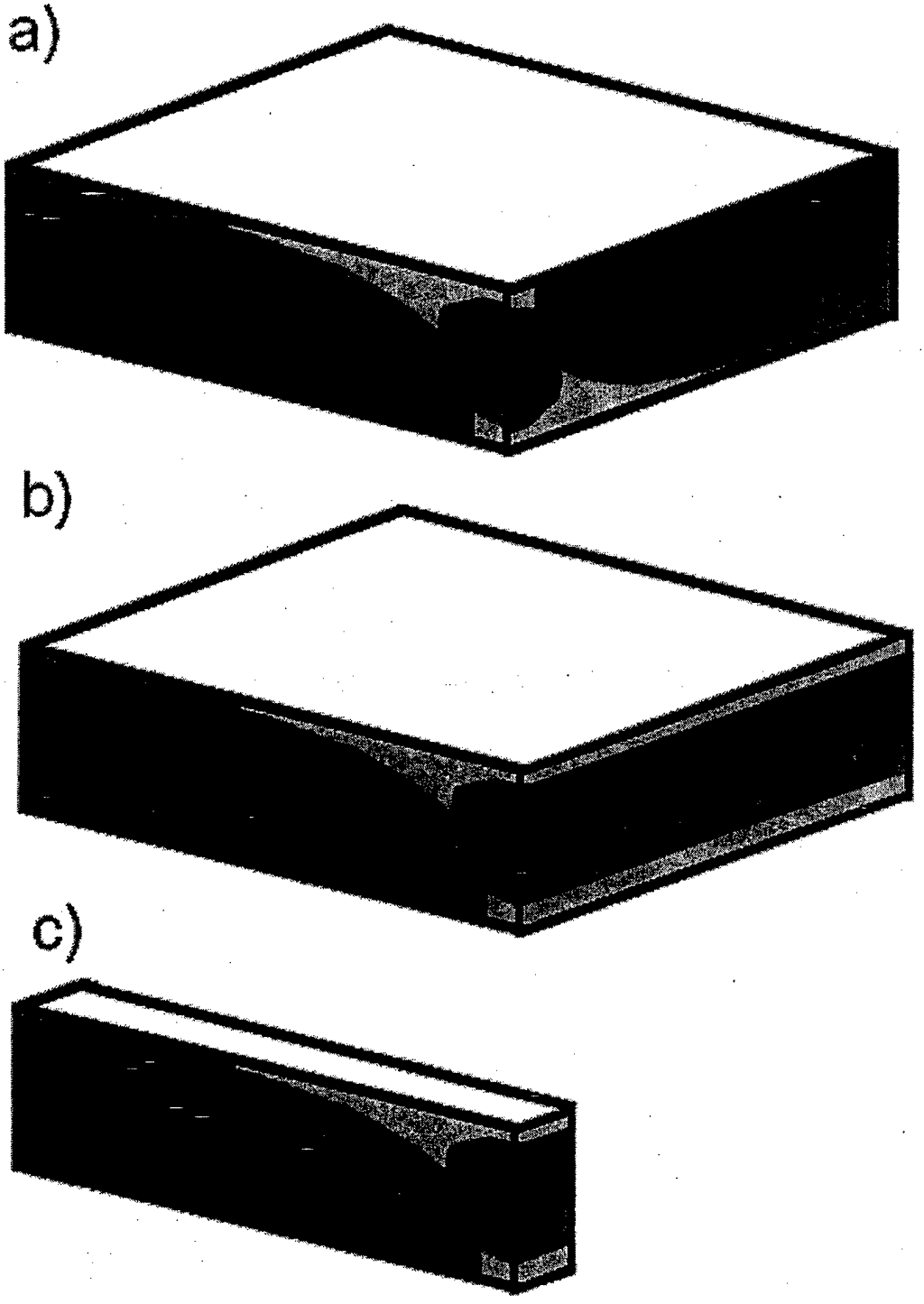

Figure 5). Transformation steps from a fully three dimensional to single-slice model.

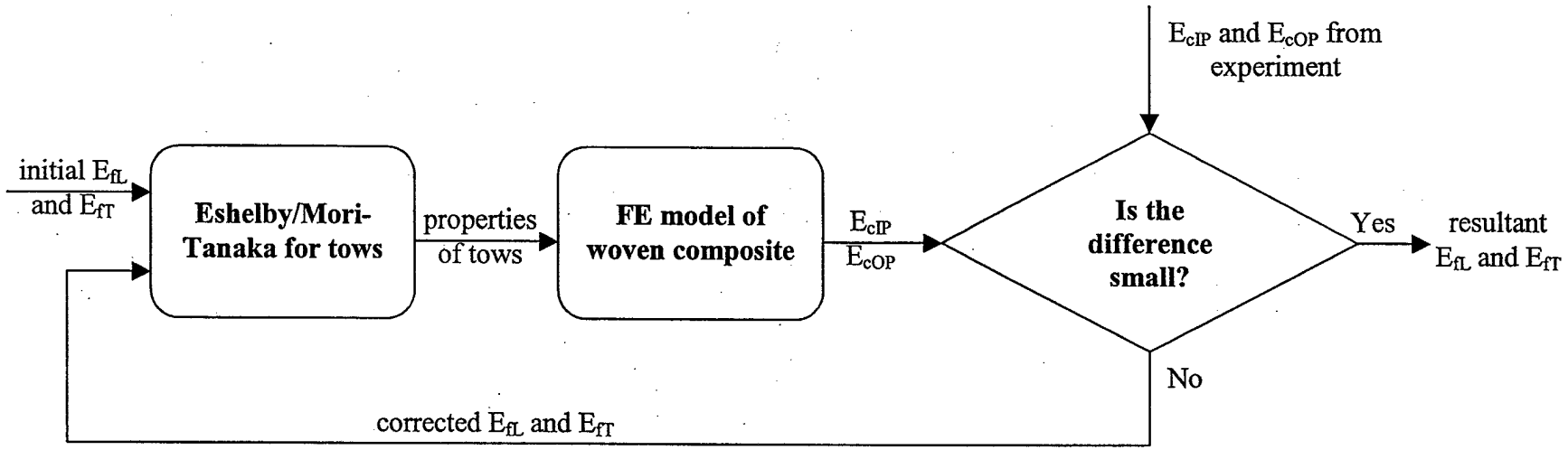

Figure 6). Numerical procedures for determining longitudinal and transverse Young's moduli of graphite fibers

Acta Materialia, submitted in December 2004

An Evaluation of Residual Stresses in Graphite/PMR-15 Composites by X-ray Diffraction

B. Benedikt*, M. Kumosa and P. K. Predecki**

Center for Advanced Materials and Structures
Department of Engineering, University of Denver
2390 South York St., Denver, Colorado 80208

Abstract

In this work, a method based on X-ray diffraction (XRD) measurements of internal stresses in embedded metallic ellipsoidal inclusions is briefly described. The method has been recently developed for the determination of residual thermal stresses in high temperature graphite/polyimide composites. The effects of external bending loads and aging on the measurements of the internal stress in unidirectional and woven graphite fiber (T650-35)/polyimide (PMR-15) composites were examined in addition to several other factors which could influence the accuracy of the stress measurements. Such factors as the volume fraction of inclusions, their aspect ratios and the interaction between individual embedded inclusions were also evaluated in this study. It has been shown that despite its complexity the proposed method can be successfully applied to the evaluation of residual stresses in high temperature polymer matrix composites subjected to external loads and aging.

* Present address: Engineering Sciences and Application Division, Los Alamos National Laboratory, Los Alamos, 87545 NM, USA

** to whom correspondence should be addressed

1. Introduction

The evaluation of the residual thermal stresses in polymer matrix composites is not a straightforward task. Several methods have been proposed for the residual stress measurements in the composites, each with its own limitations [1-22]. One of them is based on X-ray diffraction (XRD) measurements of residual strains in crystalline ellipsoidal inclusions embedded in the interlaminar regions of unidirectional and woven polymer matrix composites [8-22]. The residual interlaminar stresses in the composites are then extracted from the XRD data for the inclusions using either analytical or numerical models. The idea of employing embedded metallic inclusions as stress sensors was first proposed by Predecki and Barrett [8-11] and used to measure residual stresses in unidirectional graphite/epoxy composites with embedded aluminum, silver and niobium inclusions. In their work [8-11] Predecki and Barrett were successful in measuring the strains and stresses in the embedded inclusions including the effect of externally applied mechanical loads. However, they were unable to quantitatively evaluate the stress transfer from the composites to the embedded inclusions, which is critical for the correct determination of the state of stress in the composites.

Fenn et al. [12] used XRD to measure triaxial strains in nickel inclusions embedded in Araldite MY 753 epoxy resin as a function of the volume fraction of inclusions and the curing temperature. The authors observed little difference in measured strains over a range of metallic inclusion volume fractions (10%-30%). They also observed that the measured strains inside inclusions for the examined curing temperatures did not coincide with theoretically predicted values. This discrepancy was attributed to the lack of the incorporation of temperature dependent resin properties into the model. Meske and Schnack [13, 14] investigated strains in silver inclusions embedded between composite layers using XRD. They proposed a new micromechanical approach to study the stress–strain relationship between the measured strain in the inclusions and the stress in the composite. However, their approach was based on the assumption that the inclusions formed a continuous layer in the composite, which is rarely satisfied as revealed by SEM analyses [15, 16].

Recently, major research activities have been undertaken [15-22] to further improve the method of Barrett and Predecki and apply it to the measurements of residual interlaminar stresses in advanced high temperature polymer matrix composites based on T650-35 graphite fibers embedded in a PMR-15 polyimide matrix (see Figures 1a-b). These composites develop large residual stresses, which can, in some cases, cause premature interlaminar fracture of the composite panels during manufacturing [23-33]. The residual stresses can also greatly affect the mechanical performance of the composites, especially under shear dominated biaxial loads [24,26,31,33]. Thus, the precise determination of the stresses in these composites was found to be of primary importance. In order to measure the stresses the XRD method of Predecki and Barrett [8-11] was used and significantly improved by adding strong analytical and numerical components [15-22]. Without these two new components, it would not be possible to extract the residual stresses in the composites from the XRD residual stresses in the inclusions for different composite architectures (woven and unidirectional) as a function of manufacturing conditions, external loads and potential in-service aging conditions. The present methodology is based on XRD measurements of residual stresses in embedded inclusions and then on extracting the information about the interlaminar stresses in the composites using the Eshelby/Mori-Tanaka approach [34-36]. Throughout this paper we will refer to this methodology as the XRD-Eshelby/Mori-Tanaka (XRD-E/M-T) method.

In this work, we briefly describe the XRD-E/M-T method and present a few key examples of its application to the residual stress determination in the T650-35/PMR-15 composites. New computational results are also presented here to further verify the accuracy of the method and to establish its potential limitations.

2. Fundamental Basis of the XRD-Eshelby/Mori-Tanaka approach

2.1 XRD measurements

The experimental determination of the strains and stresses in Al inclusions embedded in composites was performed in the following way. First, the lattice spacing d_0 between 422 atomic planes for unstressed Al powder was measured using the well-established XRD technique [37-39]. Second, the lattice spacing $d_{\phi\psi}$ for 422 planes perpendicular to the diffraction vector $\mathbf{L}_{\phi\psi}$ (see Figure 2) for the Al inclusions were experimentally obtained using the same XRD technique. It can be shown that if $\frac{d_{\phi,\psi} - d_0}{d_0}$ vs. $\sin^2\psi$ plots for $\phi=0^0$ and $0^0<\psi< 90^0$, and $\phi=90^0$ and $0^0<\psi< 90^0$ are linear, then the shear stress components σ_{13} and σ_{23} are zero, there are no significant stress gradients in the diffracting volume, and the method is considered to be applicable to the specimens being measured [38].

The relationships between the measured lattice spacing and the principal components of the strain (ε_{11}, ε_{22}, and ε_{33}) in the inclusions can be obtained from equations 1a-b [38].

$$\frac{d_{\phi=0,\psi} - d_0}{d_0} = (\varepsilon_{11} - \varepsilon_{33})\sin^2\psi + \varepsilon_{33} \tag{1a}$$

$$\frac{d_{\phi=90,\psi} - d_0}{d_0} = (\varepsilon_{22} - \varepsilon_{33})\sin^2\psi + \varepsilon_{33} \tag{1b}$$

Two representative examples of $\frac{d_{\phi,\psi} - d_0}{d_0}$ vs. $\sin^2\psi$ plots are presented in Figures 3a-b. It can be seen in these figures that the $\sin^2\psi$ plots are linear within experimental error, therefore, the principal components of the strain tensors could be determined using equations 1a-b. In the numerical computations, six different values of the lattice spacing $d_{\phi,\psi}$ were measured for each ϕ angle ($\phi=0^0$ or $\phi=90^0$ by varying ψ. The fiber direction defined the $\phi = 0^0$ in-plane direction. The principal strain components were subsequently

computed using the least square method. The corresponding principal stresses in the inclusions were computed by multiplying the principal strains by the so-called x-ray elastic constants for an Al single crystal. The x-ray elastic constants used in this study were computed from the Neerfeld-Hill model [38].

2.2 Application of the Eshelby/ Mori-Tanaka approach for the stress determination

As part of the stress analysis, Benedikt et al. [15-22] proposed a model based on the Eshelby/Mori-Tanaka method [34-36], which can be used to compute average residual interlaminar stresses in the composites from the measured strains in the embedded inclusions. In this approach, the residual stresses σ^{Res} ($\sigma^{Res}=\mathbf{C}^{M}:\varepsilon^{Res}$, where $\mathbf{C}^{M}$ is the stiffness tensor for the matrix and ε^{Res} is the corresponding residual strain) caused by reinforcing graphite fibers, were modeled as far-field stresses prescribed to an unbounded matrix with embedded metallic inclusions (Figure 4). Using the Eshelby/Mori-Tanaka approach, one can calculate the magnitude of the prescribed stresses σ^{Res}, which generated the required state of stress in the embedded inclusions. However, it has been shown in Ref. 15 that this procedure yields correct results only if the elastic and thermal properties of the inclusions, the distributions of the inclusions and the visco-elastic and thermal properties of the matrix are known. In its original form, the approach proposed by Benedikt et al. [15-22] did not consider the actual interactions between the individual inclusions, the distribution pattern (morphology) and shape of the inclusions and their effects on the measurements of the residual stresses. This has been accomplished for the first time in the present work.

Throughout this paper, the stresses in the inclusions caused by the average interactions between the inclusions themselves and of the inclusions with the visco-elastic matrix, due to the temperature change during manufacturing are called the close range stresses $\sigma^{C\text{-}R}$ ($\sigma^{C\text{-}R}=\mathbf{C}^{I}:\varepsilon^{C\text{-}R}$). The close range stresses $\sigma^{C\text{-}R}$ can be approximated using the Eshelby/Mori-Tanaka method [34-36] if the properties of the embedded inclusions and the matrix are known. The close-range strain $\varepsilon^{C\text{-}R}$ at ambient temperature was computed from equation 2.

$$\varepsilon_{kl}^{C-R} = \sum_{i=0}^{f-1}\left(S_{klmn}\varepsilon_{mn}^{T}(i) + \varepsilon_{kl}^{T-M}(i) - \varepsilon_{kl}^{T^*}(i)\right) \quad (2)$$

where $\varepsilon^{T^*}(i)$ is the temperature dependent eigenstrain for an inclusion, $\varepsilon^{T\text{-}M}(i)$ is the time and temperature dependent perturbed strain computed from the Mori-Tanaka method, $\varepsilon^{T}(i)$ is the time and temperature dependent eigenstrain at time i, and f is the number of sub-steps used in the visco-elastic analysis [15].

Once the close-range stresses are calculated, the residual strains ε^{Res} and therefore the residual stresses σ^{Res} in the composite can be determined using equations 3a-c.

$$C_{ijkl}^{I}\left(S_{klmn}\varepsilon_{mn}^{T} + \varepsilon_{kl}^{T-M} + \varepsilon_{kl}^{Res}\right) = C^{M}\left(S_{klmn}\varepsilon_{mn}^{T} + \varepsilon_{kl}^{T-M} + \varepsilon_{kl}^{Res} - \varepsilon_{kl}^{T}\right) \quad (3a)$$

$$\varepsilon_{ij}^{T-M} + v_f\left(S_{ijkl}\varepsilon_{kl}^{T} - \varepsilon_{ij}^{T}\right) = 0 \quad (3b)$$

$$\sigma_{ij}^{X-Ray} - C_{ijkl}^{I}\varepsilon_{kl}^{C-R} = C_{ijkl}^{I}\left(S_{klmn}\varepsilon_{mn}^{T} + \varepsilon_{kl}^{T-M} + \varepsilon_{kl}^{Res}\right) \quad (3c)$$

where $\sigma^{X\text{-}Ray}$ is the measured stress in the inclusions, **S** is the Eshelby tensor for spherical inclusions, $\mathbf{C}^{I}$ is the tensor of the elastic constants of the inclusions, $\mathbf{C}^{M}$ is tensor of the elastic properties of the matrix, ε^{T} is the constant eigenstrain [35], $\varepsilon^{T\text{-}M}$ is the average perturbed strain caused by the presence of multiple inclusions computed from the Mori-Tanaka method (see Figure 4), v_f is the average volume fraction of the inclusions, and $\varepsilon^{C\text{-}R}$ is the close-range strain computed from equation 2.

3. Residual Stresses in Graphite Polyimide Composite

Three effects have been examined in our research using the XRD-E/M-T method. First, the effect of composite architecture was investigating by the evaluation the interlaminar

stresses in both unidirectional and woven 8HS T650-35/PMR-15 composites [15-18, 20]. Then, the composites were subjected to four-point bending and the effect of external loads on the stress distributions in the inclusions and the composites was examined [16, 17, 20, and 22]. Finally, the composites were subjected to environmental aging in either nitrogen or in air and the effect of aging on the residual stresses was determined [19-21].

3.1 Composites investigated

Two composite systems have been investigated, namely six ply unidirectional and four ply eight harness satin woven laminates. Aluminum inclusions were placed between the first and second plies (Figures 1a-b) for both composite architectures before the curing cycle [15]. The inclusions formed clusters with the volumes of fibers of 40±7% (Fig. 1a) and 46±7.4% (Fig. 1b) for the unidirectional and woven systems, respectively [15, 16]. More information about the material properties of the composites, inclusions and manufacturing conditions can be found in [15, 16, and 20].

3.2 Material properties

The PMR-15 matrix was assumed to be a visco-elastic material with its thermal expansion coefficient α depending upon temperature and its shear modulus G depending on both time and temperature. Poisson's ratio of PMR-15 was assumed to be constant. The experimental values of the shear modulus G as a function of time and temperature were taken from Ref. [40] and the thermal expansion coefficient of the post cured polyimide was measured in this study. The values of G and α were subsequently curve fitted using the non-linear least square method to obtain G(t, T) and α(T) functions. These relations are shown below.

$$G = 10^{(Exp(0.16(-Log(t)+6.5)^{0.5})+7.5)} \quad (4a)$$

$$a_v = 10^{Exp(0.012(-T+348)^{0.48})-1.076} \quad (4b)$$

$$a_h = 10^{Exp(0.41(-T+348)^{0.28}-4.3)} \tag{4c}$$

$$\alpha = 3\cdot 10^{-12}\cdot(104+T)\cdot(127160-548\cdot T+T^2) \tag{4d}$$

The shear modulus G is given in equation 4a as a function of time at T_{ref}=288°C (the master curve). The vertical, $a_v(T)$, and horizontal, $a_h(T)$, shift functions were estimated from the data presented in Ref. [40]. The horizontal shift function is used in the definition of reduced time $\xi(t)$ (see equation 5).

$$\xi(t) = \int_0^t \frac{dt'}{a_h[T(t')]} \tag{5}$$

The application of the horizontal and vertical shift functions (equations 4b and 4c) allows the determination of the G(t,T) function from the master curve. However, the formulae given by equations 4a-d are only valid for a temperature range from room temperature to 348°C and a range of time from 0 to $10^{6.5}$ seconds.

The linear elastic and thermal properties for aluminum inclusions and PMR-15 (for the linear elastic analysis) used in our models are shown in Tables 1.

Table 1. Elastic and thermal properties of Al inclusions and PMR-15

	Young's modulus [MPa]	**Poisson ratio**	**Coefficient of thermal expansion [1/°K]**
Aluminum	**71**	**0.351**	**$22.4\cdot10^{-6}$**
PMR-15	**4.35**	**0.36**	**$44.8\cdot10^{-6}$**

For the T650-35 fibers the longitudinal and transverse Young moduli and the longitudinal shear modulus were 241 GPa, 20GPa and 27GPa, respectively and their longitudinal and transverse Poisson ratios were taken as 0.2 and 0.4. Their longitudinal and transverse coefficients of thermal expansions were $\alpha_L = -0.5\cdot10^{-6}$ and $\alpha_T = 10\cdot10^{-6}$ per °K.

3.3 Effect of composite architecture

The residual thermal stresses in the two composite systems were determined under two conditions; linear elastic with a constant coefficient of thermal expansion (α) for PMR-15 and visco-elastic with α depending on temperature [40]. The actual manufacturing cycle was followed in the visco-elastic case. The stresses in the composites were also calculated using classical lamination plate theory (CLPT) [41]. From four sets of computations for each composite we could determine the extent of the visco-elastic effects in the composites and compare the predicted interlaminar stresses obtained from the XRD-E/M-T and CLPT methods. The results from the calculations are shown in Tables 2a-b. It can be seen from these data that the XRD-E/M-T method can distinguish between different composite architectures [15, 16]. Also, the solution for the stresses is three-dimensional and the residual in-plane stresses in the composites (both unidirectional and woven) agree well with the predictions from CLPT. More, importantly, the method also allows for the determination of the through thickness interlaminar stresses, which cannot be obtained from CLPT [40].

Table 2. Interlaminar residual stresses in (a) unidirectional and (b) 8HS woven composites from the XRD-Eshelby/Mori-Tanaka and CLPT methods obtained with linear-elastic and visco-elastic assumptions [15, 17].

a)

	X-ray with Eshelby			**Plate theory**		
	σ_{11} **[MPa]**	σ_{22} **[MPa]**	σ_{33} **[MPa]**	σ_{11} **[MPa]**	σ_{22} **[MPa]**	σ_{33} **[MPa]**
Linear elastic	**57±3.5**	**42±3.5**	**28±3.5**	**70.4**	**44.4**	**0**
Visco-elastic	**52.2±9**	**37.6±3.5**	**23±3.5**	**47.9**	**31.6**	**0**

	X-ray with Eshelby			Plate theory		
	σ_{11} [MPa]	σ_{22} [MPa]	σ_{33} [MPa]	σ_{11} [MPa]	σ_{22} [MPa]	σ_{33} [MPa]
Linear elastic	**70.7 ± 17**	**71.1 ± 17**	**36.7 ± 16**	**94**	**94**	**0**
Visco-elastic	**67.3 ± 17**	**67.6 ± 16**	**33 ± 16**	**63.1**	**63.1**	**0**

b)

There is also another very important observation, which can be made by evaluating the thermal residual stresses shown in Tables 2a-b. Clearly, there is a small difference between the results from the XRD-E/M-T method with and without the visco-elastic assumptions. Even, if the visco-elastic properties of PMR-15 and their temperature dependent CTE are ignored and the stresses are calculated with time independent α and a constant stiffness at room temperature, the difference between the two approaches is less than 10% for both cases. Obviously, this effect comes from the fact that the visco-elastic response of the resin is already included in the experimental XRD response of the inclusions from which the residual stresses in the composites were calculated. The relatively close agreement between the two approaches (linear and visco-elastic) might have important practical applications. Since the visco-elastic response of polymers is often very difficult to obtain, it can essentially be disregarded in the residual stress analysis using the concept of embedded metallic inclusions following the observations made in Tables 2a-b. The error caused by this assumption will be relatively small.

3.4 Effect of externally applied bending loads

Simultaneous four-point bend tests and XRD measurements were performed on the composites and the stresses in the inclusions were measured as a function of the bending moment represented by the axial strain on the surface of the specimens (Figure 5) [16, 17, 20 and 22]. The axial strains were measured by strain gages placed on the surface of the specimens. It was observed that initially the measured von Mises stresses in the

embedded inclusions increased linearly with the axial strains generated by the fixture (see Figures 6a-b). However, when the von Mises stresses reached approximately 60-65 MPa, they formed a plateau. The plateau was observed to occur in the inclusions embedded inside both the unidirectional and woven composites for very similar von Mises stresses [20, 22]. Internal cracking in the composites was eliminated as a reason for the plateau by performing four-point bend tests on the composites with and without the inclusions and by monitoring acoustic emission [20, 22]. The presence of the plateau in the von Mises stresses in the inclusions was attributed to the onset of plastic deformation of the aluminum inclusions. It was concluded from the four-point bend experiments that the XRD-Eshelby/Mori-Tanaka approach is sensitive to the external loads and is limited by the plastic deformation of the inclusions, similar to the observations made by Predecki and Barrett [9]. Obviously, the effect of plasticity of the inclusions would make the methods impossible to use in the case of very large residual stresses generating von Mises stresses in the inclusions that are much larger than the yield strength of the inclusions. It would also make the method impractical, if the yield strength of the inclusions was very low. Only, an optimum combination of the yield strength of the inclusions and the magnitudes of residual stresses, creating a distinct linear response, shown in Figures 6a-b, would make the method suitable for residual stress measurement.

3.5 Effect of aging in nitrogen and in air

Finally, the XRD-E/M-T method was also used to monitor the changes of residual stresses in the composites subjected to aging in either air or nitrogen at 315°C (Figures 7 and 8) [19-21]. However, it could not be used successfully to evaluate residual stresses in the composites aged in air due to the lack of physical properties of PMR-15 aged in air [19-21]. It was observed that the composites aged in air developed significant numbers of cracks (Figures 8a-b) [19-21], which had to be neglected in the subsequent computations due to the numerical complexity, despite the fact that the cracks must have influenced the residual stresses in the inclusions. On the other hand, the tests performed in nitrogen yielded results, which could be interpreted using the XRD-E/M-T approach. The behavior of the aged neat PMR-15 resin was either measured (volumetric shrinkage) or

obtained from the existing literature (visco-elastic properties [42] and α [43]). No cracks were found in the unidirectional composite aged in nitrogen and very few cracks were found in the woven system subjected to these conditions up to approximately 1000 hours.

Table 3. Stresses in Al inclusions as a function of aging time at 315°C in nitrogen for (a) unidirectional and (b) 8HS woven T650-35/PMR-15 composites [20, 21].

Aging Time [hours]	σ_{11}* [MPa] XRD	σ_{22}* [MPa] XRD	σ_{33}* [MPa] XRD	Von Mises* [MPa]	σ_{11}** [MPa] CLPT	σ_{22}** [MPa] CLPT	σ_{33}** [MPa] CLPT
24	85	53	15	60.7	69.6	36.5	-29.3
96	70	34	-0.5	61.1	74.3	39.0	-33.5
264	87	54	21	57.2	84.5	44.2	-42.4
600	80	51	20	52.0	104.4	54.4	-60.5
890	109	79	44	56.3	121.6	63.3	-76.4
1170	106	78	45	52.9	138.4	71.9	-91.9

(a)

Aging Time [hours]	σ_{11}* [MPa] XRD	σ_{22}* [MPa] XRD	σ_{33}* [MPa] XRD	Von* Mises [MPa]	σ_{11}** [MPa] CLPT	σ_{33}** [MPa] CLPT
24	85.3	87.7	31.8	54.0	69.3	-21.9
96	68.2	61.5	23.6	41.0	74.8	-25.8
264	90.3	88.0	6.2	83.0	87.0	-33.9
600	96.0	92.2	27.6	67.1	109.9	-50.8
890	91.1	93.5	33.7	59.0	132.3	-65.4
1170	91.7	91.0	37.0	54.5	152.7	-79.7

(b)

Table 4. Interlaminar residual stresses as a function of aging time at 315°C in nitrogen in (a) unidirectional and (b) 8HS woven T650-35/PMR-15 composites [20, 21].

Aging Time [hours]	σ_{11}* [MPa] XRD	σ_{22}* [MPa] XRD	σ_{33} [MPa] XRD	σ_{11}** [MPa] CLPT	σ_{22}** [MPa] CLPT
24	86.4	64.1	37.7	68.5	45.7
96	76.4	51.3	27.4	74.6	50.2
264	96.9	74.0	51.1	87.9	60.1
600	103.8	83.6	62.1	106.0	79.8
890	138.5	117.7	93.4	137.2	97.1
1170	146.8	127.3	104.4	159.7	113.9

(b)

Aging Time [hours]	σ_{11}* [MPa] XRD	σ_{22}* [MPa] XRD	σ_{33}* [MPa] XRD	$\sigma_{11}=\sigma_{22}$** [MPa] CLPT
24	88.6	90.4	49.8	71.8
96	76.4	71.6	44.1	78.7
264	99.3	97.7	38.3	93.6
600	115.8	113.1	66.2	123.4
890	121.9	123.7	80.3	149.3
1170	131.9	131.4	92.2	174.5

(b)

The stresses in the inclusions aged in nitrogen measured by XRD (*) and the corresponding numerical predictions of the stresses from CLPT in combination with Eshelby/Mori-Tanaka (**) are presented in Tables 3a,b for the two composite systems. The interlaminar stresses in the composites aged in nitrogen are shown in Tables 4a,b with the stresses from XRD-E/M-T indicated by (*) and from CLPT by (**). In the case of the composites aged in nitrogen, not only the stresses caused by the cooling cycle, but

also the stresses caused by the volumetric shrinkage were modeled. It can be seen from Tables 4a,b that all in-plane stress components increase with aging. The von Mises equivalent stress was also calculated to confirm that the measured stresses did not cause yielding of the inclusions. The data from the aging experiments performed in air can be found in [20, 21].

4. Effects of Inclusions on Residual Stress Measurements

It was shown above that the XRD-E/M-T method can be very useful in residual stresses measurements in high temperature polymer matrix composites and that the effects of aging and external loads can be monitored. In this section, several other important factors are examined, related to the application of embedded ellipsoidal metallic inclusions to the measurement of residual stresses. These factors have not been accounted for in our previous analyses [15-22]. In particular, the effects of the volume fraction of inclusions, their aspect ratios and the local interactions between individual inclusions on the XRD stress measurements needed to be established.

4.1 Effect of varying volume fractions of inclusions

The actual XRD stress data were obtained from many different clusters of embedded Al inclusions. Since the dimensions of the incoming X-ray beam were several orders of magnitude larger than any individual inclusion the measured strains were averaged over multiple inclusions. Based on our SEM analysis [15, 16], it was determined that most of the inclusions formed clusters with varying volume fractions. Furthermore, it was impossible to precisely determine the distributions of the inclusions in the area from which the XRD measurements were performed. Therefore, to evaluate the influence of the volume fraction of inclusions on the calculated stresses in the composite, one needs to determine these stresses assuming a different volume fraction each time. The difficulty associated with this approach is that a single set of XRD data must be arbitrarily chosen, before any calculations may take place. The scatter in the experimental XRD results was quite significant [15-22], so it was not clear if the arbitrary choice of the experimental

results could influence the calculated stresses in the composites. In order to overcome this difficulty, three sets of experimental data (the highest, the lowest and the average measured strains) for both unidirectional and woven composites were used.

Subsequently, the stresses in the composites were calculated from the chosen XRD strains assuming a different volume fraction of inclusions. The results of these computations for two composite systems are presented in Figures 9a-b. It is clearly seen in these figures that the calculated interlaminar residual stresses do not significantly depend on the assumed volume fraction of embedded inclusions for both unidirectional and woven composites. It can also be observed that the scatter in the computed residual stresses, indicated by the error bars in Figures 9a-b, due to the experimental errors in the XRD measurements is considerably larger than the effect of the volume fraction of inclusions.

4.2 Effect of inclusion shape

Another source of possible inaccuracy of the method that needed to be examined was an uncertainty related to the shape of the embedded inclusions. In our analyses we have assumed so far that that the inclusions are perfectly spherical [15-22]. However, based on our SEM observations [15], this assumption was found to be not always strictly correct. Therefore, an analytical approach proposed for the determination of strains and stresses in randomly oriented spheroidal inclusions [44, 45] was employed in this work to establish the relationship between the shape of the embedded inclusions and the calculated stresses in the composites. A random orientation of the inclusions was assumed which agreed well with our SEM observations [15]. In addition, the interlaminar stresses were also computed assuming that the inclusions were perfectly aligned along the fiber direction.

Figures 10a-b illustrates the thermal residual stresses in the composites as a function of the aspect ratio of the embedded inclusions for the unidirectional and woven composites, respectively. The results were obtained from the average XRD strains. It is evident when

examining the data in Figures 10a-b that all three stress components do not depend to any great extent upon the shape and orientation of the embedded inclusions. In particular, for the experimentally determined range of aspect ratios, denoted by the shaded areas in Figures 10a-b, the stress changes are essentially negligible for all considered composites and orientations. Also, the interlaminar stresses calculated from the aligned inclusions are generally more sensitive to the changes in the aspect ratio than the stresses determined from the randomly oriented inclusions.

4.3 Effects of interactions between individual inclusions and of distribution patterns

The aluminum inclusions used in the XRD experiments can locally form clusters with high concentrations of inclusions, even higher than 47%, as indicated in Figures 1a-b. Therefore, the average distance between the inclusions in the densely packed clusters can be very small with respect to the size of the inclusions. Consequently, the local interactions between the embedded inclusions may considerably disturb the stress and strain fields at the microscopic level, which could also affect the XRD data. The Eshelby/Mori-Tanaka approach (equations 3a-c) only accounts for the average interactions between the inclusions [46]. To numerically estimate the potential inaccuracy of our method caused by neglecting the interactions between individual inclusions, we extend the Eshelby/Mori-Tanaka approach to include the individual interactions effect using the model proposed in [47].

It would be almost impossible to numerically determine the interactions between all individual Al inclusions in an average size cluster due to the sheer number of inclusions, which could be larger than several thousands. On the other hand, the individual interactions are only considerable between the inclusions, which are located fairly close to each other [47, 48]. For these reasons, we explicitly modeled the interactions only inside a relatively small sub-cluster that consisted of up to no more than 125 inclusions (see Figures 1a-b). By prescribing the far-field strains $\varepsilon^{T\text{-}M}$ (with $\sigma^{T\text{-}M} = \mathbf{C}^{M}:\varepsilon^{T\text{-}M}$) to the sub-cluster at infinity, the average influence of the remaining inclusions in the cluster is considered in the computations. The magnitude of $\varepsilon^{T\text{-}M}$ is determined based on the

average strain field in the interacting inclusions in the sub-cluster using the following equation:

$$\frac{v}{N}\sum_{i=1}^{N}\left(C_{ijkl}^{Mat}\left(\varepsilon_{kl}^{A}+\varepsilon_{kl}^{d(i)}-\varepsilon_{kl}^{*(i)}+\varepsilon_{kl}^{T-M}\right)\right)+(1-v)\left(C_{ijkl}^{Mat}\left(\varepsilon_{kl}^{A}+\varepsilon_{kl}^{T-Ms}\right)\right)=C_{ijkl}^{Mat}\varepsilon_{kl}^{A} \qquad (6)$$

where N is the number of inclusions in the sub-cluster, $\varepsilon^{*(i)}$ is the constant eigenstrain for the i^{th} inclusion and $\varepsilon^{d(i)}$ is the disturbance strain for the i^{th} inclusion given by:

$$\varepsilon_{ij}^{d(I)}=S_{ijkl}^{\Omega_I}\varepsilon_{kl}^{*(I)}+\sum_{\substack{r=1\\(r\neq I)}}^{N}S_{ijkl}^{\Omega_r(outside)}\Big|_{x=x_p}\varepsilon_{kl}^{*(r)} \quad \text{for I=1, 2,...,N} \qquad (7)$$

where S^{Ω_I} is the Eshelby tensor for the interior points of inclusion Ω_I, and $S^{\Omega_r(outside))}$ is the Eshelby tensor for the exterior points of inclusion Ω_r (r=1, 2,...,N and r≠I) computed at the center point $\mathbf{x_p}$ of inclusion Ω_I. Since the numerical values of the Eshelby tensors for the exterior points depend on the relative position of the interacting inclusions, the disturbance strains $\varepsilon^{d(i)}$ (i=1, 2,...,N) consider also the effect of individual interactions. More information about this model and the numerical procedures used can be found in [48].

Table 5. Interlaminar stresses in unidirectional (a) and woven (b) composites calculated as a function of the number of interacting inclusions and distribution patterns.

Number of inclusions in sub-cluster	Random distribution			Simple cubic distribution			Eshelby/Mori-Tanaka		
	σ_{11} [MPa]	σ_{22} [MPa]	σ_{33} [MPa]	σ_{11} [MPa]	σ_{22} [MPa]	σ_{33} [MPa]	σ_{11} [MPa]	σ_{22} [MPa]	σ_{33} [MPa]
1	57.1	42.0	28.0	57.1	42.0	28.0	57.1	42.0	28.0
27	57.3	42.1	28.2	55.1	42.3	30.3			
125	57.0	42.3	28.7	54.8	42.37	30.8			

a)

Number of inclusions in sub-cluster	Random distribution			Simple cubic distribution			Eshelby/Mori-Tanaka		
	σ_{11} [MPa]	σ_{22} [MPa]	σ_{33} [MPa]	σ_{11} [MPa]	σ_{22} [MPa]	σ_{33} [MPa]	σ_{11} [MPa]	σ_{22} [MPa]	σ_{33} [MPa]
1	70.7	71.1	36.6	70.7	71.1	36.6	70.7	71.1	36.6
27	70.8	70.8	37.3	69.4	69.7	40.4			
125	70.6	70.9	38.1	69.2	69.3	41.1			

b)

The residual stresses in the unidirectional and woven composites computed using the Eshelby/Mori-Tanaka model and the model proposed in this study that considers the interactions between the individual inclusions are shown in Tables 5a -b. Only the results from the linear elastic computations are presented here using the actual average XRD stress data for the Al inclusions. Since the differences between the elastic and visco-elastic results in Tables 2a-b are less than 10% and the visco-elastic case is modeled as a finite sum of elastic solutions anyway, the effect of inclusion interactions and distribution

patterns shown in Tables 5a-b should be quite representative for the visco-elastic cases also. Most importantly, the effect of the interactions between individual Al inclusions should not influence the residual stress analysis discussed in this work based on the data listed in Tables 5a-b. Also, no noticeable effect of the distribution pattern (random vs. simple cubic) of the inclusions was observed.

4. Advantages and Disadvantages of the XRD-Eshelby/Mori-Tanaka approach

4.1 Advantages

It has been recently shown that the thermal residual stresses could be accurately determined from the stresses measured by XRD in embedded aluminum inclusions in high temperature polyimide matrix composites [15-22]. It was also indicated that the original work by Predecki and Barrett [8-11] was correct in concept. Most importantly, the initial observations made in [15-22] were validated by testing two composite systems much more suitable for this purpose, with much higher residual stresses than the original graphite fiber epoxy systems [23-33]. Owing to the recently gained experience in this study, several advantages and disadvantages of the XRD-Eshelby-Mori-Tanaka method can be enumerated regarding its applicability to the residual stress determination in polymer matrix composites.

With regard to the advantages, (1) the method is accurate enough to determine stresses non-destructively to within a few MPa and to distinguish between the residual stresses in unidirectional and woven composites based on the same fibers and matrix [15-18, 20]. Moreover, (2) the effect of external loads on the interlaminar stresses in the composites can be investigated using this method [16, 17, 20, and 22]. (3) The method was also found to be very useful in the investigation of graphite polyimide composites subjected to aging in nitrogen [19-21]. With additional modifications/developments it could be also useful for monitoring aging in composites aged in air, however the effect of volumetric shrinkage and internal cracking on the internal stresses in the composites would have to be determined first which might not be a straightforward task. (4) The embedded Al

inclusions were found not to affect the strength of the composites despite their relatively large numbers, which is certainly an advantage [22]. The plastic deformation of the inclusions appears to be a shielding mechanism against the initiation of micro-cracking around the inclusions under large bending loads.

Another very important feature of the method which should be treated as a major advantage (5) is its ability to gather enough visco-elastic information about the matrix that the extraction process of the stresses in the composites from the stresses in the embedded inclusions can be made under linear elastic conditions [17, 20]. Since the visco-elastic properties of a polymer are already included in the data from the inclusions, relatively small errors are created if the visco-elastic properties of the matrix are neglected in the modeling part. (6) It was also shown that if Al inclusions are used, the effect of their oxidation during aging at 315°C does not influence the stress measurements up to 1000 hours [21]. For longer exposure times or temperatures, either Au or Au-Pd inclusions would have to be used to avoid severe oxidation. The final major advantage of the method (7) is the fact the interactions between the inclusions can be ignored and the classical Eshelby-Mori-Tanaka approach can used to calculate the stresses.

4.2 Disadvantages

Despite the above advantages of the methods developed so far, there are also disadvantages. First of all, (1) the method requires that inclusions having sufficient strain response to residual stresses in the surrounding matrix be incorporated into the composite during manufacturing. (2) The methods can be successfully used only if ellipsoidal inclusions are employed as strain sensors. When irregular Ag inclusions were used [15] the results were less than satisfactory. Also, (3) the method is very sensitive to depth of the inclusions beneath the surface if conventional parafocusing optics are used, leading to errors in diffraction peak positions. To prevent these errors, parallel-beam optics must be used. Even then, it is preferable to have the embedded inclusion forming a layer parallel to the surface of the specimen to reduce scatter in the stress results. In addition, (4) the

method provides only the total residual stresses in the inclusions, averaged over the irradiated volume. To calculate residual intralaminar stresses, additional either analytical or numerical models must be used, especially in the case of woven composites [16]. (5) The method also cannot be used to monitor residual stresses larger than the yield stress of the embedded inclusions [22] and (6) cannot be used successfully in its present form to monitor weak residual stresses due to its rather low resolution with conventional laboratory diffractometers. (7) The final disadvantage of the method in its present form is that the large number of inclusions densely packed in the interlaminar regions and forming lens-shape clusters could affect the composite architecture [15] and some mechanical properties. However, this could be overcome by minimizing the volume fraction of inclusions and using stronger X-ray sources.

The above list of advantages and disadvantages clearly shows the major benefits and drawbacks of the XRD-E/M-T method as used thus far for the determination of residual stresses in graphite/polyimide composites. Most likely other advantages and disadvantages would be identified if the method was applied to other composites subjected to other mechanical and thermal conditions and exposed to aging in environments other than nitrogen or air. With additional research efforts this method could be further refined to monitor residual stress distributions even more accurately in advanced polymer matrix composite systems both in the laboratory and in the field.

Conclusions

The applicability of the method based on XRD measurements of residual stresses in embedded metallic ellipsoidal inclusions in conjunction with the Eshelby/Mori-Tanaka model for the determination of residual interlaminar stresses in polymer matrix composites was discussed in this work. The method was effectively used in this research to estimate the residual stresses in unidirectional and woven composites based on T650-35 graphite fibers embedded in a PMR-15 polyimide matrix subjected to external loads of various magnitudes and to aging. Despite several clearly identified disadvantages, the method can be recommended for the determination of residual stresses in polymer matrix

composites with moderate to large residual stress concentrations, particularly with the use of higher intensity X-ray sources.

Acknowledgments

This research was supported by the Air Force Office of Scientific Research and NASA Glenn Research Center under joint grant #F49620-00-1-0159. Additional funds were also provided by the National Science Foundation and the University of Denver from a Major Research Instrumentation Program; Instrument Development and Acquisition grant# CMS-9977735, and by the Los Alamos National Laboratory.

References

1. N. J. Rendler and I. Vigness, Hole-drilling Strain-gage Method of Measuring Residual Stresses, *Experimental Mechanics*, vol. 6, no. 12, p. 577-586, 1966.

2. R. Y. Kim, H. T. Hahn, Effect of Curing Stress on the First Ply-failure in Composite Laminates, *Journal of Composite Materials*, vol. 13, p. 2-16, 1979.

3. H. E. Gascoigne, Residual Surface Stresses in Laminated Cross-ply Fiber-Epoxy Composite Materials, *Experimental Mechanics*, vol. 34, p. 27-36, 1994.

4. G. P. Carman and G. P. Sendeckyj, Review of the Mechanics of Embedded Optical Sensors, *Journal of Composite Technology and Research*, vol. 17, p. 183-193, 1995.

5. L. S. Schadler and C. Galiotis, Fundamentals and Applications of Micro Raman Spectroscopy to Strain Measurements in Fibre Reinforced Composites, *International Materials Reviews*, vol. 40, no. 3, p. 116-134, 1995.

6. H. Fukuda, K. Takahashi and S. Toda, Thermal Deformation of Anti-symmetric Laminates at Cure, *Proc. ICCM-10*, vol. 3, p. 141-148, 1995.

7. P. G. Ifju, X. Niu, B. C. Kilday, S. C. Liu and S. M. Ettinger, Residual Stress Measurement in Composite Using the Cure-Referencing Method, *Experimental Mechanics*, vol. 40, p. 22-30, 2000.

8. C. S. Barrett and P. Predecki, Stress Measurement in Polymeric Materials by X-ray Diffraction, *Polymer Eng and Sci.*, vol.16, p. 602-608, 1976.

9. P. Predecki and C. S. Barrett, Stress Measurement in Graphite/Epoxy Composites by X-ray Diffraction from Fillers, *J. Comp. Mat.*, vol. 13, p. 61, 1979.

10. C. S. Barrett and P. Predecki, Stress Measurements in Graphite/Epoxy Uniaxial Composites by X-rays, *Polymer Composites*, vol. 1, p. 2-6, 1980.

11. P. Predecki, C. S. Barrett, Residual Stresses in Resin Matrix Composites, In E. Kula, editor, *28th Sagamore Army Materials Research Conference*, p. 409-424, Lake Placid, July 13-17 1981.

12. R. H. Fenn, A.M. Jones and G.M. Wells, X-ray Diffraction Investigation of Triaxial Residual Stresses in Composite Materials, *Journal of Composite Materials*, vol. 27, no. 14, p. 1338-1351, 1993.

13. R. Meske and E. Schnack, A Micro-mechanical Model for X-Ray Stress Analysis of Fiber Reinforced Composites, *Journal of Composite Materials*, vol. 35 (11), p. 972-998, 2001.

14. R. Meske and E. Schnack, Particular adaptation of X-ray diffraction to fiber reinforced composites, *Mechanics of Materials*, vol. 35 (1-2), p. 19-34, 2003.

15. B. Benedikt, M. Kumosa, P. K. Predecki, L. Kumosa, M. G. Castelli, J. K. Sutter, An Analysis of Residual Thermal Stresses in a Unidirectional Graphite/PMR-15 Composite Based on the X-ray Diffraction Measurements, *Composite Science and Technology,* vol. 61 p. 1977-1994, 2001.

16. B. Benedikt, P. K. Predecki, L. Kumosa, D. Armentrout, J. K. Sutter and M. Kumosa, The Use of X-ray Diffraction Measurements to Determine the Effect of Bending Loads on Internal Stresses in Aluminum Inclusions Embedded in a Unidirectional Graphite Fiber /PMR-15 Composite, *Composites Science and Technology*, vol. 61, no.14, p. 1995-2006, 2001.

17. B. Benedikt, P. Rupnowski, L. Kumosa, J.K. Sutter, P.K. Predecki and M. Kumosa, Determination of Interlaminar Residual Thermal Stresses in a Woven 8HS graphite/PMR-15 Composite Using X-ray Diffraction Measurements, *Mechanics of Advanced Materials and Structures*, vol. 9, no. 4, p. 375-394, 2002.

18. B. Benedikt, P.K. Predecki, L. Kumosa and M. Kumosa, Measurement of Residual Stresses in Polymer Matrix Fiber Reinforced Composites based on X-ray Diffraction, Denver X-ray Conference, August 2001, Steamboat Springs, Colorado, *Advances in X-ray Analysis*, vol. 45, p.218-224, 2001.

19. Benedikt, B., Gentz, M., Kumosa, L., Predecki, P.K., Armentrout, D., Kumosa, M. and Sutter, J.K., The Use of X-ray Diffraction Measurements to Determine the Effect of Aging on Residual Stresses in Unidirectional and Woven Graphite/Polyimide Composites, the 51st Annual Denver X-Ray Conference, Colorado Springs, August 2002, International Center for Diffraction Data, Advances in X-ray Analysis, vol. 46, p. 112-118, 2002.

20. B. Benedikt, Analysis of Residual Stresses in Graphite Fiber/PMR-15 Composites, Ph.D. Thesis, Department of Engineering, University of Denver, Denver, Colorado, June 2003.

21. B. Benedikt, M. Gentz, L. Kumosa, P. Rupnowski, J. K. Sutter and M. Kumosa, X-ray Diffraction Experiments on Aged Graphite Fiber/Polyimide Composites with Embedded Aluminum Inclusions, *Composites Part A,* vol. 35, no. 6 p. 667-681, 2004,

22. B. Benedikt, M. Kumosa, D. Armentrout, L. Kumosa, J. K. Sutter and P. K. Predecki, Analysis of Stresses in Aluminum Particles Embedded Inside Unidirectional and Woven Graphite/Polyimide Composites Subjected to Large Bending Loads, *Mechanics of Advanced Materials and Structures*, vol. 11, no. 1, p. 31-49, 2004.

23. G. Odegard and M. Kumosa, Elastic-Plastic and Failure Properties of a Unidirectional Graphite/PMR-15 Composite at Room and Elevated Temperatures, *Composites Science and Technology,* vol. 60, p. 2979-2988, 2000.

24. M. Kumosa, G. Odegard, D. Armentrout, L. Kumosa and J. K. Sutter, Comparison of the ±45° Off Axis and Iosipescu Shear Tests for Woven Fabric Composite Materials, *Composites Technology & Research*, vol. 24, p. 3-1, 2002.

25. J. K. Sutter, Higher Operating Temperature Propulsion Components, Proc. of the High Temple Workshop XXII, Edit. DOD/NASA Laboratories and University of Dayton Research Institute, Santa Fe, New Mexico, p. 21-24, January 2001.

26. M. Gentz, D. Armentrout, P. Rupnowski, L. Kumosa, J. K. Sutter and M. Kumosa, Mechanical Behavior of a Woven Graphite/PMR-15 Composite at Room and Elevated Temperatures Determined from the ±45° Tensile and Iosipescu Shear Tests, *Journal of Composites Technology & Research*, vol. 25, p. 22-34, 2003.

27. P. Rupnowski and M. Kumosa, Meso- and Micro-Stress Analyses in an 8HS Graphite/Polyimide Woven Composite Subjected to Biaxial In-Plane Loads at Room Temperature, Composites Science and Technology, vol. 63, no. 6, p. 785-799, 2003.

28. M. Kumosa, An Investigation of Damage Initiation in Woven Graphite Fiber/Polyimide Composites Subjected to Shear, *Key Engineering Materials,* vols. 251-252, p. 447-456, 2003.

29. B. Benedikt, P. Rupnowski and M. Kumosa, Visco-Elastic Stress Distributions and Elastic Properties in Unidirectional Composites with Large Volume Fractions of Fibers, *Acta Materialia,* vol.51, no. 12, p. 3483-3493, 2003.

30. R. E. Allerd, S. P. Wesson, E. E. Shin, L. Inghram, L. McCorkle, D. Papadopoulos, D. Wheeler and J. K. Sutter, The Influence of Sizing on the Durability of High-Temperature Polymer Composites, *High Performance Polymers*, 2003, vol.15, no. 4, p. 395-419, 2003.

31. M. Gentz, D. Armentrout, P. Rupnowski, L. Kumosa, E. Shin, K. K. Sutter and M. Kumosa, In-Plane Shear Testing of Woven Graphite/Polyimide Composites with Medium and High Modulus Graphite Fibers at Room and 316°C Temperatures, *Composites Science and Technology*, vol. 64, p. 203-220, 2004.

32. M. Gentz, B. Benedikt, M. Kumosa and J. K. Sutter J. K., Residual Stresses in Unidirectional Carbon Fiber/Polyimide Composites as a Function of Aging, *Composites Science and Technology*, vol. 64, p. 1671-1677, 2004.

33. P. Rupnowski, M. Gentz, J. K. Sutter and M. Kumosa, Mechanical Response of a Woven Graphite/Polyimide Composite to In-Plane Shear Dominated Loads at Room an Elevated Temperatures, *Acta Materialia*, vol. 52, pp. 5603-5613, 2004.

34. J. D. Eshelby, The Determination of the Elastic Field of an Ellipsoidal inclusion, and Related Problems, *Proc. R. Soc. London*, vol. A241, p. 376, 1957.

35. T. Mura, *Micromechanics of Defects in Solids*, 2nd edition, Martinus Nijhoff Publishers, Dordrecht, 1987.

36. T. Mori and K. Tanaka, Average Stress in Matrix and Average Elastic Energy of Materials with Misfitting Inclusions, *Acta Metall.*, vol. 21, p. 571-574, 1973.

37. B. D. Cullity, Elements of X-Ray Diffraction, second edition, Addison-Wesley Publishing Company, Inc. Reading, 1978.

38. I. C. Noyan and J. B. Cohen, Residual Stress. Measurement by Diffraction and Interpretation. Springer-Verlag, New York, 1987.

39. L. H. Schwartz and J. B. Cohen, Diffraction from Materials, Second edition, Springer-Verlag, New York, 1987.

40. G. D. Roberts, D. C. Malarik and J. O. Robaidek Viscoelastic Properties of Addition-Cured Polymides Used in High Temperature Polymer Matrix Composites, Composites Design, Manufacturing, and Applications; *Proceedings of the Eight International Conference on Composite Materials*, S. W. Tsai and G. S. Springer, Eds., Society for Advanced Materials and Process Engineering, Covina, CA 1991, p. 12-H-1 to 12-H-10.

41. J. N. Reddy, *Mechanics of Laminated Composite Plates. Theory and Analyses.*, CRC Press, 1997.

42. J. E. Kamvouris, G. D. Roberts, J. M. Pereira and C. Robzak, Physical and Chemical Aging Effects in PMR-15 Neat Resin, *High temperature and Environmental Effects on Polymeric Composites: 2nd Volume, ASTM STP1302*, T.

S. Gates and Abdul-Hamid Zureic, Eds., American Society for Testing and Materials, pp. 243-258, 1997.

43. L. C. Tsuji, H. L. McManus and K. J. Bowles, Mechanical Properties of Degraded PMR-15 Resin, *Time Dependent and Nonlinear Effects in Polymers and Composites, ASTM STP 1357*, R. A. Schapery and C. T. Sun, Eds., American Society for Testing and Materials, West Conshohocken PA, pp. 3-17, 2000.

44. J. Luo and R. Stevens, Micromechanics of Randomly Oriented Ellipsoidal Inclusion Composite. Part I: Stress, Strain and Thermal Expansion, *J. Appl. Phys.*, vol. 79 (12), p. 9047-9056, 1996.

45. J. Luo and R. Stevens, Micromechanics of Randomly Oriented Ellipsoidal Inclusion Composite. Part II: Elastic Moduli, *J. Appl. Phys.*, vol. 79 (12), p. 9057-9063, 1996.

46. Y. Benveniste, A New Approach to the Application of Mori-Tanaka's Theory in Composite Materials. *Mechanics of Materials*, vol. 6, p. 147-157, 1987.

47. Z. A. Moschovidis and T. Mura, Two Ellipsoidal Inhomogeneities and Related Problems Treated by Equivalent Inclusion Method, *ASME J. Appl. Mech.*, vol. 42, p. 847-852, 1975.

48. B. Benedikt, M. Lewis and P. Rangaswamy, Multi-Inclusion Model for Particulate Composite with Periodically and Randomly Distributed Reinforcements, to be submitted for publication.

Figure Captions

Figure 1. Al inclusions distributed in the interlaminar region of (a) unidirectional and (b) 8HS woven T650-35/PMR-15 composite.

Figure 2. Definition of angles ϕ and ψ, and the specimen coordinate system x_1, x_2, x_3.

Figure 3. Two examples (a and b) of $\sin^2 \psi$ plots for embedded Al inclusions.

Figure 4. Model used for the determination of residual strains and stresses in the matrix from the XRD strains and the close range strains.

Figure 5. X-ray four-point bend tests on composite specimen with embedded inclusions (schematic).

Figure 6. XRD von Misses stresses in aluminum inclusions as a function of the bending strain; (a) in two unidirectional and (b) two woven T650-35/PMR-15 specimens.

Figure 7. T650-35/PMR-15 specimens (a) unidirectional and (b) woven aged in nitrogen at 315°C up 1064 hours.

Figure 8. Examples of damage in (a) unidirectional and (b) woven T650-35/PMR-15 specimens aged in air at 315°C for 1064 hours.

Figure 9. Residual stresses in T650-35/PMR-15 composites as a function of the volume fraction of embedded inclusions; (a) unidirectional and (b) woven 8HS composites.

Figure 10. Residual stresses in T650-35/PMR-15 composites as a function of the aspect ratio of embedded Al inclusions; (a) unidirectional composite, (b) woven 8HS composite.

Figure 11. Cluster and sub-cluster of aluminum inclusions between the first and second plies.

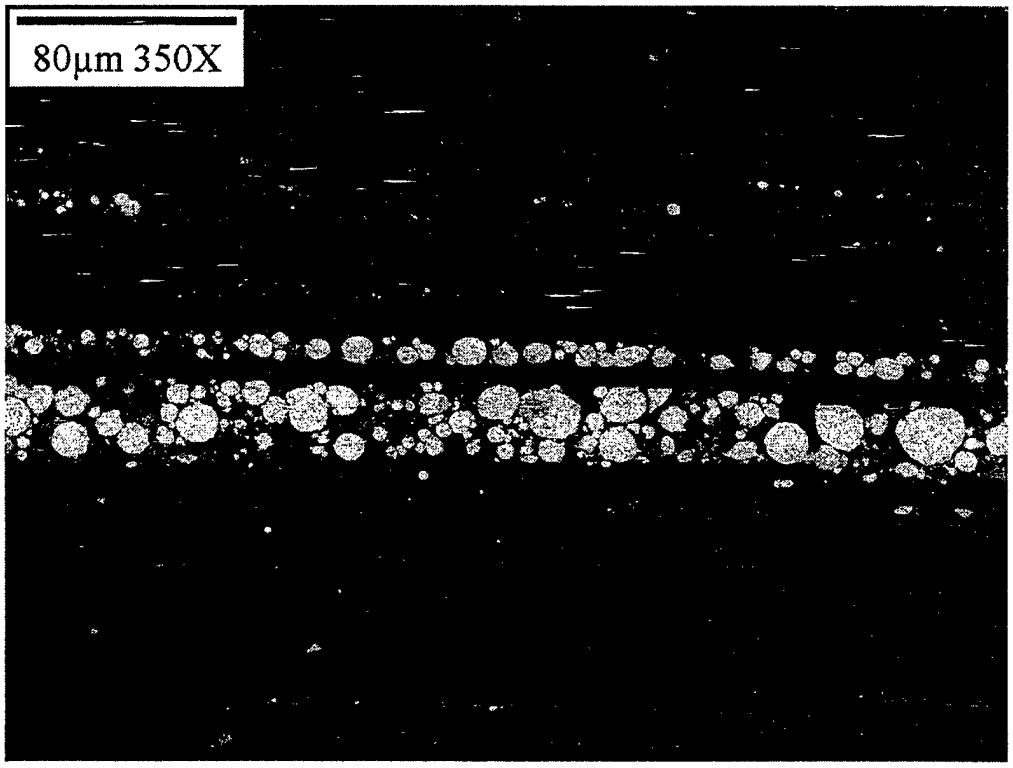

a)

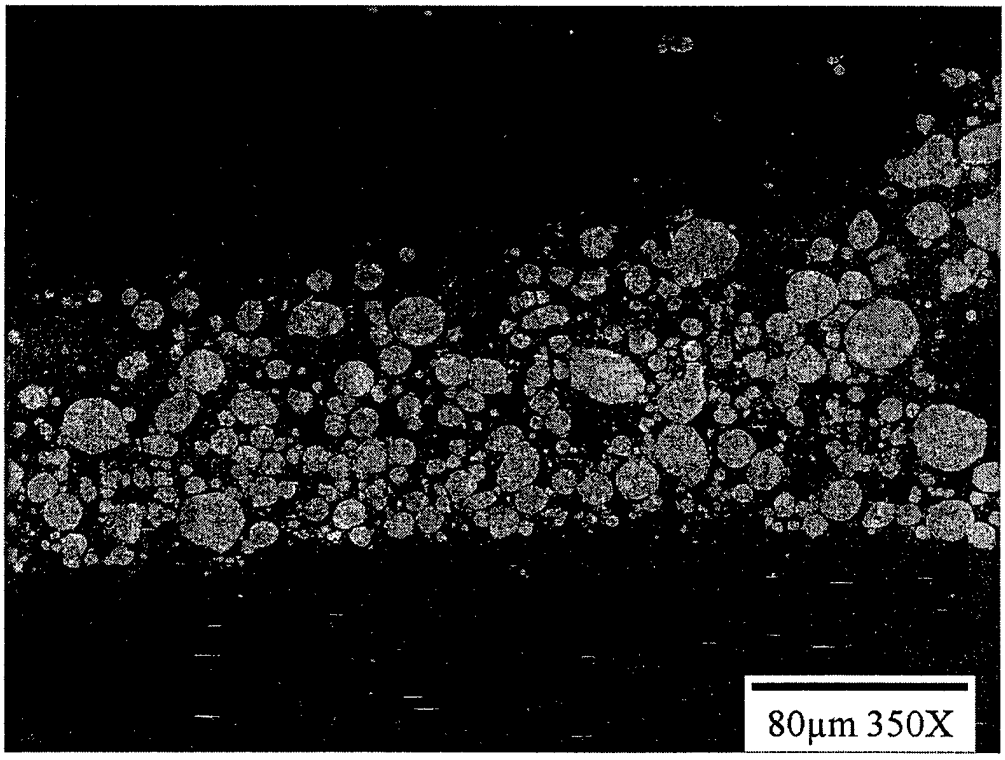

b)

Figure 1. Al inclusions distributed in the interlaminar regioon of (a) unidirectional and (b) 8HS woven T650-35/PMR-15 composite.

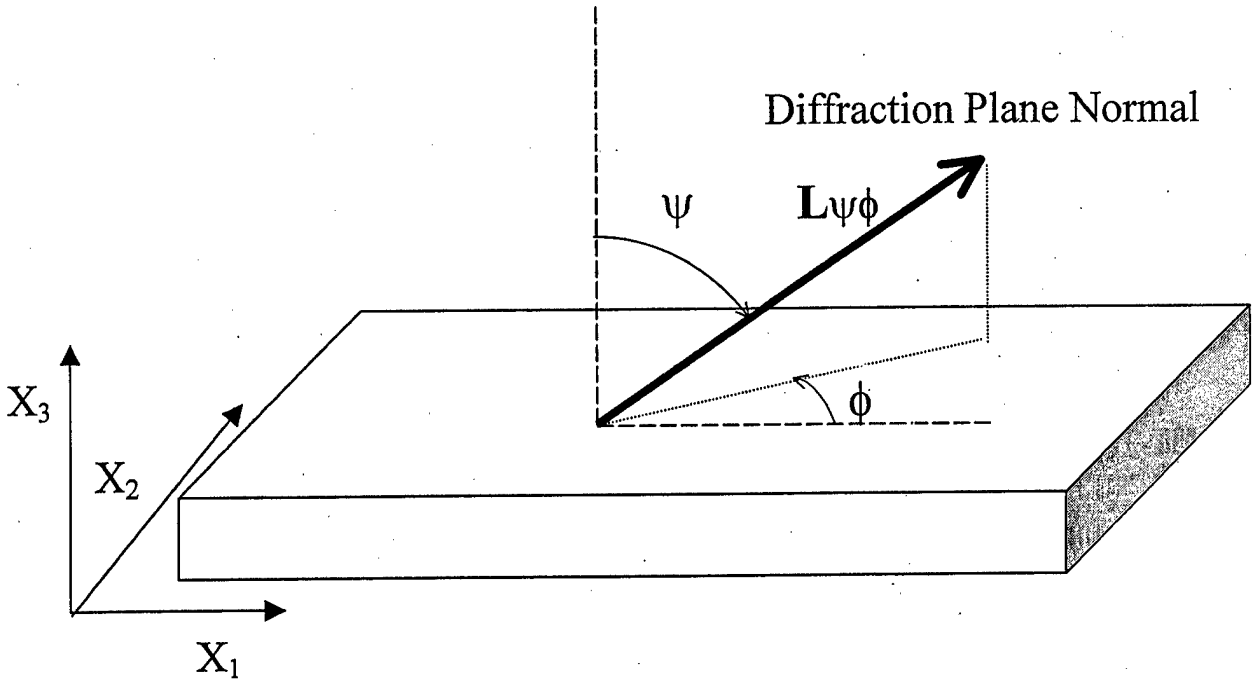

Figure 2. Definition of angles ϕ and ψ, and the specimen coordinate system x_1, x_2, x_3.

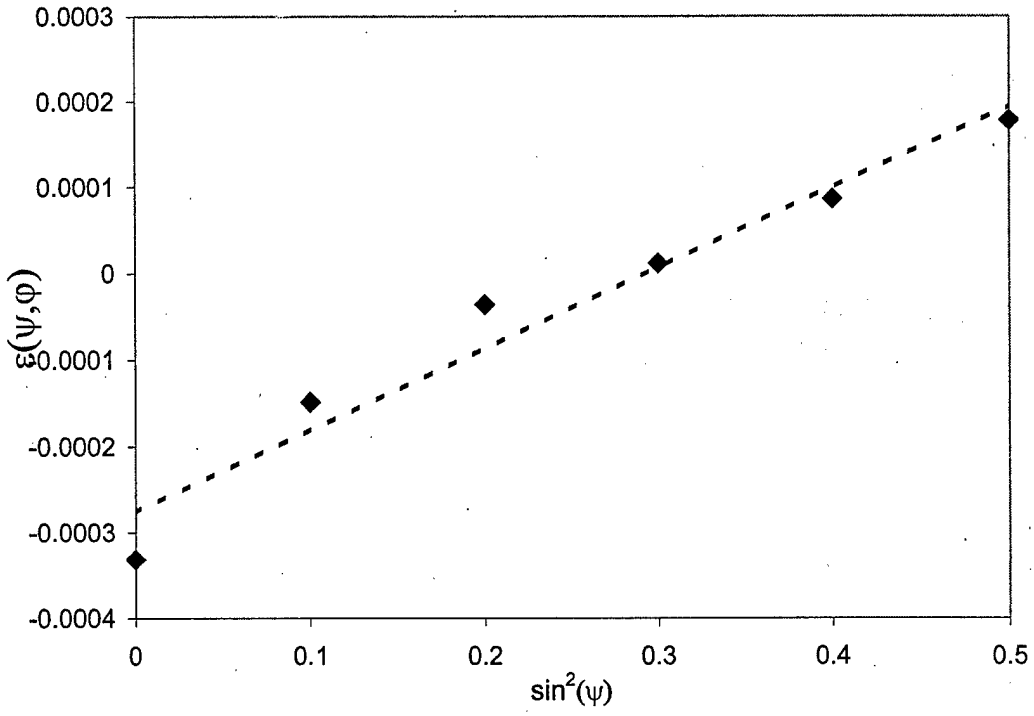

a)

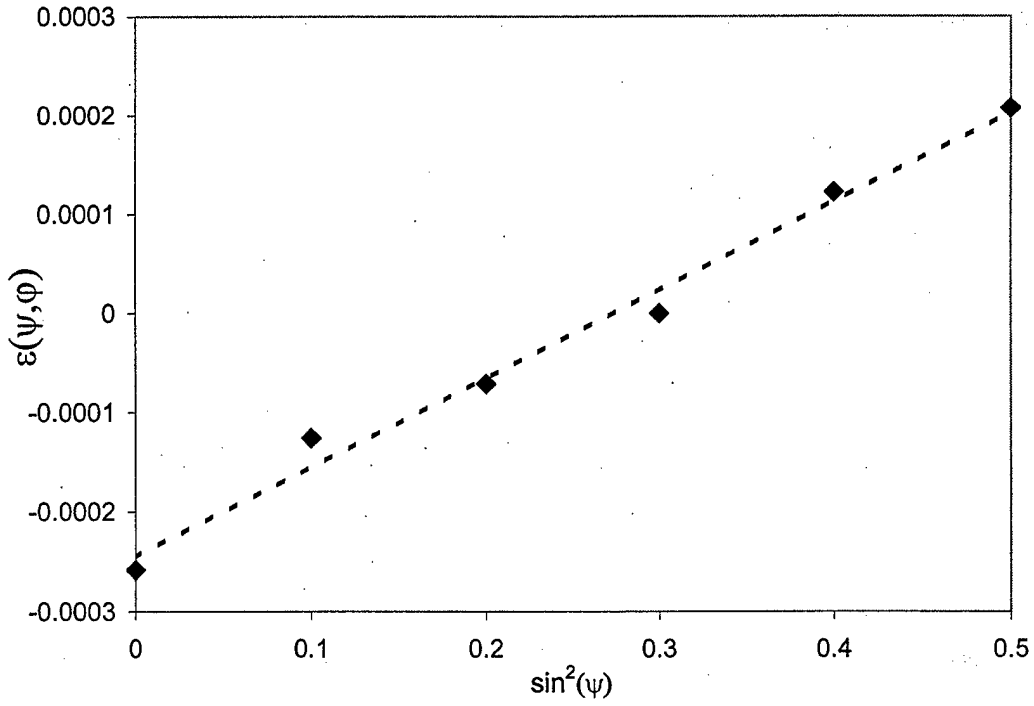

b)

Figure 3. Two examples (a and b) of $\sin^2 \psi$ plots for embedded Al inclusions.

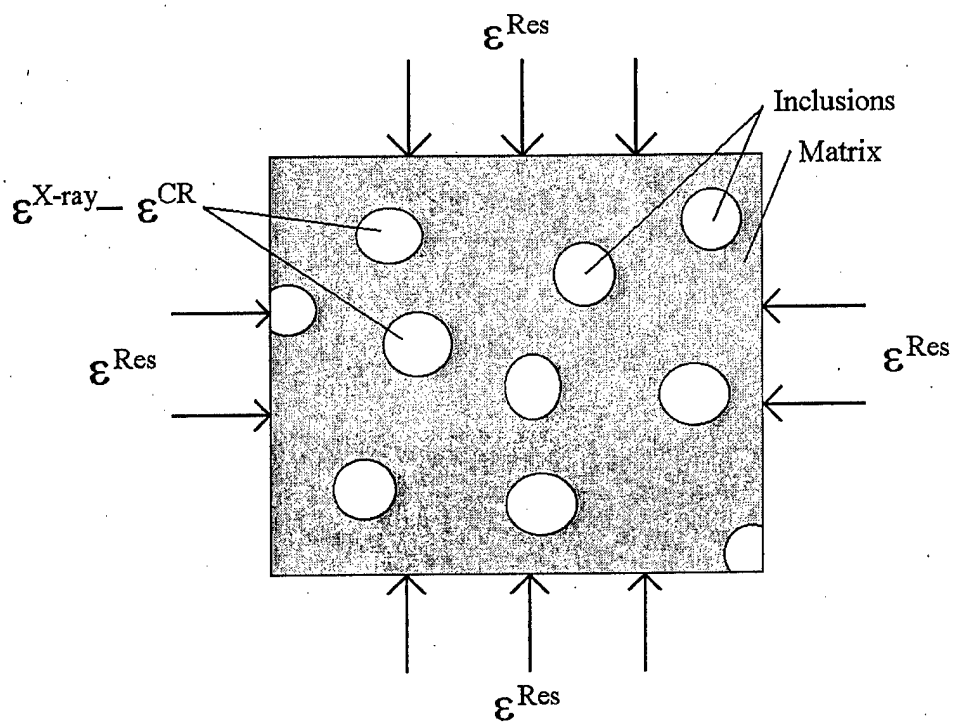

Figure 4. Model used for the determination of residual strains and stresses in the matrix from the XRD strains and the close range strains.

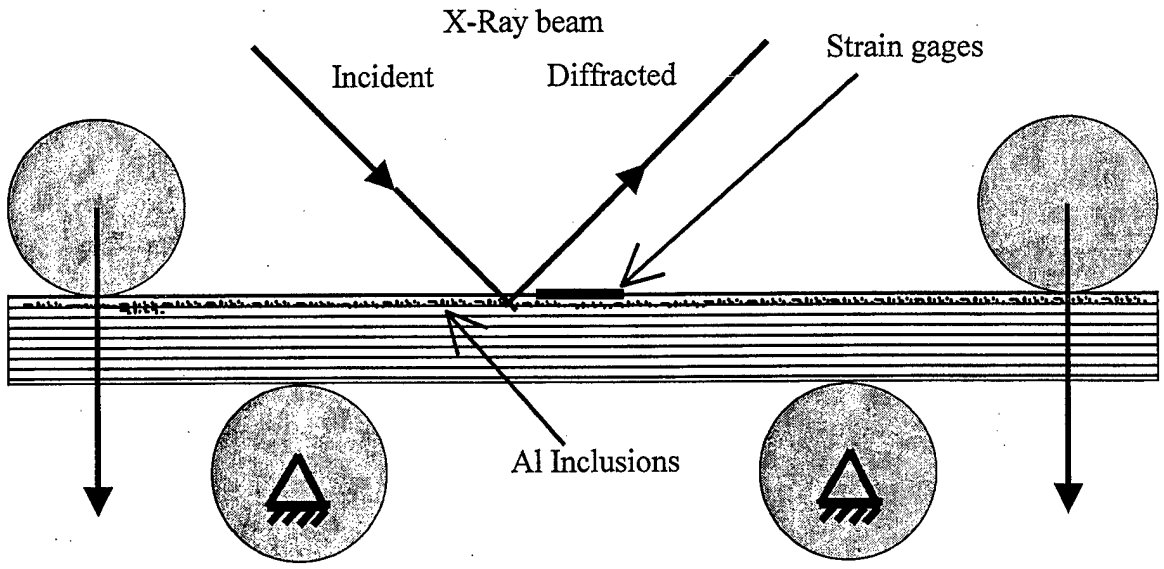

Figure 5. X-ray four point bend tests on composite specimen with embedded inclusions (schematic).

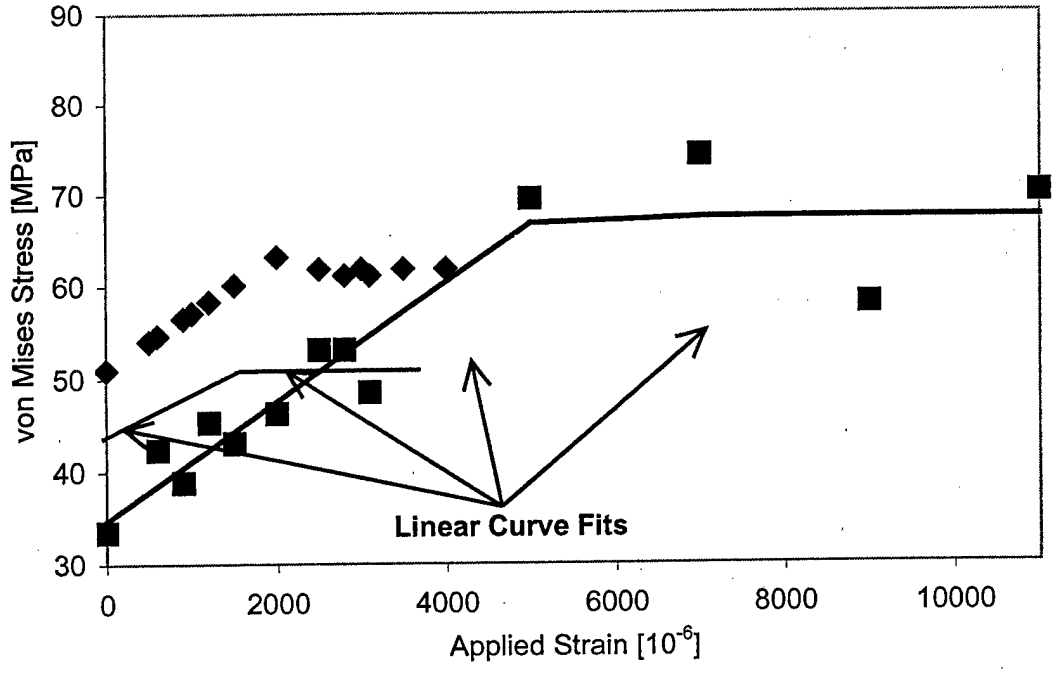

a)

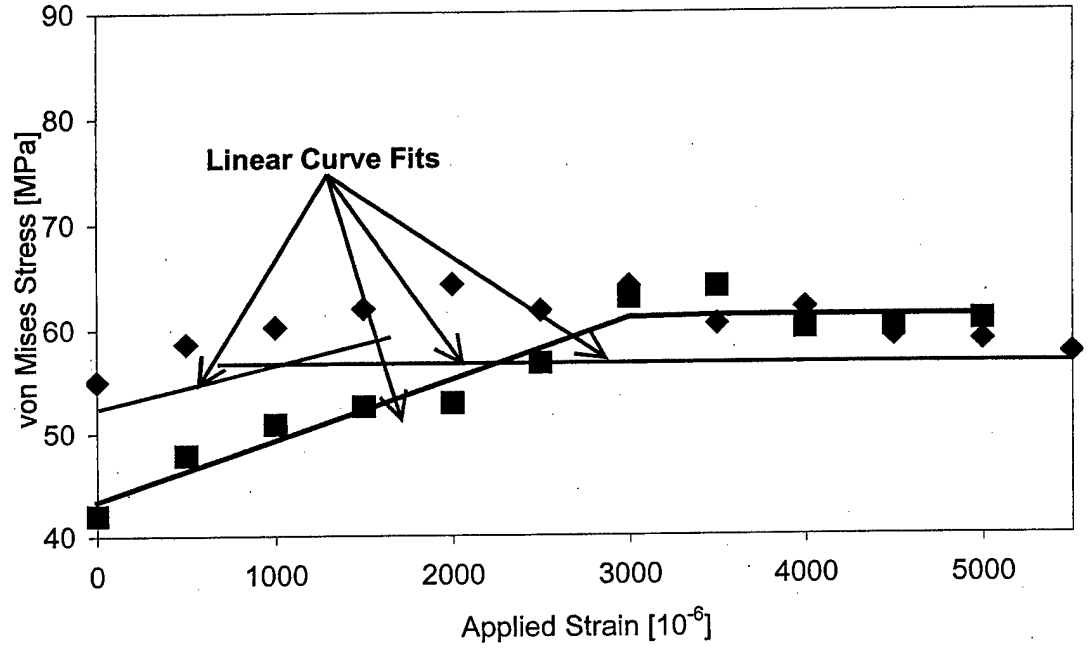

b)

Figure 6. XRD von Misses stresses in aluminum inclusions as a function of the bending strain; (a) in two unidirectional and (b) two woven T650-35/PMR-15 specimens.

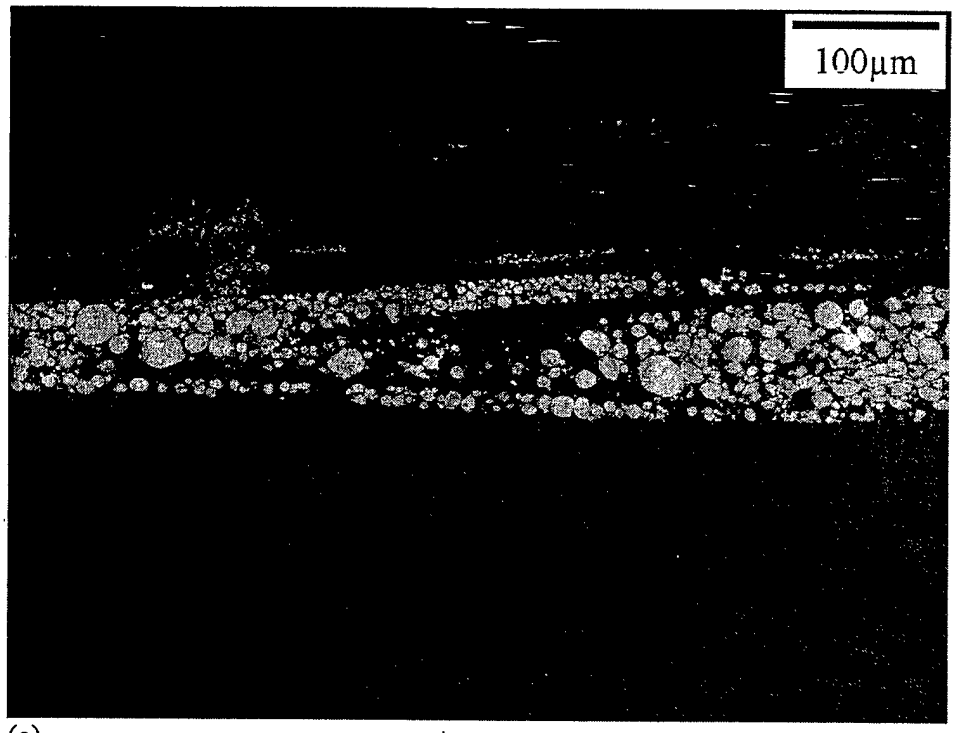

(a)

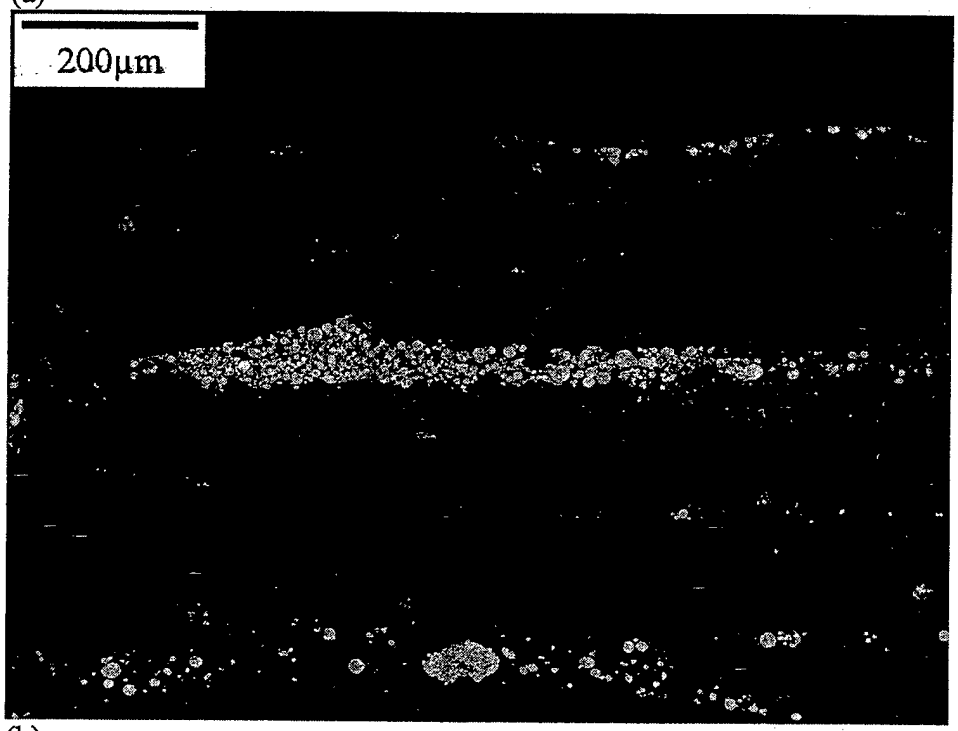

(b)

Figure 7. T650-35/PMR-15 specimens (a) unidirectional and (b) woven aged at 315°C in nitrogen up 1064 hours.

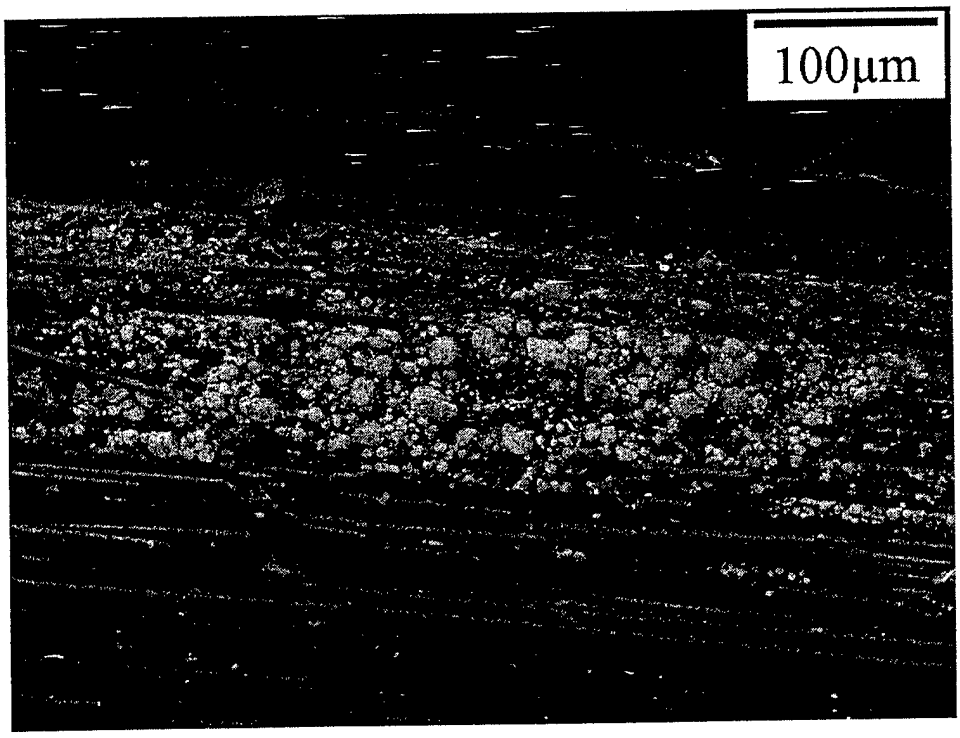

a)

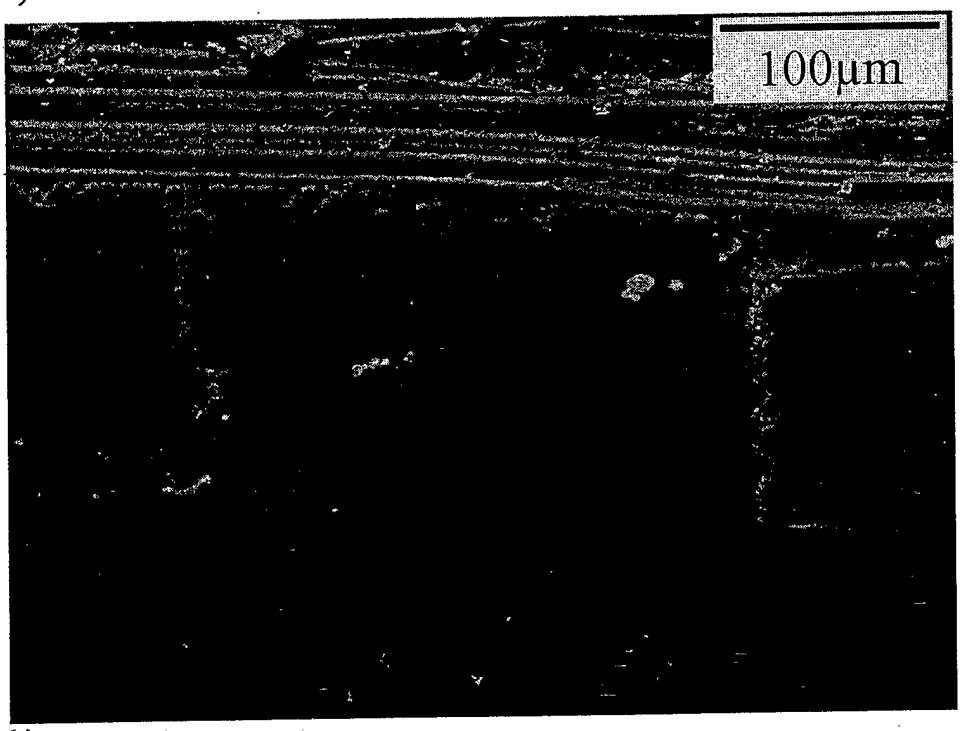

b)

Figure 8. Examples of damage in (a) unidirectional and (b) woven T650-35/PMR-15 specimens aged in air at 315°C for 1064 hours.

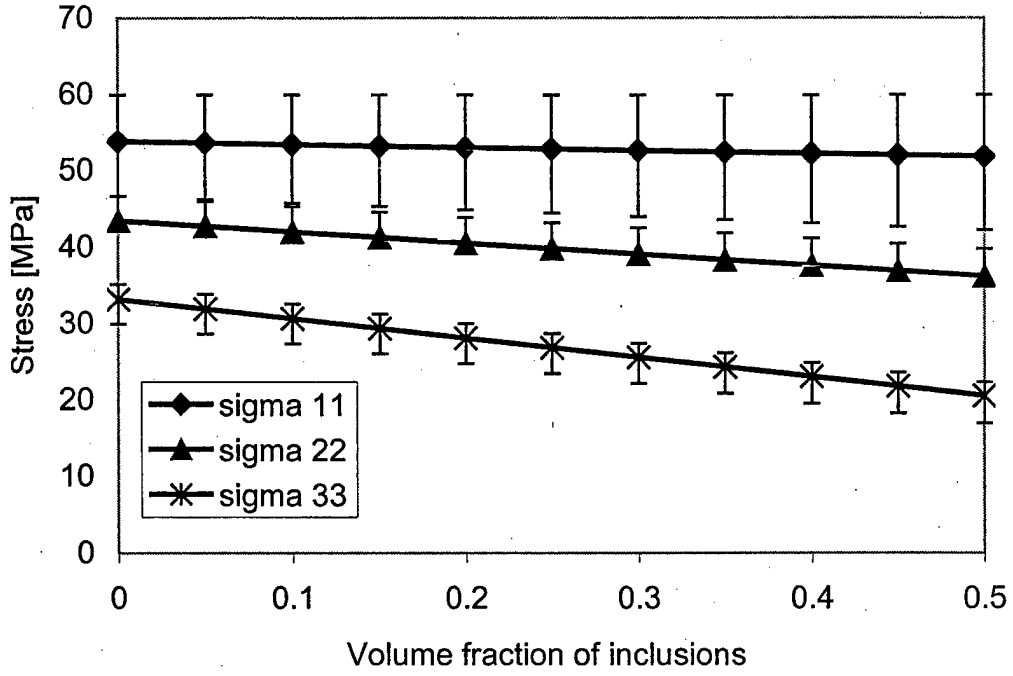

a)

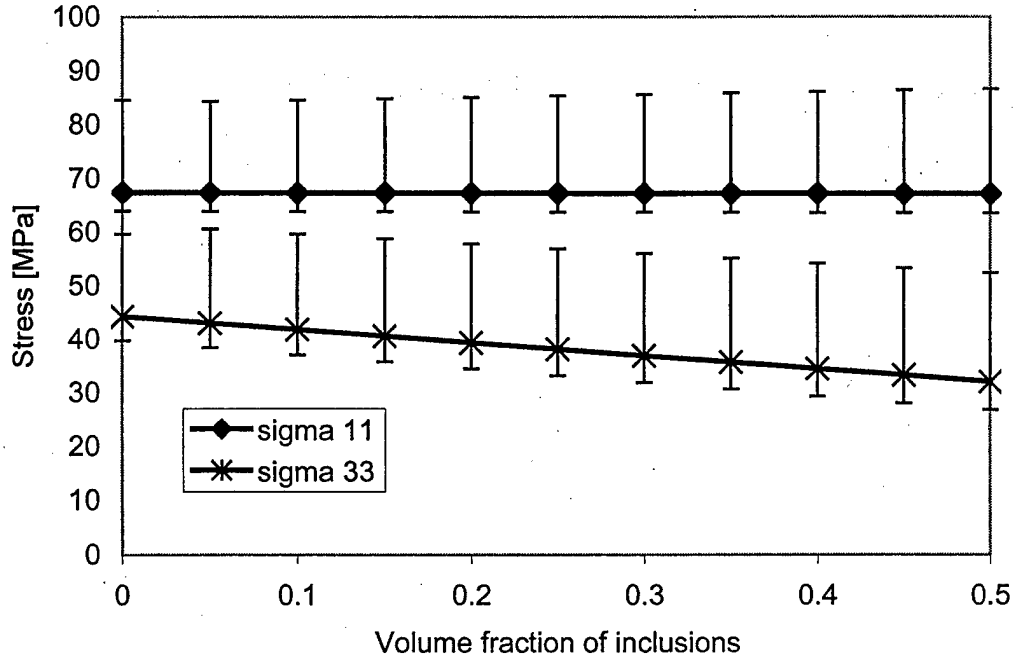

b)

Figure 9. Residual stresses in T650-35/PMR-15 composites as a function of the volume fraction of embedded inclusions; (a) unidirectional and (b) woven 8HS composites.

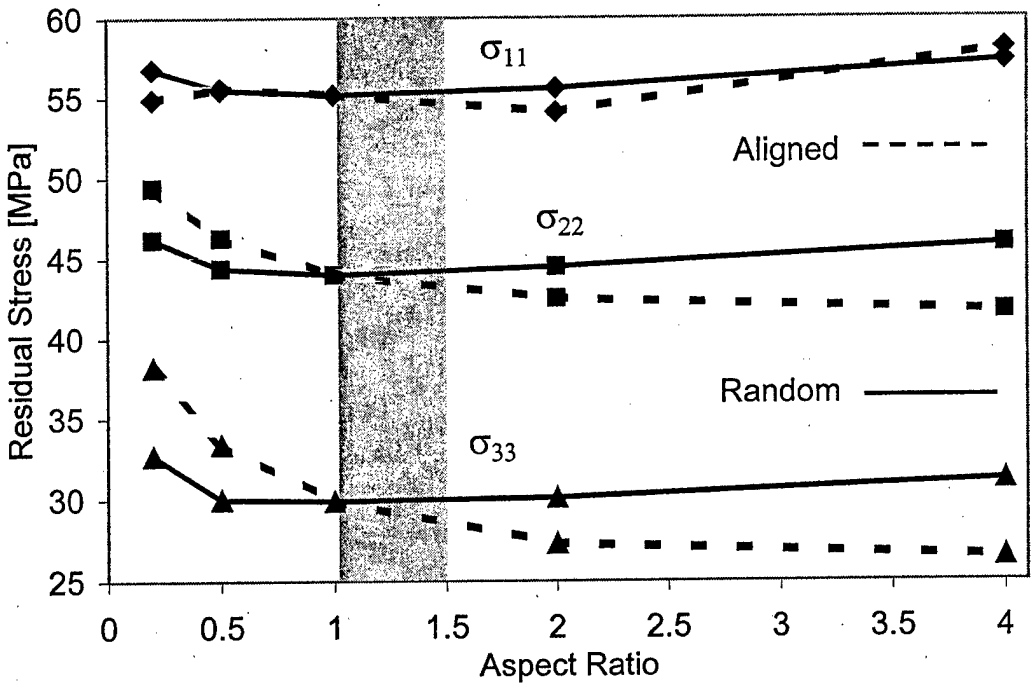

(a)

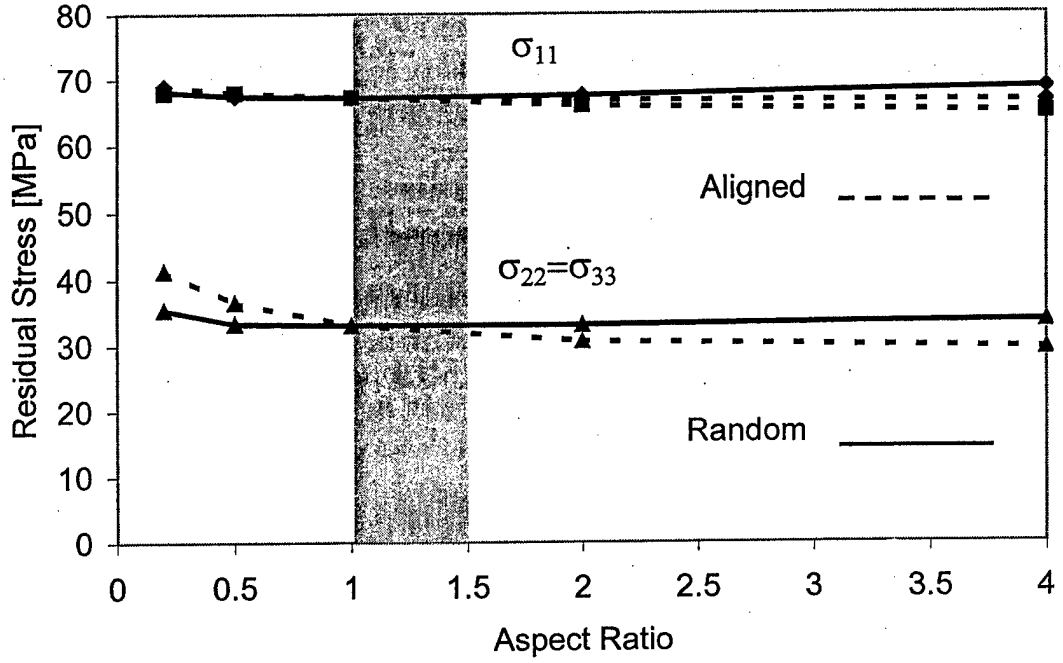

(b)

Figure 10. Residual stresses in T650-35/PMR-15 composites as a function of the aspect ratio of embedded Al inclusions; (a) unidirectional composite, (b) woven 8HS composite.

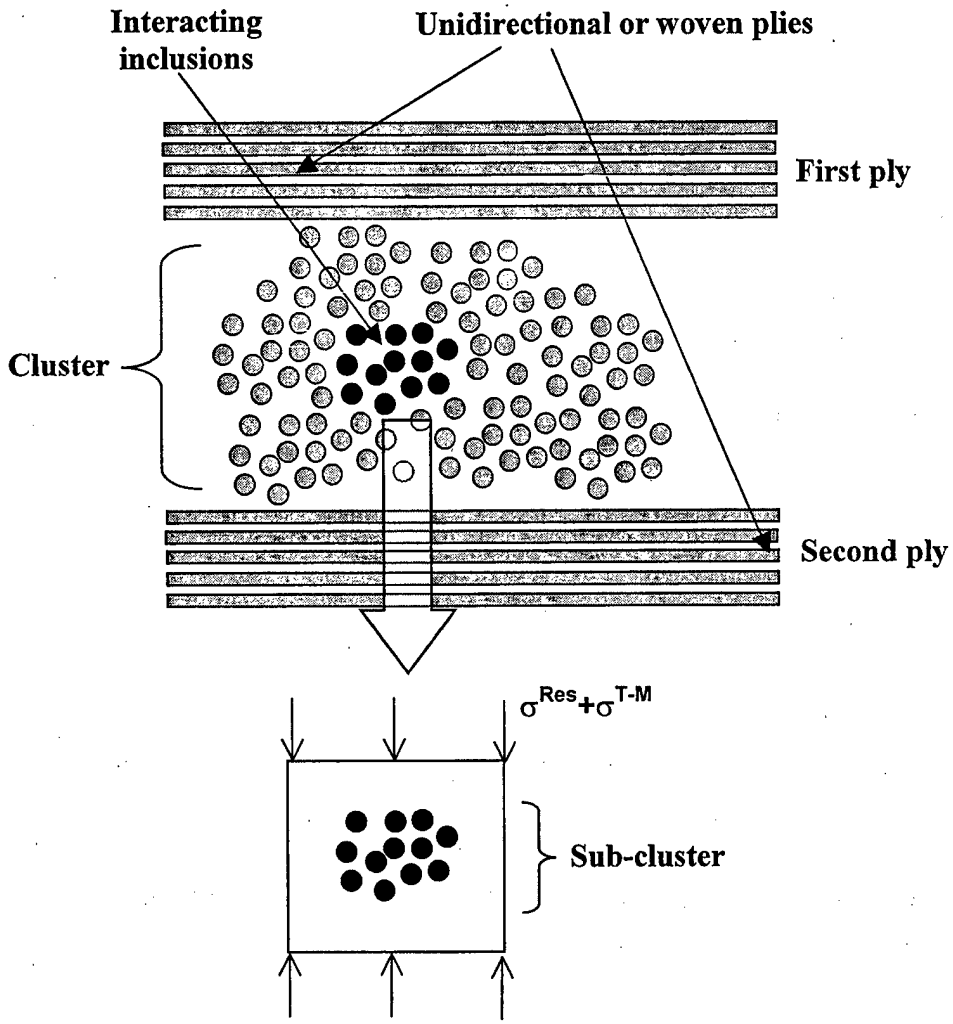

Figure 11. Cluster and sub-cluster of aluminum inclusions between the first and second plies.